Modelling of Biomass Steam Gasification in a Bubbling Fluidized Bed Gasifier

A thesis

submitted in fulfilment

of the requirements for the Degree

of

Doctor of Philosophy

in

Chemical and Process Engineering

in the University of Canterbury

by

Prasanth Gopalakrishnan

UNIVERSITY OF CANTERBURY
April, 2013

Summary

This thesis presents the numerical simulation study of the biomass-steam gasification in a bubbling fluidized bed (BFB) gasifier including the mathematical model development and the experimental validation of the model developed. The study focused on two main areas on developing the mathematical model: a one-dimensional (1D) non-isothermal reaction kinetics model and a two-dimensional (2D) model consisting of the reaction kinetics model for gasification reactions and two-dimensional CFD model for hydrodynamics characteristics.

Literature review was firstly conducted which shows that the biomass gasification with steam as the gasification agent at elevated temperatures can be considered to include two main stages: initial pyrolysis and subsequent gasification reactions. In the first stage, the pyrolysis reactions of the biomass occurred instantaneously for a short duration at the bottom of the gasifier filled with the bed materials. The biomass was decomposed into volatile gases, char and tar. The steam as gasification agent fluidizes the reactor bed facilitating good mixing and heat transfer. In an industrial biomass gasification system, the final gas composition of the producer gas was affected by the products of pyrolysis process especially the compositions of the gaseous volatiles which were quantified with a product distribution function of temperature developed from experimental results in this work.

In the subsequent stage of gasification, reactions occurred among the gasification agent (steam), the volatile gases and the char evolved from the initial stage of pyrolysis at high temperatures. Considering the low tar concentration and its slow reactions, it was assumed in the model that these tars were not involved in the reactions during the gasification process. The producer gas from biomass-steam gasification mainly consists of CO, H_2, CO_2, CH_4 and H_2O and least quantities of higher hydrocarbons at elevated operating temperature. Hence the reactions involved with these gas components were only considered in this model that mainly constitutes of Steam Gasification reaction, Water Gas-Shift reaction, Methanation reaction, Bouduard reaction, and Steam Methane Reforming reaction.

The development of the subsequent gasification reaction model was based on two-stage reactions and two-phase theory of gases and solids. The two phases considered, consists of the particle-lean bubble phase and the particle-rich emulsion phase which were distributed homogeneously when the gas velocity through the bed was in excess of the minimum fluidization velocity. Between the two phases there was certain interchange of gas or cross

flow. In the two-phase theory model, the heat and mass transfer rates were related to the fluidization characteristics of the bed. Therefore, understanding and quantitatively description of the hydrodynamics of the gas-solid within the gasifier were important. The governing hydrodynamic equations in literature were adopted in the development of the 1D model for the gasification process in the BFB.

In the 1D gasification model, the conservation equations (mass and energy balances) were described considering the convective and the diffusive flows between the phases. The gasification model developed also includes the empirical model in the pyrolysis and the subsequent gasification reactions that encompass both homogeneous and heterogeneous reaction kinetics based on Arrhenius correlations. The non-linear partial differential equations (PDEs) describing the mass and energy balances with the reactions kinetics were numerically solved using a solver function from the PDE modules of Matlab software with properly defined initial and boundary conditions.

After developing the 1D model, the Computational Fluid Dynamics (CFD) techniques were applied to the fluidized bed systems to gain better understanding of the hydrodynamic behaviour within the BFB gasifier that involves flows of steam, biomass and bed materials. Following this, a 2D mathematical Eulerian-Eulerian granular kinetic model was developed to simulate flows of bed materials and steam (gasification agent) in the BFB. Conservation equations for mass and momentum were used to compute the hydrodynamics of flows in the BFB. The model predicted the dynamics of flow of solid particles and the gas feed streams, particle bed pressure and the gas pressure. The fluidization in the BFB gasifier was modelled using CFD ANSYS FLUENT 12.1 package.

In the development of the 2D gasification model, the developed reaction kinetics model was integrated into the 2D CFD model called Gasification embedded 2D CFD model. In this 2D model, the built-in 'laminar finite-rate' model was adopted to describe the chemical kinetics using Arrhenius reaction kinetics expressions. The momentum equation considered laminar viscous model for laminar flow at low steam to biomass (S/B) ratio (lower than 0.6) and $k-\varepsilon$ turbulence viscous model for transient to turbulent flow regime for high S/B ratio. In the ANSYS FLUENT package, the non-linear coupled PDEs of multiphase flow had problems with the integration of the viscous model and the reaction equations. These were solved using a Phase Coupled SIMPLE solver algorithm based on FVM.

To provide validation data for the developed biomass gasification models, experiments were undertaken on the 100kW DFB gasifier at the University of Canterbury. In the experiments, the gasifier was operated firstly with nitrogen as the fluidization agent in order to generate experimental data of pyrolysis reactions as no gasification agent (steam) was involved. It had been found that the simulation results from the initial pyrolysis model were in close agreement with the experimental data with discrepancies of ±1.0% (mol/mol) for H_2, ±0.8% (mol/mol) for CO, ±0.6% (mol/mol) for CO_2 and ±0.3% (mol/mol) for CH_4. The correlation coefficient (R^2) of the predicted and observed mole fractions of H_2, CO, CO_2, and CH_4 were 0.89, 0.94, 0.85 and 0.93, respectively.

After this, the gasification agent steam was introduced for normal gasification operation under various operation conditions (temperature, S/B ratio). The experimental results were compared with the simulated results from both the 1D and the 2D models for gas compositions. It has been found that the model predicted results were in close agreement with the experimental data. The experimentally measured producer gas compositions for the operating conditions of 680-780°C, 1 atmospheric pressure and S/B ratio of 0.53 ranged from 17.9% to 28.3% for H_2, from 35.7% to 38.5% for CO, from 23% to 28.8% for CO_2 and from 13% to 15% for CH_4 (mol/mol on dry basis). Under the above operation conditions, the discrepancies between the experimentally measured producer gas compositions and the predicted results using the 1D model were, respectively, 4.5% for H_2, 1.4% for CO, 7.5% for CO_2 and 1.2% for CH_4 (mol/mol on dry basis). For the 2D model, the discrepancies were, respectively, 2.4% for H_2, 2.9% for CO, 4.9% for CO_2 and 0.8% for CH_4(mol/mol on dry basis). However under the operating conditions of 780°C and S/B ratio of 0.53, the predicted $CO_2$and H_2concentrations from the 2D model were, respectively, 8.6% (mol/mol on dry basis) higher and 4.8% (mol/mol on dry basis) lower than the measured value.

The experimentally measured producer gas compositions for the operating conditions of 710°C and S/B ratio of 0.33-0.84rangedfrom 24.4% to 32% for H_2, from 32.7% to 44.2% for CO, from 15% to 21.8% for CO_2 and from 13.6% to 16.4% for CH_4 (mol/mol on dry basis). The discrepancies between experimentally measured producer gas compositions and the model predicted results for the above operating conditions were 1.6% for H_2, 2.7% for CO, 1.8% for CO_2 and 0.6% for CH_4 (mol/mol on dry basis) for the 1D model while those for the 2D model were 4% for H_2, 1.6% for CO, 1% for CO_2 and 1.6% for CH_4 (mol/mol on dry basis).

From the model validation, it was found that the 1D model results and 2D model simulation results were closely in agreement and show small discrepancy with the experimental results. In addition, the 1D model uses less computing time than the 2D model; therefore, the 1D model has been used to investigate the effects of operating conditions (temperature and S/B ratio) on the producer gas composition. It was observed that the gas concentration of CO, CO_2 and CH_4in the producer gas decreased while the H_2 increased with increasing operating temperature in the examined range from 680-780^oC. Similarly the gas concentration of H_2 and CO_2 in the producer gas increased while CO and CH_4 decreased with increasing S/B ratio in the examined range from 0.33-0.84.

The 2D model can be used to predict gas distribution within the gasifier thus it can be used to gain better understanding of the gasification process and effect of gasifier configuration and operating conditions on the gasifier performance. Further studies are proposed for improvements on the 2D model.

Acknowledgement

It's my pleasure to thank the many people who made this thesis possible.

In the first place I would like to record my gratitude to Prof. Dr. Shusheng Pang for his supervision, advice, and guidance from the very early stage of this research as well as giving me extraordinary experiences throughout the work. Above all and the most needed, he provided me unflinching encouragement and support in various ways. His truly scientist intuition has made him as a constant oasis of ideas and passions in science, which exceptionally inspired and enriched my growth as a student, a researcher and a scientist want to be. I am indebted to him more than he knows.

It's my pleasure to thank my co-supervisor Dr.Chris Williamson and the entire academic staff of the Department of Chemical and Process Engineering (CAPE), University of Canterbury for their valuable time and support extended by them for my research work. Mr. Ian Gilmour who is a part of the Gasifier project team deserves a special mention for being a great support helping me out and giving me advice whenever needed.

I am very thankful for the financial support from the New Zealand Foundation for Research, Science and Technology (FRST) is also appreciated.

I would like to thank Associate Professor Zhifa Sun of Department of Physics, University of Otago, New Zealand and Dr. Reinhard Rauch of Institute of Chemical Engineering, Vienna University of Technology, Austria, for their valuable comments and corrections in preparing the thesis.

I would like to thank all my lab buddies for making the biomass gasification lab a convivial place to work and would like to mention Dr. Woei-Lean Saw and Mr. Chris Penniall for providing me a great support in running the gasifier plant. I am also thankful to the lab technicians, office staffs, and post-grad colleagues for their immense support in various forms during my research work.

Where would I be without my family? My parents deserve special mention for their inseparable support and prayers. Words fail me to express my appreciation to my wife Priya whose dedication, love and persistent confidence in me, has taken the load off my shoulder. I owe her for being unselfishly let her intelligence, passions, and ambitions collide with mine. I warmly appreciate the generosity and understanding of my extended family.

Table of Contents

List of Figures

List of Tables

Nomenclature

The following listed symbols were used in this thesis. Others defined in the appropriate locations in this thesis for one-off use were not included:

a_{ik} Number of atoms, representing k^{th} element present per molecule of chemical species *(i)*

Ar Archimedes number (-)

$b_{0,i}$ Parameters to find gas species *(i)* due to pyrolysis

C_{cs} Weight fraction of char with respect to the inert bed material (kg_{char}/kg_{sand})

C_D Drag co-efficient $(-)$

C_i Molar concentration of species *(i)*$(kmol/m^3)$

C_{ib} Concentration of the species *(i)* in the bubble phase$(kmol/m^3)$

C_{ie} Concentration of the species *(i)*in the emulsion phase$(kmol/m^3)$

$Cp_{b,g}$ Average specific heats of gas species *(i)*, in bubble phase $\left(kJ/(kmol.K)\right)$

$Cp_{b,i}$ Specific heat of species *(i)* in the bubble phase at specific bubble phase temperature$\left(kJ/(kmol.K)\right)$

$Cp_{e,i}$ Specific heat of species *(i)* in the emulsion phase at specific emulsion phase temperature$\left(kJ/(kmol.K)\right)$

$Cp_{e,g}$ Average specific heats of gas species *(i)*, in emulsion phase $\left(kJ/(kmol.K)\right)$

Cp_{sand} Specific heat of inert bed material, sand $\left(kJ/(kg.K)\right)$

d_b Average bubble diameter (m)

d_{b0} Minimum bubble diameter (m)

d_{bm} Maximum bubble diameter (m)

d_p Particle diameter (m)

$D_{b\,ik}$ Binary gas phase diffusion coefficients of species *(i)* with respect to each component of the species *(k)* in the bubble phase (m^2/s).

$D_{e_{ik}}$	Binary gas phase diffusion coefficients of species *(i)* with respect to each component of the species *(k)* in the emulsion phase (m^2/s).
D_{ib}	Effective diffusion coefficient of species *(i)* with respect to total gas mixture in the bubble phase which depicts the plug flow (m^2/s).
D_{ie}	Effective diffusion coefficient of species *(i)* with respect to total gas mixture in the emulsion phase which depicts the mixed flow (m^2/s)
e_{ss}	Restitution co efficient of particle $(-)$
E_{Aj}	Activation energy of reaction $j(kJ/kmol)$
g_0	Radial distribution function $(-)$
ΔG_i°	Standard Gibbs energy changes for formation of species *(i)* $(kJ/kmol)$
H_{be}	Inter-phase volumetric heat transfer coefficient between bubble phase and emulsion phase $\left(kW/(m^3.K)\right)$
H_{bc}	Bubble side volumetric heat transfer coefficient $\left(kW/(m^3.K)\right)$
H_{ce}	Emulsion side volumetric heat transfer coefficient $\left(kW/(m^3.K)\right)$
H_c	Mass specific enthalpy of char (kJ/kg)
$\bar{h}^0_{f_{biomass}}$	Enthalpy of formation of biomass fuel (MJ/kg)
h_{fg}	Enthalpy of vaporisation of water (MJ/kg).
$\bar{h}^0_{f_i}$	Enthalpy of formation of product species(i) under complete combustion of the solid fuel $(kJ/kmol)$
$\bar{h}^0_{f_i,298}$	Enthalpy of formation of species *(i)* at 25°C $(kJ/kmol)$
ΔH_i°	Heat of formation of species *(i)* $(kJ/kmol)$
H_{ib}	Species *(i)* specific enthalpy in the bubble phase $(kJ/kmol)$
H_{ie}	Species *(i)* specific enthalpy in the emulsion phase $(kJ/kmol)$
ΔH_r	Enthalpy change of a reaction (kJ/kg)or $(kJ/kmol)$
$H_{reactant}$	Enthalpy of each reactant at specific temperature $(kJ/kmol)$
H_{prod}	Enthalpy of each product at specific temperature $(kJ/kmol)$

HHV_{fuel}	High heating value of the solid fuel (MJ/kg)
k_{0j}	Pre-exponential factor for reactions j $(1/s)$
K_{be}	Inter phase mass transfer coefficient between bubble phase and emulsion phase $(1/s)$
K_{bc}	Bubble side mass transfer coefficient $(1/s)$
K_{ce}	Emulsion side mass transfer coefficient $(1/s)$
K_{eqj}	Equilibrium constants for reactions j $(-)$
k_j	Arrhenius rate constants for reactions j $(1/s)$
LHV_{fuel}	Lower heating value of the solid fuel (MJ/kg)
$m_{0,i}$	Parameters to find gas species *(i)* due to pyrolysis
M_{char}	Mass of char (kg_{char})
m_H	Mass fraction of hydrogen in the solid fuel $(kg_{H2}/kg_{biomass})$
M_{sand}	Total weight of the inert bed material, sand, (kg_{sand})
M_{tar}	Mass of tar (kg_{tar})
$M_{volatiles}$	Mass of gas $(kg_{volatiles})$
M_{wood}	Mass of woody biomass (kg_{wood})
M_{w_c}	Molecular weight of char $(kg/kmol)$
Mw_g	Average molecular weight of gas species $(kg/kmol)$
Mw_i	Molecular weight of species i $(kg/kmol)$
Mw_{sand}	Molecular weight of sand $(kg/kmol)$
n_d	Number of holes in the distributor
N_i	Moles of the gas species *(i)*, such as CO, CO_2, CH_4, H_2 and H_2O $(kmol)$
Nu_s	Nusselt number for granular flow $(-)$
r_{jb}	Reaction rate of the j^{th} chemical reaction in the bubble phase $(kmol/(m^3.s))$
r_{je}	Reaction rate of the j^{th} chemical reaction in the emulsion phase $(kmol/(m^3.s))$
P	Operating Pressure (kPa)

P_0	Standard pressure(kPa)
P_g,P_s	Gas pressure and solids pressure (kPa)
Pr	Prandtl number $(-)$
ΔP_{mf}	Pressure gradient at minimum fluidization condition (kPa)
Q_{loss}	Heat loss in the gasification process (kJ)
$\vec{q}_s$,$\vec{q}_g$	Heat flux for solid phases and gas phases (kW/m^2)
R	Gas constant $\left(kJ/(kmol.K)\right)$
R_{cs}	Rate of generation (or consumption) of solid char in the emulsion phase (kg/s)
R_{ib}	Rates of generation of i^{th} species in the bubble phase $(kmol/(m^3.s))$
R_{ie}	Rates of generation of i^{th} species in the emulsion phases $(kmol/(m^3.s))$
Re_s	Relative Reynolds number between gas and solids phase $(-)$
S	Cross sectional area of the BFB (m^2)
S_b	Cross-sectional area of the bubble phase region in the BFB (m^2)
S_e	Cross-sectional area of emulsion phase region in the BFB (m^2)
T	Operating temperature (K)
T_b	Bubble phase temperature (K)
T_e	Emulsion phase temperature (K)
$\nabla\vec{T}_g$, $\nabla\vec{T}_s$	Tensor forces of gas phase and solid phase (N/m^2)
u_{br}	Rise velocity of single bubble relative to emulsion solids (m/s)
u_b, u_e	Bubble velocity and emulsion velocity (m/s)
u_0	Superficial gas velocity (m/s)
u_{mf}	Gas velocity at minimum fluidization condition(m/s)
u_t	Terminal velocity (m/s)
$\vec{v}_g$,$\vec{v}_s$	Velocity of gas phase and solid phase(m/s)
V_i	Diffusion volume for species i (m^3)
$v_{r,s}$	Terminal velocity correlation for the solid phase (m/s)

$V_{gas,e}$	Total gas volume of the emulsion phase in the entire bed (m^3)
W_{in}	Rate of char into the gasification process after the initial pyrolysis (kg/s)
W_{out}	Rate of char out of the gasification process (kg/s)
y_i	Mole fraction of gas species *(i)* $(kmol/kmol)$
y_{ib}	Mole fraction of gas species *(i)* in the bubble phase $(kmol/kmol)$
y_{ie}	Mole fraction of gas species *(i)* in the emulsion phase $(kmol/kmol)$

Greek Symbols

μ_g	Average viscosity of gas species $(kg/(m.s))$
ε_b	Volume fraction of the bubble phase $(-)$
ε_e	Volume fraction of the emulsion phase $(-)$
ε_g	Volume fraction of gas phase $(-)$
ε_{mf}	Volume fraction at minimum fluidization $(-)$
ε_s	Volume fraction of solid phase $(-)$
$\nu_{i,j}^p, \nu_{i,j}^r$	Stoichiometric coefficient of species *(i)* in reaction *(j), where p and r represents products and reactants* $(-)$
τ	Residence time of the sand (s)
α	Carryover factor of the specified material $(-)$
$\lambda_{g,i}$	Thermal conductivity of gas species *i* $(kW/(m.K))$
λ_s^*	Thermal conductivity of solids $(kW/(m.K))$
σ	Stefan Boltzmann constant =5.670 x 10^{-11} $(kW/(m^2.K^4))$
θ_s	Granular temperature (m^2/s^2)
γ_s	Collisional energy dissipation due to inelastic collisions of particles $(kW/(m^3))$
κ_s	Diffusion coefficient for granular conductivity $(kg/(m.s))$
ξ_s	Bulk solid viscosity $(kg/(m.s))$
μ_s	Shear solid viscosity $(kg/(m.s))$
λ_g	Thermal conductivity of gas mixture $(kW/(m.K))$

ρ_c, ρ_g, ρ_s	Density of char, gas phase and solid phase respectively (kg/m^3)
ρ_{sand}	Density of sand (kg/m^3)
β	Fluid particulate interphase drag coefficient $(kg/(m^3.s))$

Abbreviations

ANN	Artificial neural network
BC	Boundary condition
BFB	Bubbling fluidized bed
CAPE	Chemical and process engineering
CFB	Circulating fluidized bed
CFD	Computational fluid dynamics
CV	Control volume
DFB	Dual fluidized bed
DHM	Davidson-Harrison model
ER	Equivalence ratio
EEM	Eulerian-Eulerian model
FEM	Finite element method
FICFB	Fast internally circulating fluidized bed
FVM	Finite volume method
GC	Gas chromatography
GHG	Greenhouse gas emissions
HHV	High heating value
HNN	Hybrid neural network
IC	Initial condition
KLM	Kunii Levenspiel model
KTGF	Kinetic theory of granular flow
LEM	Lagrangian-Eulerian model
LHV	Low heating value
MFNN	Multilayer feed forward neural network
PDE	Partial differential equation
S/B	Steam to biomass
SFR	Steam feed rate

Chapter 1

Introduction

This chapter begins with the energy demand and consumption, globally and in New Zealand and the impact of greenhouse gas emissions in New Zealand. A brief preface on the biomass usage and biomass gasification is overviewed, outlining the research work carried out in the University of Canterbury and the author's contribution and the main objectives of the thesis. Finally summary of the chapters are outlined.

1.1 Introduction

The world's energy consumption has been steadily increasing for a variety of reasons mainly due to industrialization, rapid economic growth of the developing countries and their population, enhancements in their quality of life and increased transportation of people and goods. In today's world, the global energy challenge is to overcome the climate change and the global warming caused by extensive use of fossil fuels such as coal, oil and natural gas. These fossil fuels have been the prime source of energy supply for the majority of the developed countries energy requirement for over a decade. These fuel resources are not sustainable and cause Green House Gas emissions (GHGs) responsible for global warming *(Fawzy and Saad, 2002)*. Therefore it is important to utilise renewable energy resources that provide low SO_2 and CO_2 emissions, being a positive contribution to limit the greenhouse effect *(Zanzi et al., 1996)*. Many researchers in the world have been looking for alternative energy resources and fuels including wind, solar and hydro power, as well as biomass. Among these forms of renewable energy resources, the woody biomass is expected to be one of the predominant forms of renewable energy sources in the future due to its abundance and manageability. Currently 14% of the total world's energy consumption is from biomass *(Bain et al., 1998)*. However, there is even a greater potential to produce more energy and liquid fuels from biomass. The least-expensive biomass resources are the waste products from wood or agro-processing operations, but their supply is limited. To overcome this limitation, countries around the world are considering biomass crops for energy purposes and have begun developing technologies to use biomass more efficiently. The potential of biomass energy derived from forest and agricultural residues worldwide is estimated at about 30 EJ/yr,

compared to an annual world-wide energy demand of over 400 EJ. To contribute larger extent to the world's energy supply, the cultivation of dedicated biomass crops for energy purposes, will be required, using uncultivated land and marginal lands *(McKendry, 2002)*.In terms of size of resource, there is the potential to produce at least 50% of Europe's total energy requirement, from purposely grown biomass using uncultivated non-agricultural land and from forest and agricultural residues *(Bridgwater, 1995)*. New Zealand has abundant forest resources of 1.8 million hectares and large areas of underutilized non-agricultural land from which 20 million m^3 of log woods are harvested annually with high potential for biomass production. Between 2015 and 2025, wood availability is forecast to increase rapidly, lifting to 35 million m^3 / year *(McKendry, 2002)*. However, the major problems with biomass is that, as an energy crop, it is has high moisture content and labour-intensive to produce, harvest and transport, as it is dispersed over large areas. Hence an effective management system must ensure that the forests continuously provide a full range of products and amenities, in perpetuity, while retaining the forests' natural values. Thus the biomass as a sustainable energy source will play an important role in future energy supply and in reducing GHGs *(Bain et al., 1998; Higman and Van der Burgt, 2003; Overend et al., 1985)*.

The major challenge for the utilisation of biomass for energy is the conversion efficiency and the production costs using the existing biomass conversion technologies *(Purvis and Craig, 1998)*. Transportation of large quantities of biomass fuels from forestry sources to the site of use is one of the major obstacles to the development of larger biomass plants. Untreated woody biomass has a relatively low energy density and high moisture content compared to fossil fuels and is difficult to comminute into small particles. These properties make transport of wood relatively expensive and therefore higher levels of transport present barriers to large-scale plants. In contract, small-scale biomass electricity generation plants can be fuelled by local resources from small adjacent catchment areas. Even though when biomass fuels are dried they can regain moisture and may rot during storage. Furthermore, enhancement of the energy density is advisable because a large amount of wood is required to replace an equivalent amount of coal in applications such as combustion and gasification.

However biomass gasification is regarded as a promising conversion technology due to its high energy efficiency, lower impact on environment and flexibility for the producer gas to be utilized considering its availability. Hence in this thesis, a mathematical model is

developed to better understand and optimize one of the biomass conversion technologies, biomass gasification.

1.2 Global energy demand and consumption

Over the last two decades there has been a rapid increase in the global energy usage. According to International Energy Outlook 2010 the projected total worldwide energy consumption would increase by about 49% from 2007 to 2035 *(Doman et al., 2010)*. Figure 1.1 shows the past trend and projected changes of various types of world's energy consumption. It can be seen that the demands of all types of energy will continue increasing but the renewable energy is expected to grow more rapidly than the fossil fuels (liquid fuels, natural gas and coal). Though the liquid fuels contribute the larger share of energy consumption worldwide, their proportion in the overall energy consumption will fall from 35% to 30% over the projected period between 2007 and 2035. On the other hand due to declining availability of the fossil fuels, increase in the world oil prices and environment awareness, the renewable energy is projected to increase from 10% in 2007 to 14 % in 2035 with more renewable fuel being as an alternative fuel.

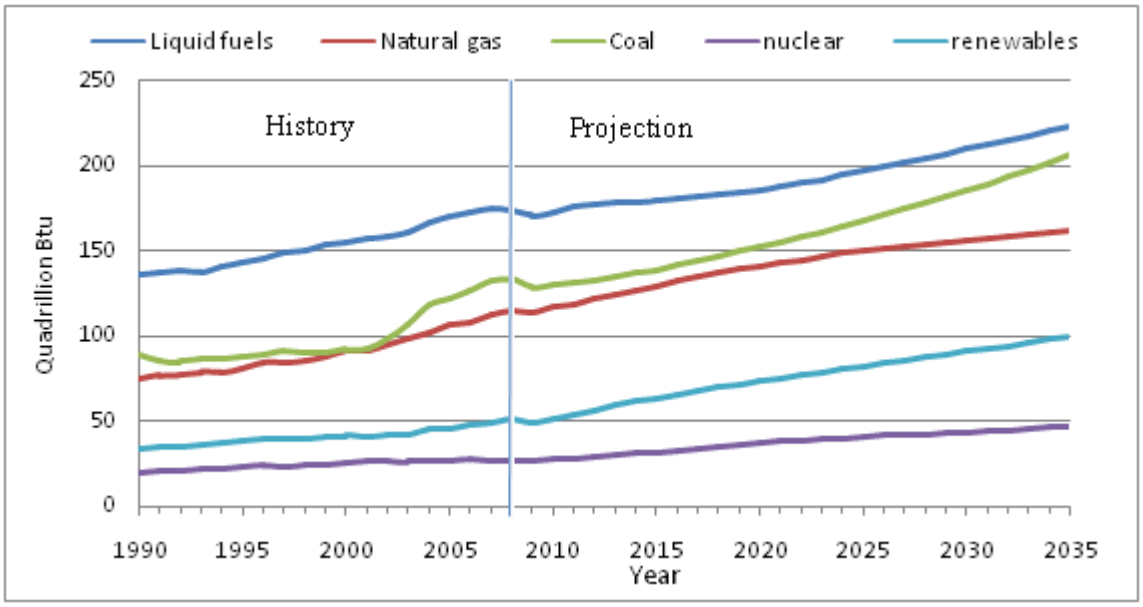

Figure 1.1: World energy consumption by fuel type, 1990-2035 *(Doman et al., 2010)*.

Figure 1.2 shows a comparison between 2007 and 2030 for application of various types of energy (coal, oil, gas, electricity, heat, biomass and other renewable fuel) in different sectors *(International Energy Agency, 2009)*. The increased use of biomass as renewable fuels in the

projected period is utilised mostly in the residential sectors and industrial sectors, however, the contribution in the transportation sector shows a promising future for biomass to meet the world energy demand. The biomass is often the choice of fuel for residential sector due to cheap and easily availability. Biomass currently provides the vast majority of renewable energy consumed in the industrial sector and continues to grow by an average of 1.8% per year throughout the projection period. In this period, the electricity in industrial sector is expected to increase by an average of 2.5% per year *(International Energy Agency, 2009)*. The world's total electricity generation from the renewable resources increases from 18% to 23 % between 2007 and 2035 by an average of 3% per year *(Doman et al., 2010)*.

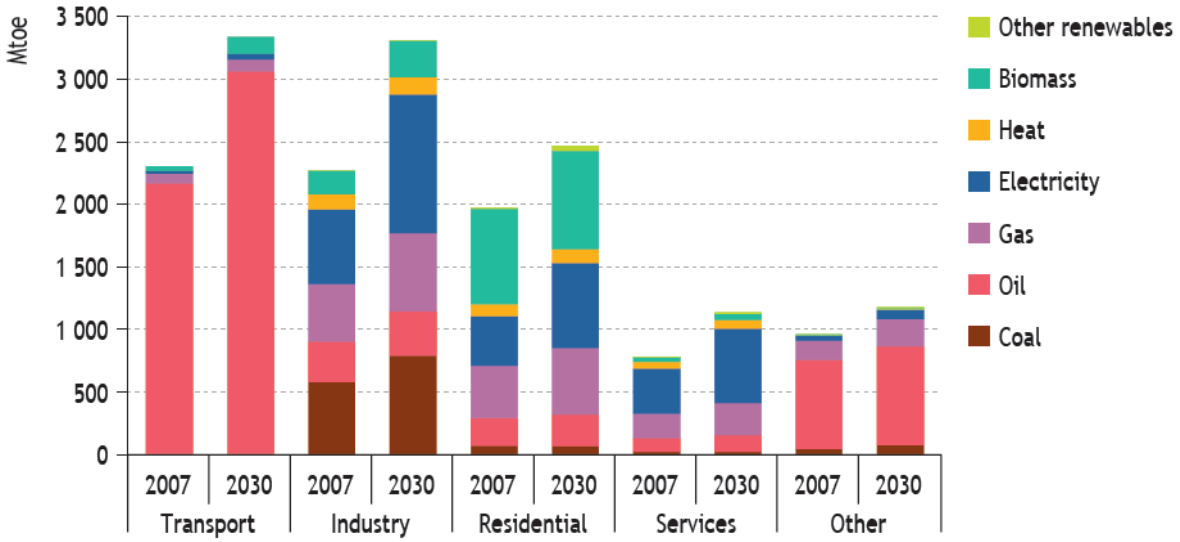

Figure 1.2: World energy consumption by energy type and sectors between 2007 and 2030 *(International Energy Agency, 2009)*

1.3 New Zealand's energy demand and consumption

The report published by the Ministry of Economic Development shows that over the past few decades, large proportion of New Zealand energy demand is from non-renewable energy sources, accounting for about 65-70% of energy supplies, of which crude oil is the major contributor followed by coal and natural gas *(Dang et al., 2010)*. The crude oil is imported mainly from Middle East countries such as Qatar, United Arab Emirates, and from Asian countries such as Brunei, Indonesia and Malaysia *(The Ministry of Foreign Affairs and Trade, 2011)*. According to the report from New Zealand's Ministry of Economic

Development, the demand for energy by coal is less compared to other fuel types of energy *(NZ Energy Outlook, 2010)*. New Zealand's total energy demand is projected to grow at 1.5% pa between 1990 and 2030 from 406PJ to 645PJ as seen in Figure 1.3. With the vast resources available, around 30-35% of New Zealand's primary energy supply would come from renewable resources which are expected to grow at a rate of 1.1% pa from 50PJ in 1990 to 100PJ in 2030 as shown in Figure 1.3.

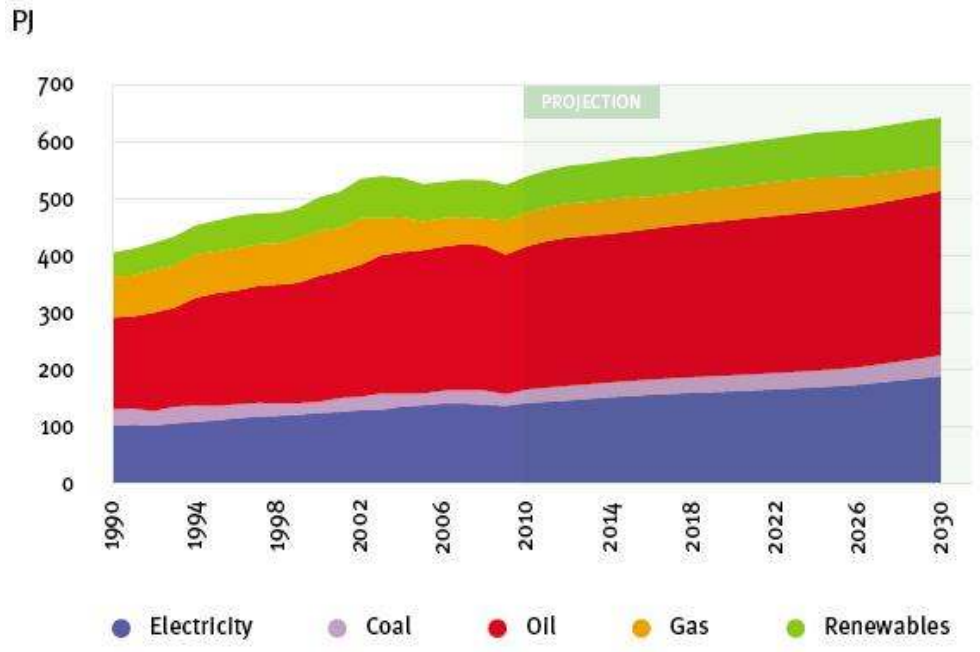

Figure 1.3: Total energy demand in New Zealand by different fuel types of energy in the recent past and projected period to 2030 *(NZ Energy Outlook, 2010)*.

Further detailed data has shown that the primary energy supply of renewable energy sources in New Zealand; mainly include hydro, geothermal resources and woody biomass. The woody biomass as the primary energy supply, increased from 15.2% in 1990 to 19% in 2007 as shown in Figure 1.4 *(Dang et al., 2008)*.

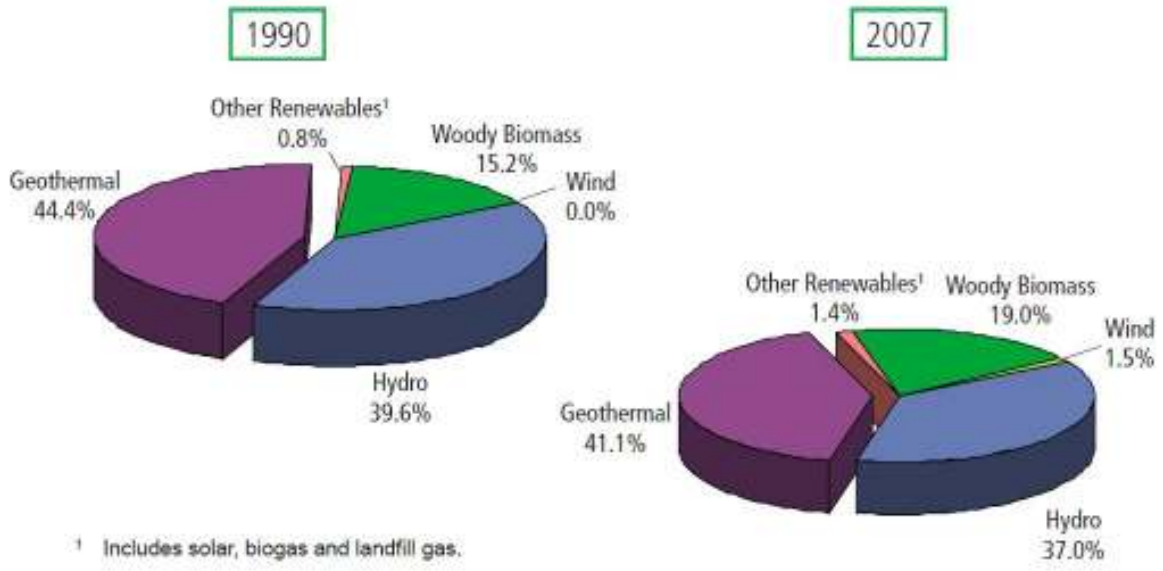

Figure 1.4: Distributions of various types of renewable energy in the primary energy supply in New Zealand *(Dang et al., 2008)*.

The report from Ministry of Economic Development also shows that in 2008, 65% electricity generation came from renewable resources and this increased to 73% in 2009 in which 21% was generated using woody biomass *(Dang et al., 2010)*. This report also projects that the demand for energy will increase steadily. Biomass will contribute more to the national energy demand in the future.

1.4 New Zealand's Green House Gas Emissions (GHGs)

One of the important drivers for using renewable energy resources is the concern for environmental impacts such as Green House Gas Emissions (GHGs) from the fossil fuels. The GHGs emissions are represented as carbon dioxide equivalent (CO_2–e) from the direct greenhouse gases – carbon dioxide (CO_2), methane (CH_4) and nitrous oxide (N_2O) – based on their global warming potential. New Zealand's GHGs emissions have been increasing at a rate of 2.6% pa from 1990 to 2008 as a result of enormous use of fuels in transportation and increased utilisation of coal and natural gas in electricity generation. Although New Zealand's contribution to the total world energy GHGs emissions is only approximately 0.12%, their emission per capita remains at relatively high with a value of 11.4 tonnes of CO_2–e emissions per annum. This sustained increase in GHGs emissions over the years has caused concerns and thus the government ratified the Kyoto protocol in 2002 along with

other nations *(Godber et al., 2010)*. Over the last two decades the major contributors of GHGs emissions come from crude oil followed by natural gas and coal, while on the other hand the biomass has near zero GHGs emission. It is encouraging to see that between 2008 to 2009 the GHGs emission in New Zealand had fallen down by 7% due to the measures to promote utilization of more renewable resources available nationwide.

1.5 Biomass combustion and gasification

Currently the biomass is mainly used for electricity and heat through combustion. There are various biomass combustion techniques being used around the globe to contribute 15% of the world's energy demand. The chemical composition of biomass varies among different species, but it generally contains of approximately 50% Carbon, 44% of Oxygen and 6% of Hydrogen *(Rapagnà et al., 2000; Rath et al., 2003)* in the forms of lignin (25%), and cellulose and hemicelluloses (75% in total) *(Antal,1983; Di Blasi et al., 2001)*. The biomass is non-homogeneous in its natural state having high volatile content of 71.5 wt % and low ratio of fixed carbon to volatile matter of 0.2 *(Franco et al., 2003)*. The heating value of the biomass is normally 18-19 MJ/kg oven dry which is much lower than that of coal at 27.2 MJ/kg with 5% moisture content *(Bull, 2008)*.

Although biomass gasification has shown advantages for commercial application, there are some technical issues which have to be resolved and thus further improvement and operation optimisation are needed. Improving the heating value of producer gas obtained from the biomass gasification is one of the improvements and the producer gas heating value depends on several factors such as type of gasifier used, types of biomass feed and gasification agent (air, oxygen or steam), and operation conditions. Detailed studies on different types of gasifier are discussed in Chapter 2. The research of *Hofbauer et al (1997)* showed that the partial combustion of biomass in the air blown gasification system produced low quality gas with a low heating value (LHV) of 4-7 MJ/Nm^3, while high quality gas heating value of 10 - 18 MJ/Nm^3 is produced using gasification with pure oxygen instead of air which is relatively cheap. On the other hand fast internal circulating fluidized bed (FICFB) gasification using steam as the gasification agent produced high quality product gas with a LHV of 10 - 14 MJ/Nm^3.

1.6 University of Canterbury-contributions and research on bio-energy

As mentioned above, in most gasification systems air or oxygen is used as the gasification agent for partial combustion to supply heat in the endothermic gasification process. Recently fluidized bed gasification with steam as the gasification agent has attracted great attention because of its apparent advantages that no nitrogen is present in the producer gas compared to air gasification and the cost is lower than the oxygen gasification technology. The fluidized bed gasification is in the development stage but the steam-blown fluidized bed gasification has shown promising results by the recent studies *(Hofbauer et al., 2003; Hofbauer et al., 2002a; Pfeifer et al., 2007)*.

The conventional method of biomass combined heat and power (CHP) based on steam turbine technology usually has a low power-to-heat ratio. With the advanced technology based on the biomass gasification and the gas turbine combined cycle technology (hereafter referred to as Biomass Integrated Gasification Combined Cycle, BIGCC), higher power-to-heat ratios can be achieved, thereby increasing the potential for electric power generation for a given heat demand. A pictorial representation of general BIGCC system is shown in Figure 1.5. The BIGCC technology is yet to be commercialized, but the technical performance (electric efficiency and power-to heat ratio) for BIGCC power generation is much higher than for conventional biomass steam turbine systems *(Marbe et al., 2004)*.

A review of various technologies are reported by *Li and Pang (2005)* and *Brown (2006)* who concluded that the FICFB is the most advanced and suitable technology for application in the Biomass Integrated Gasification Combined Cycle (BIGCC) system. The FICFB has been applied in a demonstration biomass gasification plant in Güssing, Austria, with a feed capacity of 8MW. The total system energy from the Güssing power plant produced an efficiency of 85% accounting for 2 MW electricity and 4.8MW heat. The producer gas is nearly free of nitrogen with high calorific value of 12-14 MJ/Nm^3 *(Hofbauer et al., 2002b)*.

The research team in the Department of Chemical and Process Engineering (CAPE), University of Canterbury, has been conducting a research programme, and one of the goals of this programme is to develop a self-generated power and heat system for the wood processing industry. The BIGCC is further developed and a laboratory scale FICFB gasifier is built in collaboration with a research team at the Vienna University of Technology in Austria. Recently the programme is extended to include liquid fuel synthesis using Fisher-Tropsch process. This PhD project is part of the programme with objective to develop a mathematical

model to simulate the biomass gasification process with steam as the gasification agent. The developed model will then be used to better understand the gasification process and to investigate the effects of the operation conditions including gasification temperature and biomass to steam ratio.

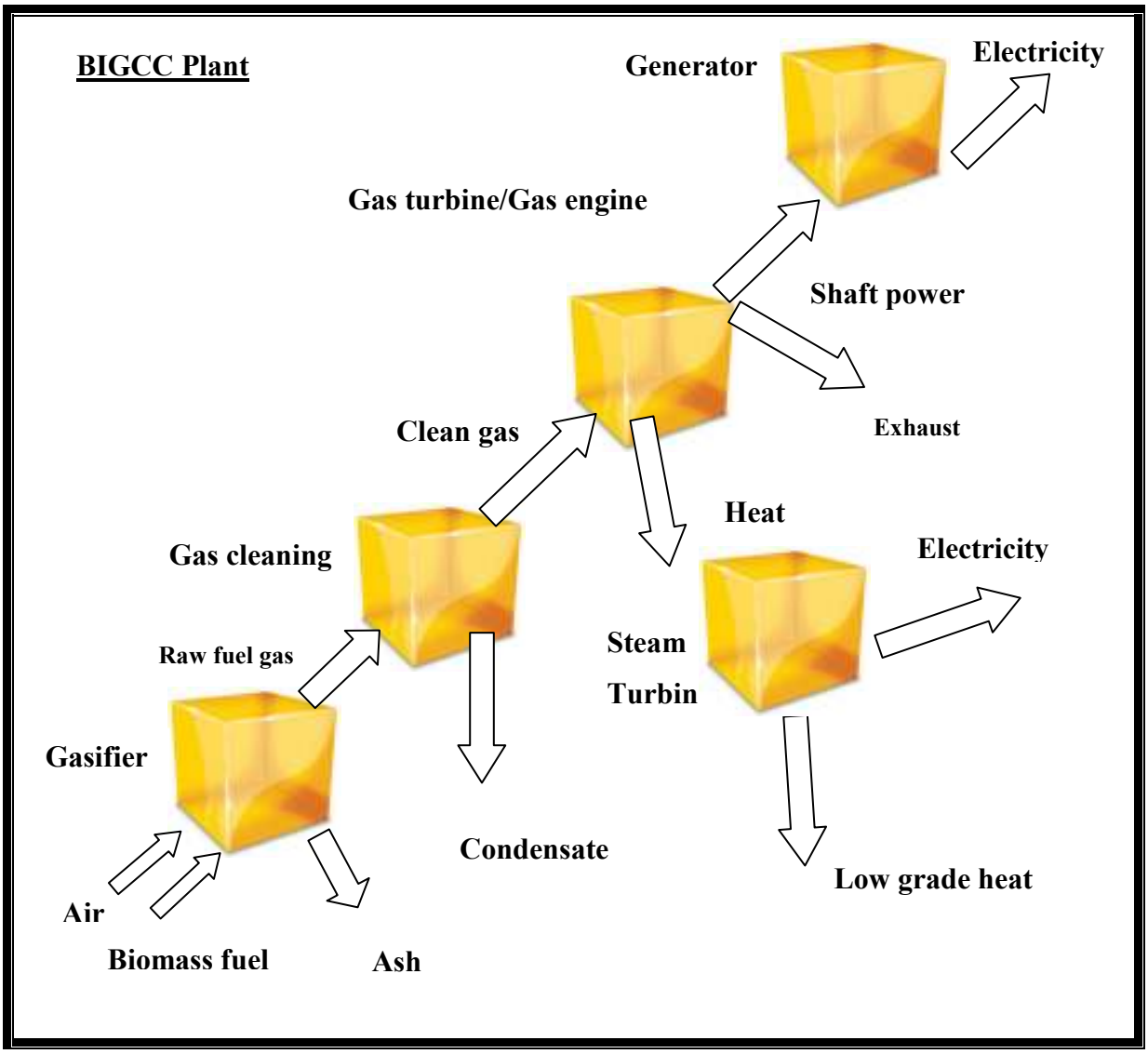

Figure 1.5: More efficient heat and power generation using Biomass Integrated Gasification Combined Cycle (BIGCC).

1.7 Authors contribution and focus in this thesis

In this thesis, the existing modelling of solid–fuel gasification in a fluidized bed was firstly reviewed with emphasis on biomass and waste materials as feedstock. Modelling of bubbling fluidized bed (BFB) was proposed and methods for calculation of the fluid dynamics and reaction processes were developed in details. From the literature review, it is found that most of the existing gasification models are developed based on simplified assumptions for the reaction process and the fluid dynamics due to uncertainty and complex processes of the fluidized bed gasification process. The biomass gasification models can be divided into two categories: namely the kinetic models and the equilibrium models. Considering the fact that the equilibrium models can only predict the end reaction product distribution and cannot describe the instantaneous product distribution within the reactor, this type of models cannot be used for reactor analysis and design. Therefore, the kinetic model was chosen in this work that can simulate the reaction condition at different time and position within the biomass gasifier which makes it suitable for reactor scale-up design and operation parameters optimization. In this work, non-isothermal one-dimensional (1D) mathematical model was firstly developed based on the dual phases (bubble phase and dense phase) in which reaction kinetics of the produced combustible gases were proposed. The model was able to simulate gas composition in biomass-steam gasification in the BFB gasifier. In this model the effects of some parameters such as steam/biomass ratio, and temperature were studied.

After developing the 1D model, the computational fluid dynamics (CFD) techniques were applied to the fluidized bed systems to gain a better understanding of the hydrodynamic behaviour involved, as the BFB gasifier involves flows of steam and bed materials within the gasifier. After gaining sound knowledge of hydrodynamics characteristics in the fluidized bed, the developed CFD model for the behaviour of a gas-solid fluidized bed systems were integrated with the earlier developed gasification reaction kinetics model into the two-dimensional (2D) CFD model called Gasification embedded 2D CFD model. The steam-biomass gasification product distributions along the reactor length and along the radial distribution from the developed 2D model were studied at different operating conditions. Finally the developed model was validated with several experiments that were undertaken on the 100kW dual fluidized bed (DFB) biomass gasifier at the University of Canterbury.

1.8 Outline of thesis

In this thesis Chapter 2 presents a literature review on the mathematical modelling of the biomass gasification and related topics. In this chapter the process of biomass gasification and characteristics of the biomass related to gasification were discussed. Following this, the details of biomass gasification processes such as initial pyrolysis, char gasification and gas phase volatile reactions were outlined. The influence of the operating gasification parameters such as S/B ratio and temperature were examined on the gas composition. This chapter also discusses the different types of reactor bed design available with different options of gasification agent. This chapter concludes with the fundamentals of fluidization, flow regimes, gas-particle interactions and particle-particle interactions in the fluidized bed. Based on the literature review as presented in Chapter 2, existing technology/system is evaluated, and areas and gaps for further development are identified in terms of development of the biomass gasification models.

In Chapter 3 the modelling of biomass gasification in BFB gasifier is described. This chapter begins with the analysis of the gasification process including the initial pyrolysis reactions and the subsequent gasification reactions in the fluidized bed gasifier. Following this, the reaction kinetics both in the pyrolysis and in the gasification process is quantified. Based on these analyses, a simple 1D model of the fluidized bed gasification is proposed. The governing equations for heat and mass transfer, and fluid flow are mathematically described for the BFB.

To understand and to quantify the flow of gases and solid particles in the BFB (gasification reactor), a hydrodynamic model is developed in Chapter 4 in which a gas-solid approach using CFD model is applied based on Eulerian-Eulerian model. From this hydrodynamic model developed, the hydrodynamic characteristics in the BFB, such as the profiles of solids concentration, particle velocity, solid flux and pressure gradient distributions, and the developments of these profiles are investigated.

Chapter 5 presents 2D model of the BFB gasifier which expands the 1D model as presented in Chapter 3 by including the variations in the radial direction in the gasification reactor.

Chapter 6 discusses the model validation and application for parameter sensitivity analysis. This chapter begins with the description and the experimental procedures of the FICFB gasifier built in the Department of Chemical and Process Engineering (CAPE) at the

University of Canterbury. After this, the simulation results from the mathematical models are compared with the measured results which were obtained from the experiments of this work. Finally the effects of operating parameters on the model such as temperature and steam/biomass ratio analyzed.

Finally in Chapter 7, a summary of conclusions are presented and recommendations for future work are given.

1.9 References

Antal, M.J., 1983. Effects of Reactor Severity on the Gas-Phase Pyrolysis of Cellulose and Kraft Lignin-Derived Volatile Matter. Industrial & Engineering Chemistry Product Research and Development 22, 366-375.

Bain, R.L., Overend, R.P., Craig, K.R., 1998. Biomass-Fired Power Generation. Fuel Processing Technology 54, 1-16.

Bridgwater, A.V., 1995. The technical and economic feasibility of biomass gasification for power generation. Fuel 74, 631-653.

Brown, J., 2006. Biomass Gasification: Fast Internal Circulating Fluidized Bed Gasifier Characterisation and Comparison, Chemical and Process Engineering. University of Canterbury, Christchurch.

Bull, D.R., 2008. Performance Improvements to a Fast Internally Circulating Fluidised Bed (FICFB) Biomass Gasifier for Combined Heat and Power Plants University of Canterbury, New Zealand

Dang, H., Field, B., Gadber, D., Hunt, P., Lawrence, S., Thornton, S., Tsui, K., 2010. New Zealand energy data file 2010. Ministry of Economic Development.

Dang, H., Lawrence, S., Pittams, M., Tamayo, J., D, S.T., Wilkinson, D., 2008. New Zealand Energy in Brief August 2008.

Di Blasi, C., Branca, C., Santoro, A., Gonzalez Hernandez, E., 2001. Pyrolytic behavior and products of some wood varieties. Combustion and Flame 124, 165-177.

Doman, L.E., Smith, K.A., Mayne, L.D., Yucel, E.M., Barden, J.L., Fawzi, A.M., Martin, P.D., Zaretskaya, V.V., Mellish, M.L., Kearney, D.R., Murphy, B.T., Vincent, K.R., Doman, L.E., Lindstrom, P.M., Leff, M.T., Geagla, A., Holte, J., Kapilow-Cohen, B., LaRiviere, M., Smith, C.L., Staub, J., Sweetnam, G., Wells, P., 2010. International Energy Outlook 2010, in: DOE/EIA-0484(2010) (Ed.). U.S. Energy Information Administration.

Fawzy, E.-M., Saad, E.-D.H., 2002. Fundamentals and Technology of Combustion. Elsevier Science Ltd.

Franco, C., Pinto, F., Gulyurtlu, I., Cabrita, I., 2003. The study of reactions influencing the biomass steam gasification process. Fuel 82, 835-842.

Godber, D., Lawrence, S., Tsui, K., 2010. New Zealand Energy Greenhouse Gas Emissions. Energy Information and Modelling Group of the Ministry of Economic Development New Zealand.

Higman, C., Van der Burgt, M., 2003. Gasification. Elsevier.

Hofbauer, H., Rauch, R., Bosch, K., Koch, R., Aichernig, C., 2003. Biomass CHP plant Guessing – a success story, In Pyrolysis and Gasification of Biomass and Waste; Bridgwater, A. V. CPL Press: Newbury, U.K, pp. page 371-383.

Hofbauer, H., Rauch, R., Loeffler, G., Kaiser, S., Fercher, E., Tremmel, H., 2002a. Six years experience with the FICFB Gasification process, In Twelfth European Biomass Conference, Florence, Italy, pp. pp 982-985.

Hofbauer, H., Reinhard, R., Klaus, B., Reinhard, K., Christian, A., 2002b. Biomass CHP Plant Güssing – A Success Story, Expert Meeting on Pyrolysis and Gasification of Biomass and Waste. Renet-Austria, Vienna, Stasbourg, France.

Hofbauer, H., Veronik, G., Fleck, T., Rauch, R., MacKinger, H., Fercher, E., 1997. The FICFB - gasification process. Developments in Thermochemical Biomass conversion 2, 1016-1025.

International Energy Agency, 2009. World Energy Outlook, (Online) Retrived on 28th September 2011, Available:http://www.iea.org/textbase/nppdf/free/2009/weo2009.pdf.

Li, J., Pang, S., 2005. Evaluation of BIGCC Technologies Developed Overseas., Confidential Internal Report. Canterbury University., Christchurch.

Marbe, Å., Harvey, S., Berntsson, T., 2004. Biofuel gasification combined heat and power--new implementation opportunities resulting from combined supply of process steam and district heating. Energy 29, 1117-1137.

McKendry, P., 2002. Energy production from biomass (part 1): overview of biomass. Bioresource Technology 83, 37-46.

NZEnergyOutlook, 2010. New Zealand's Energy Outlook 2010., (Online) Retrived on 28thSeptember 2011, Available:http://www.med.govt.nz/energyoutlook

Overend, R.P., T.A.Milne, L.K.Mudge, 1985. Fundamentals of Thermochemical Biomass Conversion. Elsevier Applied Science Publishers.

Pfeifer, C., Puchner, B., Hofbauer, H., 2007. In-Situ CO2-Absorption in a Dual Fluidized Bed Biomass Steam Gasifier to Produce a Hydrogen Rich Syngas. International Journal of Chemical Reactor Engineering 5, 15.

Purvis, C.R., Craig, J.D., 1998. A Small Scale Biomass Fueled Gas Turbine Power Plant, BioEnergy, Madison, WI USA.

Rapagnà, S., Jand, N., Kiennemann, A., Foscolo, P.U., 2000. Steam gasification of biomass in a fluidised bed of olivine particles. Biomass and Bioenergy 19, 187-197.

Rath, J., Wolfinger, M.G., Steiner, G., Krammer, G., Barontini, F., Cozzani, V., 2003. Heat of wood pyrolysis. Fuel 82, 81-91.

The Ministry of Foreign Affairs and Trade, 2011. Information Paper: NZ Ministry of Foreign Affairs and Trade. (Online) Retrieved on 27th September 2011, Available:http://www.mfat.govt.nz/Countries/Middle-East/United-Arab-Emirates.php

Zanzi, R., Sjoestroem, K., Bjoernbom, E., 1996. Rapid High-Temperature Pyrolysis of Biomass in a Free-Fall Reactor. Fuel 75, 6.

Chapter 2

Literature review

This chapter covers the overview of biomass, its properties in relation to gasification, pyrolysis and other biomass conversion pathways. A comprehensive biomass conversion process is outlined. The description and discussion on biomass pyrolysis, char gasification and gas phase volatile reactions involved in the biomass gasification process is summarized. A brief discussion is provided for different types of reactor design for biomass gasification, with significance given to the fluidized beds on fundamentals of fluidization and flow regime. Finally different types of modelling methods that has been used for biomass gasification such as equilibrium modelling approach, kinetic reaction modelling approach and CFD model with reactions are discussed and summarized.

2.1 Biomass as renewable source of energy

The biomass can be utilized as an energy resource by thermal or biological conversion routes into a range of useful energy products such as heat, electricity, hydrogen, liquid fuels and synthesis gas. The latter three can also be further used for production of heat and/or electricity. The biomass is broadly defined as any material of recent biological origin and includes plant materials such as stems of trees and agricultural crops as well as animal manures and sewage bio-solids.

2.2 Properties of biomass relevant to gasification and pyrolysis

Due to the complex characteristics and variability of the bio-origin biomass, better understanding of structure and properties of the biomass material is necessary in order to evaluate their utility as feed stocks. This section provides a summary on the biomass properties which are related to biomass gasification performance and gasification products with focus on *Pinus radiata***,** the most abundant form of woody biomass available in New Zealand.

The characteristics of general pine wood biomass such as wood pellets, wood chips and wood sawdust from forestry, bark, and wood waste were investigated and compared as fuel feedstock for the DFB gasifier. The wood pellets are standardised fuel with defined particle size (6 mm in diameter and 10-20 mm in length) and shape while the sawdust processed had particle size ranging from 200μm to 900 μm *(Garcı´a. L. et al., 1999; Lv et al., 2004b)*, however the wood chips used varied in size and shape largely. The elemental analysis (in % mass) and the proximate analysis (in % mass) of the pine sawdust, pine wood pellets and pine wood chips were listed in Table 2.1 and Table 2.2 respectively. The molecular formula of woody biomass was defined as CH_aO_b where, a and b are the H/C and O/C mole ratio, respectively and were determined based on the chemical analysis of the feedstock and were on a dry, ash-free basis from the Table2.2.

The size and shape of the woody biomass are important factors for determining flow characteristics of the fuel as well as their behaviour inside the gasifier. Gasifiers frequently endure from bridging and channeling of the fuel. The size and shape of the biomass have influence on the product distribution. A uniform particle sized fuel such as biomass wood pellets and sawdust reduces these problems to some extent. This smooth uniform shape biomass wood pellet provides good mechanical flow characteristics, however the usage of wood chips results in the bridging problem. Improving the grate design and added agitation or stirring can provide trouble free gasification operation, however excessive agitation results in excessive carbon carryover which in turn reduces gasification efficiency.

Small particle sizes such as pine sawdust and pine pellets produce a greater gas yield and a lesser char yield than the wood chip particles. The gas yield and composition are related to the heating rate of the biomass particles: high heating rates produce more light gases and less char and condensate. Since smaller particles have larger surface area and therefore faster heating rate, it can be expected that the size of biomass particle will have influence on product gas composition and yield. The smaller particles produced more CH_4, CO and C_2H_4 and less CO_2 than the larger ones. Hence the gas yields, gas LHV, and carbon conversion efficiency were all improved when biomass particle size decreased *(Lv et al., 2004b)*.

Gasification of different biomasses was studied by *Prasad and Kuester (1988)* using a DFB gasification system. The HHV and heat of formation of pine sawdust are 19.95MJ/kg and 2.36 MJ/kg respectively (Prasad and Kuester, 1988). *Lv et al. (2004b)* investigated four different size pine sawdust ranges (0.6–0.9, 0.45–0.6, 0.3–0.45, and 0.2–0.3 mm,

respectively) and found that the gas yield varied from 1.53 to 2.57 Nm^3/kg biomass; gas LHV ranged between 6976 and 8737 kJ/Nm^3; carbon conversion efficiency varied from 77.62% to 95.10%. The thermal effectiveness or energy recovery defined as the percentage of the energy content in the sawdust fed that appears in the exit gas (tars free) increases from 35% to 75% on increasing the temperature from 660 to 810°C *(Corella et al., 1991)*. Steam biomass gasification process demonstrated in Güssing power plant has a fuel capacity of 8 MW and an electrical output of about 2 MWel with an electrical efficiency of about 25 % and total efficiency of 80%. Wood chips with a water content of 20 - 30 % were used as fuel and the calorific value of the dry producer gas is about 12 MJ/Nm^3 *(Hofbauer et al., 2002)*. It was found in Güssing gasifier, that higher gasification temperatures lowered the heating value of the producer gas which caused the electrical efficiency of the whole CHP plant to decrease. In 100kW DFB gasifier established in University of Canterbury, the cold gas efficiency increased from 16-30 % as gasification temperature increased from 642- 758 °C. The LHV of the producer gas increased from 12.6-13.4 MJ/Nm^3 as gasification temperature increased. This is because the higher producer gas yields increased the total combustion energy output (in kW) of the gasifier for the same wood input rate *(Bull, 2008)*.

In any biomass gasification system, the moisture content of the biomass feed is important. The moisture content of the biomass feedstock has a noticeable effect on the efficiency of the conversion process and is directly proportional to the gas yield and composition. More energy must be supplied to the gasifier to evaporate increased moisture in the feedstock thereby increasing carbon dioxide content of the produced gas increase with fuel moisture. In addition, carbon monoxide decreases changing the heating value and substantial amount of the heating value of the biomass fuel is considerably lost *(Ebeling and Jenkins, 1985)*. *Black et al (1980)* achieved reliable operation using fuels with moisture contents of 30-50%. However, the recommended moisture value for biomass should be below 25% to optimize the efficiency of the gasifying process but not necessarily very low, because moisture is required in the reaction and part of the water is broken down, yielding hydrogen *(Melgar et al., 2007)*. The moisture content also directly affects the handling, storage and transportation of biomass fuels. Decomposition and the resulting energy loss and increase in ash content of high moisture fuels during storage will be a problem. Transportation of high moisture fuels is generally undesirable because of the high costs involved *(Ebeling and Jenkins, 1985).*

2.2.1 Proximate analysis

The proximate analysis provides data to characterize the fuels in terms of volatile matters, ash content and fixed carbon content on dry basis which are measured when the fuel to be analyzed is heated to 950°C. The ash (mineral) in the sample and the high heating value (HHV) are measured based on the complete combustion of the fuel sample to carbon dioxide and liquid water. The volatility of biomass is affected by the heating rate, with higher heating rate yielding more volatile matters. The moisture content in the proximate analysis represents the physically bound water molecules in the biomass which are removed simply by heating of the materials without chemical reactions occurring. The gas components released during heating of the material to high temperatures with chemical reactions occurring such as in pyrolysis and gasification of the biomass is classified as volatiles. Typical proximate analysis results for solid fuels are given in Table 2.1, from which it is evident that the biomass materials are more volatile and are easily pyrolysed than lignite and bituminous coals. In addition, the biomass contains considerably less fixed carbon and infinitesimal small amount of ash compared to coals. The higher volatile content of biomass makes it a potentially useful energy resource.

Table 2.1: Proximate analysis results for selected solid fuels of biomass and coals on dry basis

Proximate analysis (wt%)	Volatile Matter	Fixed Carbon	Ash	*References*
Pine sawdust	80.4-86.3%	13-14.8%	0.5-2.3%	*(Prasad and Kuester, 1988)*
Pine wood pellets	84.1	15.4	0.43	*(Bull, 2008)*
Pine wood chips	84.0	15.6	0.42	*(Bull, 2008)*
Eucalyptus (hardwood)	83.6	15.5	0.78	*(Franco et al., 2003)*
Holm Oak (hardwood)	77.6	19.7	2.70	*(Franco et al., 2003)*
Lignite	37.0	58.1	4.90	*(Yan et al., 1998)*
Coal C	22.0	62.2	15.80	*(Yan et al., 1998)*

2.2.2 Ultimate analysis

The ultimate analysis represents elemental composition of solid fuels in weight percentage of carbon, hydrogen, and oxygen as major components and sulphur and nitrogen as minor components. Normally the ultimate analysis is done on dry basis to eliminate the effect of moisture content. The typical ultimate analyses for a variety of solid fuel feed stocks are represented in Table 2.2. Based on the data presented in Table 2.2 and the molar weights, the H/C molar ratio for coal is nearly unity and that for biomass is about 1.5 due to the fact that coals normally contain much higher carbon than biomass. It is important to note that the oxygen content in biomass is considerably higher than that in the coal due to the acid and alcoholic groups in the cellulose, hemicellulose and lignin of the biomass which will be discussed later in this section. The ash content is high in coal compared with the biomass. With the ultimate analysis of the solid fuels, relative quality based on volatile matters can be assessed *(Reed, 1981)*.

Table 2.2: Ultimate analysis data for selected solid fuels and biomass materials based on dry ash free basis

Ultimate analysis (wt% daf*)	C	H	O	N	S	
Pine wood chips (softwood)	51.6	4.9	42.6	0.9	n.d^{+}	*(Franco et al., 2003)*
Pine sawdust	47.36	5.84	46.76	0	0.04	*(Prasad and Kuester, 1988)*
Pine wood pellets	51.3	5.81	42.4	<0.2	0.01	*(Bull, 2008)*
Eucalyptus (hardwood)	52.8	6.4	40.4	0.4	n.d	*(Franco et al., 2003)*
Holm Oak (hardwood)	51.1	5.3	42.7	0.9	n.d	*(Franco et al., 2003)*
Lignite	68.03	5.15	25.24	0.53	1.05	*(Yan et al., 1998)*
Coal C	80.04	4.16	14.73	0.94	0.12	*(Yan et al., 1998)*

+: not detected; *: dry ash free basis

2.2.3 Heating value

In addition to the proximate and the ultimate analyses, the solid fuels can also be characterized by the energy contained within the fuels in terms of higher heating value (HHV) as gross calorific value and lower heating value (LHV) as net calorific value. The

HHV refers to the amount of heat released from the combustion of the solid fuel including the latent heat of vaporization of water from the sample while LHV does not include the contribution of the latent heat of vaporization. Though HHV can be measured using bomb calorimetric methods, it is a tedious process and hence a correlation has been developed using the composition of the solid fuels. Two major factors affecting the heating value of biomass materials are ash content and moisture content. High contents of these two components lower the heating value of the biomass materials. The most reliable correlation, with more than 90% predictions in the range of ±5% error, is illustrated by *Sheng and Azevedo (2005)* to determine HHV based on ultimate analysis with their elemental composition.

$$HHV_{biomass} = -1.3675 + 0.3137C + 0.7009H + 0.0318\,O^{*}\ \ (MJ/kg) \qquad (2.1)$$

In which, C, H and O* are based on the elemental composition of biomass (in wt %). O* is the sum of the contents of oxygen and other elements such as sulphur, nitrogen in the organic matter.

The measured heating value for hardwood ash free biomass is 19.6 MJ/kg while that of softwood is 19.4 MJ/kg from their elemental composition taken from the Table 2.2. In contrast, fossil fuels have high heating values, for example, bituminous coal C with 5% moisture content has $HHV_{bituminous\ coal\ C}$ of 27.2 MJ/kg.

2.2.4 Energy density of biomass

Although the biomass can be used as a potential energy resource, chemical composition of woody biomass varies significantly from those of fossil fuels like coal or oil, since wood mainly consists of oxygen-containing organic polymers. Biomass from green trees has higher moisture content up to 150% (dry-basis) and low density which would induce high costs for transportation and storage thus pre-drying is necessary to improve process efficiency and reduce transportation costs. Hence the biomass has low energy density defined as the heating value per unit volume of origin material compared to that of most fossil fuels *(Bridgeman et al., 2008).*

2.3 Biomass microstructures and chemical composition

In characterizing and correlating reactivity data for biomass pyrolysis and gasification, it is necessary to know the microstructure and chemical structure of the biomass. Wood, as the target biomass in this thesis, can be basically separated into three fractions such as extractable, cell-wall components and ash. The cell-wall components represent the bulk of the wood and they are the dominant chemical species which can be categorized as lignin, cellulose and hemicelluloses with the latter two being termed together as holocellulose *(Rowell, 2005)*. Several minor components, including a complex mixture of low molecular weight sugars, inositols, amino acids, simple fats, carboxylic acids, terpenes, and phenolic compounds are included in the extractable organic fraction of the biomass *(Di Blasi et al., 2001)*.

Depending on the wood species, the chemical composition varies. For softwoods such as Douglas fir, redwood and pine, the lignin composition is higher compared to hardwood (beech) i.e., 24–33% (softwood) against 16–24% (hardwood), and the cellulose is in the range of about 42 ± 2% for both species of the wood while hemicelluloses are present in complementary proportion *(Di Blasi et al., 2001; Rowell, 2005)*. Cellulose with a chemical formula $(C_6H_{10}O_5)_n$ is typically comprised of less than 10,000 anhydroglucose units, containing 49 wt% oxygen and is insoluble in water *(Klass, 1998)*. It is a glucose-based polysaccharide with covalent bond, hydrogen bond and van der Waal forces within the polymer consisting of highly ordered crystalline regions as well as of disordered or amorphous regions with lower packing density.

Hemicelluloses with a chemical formula $(C_5H_8O_4)_n$, the second major wood components which are part of the cell walls, are chemically similar to cellulose except that they are not polymers in that they have no consistently recurring monomer unit and they are much shorter, with a degree of polymerization (DP) between 100~200 *(Klass, 1998; Serdar, 2004)*. Hemicelluloses include several carbohydrate monomers (heteropolysacharides), mainly heterogeneously linked by six-carbon and five-carbon anhydro-sugars, with the five-carbon sugar containing about 54 wt% oxygen by mass *(Hon and Shiraishi., 2001; Rowell, 2005)*.

Lignin as the third major component of wood is an aromatic, phenolic, amorphous cross-linked resin with no exact structure. The thermal decomposition of wood lignin begins at 280°C and the decomposition is accelerated with temperature up to 450°C. with a maximum decomposition rate at 350°C to 450°C. Phenols are formed during lignin pyrolysis due to

cleavage of the ether and carbon-to-carbon linkages. In comparison to cellulose and hemicellulose, lignin is more difficult to dehydrate. Furthermore, the pyrolysis of lignin produces more residual char than the pyrolysis of cellulose. The gaseous products represent 10wt% of the original lignin contains methane, ethane, and carbon monoxide *(Mohan et al., 2006)*.

2.4 Overview of pathways for biomass conversion to energy products

Biomass can be converted into useful form of energy products via two major conversion routes: biochemical/biological and thermo-chemical conversions. Biological conversion processes, which include anaerobic digestion and alcoholic fermentation, involve the anaerobic decomposition of biomass to yield methane from bacterial fermentation or ethanol from yeast fermentation. This technology preserves the nutrient components of the feedstock in a form that can be used as animal feed or fertilizer. Thermo-chemical processes that produce useful energy from biomass are direct combustion, gasification and pyrolysis. In the paper of *Bridgwater (2003)*, different possibilities for production of energy products and chemicals from biomass are reviewed. These conversion routes are summarized in Figure. 2.1 in which the main energy products and applications are also indicated.

Combustion of biomass is widely practiced commercially to provide heat and electricity with net conversion efficiencies commonly ranging from 20% to 40%, however, the efficiency may be increased when the biomass is co-combusted in coal-fired power plants *(Caputo et al., 2005)*. Combustion involves heating the biomass fuel with an oxidiser (typically air/oxygen) to a temperature at which the biomass constituents (C, H) react and combust completely in exothermic reactions. Though emissions and ash handling remain technical problems in combustion process, the fluidized bed designs have become the preferred technology because of low NO_x emissions and reliable scalability.

Pyrolysis is the thermal degradation of carbonaceous material in absence of air/oxygen. The products of pyrolysis are char, liquid fuel and gaseous fuel. The proportion of each product component depends mainly on the process conditions chosen, i.e. heating rate, operating temperature, pressure and gas residence time in the reactor. Depending on the heating rate and residence time of the biomass particles, the pyrolysis process is classified into slow pyrolysis (heating rates in the order of 10°C/s) and fast pyrolysis (heating rates up to 10^3 to

10^4 °C/s), while the product yield and distribution are significantly different between the slow and fast pyrolysis. Pyrolysis gas can be used for heat and power generation.

Gasification is the process which converts biomass into a gas mixture which has flexibility for applications such as for gas turbines, engines, fuel cells, hydrogen production and liquid fuel synthesis. The main purpose of the biomass gasification is the production of gas, called producer gas, which can be used as fuel gas in an internal combustion (IC) engine for power production.

Among all the possible thermo-chemical conversion processes, biomass gasification is one of the most promising technologies as it offers higher efficiencies compared to combustion and pyrolysis. A broad variety of combustion and gasification technologies producing heat, CHP or power at different scale ranges were studied by *Dornburg and Faaji (2001).* The atmospheric and pressurized BIGCC employed on large scales up to 300 MWth-input produces electrical efficiency of 35 to 45% while the fluidized bed combustion reactor combined with steam turbine (FBC/ST) with fuel capacities between 10 to 200 MWth-input could produce electrical efficiency of 25 to 35% *(Bridgwater, 1995; Dornburg and Faaij, 2001)*. The combustion of vacuum fast pyrolysis biomass products through an Integrated Pyrocycling Combined Cycle (IPCC) system can result in 18–30% increase of electricity output per ton of biomass compared to direct biomass combustion *(Bridgwater and Peacocke, 2000)*. The electricity generation cost for the same power generation systems such as BIGCC and FBC/ST were high range of 10000 $/KWe for smaller fuel capacities.The economic performanceelectricity generation cost of the generation improves with increasing scales up to 100 MWe. The cost of BIGCC is higher by 400 $/KWe at 2000$/KWe over the FBC/ST. The lowest costs per unit of primary energy saved are observed for BIGCC. These are therefore favourable with regard to both economic and efficiency *(Bridgwater, 1995)*. In addition, the producer gas from the biomass gasification has flexibility for further applications. For any fuel constituents (C, H, O), at fixed pressure and operating temperature, the fuel feed-rate and air supplies in a fluidized bed gasifier (normally gasified with air), can be controlled independently and the thermo-chemical conversion process of the system is determined by the term equivalence ratio ER. The ER is often used in connection with gasifier air supply and defined as the ratio of actual air fuel ratio to the stoichiometric air fuel ratio. The classification of the thermo-chemical conversion is based on ER, i.e., pyrolysis (ER=0), gasification (ER=0.25–0.50) or complete combustion (ER≥1) and mixed processes when ER is between the boundaries such as mixed pyrolysis and gasification when ER is

between 0 and 0.25, while gasification and combustion between 0.5 and 1 *(Desrosiers, 1981).* The quality of gas obtained from a gasifier depends strongly on the value of ER employed and the gasification yield initially increases with ER, and then it starts decreasing when the ER > 0.5 where combustion reactions begins to predominant gasification process.

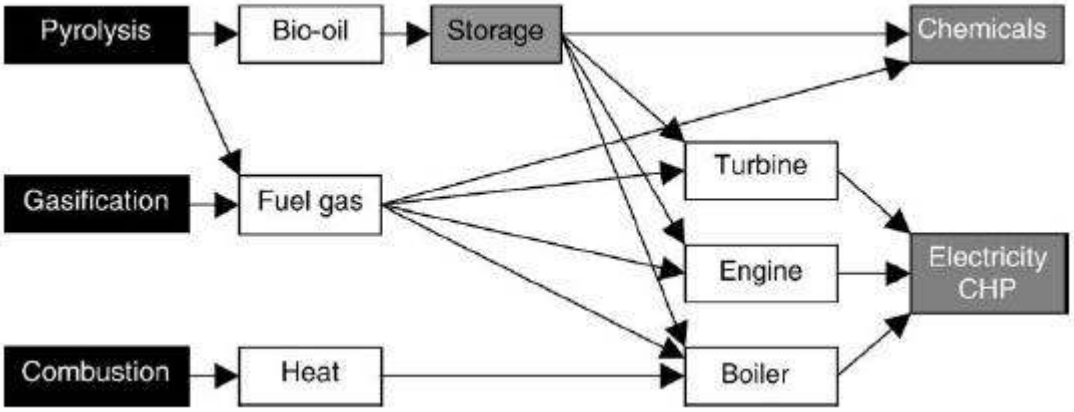

Figure 2.1: Biomass conversion routes

2.5 Gasification process

The gasification process of biomass and other solid fuels is a complex thermo-chemical process comprising of a number of steps as shown in Figure. 2.2. The biomass gasification consists of two stages of physical changes and chemical reactions after the drying process to remove water. In the initial stage, called initial pyrolysis, where thermal decomposition of the biomass under high temperatures occurs to produce pyrolysis gases (CO, CO_2, H_2 and CH_4), tar, char and minor quantity of oxygenated compounds such as phenols. The subsequent gasification process includes chemical reactions among derived gases from the initial pyrolysis, gasification agent (oxygen or steam) and char also at elevated temperatures *(Bridgwater, 1995).*

The gaseous product from the biomass gasification is called producer gas with the major components after removing water vapour being CO, CO_2, H_2, CH_4, H_2O and some minor components of higher hydrocarbons and tars. Close coupling of gasification and the power system increases the overall conversion efficiency by utilizing the thermal and the chemical energy of hot product gases.

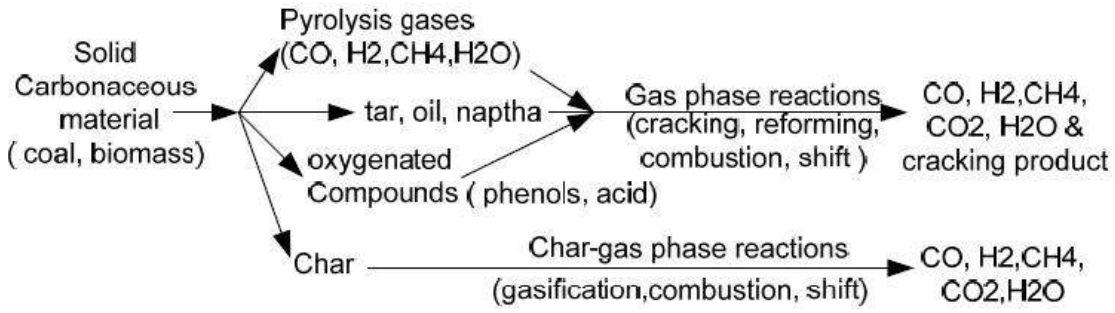

(2.2)

Figure 2.2: Gasification of coal or biomass *(Higman and Van der Burgt, 2003).*

In typical gasifier the following physicochemical processes take place at different temperatures as indicated in Table 2. 3.

Table 2.3: Physicochemical processes *(Basu, 2006)*

Thermo-chemical process	Temperature
1. Drying	(>150°C)
2. Pyrolysis (Devolatilization)	(150 - 700°C)
3. Combustion	(700-1500°C)
4. Gasification	(800-1100°C)

Though all the thermo-chemical process steps listed above are frequently modelled in sequences, there is no clear boundary dividing them and they often overlap. Among all the thermo-chemical processes, the combustion process is exothermic while all the other processes (drying, pyrolysis, and gasification) are endothermic on overall and hence these processes consume heat provided by the exothermic combustion process (in air and oxygen gasification) or by external heat sources (in case of steam gasification). These processes are described in details in the following sections.

2.5.1 Drying

The drying process occurs once the material is heated up in which the moisture is evaporated. The drying process strongly depends on the amount and thermodynamic state of water in the

biomass. The moisture in wood can exist as liquid water in the voids of wood (free water), the bond water held physio-chemically bonded to the hydroxyl groups of the main constituents of wood in the cell walls and water vapour also in the void space in the wood. For green wood of *Pinus radiata*, moisture content in green can range from about 30% in the core part of a tree to up to 200% in the outer part of the tree, whereas most gasification systems use dry biomass with moisture contents of 10–20%. Therefore in order to generate a producer gas with high heating values, the green biomass should be dried to this range of moisture content before the gasification operation.

In the gasification, once the biomass feed enters the gasifier it is heated up and dried releasing water till about 200°C. The fuel's moisture content in general has a comprehensive role in thermo-chemical biomass conversion. With increasing moisture content, the heat consumption for drying and for heating up of the biomass to pyrolysis temperature increases considerably. Hence, in the air/oxygen gasification process increasing fuel moisture content lowers the temperatures of pyrolysis and subsequent gasification processes. Therefore, the biomass moisture content has a considerable effect on the pyrolysis and gasification product distribution. The effect of moisture content and drying on gasification is studied by a number of researchers *(Di Blasi, 1998b; Galgano and Di Blasi, 2004; Thunman et al., 2001)*.For modelling the gasification process it is a common practice to couple drying with pyrolysis *(Bilbao et al., 1996; De Diego et al., 2002; Gray et al., 1985)*. A comprehensive discussion of drying and related phenomena, especially with respect to models for thermo-chemical biomass conversion, is given by *Di Blasi (1998b)*.

2.5.2 Pyrolysis or devolatilization

After drying, while the biomass is further heated up to 230°C or higher, devolatilization or pyrolysis occurs in which a series of complex physical and chemical changes can be found. During pyrolysis the thermally unstable components, such as lignin in biomass and saccharine polymer in the biomass cellulose, and volatiles evolved out of thermo-chemical processes, are broken down and evaporate with other volatile components. The composition of the evolved products is a function of the temperature, pressure, and gas composition during devolatilization. After the initial pyrolysis step, partial oxidation of the primary products occurs in case of air or oxygen gasification or char gasification reactions occur in case of steam gasification. In the meantime, chemical reactions among the derived gases, gas agent

and char also occur. Generally in a gasification process, pyrolysis proceeds at a much quicker rate than the subsequent gasification reactions and therefore, the gasification reactions are the rate controlling step. Therefore, quantification of the gasification reactions is critically important in the modelling of the biomass gasification process which needs data of reaction kinetics, phase transitions, heat and mass transfer rates *(Bridgwater, 2003)*. The yield of volatiles increases with the heating rate, but for the highest temperatures, the condensable tars are cracked and the gas yield is increased mainly due to higher lignin content *(Di Blasi, 2008)*. In the biomass pyrolysis, lower process temperature and longer residence time favour the production of solid char *(Capart et al., 1989)*. On the other hand, high temperature and shorter residence time increase the biomass conversion to gas at the expense of char and tar *(Font et al., 1989; Maniatis et al., 1989)*.

Currently, the exact pyrolysis mechanisms of biomass occurring as the first step in the gasification are not clear, although several reaction mechanisms have been proposed by researchers for pyrolysis as a separate process *(Babu and Chaurasia, 2003; Di Blasi, 1996; Janse et al., 1998; Thunman et al., 2001; Thurner and Mann, 1981)*. These are illustrated in Figure 2.3. All of these models were usually used to describe low or medium temperature and low-heating-rate pyrolysis conditions. They are not applicable for simulating biomass conversion because they assume a constant ratio of the char to volatiles yield and thus are only suitable for low to medium operation temperature. Cellulose thermal decomposition models, together with phase changes and tar production, provide a framework from which a lot of investigators have developed mathematical models on the biomass pyrolysis or biomass devolatilization.

In general, kinetic models of biomass pyrolysis process can be grouped into two main categories: One-step reaction and successive multistage reactions or two-stage models or semi-global models where the kinetic mechanism includes both primary and secondary reactions and pyrolysis products exist in the form of tar, gas and char. The one step model predicts the characteristic time of the pyrolysis process, and the semi-global models are useful for gasifier design and optimization as they are suitable for coupling with subsequent gasification reactions for chemical reactions with transport phenomena *(Di Blasi, 1998a)*. *Wagenaar et al. (1993)* developed pyrolysis kinetics as a function of temperature for pine sawdust particles using single first order Shafizadeh mechanism (Kinetic Scheme 2 in Figure 2.3) which shows good agreement with experimental data. The product yields from the pyrolysis model developed by *Di Blasi (2008)* as a function of temperature using the Kinetic

scheme 1 as shown in Figure 2.3 also show good agreement with the experimental data. Although the initial pyrolysis in the gasification process is different from slow pyrolysis, the application of kinetic constants estimated at lower temperatures (250-360°C) improves the model predictions at least for char yields and not for other components.

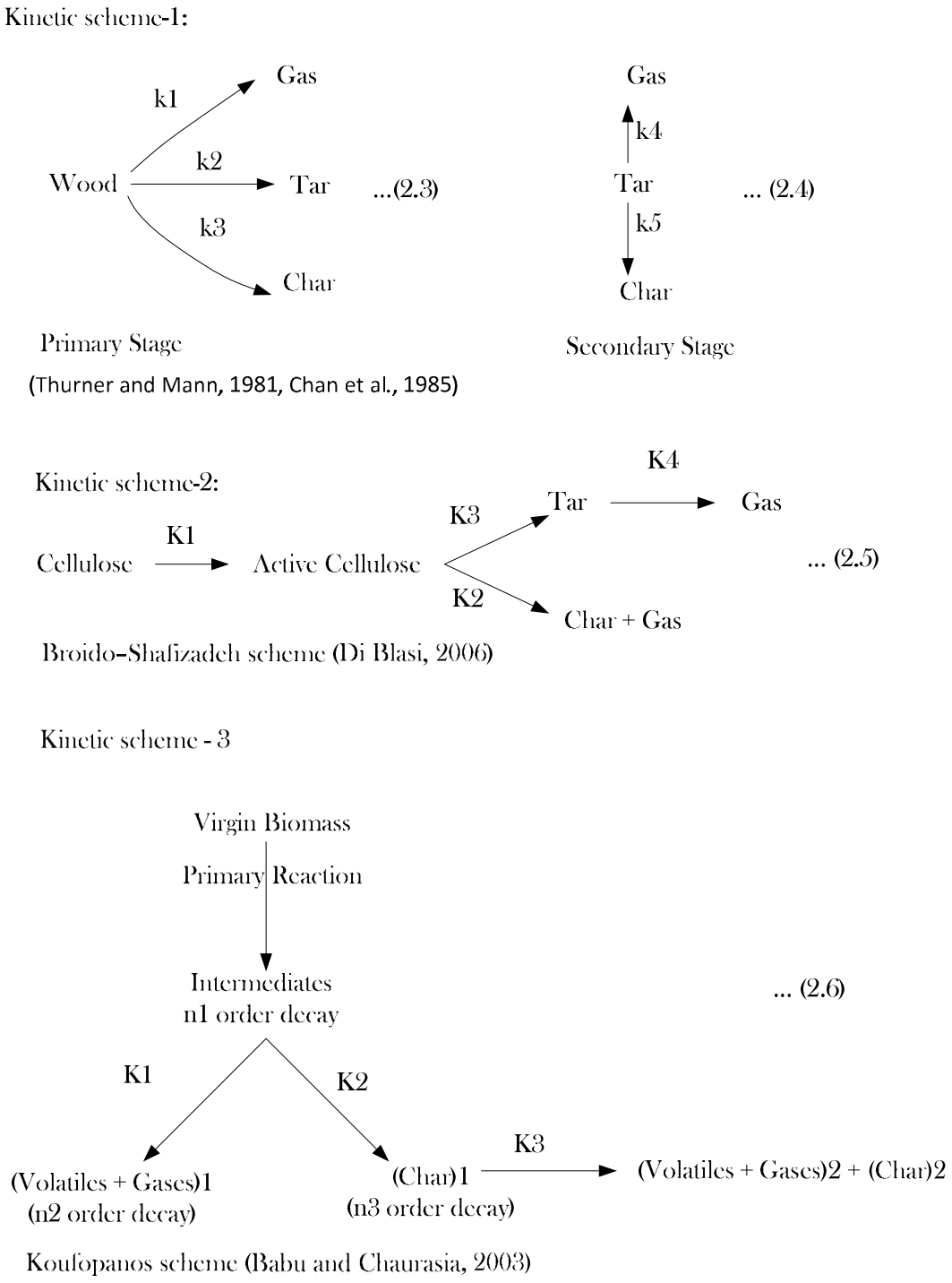

Figure 2.3: Various kinetic models for simulation of initial pyrolysis process.

It is generally accepted that the cellulose component of biomass undergoes pyrolysis according to a high activation energy step *(Di Blasi, 2008; Janse et al., 1998; Janse et al., 2000)*. The kinetic parameters (A, pre-exponential constant and E_A, activation energy) reported in the literature vary over a wide range, depending on the type of biomass sample and experimental conditions. Pyrolysis yields and product distributions are mainly determined by the composition of the original biomass. Usually cellulose has the lowest char yield; lignin produces highest char yield; hemicellulose has a medium char yield while the tar yield exhibiting the opposite trends *(Miller and Bellan, 1997)*.

2.5.3 Combustion process of carbon and hydrogen

In the biomass gasification with air or oxygen as gasification agent, oxidation or combustion of carbon and hydrogen constituents in the biomass is one of the most important chemical reactions taking place inside a gasifier, resulting in an overall exothermic gasification process. If excess oxygen is supplied to the gasifier where ER ≥ 1, the thermo-chemical conversion becomes complete combustion resulting in the formation of CO_2 (as in Equation 2.7).However, while the oxygen is supplied with the sub stoichiometric quantities (i.e., 1> ER > 0.5), partial oxidation of carbon occurs, resulting in the generation of CO (Equation 2.8). Hydrogen present in the biomass is also oxidized to generate steam (Equation 2.9).

$$C + O_2 = CO_2 + 393.77\ kJ/mol\ carbon \quad (2.7)$$

$$C + 0.5O_2 = CO + 111\ kJ/mol\ carbon \quad (2.8)$$

$$H_2 + 0.5O_2 = H_2O + 742\ kJ/mol\ hydrogen \quad (2.9)$$

2.5.4 Gasification reactions

Gasification reactions, as the last step of gasification process, are the most important and critical on the gasification rate, producer gas yield and gas composition. The gasification reactions, as overall, take an order of magnitude longer time than that for pyrolysis. Gasification reactions involve a series of reactions some of which are endothermic and remaining of which are exothermic. The model of gasifier often turns out to be a model of reactions of char and its intermediate products (CO, CH_4). These reactions that occur in the gasifier are classified as Water-gas reaction, Bouduard reaction, Water–Gas Shift reaction Methanation reaction *(Wang and Kinoshita, 1993)* and Steam Methane Reforming reaction *(Yan et al., 1998)*.

2.5.4.1 *Water-Gas reaction*

Water–Gas reaction also called Char Steam Gasification reaction is the partial oxidation of char by steam, which could come from different sources, such as water vapour associated with the incoming air, vapour produced from the evaporation of water in the biomass feed, and from pyrolysis of the solid fuel. In some gasifiers, steam is supplied as the gasification agent with or without air or oxygen. Steam reacts with the hot char according to the heterogeneous Water–Gas reaction which is endothermic.

$$C + H_2O = H_2 + CO - 138.33\ kJ/mol\ carbon \quad (2.10)$$

2.5.4.2 *Bouduard reaction*

The CO_2 formed from the initial pyrolysis process of the biomass gasification in the gasifier reacts with char to produce CO according to the following endothermic reaction, which is known as the Bouduard reaction.

$$C + CO_2 = 2CO - 170.45\ kJ/mol\ carbon \quad (2.11)$$

2.5.4.3 *Water Gas-Shift conversion*

The heating value of H_2 is about 12.77 MJ/Nm^3 (142 MJ/kg) which is higher than that of CO at 12.62 MJ/Nm^3 (10.7 MJ/kg) *(Waldheim and Nilsson, 2001)*. Therefore, the reaction of available steam with CO to produce H_2 is a highly desirable reaction. This exothermic reaction, known as Water–Gas Shift reaction, results in an increase in the ratio of H_2 to CO in the gas, and is employed in the synthesis gas production. According to *Graboski (1981)* this Water–Gas Shift reaction can be prioritized by heterogeneous catalysis on the carbon surface at temperature below 1100°C. At higher temperatures it may occur as a homogeneous reaction.

$$CO + H_2O = H_2 + CO_2 + 41.98\ kJ/mol \quad (2.12)$$

2.5.4.4 *Methanation reaction*

Methane is formed in the gasifier through the Methanation reaction (Equation 2.13) which is exothermic. Methane formation is preferred especially when the gasification products are to be used as a feedstock for other chemical process. It is also preferred in BIGCC applications

due to methane's HHV about 39.78 MJ/Nm^3 (55.5 MJ/kg) *(Waldheim and Nilsson, 2001)*. Methanation reaction can be enhanced by application of nickel-based catalysts at 1100°C and 6 to 8 bar *(Graboski, 1981)*.

$$C + 2H_2 = CH_4 + 93.80\ kJ/mol\ carbon \quad (2.13)$$

2.5.4.5 *Steam Methane Reforming reaction*

Steam Methane Reforming reaction, an endothermic reaction, produces H_2 and CO with the consumption of formed CH_4 due to initial pyrolysis reaction. The Steam Methane Reforming reaction is the slowest among the endothermic reaction and hence the net consumption of H_2O is less for lower operating temperature of 700°C and consumption of steam increases at higher temperatures.

$$CH_4 + H_2O = CO + 3H_2 - 232.78\ kJ/mol \quad (2.14)$$

The Char Steam Gasification reaction and Bouduard reactions are often referred as temperature stabilizing reactions in the gasification zone. These reactions are kinetically slow at temperatures below 800°C, but become very fast at temperatures above 1200°C. Thus in steam gasification, with sufficient amount of CO_2 available within the hot bed, a rise in temperature can be prevented due to the endothermic reactions. This temperature buffer results in a relatively stable composition of the producer gas *(Desrosiers, 1981)*.

The rate of the above reactions (mainly comprising carbon and carbon reaction products) depends primarily on the reactivity of char and the reaction potential of the gasifying medium in the ordering of O_2 followed by steam and then by CO_2, respectively. In general, if air or O_2 is used as the gasification agent, the rate of Char-Oxygen reaction (Equation 2.7 and 2.8) are the fastest compared to the Methanation reaction (Equation. 2.13) in the steam gasification. The rate of Char Steam Gasification reaction (in Equation. 2.10) is orders magnitude higher than the Bouduard reaction (in Equation. 2.11). Thus the relative rates of these reactions are: $R_{C+O2} >> R_{C+H2O} > R_{C+CO2} >> R_{C+H2}$ *(Smoot and Smith, 1985)*. Also it is estimated that the relative rates of these four reactions with char or char reaction products at 800°C temperature and 10 kPa pressure are 10^5 for O_2, 10^3 for H_2O (steam), 10^1 for CO_2 and $3x10^{-3}$ for H_2*(Walker Jr et al., 1959)*.

2.6 Types of gasifiers

Gasification reactor designs have been researched for more than a century, which has resulted in the availability of several designs at both small and large scales. There are different ways to categorize the gasifier based on the process, gasifier structure or heat supply. Though the chemistry and physics involved in the operation of gasifier reactor is complex, their construction is relatively simple. A gasifier type is selected depending on the end use and the quantity of producer gas required.

Based on heat supply for the gasification, the gasifiers can be grouped into two: auto-thermal and allo-thermal gasification. In the auto-thermal or direct gasification, the heat is supplied by partial oxidation of the feed fuel in the gasifier itself. The partial oxidation can be carried out using air or oxygen as the gasification agent, while supplementary steam could also be added to these oxidants. Air gasification produces a LHV gas (4–7 MJ/Nm^3) suitable for boiler, engine or turbine applications *(Zainal et al., 2001)*. If pure O_2 is used as the gasification agent, the heating value of producer gas will increase (10–18 MJ/Nm^3) which is suitable for use as synthesis gas for conversion to methanol and liquid biofuels *(Reed, 1981)* but the gasification operating costs will also increase due to the O_2 production costs. Allo-thermal or indirect gasification uses steam as gasification agent and the heat necessary for gasification is provided from internal recirculation of hot gas, char and hot bed material or by external heat sources. This concept allows for generating producer gas of medium heating value (14–18 MJ/Nm^3), rich in H_2, without the need for O_2 *(Gil et al., 1999; Rapagnà et al., 2000; Schuster et al., 2001)*.

Depending upon the structural design and the contact made by the gasification agent with the feed fuel, gasifier can be divided into following four types:

1. Entrained flow gasifier;
2. Fixed (updraft, downdraft);
3. Fluidized bed (Bubbling or Circulating); and
4. Spouted bed.

A review of gasifier manufacturers in Europe, the United States and Canada identified 50 manufacturers offering commercial gasification systems, of which 75% were the fixed-bed

downdraft type, 20% were the fluidized bed systems, 2.5% were the fixed bed updraft type, and 2.5% were various other designs *(Knoef, 2000)*.

2.6.1 Entrained flow gasifier

In entrained flow gasifier a finely reduced feedstock is gasified commonly with O_2 as gasification agent which operates at much higher temperatures of about 1200-1500°C and very short residence time usually few seconds compared to the fluidized bed and updraft fixed bed gasifiers as shown in Figure 2.4. Due to the high gasification temperature, the producer gas has low concentrations of tars and condensable gases and the char conversion rate is high. However, this high-temperature operation creates difficulties for materials selection of the gasifier and problem of ash melting. Although conversion in entrained flow gasifier effectively approaches 100% efficiency, its application for biomass gasification is limited by the requirement of fine fuel particles. In the IGCC systems in the world, about 10% utilizes entrained flow gasifiers which have capacities of greater than 100 MWe for coal gasification *(Bridgwater, 1995)*.

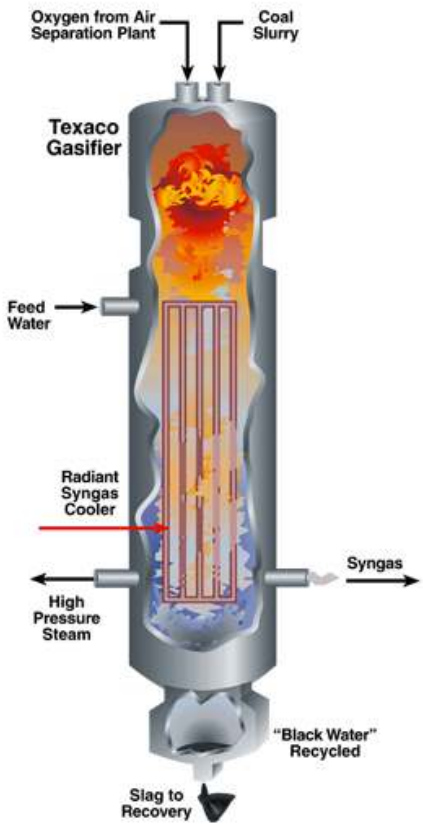

Figure 2.4: Entrained flow gasifier (NETL, 2012)

2.6.2 Downdraft fixed bed gasifier

In the fixed bed gasifiers, there is a stationary grate above which the gasification occurs. The feed fuel is normally fed at the top of the gasifier. The fixed bed gasifiers can be further divided into downdraft or updraft gasifier depending on the flows of gasification agent and producer gas. Figure 2.5 shows a sketch of the downdraft fixed bed gasifier in which the gasification agent, air or O_2, is fed into the middle of the bed or together with the feed fuel, and the producer gas flows out of the gasifier from the lower part of the gasifier beneath the stationary grate. In this type of gasifier, fuel feeding is quite easy as the temperature at the feeding position is not too high and the pressure inside the gasifier is close to atmospheric pressure. Drying, pyrolysis, combustion and mass reduction occur, sequentially, in the drying zone, the pyrolysis zone, the gasification zone and the reduction zone from the top to the bottom of the gasifier. The fuel is dried in the top section before it enters into the pyrolysis zone. Radiant and conductive heat transfer from the partial combustion sections provides the heat for drying and pyrolysis of the biomass fuel. Under the influence of gravity the dried solid fuel moves to the hot pyrolysis zone where volatile matters and char are evolved. The gaseous products of the pyrolysis reactions along with the char are drawn downwards into the combustion zone of the gasifier. In the combustion zone, the reaction with oxygen results in sharp increase in temperature up to 1200-1800°C. At this temperature the tars and other heavy hydrocarbons will be cracked down thermally into lighter hydrocarbon gas constitutions. The extent to which the pyrolysis gases are actually burned depends on design, biomass feedstock. Below the combustion zone, the remaining char if there is any, ash and the producer gas and water vapour pass to the reduction zone where the main constituents of producer gas, CO and H_2 are formed *(Reed, 1981)*.

The main advantage of a downdraft fixed bed gasifier is the production of a gas with low tar content. In practice, a tar free gas is seldom unless all gases passes through the hottest zones. On the other hand the downdraft gasifier is prone for high amount of ash and dust particles when they are passed through the combustion zone at the bottom of the reactor. Selection of uniformed size fuel is important for this kind of gasifier; otherwise the throat of the combustion zone might be blocked, restricting the pyrolysis gases flowing downward and heat transferring from the combustion zone upwards. Another set-back with this type of gasifier is relatively high temperature of the exit flue gas results in lower gasification efficiency.

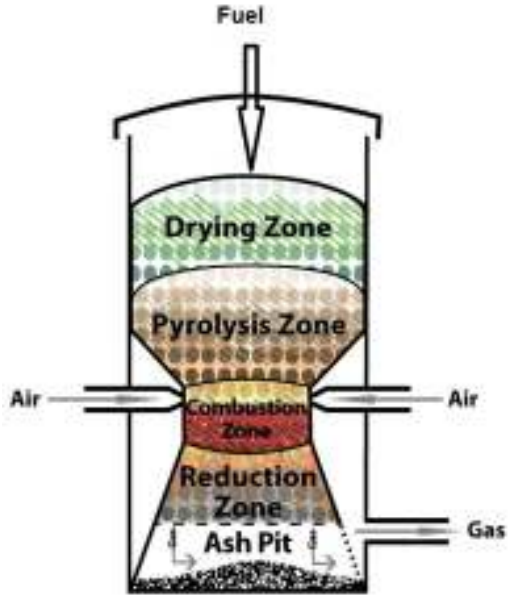

Figure 2.5: Downdraft fixed bed gasifier (GEK, 03May 2011)

2.6.3 Updraft fixed bed gasifier

In an updraft fixed bed gasifier, the solid fuel is also fed from the top, the gasification agent (air or O_2) is introduced from the bottom then flowing through the stationary grate and the producer gas is drawn out from the upper part of the gasifier above the grate, as illustrated in Figure 2.6. The gasification process in the updraft fixed bed gasifier is similar to that in the downdraft gasifier with all the four stages of drying, pyrolysis, partial combustion and reduction except for the fact positions of the combustion and reduction zones are swapped. Initially at the top layer of the bed, the solid fuel is dried by the pyrolysis gases and gases from the lower reduction zone and the combustion zone while these gases move upwards. In the same time, the char from pyrolysis zone moves downwards to the reduction zone and the combustion zone where the hot combustion gas provides energy for the endothermic reactions. The tars in the vapour either condense on the descending fuel or are carried out of the gasifier with the producer gas contributing to its high tar content. This tar contains about 30% of the energy content of the biomass fuel *(Overend et al., 1985)*. The remaining char reacts with the gasification agent (air/O_2) injected at the bottom of the reactor vessel. Finally ash is extracted at the bottom of the reactor.

The major advantages of this type of gasifier are its simplicity and high carbon conversion rate. The producer gas at the top of this type of gasifier leads to low gas exit temperature due to internal heat transfer to heat the incoming solid fuel and high gasification efficiency. Because of the efficient heat exchange between the out-flowing gases and the incoming solid fuel, this type of gasifier can handle biomass with high moisture content of up to 50% *(Overend et al., 1985, Speight, 2011)*. However, the major drawback of this gasifier is the high tar content in the producer gas mainly from the initial pyrolysis. As a result of the highly tar contaminated gas, there is a need for extensive gas cleaning if the producer gas is used for gas engines. Gas cleaning is less important if the gas is used for direct heat appliances where the tars will be simply burnt.

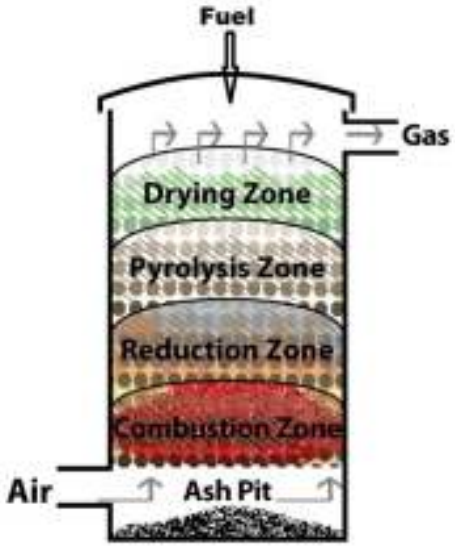

Figure 2.6: Updraft fixed bed gasifier (GEK, 03May 2011)

2.6.4 Fluidized bed gasifier

Fluidization is a process where a bed of solid particles behaves as a fluid when it comes in contact with fluidization agent, generally air, steam, producer gas from gasification or flue gas from combustion. The fluidized bed gasifier uses inert medium such as sand, dolomite or alumina to mix the solid fuels with gas phase and to help maintain the operating temperature steady at the desired level. In the conventional fluidized bed gasifier, the bed is initially heated from an external source to a sufficiently high temperature and the fuel is then introduced either by a continuous mechanical feed directly into the dense bed or by gravity

from the top or middle of the fluidized bed based on their design. The fuel-sand mixture is subjected to upward flowing gas agent through a distributor plate at sufficient velocity such that the mixture starts to be fluidized. At this point, the frictional drag force and the upward flowing fluid counteract particle gravity force. The gas agent velocity is called minimum fluidization velocity. On entering the bed, the solid fuel is rapidly heated to the reactor bed temperature and pyrolysed, releasing char, volatile high molecular compounds and gas as the initial products. The pyrolysis gases are then thermally cracked and/or gasified by steam, while the char particles are gasified via reactions as described in Section 2.5.3 and Section 2.5.4. When the gas agent velocity is relatively low above the minimum fluidization velocity, the gas flows through the bed as bubbles thus this type of gasifier is also called bubbling fluidized bed (BFB) gasifier as shown in Figure 2.7(a). However, if the gas agent is sufficient high so that the bed of solid particles is carried out of the gasifier, the gas agent velocity is called terminal velocity and the gasifier is called circulating fluidized bed (CFB) gasifier (Figure 2.7b). In the fluidized bed gasifier, the producer gas can be directed into a cyclone to remove the solid particles from the producer gas. In the BFB gasifier, the solid particles are mainly ash thus these particles can be collected for disposal. In the circulating fluidized gasifier, the solid particles are the inert bed materials and ash, therefore, the inert bed materials can be further separated and then returned back to the gasifier. The producer gas leaves from the top of the cyclone and is then cooled and cleaned before further applications *(Overend et al., 1985)*.

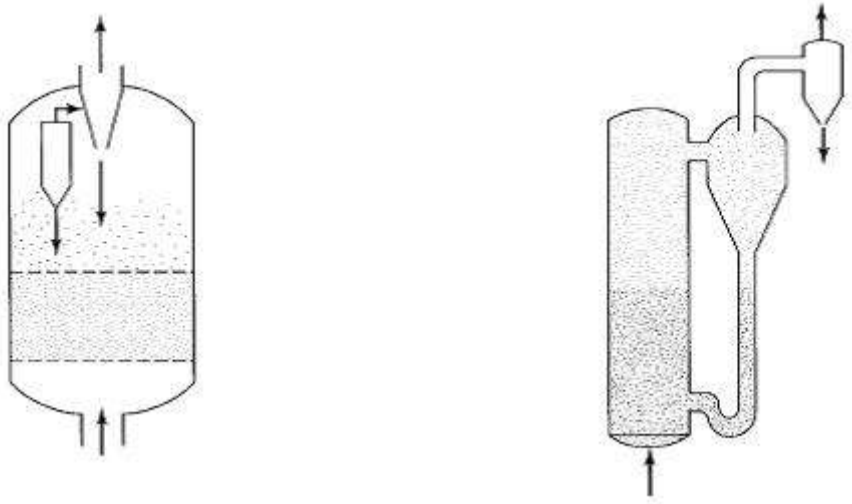

(a) BFB gasifier (b) CFB Gasifier

Figure 2.7: BFB gasifier (a) and CFB gasifier (b).

As the overall gasification process is endothermic; heat is required to sustain the gasification operation. The required heat can be provided by partial combustion of the biomass within the gasifier using stoichiometric amount of air as gasification agent or supplied indirectly by a heat carrying medium circulating through the gasifier *(Rezaiyan and Cheremisinoff, 2005)*.

In contrast to fixed bed reactors there are no stationary grate in the fluidized bed gasifier during gasification. Drying, pyrolysis and gasification occur simultaneously over the whole reactor volume, which is almost perfectly mixed and thus isothermal *(Buekens and Schoeters, 1985)*.

Since the residence time is shorter and the gasification temperature (800-900°C) is lower compared to the fixed bed gasifier, tar content in the gasification producer gas is generally higher than the downdraft fixed bed gasifier *(Rapagnà et al., 2000)*. In addition, the fluidized bed gasifier is applied for large scale plants thus the biomass loading is high. Therefore, gas cleaning is important in the biomass gasification with the fluidized bed gasifier. To prevent tar deposition and fouling, the cyclone surface should be maintained at a temperature greater than 700°C *(Reed, 1981)*. The carbon conversion could be increased by injecting a portion of recovered particles into the bed. The degree of particles will increase with gasifier load since the superficial velocity will increase proportionally. The bed temperature is maintained in an isothermal state in a fluidized bed as a result of turbulent fluidized medium promoting high heat transfer rate. The major challenge for BFB gasifier is to maintain the superficial velocity which must be several times higher than the minimum fluidization velocity and also lower than the terminal velocity of the smallest particle of the fuel to avoid carryover in a BFB gasifier. With the increase in load demand the superficial velocity must be increased proportionally. Otherwise the bed could become defluidized or slumped leading to hotspots and possibly agglomeration of char, inert bed material (such as sand) and ash particles.

The above problem can be solved by using the CFB gasifier in which the cross sectional area of the BFB gasifier is designed to be much smaller than the BFB gasifier and thus the superficial velocity of the gasification agent is higher than the terminal velocity of particles to elutriate and a cyclone to capture and re-circulate the solids as shown in Figure. 2.7(b). CFB gasifier offers longer residence time to achieve a higher degree of gasification and conversion of other components. CFB biomass gasifier could potentially achieve high carbon conversion, high cold gas efficiency, and low tar content and low emissions in terms of downstream

application of fuel gas. If these expectations could be met, fluidized bed gasifier can provide a major boost to the bio-energy industry.

To overcome the operational problems found in fixed bed gasifier and the BFB gasifier, such as handling high ash solid fuel, hot spots within the gasifier, scale-up limitations, particle size limitations, a DFB gasifier also called FICFB system has recently been developed *(Hofbauer et al., 1997, Murakami et al., 2007, Saw et al., 2011, Xu et al., 2009)*. This FICFB system isolates the gasifier reactor (BFB) and combustion reactor (CFB) with a circulating bed material to transfer heat from the combustion reactor to the gasification reactor. Therefore, this system offers an ideal opportunity to use steam as gasification agent to produce the producer gas with higher calorific value and higher H_2 content compared to other types of existing gasifiers.

2.6.5 Spouted bed gasifier

Spouted bed gasifier provides an alternative to fluidized beds for relatively coarse and uniformly sized particles (larger than about 1 mm in diameter) as illustrated in Figure 2.8. The spouted bed gasifier is characterized by a high-velocity spout of gas moving up the centre of the bed, carrying particles to the top. A spouted bed is composed of three separate regions: a relatively dilute spout (or jet) region at the centre of the bed extending right up to the bed surface surrounded by the moving-packed-bed annulus region, and a fountain region above the bed surface, where particles travel upward through a certain distance from the top of the spout and then falls back under gravity onto the bed surface. Spouted beds have been used for coal gasification, drying and low temperature chemical treatment operations. Recently spouted bed gasifer has been studied to understand the hydrodynamics characteristics such as minimum spouting velocity, pressure drops of biomass particles and has been applied for thermochemical conversion processes such as gasification, pyrolyiss, combustion and drying*(Cui and Grace, 2008).*Further consideration of spouted beds is outside our scope and more comprehensive reviews is available *(Epstein and Grace, 1997)*.

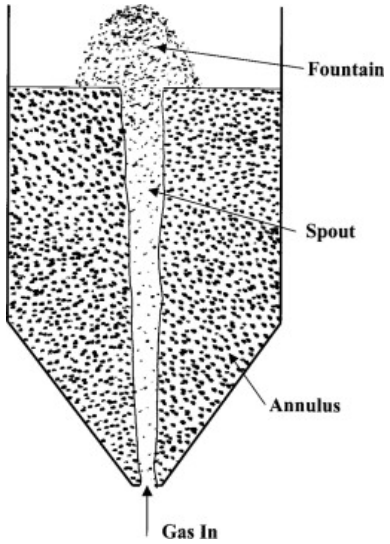

Figure 2.8: Spouted bed gasifier (Cui and Grace, 2008)

2.7 Modelling of fluidized bed gasification

The design and operation of a fluidized bed gasifier requires thorough understanding of the influence of solid fuel and operating parameters on the gasification process. For this purpose, modelling is an important means to design a unit based on results obtained from the model predictions with varying feedstocks and operating conditions. A good model, once validated, will help identify the sensitivity of the performance of a gasifier to variation in different operating and design parameters. The designers can speculate the effects of many parameters even without any further experimental data. The main goals of these models are to understand and quantify the thermo-chemical processes during the gasification of the biomass and to evaluate the influence of the main input variables, such as moisture content, air/fuel ratio, steam to biomass (S/B) ratio, producer-gas composition and the calorific value of the producer gas.

Modelling of a complex physio-chemical system is largely a process of simplifying the system so that the process can be quantitatively described by mathematical equations based on physical and thermodynamic laws. Models could be developed in various ways e.g., simpler zero-dimension models, one-dimensional, multi-dimensional and expert systems. Early models treated fluidized bed reactor models as zero dimensional equilibrium models or single phase models, which neglected the segregation of gas, solids and bubble of voids. Lately more and more comprehensive but complex 3D models have been developed with consideration of fluidization hydrodynamics, gasification kinetics and balances (momentum,

mass and energy). These considerations were mostly applied to general chemical reactors but the application to fluidized bed gasifier came only recently *(Petersen and Werther, 2005b).*

In general, the gasification process can be modelled using four basic approaches, namely,

1. Equilibrium;
2. Reaction kinetic;
3. Gasification model embedded into CFD;
4. Neural network.

Over the years large numbers of kinetic models for fluidized bed coal gasifier have been developed *(De Souza-Santos, 1989; Yan et al., 1998; Chejne and Hernandez, 2002)*. Though these models cannot be applied directly to biomass gasification, they can be modified accordingly by considering the thermo-chemical properties of the biomass, operating conditions and the reactions involved based on the gasifying medium used. The important factors that need to be noted for reaction kinetics in biomass gasification are listed below *(Corella and Sanz, 2005)*:

- Biomass is more reactive than coal, and it pyrolyzes much quickly as its ash and carbon contents are low. In biomass gasification, the secondary reactions of the high volatile gases with the gasifying agent are more dominant compared to the coal gasification. Biomass is relatively rich in oxygen, which reacts with carbon and hydrogen in the biomass during pyrolysis process to produce oxygenated gases of CO, CO_2 and H_2O *(Biagini et al., 2005)*. Hence adapting the pyrolysis kinetics of coal for biomass is not appropriate.

- Gasification of biomass below 1000°C always produces a measurable amount of tar. There is no tar kinetics available for the biomass tar products. Researchers have developed tar kinetics for different types of biomass in recent years, but the kinetics vary from different type of biomass used and different operating conditions *(Bryden and Ragland, 1996; Westbrook and Dryer, 1984).*

In addition, quantification of the hydrodynamics is important for the kinetic modelling, and the gasification embedded into CFD modelling, but the hydrodynamics are not needed in the equilibrium and neural network models. A typical kinetic model predicts the gas composition profile along the height of the gasifier while the equilibrium model predicts the maximum

product yield and the overall gas composition from the gasifier *(Li et al., 2004)*. The kinetic modelling includes the reactor hydrodynamics primarily to consider the heat and mass transfer within the reactor in addition to the consideration of reaction kinetics. Thus, while the equilibrium model predicts the result to be attained after infinite time, the kinetic modelling gives that for any time of operation in the reactor.

The artificial neural network based models, unlike other two, require little knowledge of the gasification process. It is based on input-output correlation developed from a large pool of experimental data. The CFD based model relies on examination of heat, mass, momentum and species balance in discrete regions in the reactor.

2.7.1 Equilibrium modelling

Due to its simplicity and easy to use, equilibrium modelling still attracts interests from researchers and recent studies have been focused on prediction of performance of commercial gasifiers *(Altafini et al., 2003; Jarungthammachote and Dutta, 2007; Jarungthammachote and Dutta, 2008; Li et al., 2001; Li et al., 2004; Melgar et al., 2007; Ruggiero and Manfrida, 1999; Schuster et al., 2001; Zainal et al., 2001).* These authors have shown reasonable agreement between model predictions and experimental data in a certain range of operation conditions.

Li et al. (2001), Melgar et al. (2007) and Zainal et al. (2001) proposed that thermo-chemical equilibrium models have to include some important hypotheses. Firstly, the residence time of the solid fuels in the gasifier is supposed to be high enough to reach chemical equilibrium. Secondly all the carbon in the biomass is gasified, and thereby, the char formation process can be neglected *(Melgar et al., 2007; Schuster et al., 2001)*. Thirdly the resistance to heat transfer and mass diffusion inside the char particles is ignored, although the heat of formation of the species involved will be considered. Finally, in thermodynamic calculations, the tar formation will either be treated as non-reactive or be neglected because of its low concentrations and there is no information about reaction pathways or its formation.

In general, equilibrium modelling can be termed as a zero-dimensional which approaches the conditions of the ideal, well-stirred chemical reaction where the residence time is supposed to be substantially larger than the time interval needed for complete reaction kinetics. This is a simple modelling approach which provides only the final gas composition as a function of

temperature and not with respect to changes over time or position in a gasifier *(Li et al., 2004)*. At chemical equilibrium, a gasifier is at its most stable composition, a condition achieved when the entropy of the system is maximized while its Gibbs free energy is minimized. This model gives the maximum conversion for a given reaction condition which may be used as a bench mark for assessment of different gasifiers. There are two approaches in the equilibrium modelling *(Li et al., 2001; Li et al., 2004)*:

1) Stoichiometric - mechanism based on all chemical reactions and species involved.
2) Non-stoichiometric – mechanism based on elemental composition, obtained from ultimate analysis data and the final gas components.

2.7.1.1 *Stoichiometric equilibrium model*

In stoichiometric approach, the reaction mechanism incorporates chemical reactions and species involved. It usually starts by selecting all species containing C, H and O or any other dominant atoms. If other elements form minor part, they are often neglected. In the equilibrium modelling, it is always considered that all the reactions involved are thermodynamically at equilibrium and the producer gas formed comprises CO, CO_2, H_2, CH_4, N_2, and H_2O as ideal gas with carbon conversion being 100% in case of excess gasification agent used *(Schuster et al., 2001)*.

The stoichiometric chemical equilibrium model is based on selecting those species in the product gases that are present in the largest amounts, i.e. those which have the lowest value of free energy of formation. As noted by *Prins et al. (2003)* and *Desrosiers (1981),* under the gasification conditions with temperatures between 600^{o}C and 1200^{o}C the only species present at concentrations higher than 10^{-4} mol% are CO, CO_2, CH_4, C_2H_4, H_2, N_2, H_2O and solid carbon (graphite). A generalized reaction of biomass with air and steam is formed with these gas species as shown in Equation (2.15). Using the Equation (2.15) an atomic balance of carbon, hydrogen and oxygen are formulated providing three independent Equations (2.16 – 2.18). For a heterogeneous system of species, three independent chemical reactions (Water gas reaction, Bouduard reactions and Methanation reaction) are required, according to Duhem's theory *(Smith et al., 2001)*. Similarly for a homogeneous system that consists of CO, CO_2, CH_4, H_2, N_2, H_2O, there are two independent chemical reactions, resulting from the Water Gas-Shift reaction and Steam Methane Reforming reaction. All these reactions have their equilibrium in the temperature ranging from 545 to 825°C.

$$[N_{wood}CH_{1.44}O_{0.66} + N_{O2}O_2 + N_{N2}N_2 + N_{steam}H_2O] \xrightarrow{\Delta hightemp}$$
$$\begin{bmatrix} N_{CO}CO + N_{CO_2}CO_2 + N_{H_2}H_2 + N_{CH_4}CH_4 + N_{C_2H_4}C_2H_4 + \\ +N_{char}(char) + N_{N_2}N_2 + N_{H_2O}H_2O \end{bmatrix} \quad (2.15)$$

Carbon Balance:

$$f_1 = 0 = N_{wood} - \left(N_{CO} + N_{CO_2} + N_{CH_4} + N_{C_2H_4} + N_{char}\right) \quad (2.16)$$

Hydrogen Balance:

$$f_2 = 0 = 1.44N_{wood} + 2N_{steam} - \left(2N_{H_2O} + 2N_{H_2} + 4N_{CH_4} + 4N_{C_2H_4}\right) \quad (2.17)$$

Oxygen Balance:

$$f_3 = 0 = 0.66N_{wood} + N_{steam} + 2N_{O2} - \left(N_{H_2O} + N_{CO} + 2N_{CO_2}\right) \quad (2.18)$$

The generalized Equilibrium constant for the gasification reactions (Equations $2.10 - 2.14$) is given as

$$K_{eq,i} = \prod_i (y_i)^{\nu_i} \left(\frac{P}{P_0}\right)^{\sum_i \nu_i} \quad (2.19)$$

where $y_i = N_i/N_{total}$ is the mole fraction of the species i and N_{total} is the total moles of the product species$i$. ν_i is the stoichiometric coefficients of the product gas species i. P, P_0 are the operating pressure and the standard pressure. The equilibrium constants K_{eqi} in the above equations are a function of temperature only are calculated from the Gibbs free energy *(Perry et al., 1997)*.

The unknown coefficients such as $N_{CO}, N_{CO_2}, N_{H_2}, N_{CH_4}, N_{N_2}, N_{C_2H_4} and\ N_{H_2O}$ in Equation (2.15) form the composition of the producer gas which is solved using the elemental balance equations, overall heat balance and the equilibrium constant K_{eqi} for the different gasification reactions considered. The chemical equilibrium constants and the thermodynamic characteristics of the gases, such as the specific heats, are functions of temperature. The model can be solved by iteration of the fitting chemical equilibrium constants, reaching a thermodynamic as well as chemical equilibrium in the end.

Though the equilibrium constant of the exothermic reactions are chosen for solving the stoichiometric equilibrium model, the overall gasification reaction of biomass with steam is an endothermic reaction. The heat generated from the exothermic reactions is consumed by the endothermic reactions and the reaction process is assumed to be adiabatic. Hence, heat

balancing of the reactants and products of the global reaction leads to a balance equation for the gasification process is defined by the first law of thermodynamics as

$$H_{prod}(T) + Q_{loss} = H_{reactant} \tag{2.20}$$

$$H_{reactant} = \sum_{i=reactant} N_i \, \bar{h}^0_{f_i,298} + \sum_{i=reactant} N_i \int_{298}^{T} C_{pi} dT \tag{2.21}$$

$$H_{prod}(T) = \sum_{i=prod} N_i \, \bar{h}^0_{f_i,298} + \sum_{i=prod} N_i \int_{298}^{T} C_{pi} dT \tag{2.22}$$

where $H_{reactant} and \, H_{prod}$ are the enthalpies of each reactant and each product at specific temperatures, respectively. Q_{loss} is the heat loss in the gasification process, which is zero as a result of adiabatic condition. $\bar{h}^0_{f_i,298}$ is the enthalpy of formation of species *i* at 25°C. N_i is the number of moles of the reactant species *i* in Equation (2.21)and product species *i* in Equation (2.22). The values of specific heat C_{pi} and the enthalpy of formation of gas species are evaluated from *Perry et al. (1997)*.

The relationship to find the enthalpy of formation of biomass fuel, $\bar{h}^0_{f_{biomass}}$is suggested by *De Souza-Santos (1989)* as

$$\bar{h}^0_{f_{biomass}} = LHV_{fuel} + \sum_{k=prod} N_i \, \bar{h}^0_{f_i} \tag{2.23}$$

where $\bar{h}^0_{f_i}$is the enthalpy of formation of product i under complete combustion of the solid fuel, and LHV_{fuel} is the lower heating value of the solid fuel which as estimated as shown in Equation (2.24)

$$LHV_{fuel} = HHV_{fuel} - 9m_H\left(h_{fg}\right) \tag{2.24}$$

where HHV_{fuel} the higher heating value of the solid fuel as estimated from Equation (2.1) and m_H is the mass fraction of hydrogen in the solid fuel and h_{fg} is the enthalpy of vaporisation of water.

Two parameters that significantly affect the temperature of the system in an equilibrium model of biomass gasification are the relative gasifying fuel/air ratio and the biomass moisture content that have been studied in greater detail by *Melgar et al. (2007)*. *Jarungthammachote and Dutta (2007)* in their stoichiometric equilibrium model used Gibbs free energy constrained methods to analyze the performance of a downdraft fixed gasifier. They used coefficients for correcting the equilibrium constant of the Water–Gas Shift

reaction and the Methane reaction in order to improve the model. Those coefficients were obtained from the comparison between the model and the results of other researchers' experiments. The predicted results from the modified model agree closely with experimental results reported by *Jayah et al. (2003)*. An equilibrium biomass gasification model in combination with thermodynamics was developed by *Nordgreen et al. (2006)* especially for tar breakdown in fluidized beds. Results agreed well with experimental results.

2.7.1.2 *Non stoichiometric equilibrium model*

Unlike the stoichiometric model, the non-stoichiometric approach is based on the fact that for a specified temperature and pressure, the Gibbs free energy of the system is minimal at equilibrium and the elemental composition of the feed is known from its ultimate analysis. This method is particularly applicable to gasification of fuels like biomass whose exact chemical formula is not always known.

Li et al. (2001) developed a regressive non-stoichiometric equilibrium model for a CFB coal gasifier, considering five elements and 44 species in both the gas and solid phases, where they used random (RAND) algorithm to solve the equations. Later *Li et al. (2004)* used the above model to simulate gasification of sawdust in a CFB gasifier, where they observed that gasification processes deviated significantly from chemical equilibrium model. Therefore, in order to correct the deviations, they developed a phenomenological model to modify the equilibrium-based framework to account for key non-equilibrium factors.

Altafini et al. (2003) developed an equilibrium model to simulate a sawdust waste gasification based on Gibbs free energy minimization. The model has identified the influence of moisture in fuel and several other operation parameters on gasification. Reasonable agreement between the model predicted results and experimental data was found for gasification process at very high temperatures.

A thermodynamic equilibrium model was developed by *Schuster et al. (2001)* for steam gasification of biomass. Based on the developed model, extensive parametric studies were performed for the influence of operating conditions and fuel parameters on the heating value of the product gas and the overall performance of the gasifier. In separate studies of *Zainal et al. (2001) and Melger et al. (2007)*, the equilibrium modelling approach gave reasonable predictions for the gasification process in a downdraft gasifier. Similarly the equilibrium

model by *Rutherford (2006)* also gave predictions in close agreement with measured data from a commercial updraft fixed bed gasifier. However, the model developed by *Rutherford (2006)* did not perform well for small scale (100 kW) FICFB gasifier. The limitation and inconsistency results of equilibrium model facilitate the need for kinetic model especially at lower temperatures.

However, it is known that the thermodynamic equilibrium may not be achieved mainly because of the relatively low operation temperatures (producer gas outlet temperatures between 750-1000°C) for air gasification *(Bridgwater, 1995; Buekens and Schoeters, 1985)*. The equilibrium model has some limitations. In this type of model the carbon conversion is assumed to be 100% which is not true in actual gasification process and hence a kinetic model is preferred. At low reaction temperatures the reactions rates are slow and thus the reactions cannot reach equilibrium with limited residence time. Therefore, the kinetic modelling is more suitable and accurate at moderate (<800°C) operating temperatures of the gasifier *(Altafini et al., 2003)*. At higher temperatures (>1200°C) when the reaction rate is high, the equilibrium model is more appropriate.

2.7.2 Kinetic modelling

Kinetic models provide essential information on kinetic mechanisms to describe the chemical reactions involved in the biomass gasification, which is crucial in designing, evaluating and improving gasifiers. These models are based on the chemical reaction rates and are able to predict both overall and profiles of producer gas yield and compositions with time and location within the gasifier. However, as the models involve a number of reactions and transfer process, the models are computationally intensive *(Sharma, 2008)*. Nevertheless, several researchers have made comprehensive study on kinetic models of biomass gasification with varied degrees of complicity, accuracy and adaptability to different reactor configuration *(Babu and Sheth, 2006; Damartzis et al., 2012; Di Blasi, 2000; Fiaschi and Michelini, 2001; Giltrap et al., 2003; Gómez-Barea et al., 2007; Nikoo and Mahinpey, 2008; Radmanesh et al., 2006; Wang and Kinoshita, 1993)*.

In the kinetics models, reaction kinetics is needed for each reaction involved. In addition, the models should be solved simultaneously with separate models of bed hydrodynamics and models of mass and energy balances to obtain the producer gas yield, gas composition and char conversion at different operating conditions. The reactions kinetic rate expressions can

be obtained from experiments or from semi-empirical correlations. *De Souza-Santos (2004)* has given a comprehensive account of the modelling of BFB gasifiers using essentially the two-phase theory of fluidization. Due to the lack on the necessary data in steam gasification process, many of the modelling parameters in the published models have been derived from coal gasification studies *(Macak and Malecha, 1978; Yan et al., 1998).*

The kinetics for the biomass gasification reactions vary with the biomass type and gasification agent used *(Biba et al., 1978; Gil et al., 1999; Radmanesh et al., 2006; Wurzenberger et al., 2002)*. As discussed earlier during the gasification operation in a fluidized bed, the biomass firstly undergoes pyrolysis decomposing into volatile gases mainly constituting CO_2, CO, H_2, CH_4, high molecular weight of hydrocarbon gases (defined as tars) and char *(Lv et al., 2004a; Wurzenberger et al., 2002)*. The initial pyrolysis is followed by the gasification reactions or also called secondary reactions among the evolved gases, gasification agent and char. Most important reactions considered in gasification of biomass are the Water Gas-Shift reaction, Methanation reaction, Bouduard reaction, Char Steam Gasification reaction and Steam Methane Reforming reaction as considered by many researchers. The reported rate kinetics for each of these reactions varied with the fuel type chosen and the operation conditions.

The next step of modelling involves combining kinetics of reaction with the reactor hydrodynamics. The approach for reactor modelling may be divided into two broad groups *(Nemtsov and Zabaniotou, 2008).*

- Single particle model
- Fluidized bed reactor model

In the first approach the modeler follows what happens to the fuel particle as it goes through different physical and chemical conversion processes in the gasifier (*Dupont et al., 2011; Gómez-Barea et al., 2007; Pröll and Hofbauer, 2008; Xu et al. 2011a, 2011b)*. Here the gas-phase is described as a continuum *(Enwald et al., 1996; Nemtsov and Zabaniotou, 2008)*. The first approach is to predict reaction rate data which can be used in the reactor scale modelling in the second approach. The second approach, on the other hand, considers the reactor volume and it could even work with average condition of the gasifying particle. The present review concentrates on fluidized bed reactor models.

The kinetic modelling of fluidized bed gasifiers requires several assumptions or sub-models. These include the sub-model for fluidization, the mode of gas flow through the fluidized bed and how the char particle changes with conversion. Each of these sub-models is described in the following sections.

2.7.2.1 *Fluidization model*

The fluidized bed is a complex process of gas-solid interaction; however, the interaction dominates the heat and mass transfer between the gas phase and the solid phase which, in turn, affects the gas composition and reaction rates. Though progresses have been made in application of CFD software for modelling of fluid hydrodynamics, the mechanistic models are still widely employed in the modelling of hydrodynamics in the gasification. Earlier researchers modelled fluidized bed reactors by treating both the gas and solids particles as a well-mixed phase, avoiding the multiphase nature of the bed. In the gasification kinetics modelling, classical methods of reaction engineering were applied as for modelling of either the simplest completely-stirred and ideal plug-flow reactors to the state of turbulent mixing flow reactor. In these model, flow profiles as a function of time can be predicted and validated by tracer experiments *(Reman, 1955)*. However, these models are unable to describe all aspects of the fluidized bed behaviour which involves gas and solid. Therefore, in order to maintain the effects of fluid dynamics characteristics of gas-solid system, the concept of dividing the flow regimes in the fluidized bed reactor into two regions or phases was introduced by *Toomey and Johnstone (1952)* and isknown as two-phase theory of fluidization. Here in this context the term 'phase' differs from the thermodynamic consideration of state of matter. The regions in a two-phase theory of fluidization are divided into bubble phase flow and emulsion phase flow. Here the emulsion phase considers all the solid particles and a fraction of the gas which is perfectly and uniformly mixed and is said to remain in incipient fluidization condition, whereas the bubble phase contains only the gas phase and is considered to be in plug-flow.

Later comprehensive two-phase models for BFB combustion coupled with hydrodynamics were developed by *Horio and Wen (1977)* as cited in *Overend et al. (1985)*. In this fluidized bed model the key factors taken into account were the contact time of the gas with the solid reactant and hydrodynamics parameters such as minimum fluidization velocity, voidage at minimum fluidization and the terminal velocity *(Kunii and Levenspiel, 1991)*. The two phase

model was further improved by Davidson and his colleagues *(Davidson et al., 1985)* by incorporating semi empirical relationships to estimate the gas flow between the bubble and emulsion phases, the gas fraction occupied by bubbles in the bed, the porosity, and the velocity and size of the bubbles. The transport rates of heat and mass of the reacting particles and the degree of gas and solid mixing are determined from the flow pattern obtained from these semi empirical relationships.

Modifications and simplifications have been made over the last decades on the fluidization models for various reaction systems *(Gidaspow, 1994; Gidaspow et al., 1992; Grace, 1990; Gururajan et al., 1992; Kunii and Levenspiel, 1991; Nemtsov and Zabaniotou, 2008)*. These models are commonly referred to by the names of the authors: Davidson–Harrison model (DHM) *(Davidson et al., 1985)* and Kunii–Levenspiel model (KLM) *(Kunii and Levenspiel, 1991)*. However, there are no fundamental differences between these two models which are all based on empirical or semi-empirical correlations to estimate hydrodynamics parameters (such as bubble velocity and diameter, fraction of bubbles in the bed, velocity of gas in emulsion, minimum fluidization velocity, voidage at minimum fluidization, termial velocity and bubble to emulsion heat and mass transfer coefficient).

The gasification process in the fluidized bed gasifier is more complicated than that in the fixed bed gasifier. In view of this complexity in modelling the fluidized bed gasification process, different mechanisms for heat and mass transfer in the bubble and in the emulsion phases are considered separately. The mass transfers between the gases in the bubble and emulsion phase are due to molecular diffusion driven by the concentration differences of the gases between the regions and by convective mass flow. The convective mass transfer is considered to be dominant in the bubble phase which is caused by the combination effect of the biomass devolatilization and heterogeneous and homogeneous reactions. These reactions generate gases in excess of the requirement for maintaining the incipient fluidization condition from emulsion to bubble phase. In the emulsion phase, molecular diffusion is more dominant as the gas flow is much lower than that in the bubble phase *(Yan et al., 1998)*.

2.7.2.2 *Reaction models*

The rates of gasification reactions in a gasifier have been modelling in various ways, but the models are broadly classified under three approaches: volumetric reaction rate model, shrinking core model and the shrinking particle model. Volumetric reaction rate model

expresses the gasification or combustion reaction rate on the unit volume of the bed basis thus it is employed for modelling of the gasification process at the gasifier scale. On the other hand, the shrinking core model reaction occurs at the surface and the ash formed remains attached to the particle, retaining its size and becomes an additional resistance to mass and heat transfer. The zone of reaction moves into the solids by diffusing through gas film surrounding the particle and the ash layer while its interior is gasified or combusted depending on the gasification agent, thus its density decreases through the char conversion reaction. The shrinking core model is used for modelling of gasification of a single solid particle *(Fiaschi and Michelini, 2001; Lee et al., 1998; Nikoo and Mahinpey, 2008; Xu et al. 2011b)*. In this model, first the reacting gas diffuses through the outer skin of the particle as reaction occurs. The reaction layer then moves into the interior of the solid particle, leaving behind completely converted material and inert solid. *Ishida and Wen (1971) and Wen (1968)* on the basis of the studies of numerous systems, conclude that the shrinking core model is the best simple representation for the single particles, although they do not precisely represent the whole mechanism of gas–solid reactions and can be accurate when the reaction is slow *(Fiaschi and Michelini, 2001)*. Detailed shrinking core model is elaborated by *Levenspiel (1999)*.

The third model, the shrinking particle model, considers that the reactions are confined at the surface of the particle where the abrasion in a fluidized bed is sufficient aggressive to break down the char and ash particles and the size of the particle is reduced by gasification or pyrolysis of the products. In this model two mechanisms responsible for the global reaction rate are considered: diffusion through the gas film surrounding the shrinking particle, and intrinsic chemical kinetics. As a consequence of the heterogeneous reactions, the particle diameter shrinks and the density of the bed (and porosity) remains constant, causing a gradual decrease in the solid velocity *(Hobbs et al., 1993)*.

2.7.2.3 *Reaction model in BFB*

De Souza-Santos (1989) developed one of the earliest and moderately comprehensive BFB models considering the reactions in the bottom dense zone and in dilute zone on the top called freeboard. The dense zone in the bubbling bed consists of both emulsion and bubble phases whereas the freeboard is a region above the bed in the gasifier which constitutes only gas phase reactions in a plug flow with small fractions of solids carried away upwards from

the bed due to incipient velocity. The model is generalized for application to both combustion and gasification of coal or biomass. However the model was validated only for coal combustion in a boiler. The author subsequently developed a comprehensive 1D model to simulate steady state gasification process in a fluidized bed gasifier from which gas composition, bed temperature, particle size distribution, heat transfer and pressure loss were predicted at any point in bed. The model is primarily based on mass and energy balance as well as the heterogeneous gasification reactions. These reactions were formulated by integrated shrinking core model and shrinking particle model *(Yoon et al., 1978, Fiaschi and Michelini, 2001)*.

Sadaka et al. (2002) applied the two-phase model for gasification in a BFB gasifier to predict the performance of air-steam gasification of biomass under dynamic and steady state operations. The gasifier was divided into three zones: jetting, bubbling and slugging. Each zone constitutes two-phases (bubble and emulsion) and mass and heat transfers within these phases were implemented. The free energy minimization technique was used in this model to calculate the gas mole fractions. This model can predict the temperature and product distribution along the height of the bed in both bubble and emulsion phases, the quantity, and composition and heating value of the producer gas. *Nemtsov and Zabaniotou (2008)* recently present a summary of such modelling efforts for BFB gasifier.

2.7.2.4 *Reaction model in CFB*

CFB technology has been used in coal and petroleum industry successfully for more than two decades but its application for commercial biomass gasification is still in the early stage. A 1D model for gasification of woody biomass in a CFB was developed by *Jennen et al. (1999)* where the lower dense bed was treated similar to a BFB, and was modelled according to the two phase theory i.e. bubble and emulsion phase. The bubble phase (rich in gas) was modelled as plug flow while the emulsion phase (rich in solids) was modelled as a uniform mixture. The freeboard in the upper bed used core annulus structure. Both gas and solids flow upwards in a dilute suspension in the core where gasification reactions take place. Simultaneously, some solid particles flow down through the annulus in dense suspension, carrying little gas with it. There is, however, continuous gas and solid exchange between the core and annulus. Drying and devolatilization of the biomass is generally considered to be complete in the lower bed. In this model, the initial pyrolysis was modelled in two steps: in

the first step primary tar and volatiles were set free, and in the second step, the primary tar reacted with intermediate gases and char to produce secondary tar and gases. Simultaneous occurrence of gasification reactions and pyrolysis reactions was considered. The authors (*Jennen et al., 1999)* reported that the predicted composition, pressure and temperature from the proposed model agreed well with their experimental results.

Similar modelling approach has been made recently for the gasification process in a CFB gasifier where the bed is divided into two parts: dense bubbling bed at the bottom and a core-annulus type dilute bed at the top *(Adánez et al., 2003;Corella and Sanz, 2005; Petersen and Werther, 2005b; Tsui and Wu, 2003)*. In their CFB models of *Corella and Sanz, (2005)* and *Petersen and Werther, (2005b)*, the char is well mixed in the bottom bed, differences in concentration and particle-size distribution may arise in the freeboard. Hence the efficiency of carbon conversion and the tar content of the gas may greatly depend on the movement of solids and gas in bed and freeboard. In the mathematical model developed by *Adánezet al, (2003)* for the performance of the combustion of pine wood chips in CFB boilers, the sub-models such as hydrodynamics, woodchip drying and devolatilization, volatiles combustion, and char combustion occurring in the different regions were analyzed. In their attempt, they showed that a population balance on devolatilization of biomass particles seems to be essential for the detailed analysis which was obtained experimentally from the feed biomass distribution. The model developed shows a better agreement between experimental results. In conclusion, the behaviour of fuel particles (such as density, size, and volatile content) and the location of the feeder where the conversion process in an FB depend greatly on the relative rates of mixing (solids and gases) and reaction.

2.7.3 Gasification model embedded into CFD model

The CFD model could have an important role in the modelling of gasification process in a fluidized bed gasifier. The CFD modelling of fluidized bed gasification involves conservation of mass, momentum, species and energy over a defined domain or region represented by a matrix mesh, and the CFD model can be integrated into a gasification reaction model. With the CFD tool, the equations involved can be defined in the CFD element matrix, where fluxes of above quantities moving in and out of the control domain are considered with suitable boundary conditions.

Using the CFD tool all the changes and reactions in the gasification, such as vaporization of biomass particle, its pyrolysis (devolatilization), gasification reactions *(Babu and Chaurasia, 2004; Di Blasi, 1998a)* could be incorporated as a set of sub-modules for solving using a solver. Furthermore it is possible to couple the modules with transport phenomenon especially in case of fluidized bed gasifier. The hydrodynamic or transport phenomenon for any flow situation is completely defined by Navier-Stokes equation. But in case of turbulent flow its solution becomes difficult. A complete time dependent solution of the instantaneous Navier-Stokes equation is beyond the computation capabilities of the CFD model at the moment *(Wang and Yan, 2008)*. Reynolds averaged Navier-Stokes (ke) model or large eddy simulations filters are two means for taking account of the turbulence in the flow. The drag force on a single spherical particle has been widely studied *(Bird et al., 2002; Gibilaro, 2001)*. However, when a single particle moves in a dispersed two-phase flow, the drag force is affected by the surrounding particles. Correlations for calculating the momentum exchange coefficient of gas–solid systems have been reported in the literature, such as the models of *Gidaspow (1994), Syamlal and O'Brien (1989) and Wen and Yu (1966).*

CFD model has been applied to fluidized bed gasifier over the last few years for coal gasification in BFB *(Chejne and Hernandez, 2002)*, CFB *(Gräbner et al., 2007)*, and spouted bed gasifiers *(Deng et al., 2008; Du et al., 2006; Gao et al., 2006).* However, most of the reported CFD models were used in simulation of gasification in an entrained flow gasifier both for coal *(Chen et al., 2001; Wang and Yan, 2008)* and for biomass *(Fletcher et al., 2000)* because the solids flow is more disperse and this application is computationally less expensive.

There is an apparent lack of information on employing the CFD tool for biomass gasification in a BFB gasifier *(Wang and Yan, 2008)* and in a CFB gasifier. Generally modelling of gasifier with the CFD is computationally complicated and hence most of the models available are based on other techniques rather than CFD. In contrast to fluidized bed gasification, a great deal of models has been published applying CFD to simulate fluidized bed boilers burning biomass and wastes *(Ravelli et al., 2008)*. Some efforts have also been made to use CFD to model pyrolysis in fluidized bed *(Papadikis et al., 2009)*.

The hydrodynamics of the fluid bed are dealt in detail in a CFD model in a way that differs from normal fluid flow. In the fluidized bed CFD modelling, the momentum equations are solved for the gas and the solids phases separately. The gas phase is described by a

continuum approach, adopting an Eulerian framework and modelled similarly to the modelling of single phase flow with an additional term, accounting for the interaction with the solid phase. The choice of turbulence model in the gas phase is a key issue. CFD models for the gas-solid flow can be described by two distinct approaches: Eulerian–Eulerian model approach and Lagrangian Eulerian model approach. If the solid phase is treated as a continuum, an Eulerian framework is applied to describe the motion of the solids, called Eulerian–Eulerian model (EEM) *(Enwald et al., 1996)*. Lagrangian-Eulerian models (LEM) considers the particle size changes and other variables as a function of time, using the particle motion equations in a natural way by tracking each individual particle with its physical properties *(Oevermann et al., 2008)*. The Lagrangian approach describes the solid phase at a particle level and the gas phase as a continuum. On the other hand the Eulerian-Eulerian model is based on two fluid models that treat each phase as continuum. In the Lagrangian-Eulerian models, either the discrete element method (DEM) or discrete particle method (DPM) is commonly applied, motivated by molecular dynamics. Finite difference, finite element and finite volume are three discretization methods used for Eulerian-Eulerian model. Several equations with semi-empirical parameters have to be solved simultaneously. The kinetic theory of granular flow (KTGF) is used in the two-fluid model to simulate particle collision for closure. Computational modelling of the Eulerian-Eulerian model formulation using KTGFs is less intensive than using Lagrangian approach for the fluidized bed simulations *(Papadikis et al., 2008)*. A comparative analysis of CFD models for fluidized bed has been made *(Van Wachem et al., 2001).*

This Eulerian-Eulerian approach is the most accurate than the mixture model and is commonly used for predicting the dynamic behaviour of the fluid particle systems *(ANSYS FLUENT12.0., 2009).* The particulate phase is treated as a continuum with an effective viscosity, and thus the method is also called *two-fluid* approach. Due to the significant increase in computing power of recent years, these models have now made computational modelling of multiphase granular flows possible, though it is still very challenging, particularly so for industrial scale reactor units. The discrete phase is applied to the particle flow and continuous phase to the gas. Both Euler-Euler and Euler-Lagrange approaches to model wood gasification in a BFB were applied *(Oevermann et al., 2008)*, and based on their preliminary results they found both approaches to have comparable agreement with experiments.

Finally simplifications are needed also for CFD solutions, and experimental validation is necessary before using the models with confidence *(Grace and Taghipour, 2004)*. Recent efforts in numerical solution and modelling of complex gas-solid interaction have been made attempting to close the gaps between the CFD simulation with integration of chemical reactions and the practical phenomena. If successful, it could provide a powerful tool for optimization and even design of thermo-chemical reactors like gasifier *(Wang and Yan, 2008)*. Particle-particle interaction and gas-particle interaction of CFD modelling are especially at high solid concentration as prevalent in fluidized beds is still a major challenge. Several models were developed to predict the formation of bubbles and their motion around the bed. Some of these models show qualitative agreement with observed behaviour. But prediction of the complete behaviour of a BFB from first principle is yet to be achieved.

Models developed by several investigators used sophisticated reaction kinetics and complex particle-particle interaction. Yet most of them had to use some sub-models, fitting parameters or major assumption in areas where precise information were not available. Such weak links in the long array make the final result susceptible to the accuracy. Thereafter the CFD model can predict the behaviour of that gasifier over a range of parameters from which the needed data for the CFD modelling are experimentally measured. However, the CFD mode can be inaccurate if this CFD model is used beyond the above range of conditions or for a different gasifier. CFD for fluidized bed gasification are relatively new, and in spite of offering promising expectation, much has to be added. Finally, zero dimensional models are quite useful in some cases, but the treatment is limited and the prediction capability is lower than that of reaction kinetics fluid model and CFD models. CFD model computation becomes tedious when modelling the actual component using 2D or 3D; Because of the considerable computational times required for CFD computations, especially when chemical reactions are involved, reaction kinetics fluid model are still the most common approach.

2.7.4 Neural network

An alternative to the sophisticated modelling of a complex process especially where the process is not fully understood is to use Artificial Neural Networks (ANN) approach. ANN has been extensively used in the fields of pattern recognition; signal processing, function approximation and process simulation. ANN cannot produce an analytical solution, but provides useful results. *Guo et al. (2001)* used Hybrid Neural Network (HNN) technique to

model biomass gasification for a steam fluidized bed gasifier to predict gas yield and composition from gasification of four biomasses: bagasse, cotton stem, pine sawdust and poplar. The data obtained from these experiments were used to train the HNN model. Accuracy of the prediction model can be improved by adding more training samples for each of this biomass, which can easily be achieved using ANN.

In this model, the dynamic performance of the gasification process is derived from first principles. However the most crucial parameter to this modelling approach, the transient production rate of gas species from unit mass of biomass, with which one can predict the gasification process of a biomass under certain conditions, is not measurable and the Multilayer feed Forward Neural Network (MFNN) is used to identify the gasification profiles for each biomass. In this network the comprehensive production rate of the individual gas species both from pyrolysis of biomass and the subsequent gasification reactions, on the basis of unit mass of biomass is a function of gasification time and gasification temperature. These comprehensively generated production rates of individual gas species are transient production rates used as training data. The neural networks must be trained with the experimental data before they could reasonably identify transient production rate of individual gas species for a given biomass. The training was done not by comparing the outputs of the neural network with the "desired outputs", but by comparing the model prediction with the previous known set of experimental data. This was because the "desired outputs" of the neural networks, which were the real comprehensive production rates of four major gas species, were not measurable in the experiment. Training of the networks was conducted by comparing the model predicted production rate of each gas species in the gasification runs, with those corresponding data measured in the experiment.

Xiao et al. (2009) have used ANN with the MATLAB Neural Network Toolbox to model gasification characteristics of MSW. The model predicted results were consistent with the experimental data for the gas production rates of the biomass gasification processes. This method is able to deal with complex gasification problems. ANN model, once gathered experience through training with data, can perform predictions at high speed using architecture of multiple hidden layers. The ANN architecture is broadly composed of three layers of neurons: 1) to receive the input(s), 2) process them and 3) deliver output(s). In this network when the training process satisfies the required tolerance, network holds the weights constant and uses the network to make output predictions. Back propagation algorithm is used to perform the learning of network. Multilayer feed forward neural networks are used to

approximate the function. Neural network may return poor results for data that differ from the original data which the neural network was trained. This happens sometimes when limited data are available to calibrate and evaluate the constants of the model *(Hajek and Judd, 1995)*.

2.8 Char reactivity

In biomass gasification, char reactivity is defined as char conversion rate per unit mass or per unit surface area of the formed chars is an important factor to be considered during modelling of any type of gasifier. There is larger number of models developed for reactivity of coal-based chars, and only recently *Xu et al. (2011a)* reported reactivity of biomass char, coal char and chars of blended biomass and coal. In literature, so, it has been a common practice to use coal char data for modelling biomass gasification, even though there are some intrinsic differences between the coal char and the biomass char due to the nature of the biomass fuels *(Ross et al., 2004)*. Biomass chars vary greatly in porosity, directionality, and catalytic activity. Therefore, caution should be exerted in applying expressions from one char to another *(Buekens and Schoeters, 1985)*. Biomass char has an important distinguishing feature. The reactivity of char from fossil fuels such as coal, lignite decreases with conversion or time while that of biomass generally increases with conversion and is much higher than that of coal-char *(Scott et al., 2005, Xu et al., 2011a)*. For this reason *Liu and Gibbs (2003)* used reactivity data for coal-char for biomass but multiplied it with an empirical factor from 1 to 10.

The rate of char conversion is influenced by variables, such as temperature, partial pressure of the gasifying reactants and products, particle size, porosity, and mineral content of the char, some of which vary with time due to chemical conversion and attrition. Therefore, char reactivity is also influenced by gasification conditions including temperature, pressure, nature of the gasification agent (O_2, CO_2, H_2O, H_2) and the degree of conversion. The dependence of the char reactivity on the concentrations of the reactants CO_2 and H_2O and on the temperature can be represented by Langmuir–Hinshelwood kinetics, which is based on surface mechanisms, especially when inhibition by the products (CO and H_2) must be taken into account *(Barrio and Hustad, 2008; Ollero et al., 2003)*. Char reactivity depends on the parent fuel and on the form of preparation, especially the heating rate and peak temperature *(Luo et al., 2001)*. The reactivity of coal chars varies widely depending on the rank of the parent coal.

Langmuir–Hinshelwood kinetics obtained by *Matsui et al. (1987)* for coal chars were used to model char gasification of sewage sludge in a CFB *(Petersen and Werther, 2005a, b)*. The same assumption was adopted in another biomass model *(Liu and Gibbs, 2003)* where char kinetics for gasification of coal in a jetting FB gasifier *(Luo et al., 1998)* were employed.

In the model developed for downdraft gasifier *(Babu and Sheth, 2006; Giltrap et al., 2003),* the char reactivity factor is the key parameter representing the reactivity of the char in the reduction zone. In their simulation study, char reactivity factor was varied from 1 to 10,000 both linearly and exponentially, and the model established was found to work properly. The porous char formed during the devolatilization process in steam gasification of lignin, a higher heating rate significantly increases both the reactivity of lignin char and its final conversion *(Fushimi et al., 2003)*.The reactivity of biomass char with CO_2 in a bench-scale fluidized bed reactor shows that the char reactivity increases with heating rate and temperature *(Gómez-Barea et al., 2006; Luo et al., 2001)*.

2.9. Performance of biomass gasifiers

The performance of biomass gasifiers could be characterized by parameters of producer gas yield, gasification efficiency and producer gas composition which directly influence the heating value of the gas. The composition of the producer gas obtained from any type of gasifier depends on a number of parameters, such as fuel composition, gasifying medium, operating pressure, temperature, moisture content of the fuels, gasifier design and hence prediction of the producer gas composition is not an easy task *(Basu, 2006)*. *Gil et al. (1997), Herguido et al. (1992) and Narvaez et al. (1996)* carried experimental research on biomass gasification in atmospheric BFB gasifiers under similar conditions but using different gasification agents of air, steam and steam-O_2 mixture, respectively, as shown in Table 2.4 *(Gil et al., 1999)*. All of these gasification agents can be represented by two parameters: (1) equivalent ratio (ER) which is defined as the ratio of air required for stoichiometric combustion to that actually added; and (2) S/B ratio which is defined as the ratio of water input (including that in the biomass and gasification agent) to the fed biomass. The above studies show that as the S/B ratio is increased, H_2 and CO_2 contents in the producer gas increase and the CO content decreases. Similarly methane content and C_2-hydrocarbons content decrease as the S/B increases. This behaviour is due to gasification reactions of Water-Gas Shift, partial oxidation and steam reforming. Using steam as gasification agent,

the H_2-content in the gas is the maximum (around 55 vol%) for S/B ratios of 0.8±0.9 kg/kg daf.

Table 2.4: Operation conditions and producer gas compositions for biomass gasification in atmospheric BFB gasifiers *(Gil et al., 1999)*

Gasification agents	Air *(Narvaez et al., 1996)*	Steam (pure) *(Herguido et al., 1992)*	Steam–O_2 mixture *(Gil et al., 1997)*
ER	0.18–0.45	0	0.24–0.51
S/B (kg/kg daf)	0.08–0.66	0.53–1.10	0.48–1.11
T (^oC)	780–830	750–780	785–830
Gas composition(vol%, dry basis)			
H_2	5.0–16.3	38–56	13.8–31.7
CO	9.9–22.4	17–32	42.5–52.0
CO_2	9.0–19.4	13–17	14.4–36.3
CH_4	2.2–6.2	7–12	6.0–7.5
C_2H_n	0.2–3.3	2.1–2.3	2.5–3.6
N_2	41.6–61.6	0	0
Steam	11–34	52–60	38–61
Yields			
Tars (g/kg daf)	3.7–61.9	60–95	2.2–46
Char (g/kg daf)	Na	95–110	5–20
Gas (Nm^3/kg daf)	1.25–2.45	1.3–1.6	0.86–1.14
LHV (MJ/Nm^3)	3.7–8.4	12.2–13.8	10.3–13.5

na: not available; daf: dry ash-free basis; ER: equivalence ratio;

Prins et al. (2007) and Ptasinski (2008) have focused their studies on the efficiency of biomass gasification which is based on energy (lower heating value, LHV) (Equation 2.25) or exergy (chemical, and chemical and physical, exergy) (Equation 2.26).

$$Energy\ efficiency\ \eta = \left(n_{gas}.Mw_g\right).\ LHV_{gas}/(M_{wood}.\ LHV_{wood}) \quad (2.25)$$

$$Exergy\ efficiency\ \psi = \frac{n_{gas}.\left(e_{ch,gas}+e_{ph,gas}\right)}{\left(\frac{M_{wood}}{Mw_{wood}}\right)e_{ch,biomass}+n_{gasification\ media}.e_{gasification\ media}} \quad (2.26)$$

where n_{gas} is the molar number of the producer gas *(kmol);* $n_{gasification\ media}$ is the molar number of the gasification media *(kmol);* M_{wood} is the mass of the woody biomass *(kg);* Mw_{wood} is the molecular weight of biomass *(kg/kmol);* Mw_g is the molecular weight of producer gas *(kg/kmol);* $e_{ch,gas}$ is the chemical exergy of the producer gas *(kJ/kmol);* $e_{ph,gas}$ is the physical exergy of the producer gas *(kJ/kmol);* $e_{ch,biomass}$ is the chemical

exergy of the biomass *(kJ/kmol)*; $e_{gasification\ media}$ is the specific molar exergy of air *(kJ/kmol)*. In Equation (2.25), LHV_{gas} and LHV_{wood} are the lower heating value of producer gas and that of the woody biomass, respectively.

*Ptasinski (2008)*analyzed the efficiency of biomass gasification using the triangular C–H–O diagram and found the exergetic efficiency of air blown biomass gasification to be 80.5% while for gasification with steam, the optimal gasification occurs at the S/B ratio of 1.30 kg/kg resulting in an overall exergetic efficiency of 87.6%. Steam gasification is thus more efficient than the air gasification, provided the exergy losses during steam production are minimized. The exergetic efficiency of gasification also depends on the chemical composition of the solid fuel used as feedstock. Efficiency based on chemical exergy is higher for coal than for the biomass. The same trends can be observed for gasification efficiencies based on chemical and physical exergy. Because coal is gasified at higher temperatures, their gasification efficiencies are much improved by the inclusion of the physical exergy. These results assume that gasification reaction rates are fast enough and residence time is long enough for the equilibrium state to be reached.

2.10 Conclusions

Various mathematical models have been reported for simulation of gasification process in a fluidized bed gasifier and these models include equilibrium models, kinetics models, gasification models embedded in the CFD model and neural network based models. Each type of these models has its advantages and disadvantages as the models have different approaches to handle the complicated process involving hydrodynamics, heat and mass transfer, and various chemical reactions.

The artificial neural network based models fundamentally uses the experimental knowledge based on the operating conditions to make intellectual estimation and possible effect of change in reasonable operating range is applicable only if experimental data are available. The equilibrium model on the other hand predicts the maximum achievable yield or gas composition for a set of operating parameters. Though the equilibrium model only predicts the final gas composition in a thermodynamically equilibrium state, the possible gasification reactions involved in the gasifier can be predicted by comparing the net gas species formed

from the two different approaches of equilibrium models: the stoichiometric model and non-stoichiometric model.

The fluidized bed reactor kinetic rate model combines kinetics of reaction of biomass gasification with the reactor hydrodynamics, mass and energy balances. This model predicts the progress and product composition at different positions along a reactor and over time in one dimension. It is understood that the kinetic rates depend on the fuel type the gasification agent and the operating conditions mainly temperature and pressure. Though many researchers have developed mathematical models for fluidized bed gasifier based either on one continuum flow or the two-fluid theory, the kinetics rate adapted follows that of fossil fuels which leads to uncertainty. From the literature survey it was studied that the product yields of biomass gasification in a fluidized bed gasifier were affected mainly by two factors: operating temperature and mixing effect of solid and gas in the bed. To counteract the effect of temperature, the reaction kinetics of the biomass gasification process is controlled by the Arrhenius type temperature dependence mechanism and hydrodynamic closure correlations. Hence in this research work attempts have been made to use the Arrhenius type rate kinetics of biomass esp. derived from gasification of *Pinus radiate* with steam by *Wang and Kinoshita, (1993)* under similar operating conditions as that of the model developed. On the other hand the mixing effect of solids and gases were handled with the two phase (emulsion and bubble phase) model accounting for mass and energy balance, with the semi-empirical hydrodynamic relationship was developed which give proper closures for chemical reactor modelling.

In this literature review fields for further research have been identified. In the biomass gasification process the initial stage of biomass decomposition called the pyrolysis under high temperature is recognized as the processes that require major modelling efforts. Though the pyrolysis process is well defined by various researchers, a reliable kinetics is limited under the definite operating conditions and they varied from biomass to biomass and from coal to coal. Most of the fluidized bed models still treat the pyrolysis stage of the gasification process in a semi-empirical way with the correlation of coal kinetics or product distribution function derived from the coal kinetics. Much has to be done to develop reliable computational models. Hence in this work, the need for a definite kinetics of biomass pyrolysis is developed in terms of product distribution function from the experiments conducted in a 100kW DFB gasifier. The product distribution function describing the char reduction process in pyrolysis

obtained from experiments permit better simulation of the experimental data where the residence time of gas and biomass is relatively short.

The gasification embedded CFD model provides as a tool to understand the hydrodynamics characteristics better and the gas composition across the cross section and along the height of bed for biomass–steam gasification. Unlike the fluidized bed reactor kinetic rate model, they are computationally intensive and hence in this research it is limited with simple two-dimensional model. In the CFD modelling Eulerian-Eulerian model formulation using KTGF is based on two-fluid model that treats each phase as continuum is less intensive and more accurate compared with Lagrangian-Eulerian modelling approach. Hence in this work it is necessary to use an Eulerian modelling approach to simulate hydrodynamics of fluidization and the reactions were modelled by the laminar finite-rate model with Arrhenius kinetics. Models developed for coal gasification are not necessarily applicable to biomass gasification in a fluidized bed unless suitable modifications are made. The major obstacle is to correctly fit the kinetic parameters on experimental observation, which is able to depict a wide range of operating cases.

Though the knowledge of the chemistry of tar generation and conversion has to be significantly improved over the last few decades, the focus on tar kinetics in this model has been neglected considering the operating temperature range is high where the concentration of tar obtained is lower.

As the critical operating parameters in a fluidized bed gasifier, the gasification agent, fuel type and size also have a strong influence on the gasification reaction. To optimize the gasification process, the sensitivity study is carried out on developed model by varying model parameters such as S/B ratio and operating temperature to find the best combination for the desired result.

2.11 References

Altafini, C.R., Wander, P.R., Barreto, R.M., 2003. Prediction of the working parameters of a wood waste gasifier through an equilibrium model. Energy Conversion and Management 44, 2763–2777.

ANSYS FLUENT12.0., 2009. Theory Guide. ANSYS, Inc.

Babu, B.V., Chaurasia, A.S., 2003. Modeling for pyrolysis of solid particle: kinetics and heat transfer effects. Energy Conversion and Management 44, 2251-2275.

Babu, B.V., Chaurasia, A.S., 2004. Pyrolysis of biomass: improved models for simultaneous kinetics and transport of heat, mass and momentum. Energy Conversion and Management 45, 1297-1327.

Babu, B.V., Sheth, P.N., 2006. Modeling and simulation of reduction zone of downdraft biomass gasifier: Effect of char reactivity factor. Energy Conversion and Management 47, 2602-2611.

Barrio, M., Hustad, J.E., 2008. CO2 Gasification of Birch Char and the Effect of CO Inhibition on the Calculation of Chemical Kinetics. Blackwell Science Ltd.

Basu, P., 2006. Combustion and Gasification in Fluidized Beds. CRC Press.

Biagini, E., Cioni, M., Tognotti, L., 2005. Development and characterization of a lab-scale entrained flow reactor for testing biomass fuels. Fuel 84, 1524-1534.

Biba, V., Macak, J., Klose, E., Malecha, J., 1978. Mathematical model for gasification of coal under pressure. Industrial & Engineering Chemistry Process Design and Development 17, 92-98.

Bilbao, R., Mastral, J.F., Ceamanos, J., Aldea, M.E., 1996. Modelling of the pyrolysis of wet wood. Journal of Analytical and Applied Pyrolysis 36, 81-97.

Bird, R.B., Stewart, W.E., Lightfoot, E.N., 2002. Transport Phenomena, second ed. Wiley, New York.

Bridgeman, T.G., Jones, J.M., Shield, I., Williams, P.T., 2008. Torrefaction of reed canary grass, wheat straw and willow to enhance solid fuel qualities and combustion properties. Fuel 87, 844-856.

Bridgwater, A.V., 1995. The technical and economic feasibility of biomass gasification for power generation. Fuel 74, 631-653.

Bridgwater, A.V., Peacocke, G.V.C., 2000. Fast pyrolysis processes for biomass. Renewable and Sustainable Energy Reviews 4, 1-73.

Bridgwater, A.V., 2003. Renewable fuels and chemicals by thermal processing of biomass. Chemical Engineering Journal 91, 87-102.

Bryden, K., Ragland, K., 1996. Numerical modeling of a deep, fixed bed combustor. Energy Fuels 10, 269-275.

Buekens, A.G., Schoeters, J.G., 1985. Modeling of biomass gasification., in: Overend, R.P., Milne, T.A., Mudge, K.L. (Eds.), Fundamentals of Thermochemical Biomass Conversion. Elsevier Applied Science Publishers, London, UK, pp. 619-689.

Bull, D.R., 2008. Performance Improvements to a Fast Internally Circulating Fluidised Bed (FICFB) Biomass Gasifier for Combined Heat and Power Plants University of Canterbury, New Zealand

Capart, R., Elamin, A., Ammar, S., Gelus., M., 1989. Survey of biomass liquefaction., in: G. L- Ferrero, K. Maniatis, A. Buekens, Bridgwater, A.V. (Eds.), Pyrolysis and Gasification. Elsevier Applied Science, London, UK, pp. 158- 168.

Caputo, A.C., Palumbo, M., Pelagagge, P.M., Scacchia, F., 2005. Economics of biomass energy utilization in combustion and gasification plants:effects of logistic variables. Biomass and Bioenergy 28, 35–51.

Chejne, F., Hernandez, J.P., 2002. Modelling and simulation of coal gasification process in fluidised bed. Fuel 81, 1687-1702.

Chen, C., Horio, M., Kojima, T., 2001. Use of numerical modeling in the design and scale-up of entrained flow coal gasifiers. Fuel 80, 1513-1523.

Corella, J., Aznar, M.P., Delgado, J., Aldea, E., 1991. Steam Gasification of Cellulosic Wastes in a Fluidized Bed with Downstream Vessels. Industrial & Engineering Chemistry Research 30, 2252-2262.

Corella, J., Sanz, A., 2005. Modeling circulating fluidized bed biomass gasifiers. A pseudo-rigorous model for stationary state. Fuel Processing Technology 86, 1021–1053.

Cui, H., Grace, J.R., 2008. Spouting of biomass particles: A review. Bioresource Technology 99, 4008-4020.

Damartzis, T., Michailos, S., Zabaniotou, A., 2012. Energetic assessment of a combined heat and power integrated biomass gasification–internal combustion engine system by using Aspen Plus®. Fuel Processing Technology 95, 37-44.

Davidson, J.F., Clift, R., Harrison, D., 1985. Fluidization. Orlando : Academic Press, London

De Diego, L.F., Garcia-Labiano, F., Abad, A., Gayan, P., Adanez, J., 2002. Modeling of the devolatilization of nonspherical wet pine wood particles in fluidized beds. Industrial & Engineering Chemistry Research 41, 3642-3650.

De Souza-Santos, M.L., 1989. Comprehensive modelling and simulation of fluidized bed boilers and gasifiers. Fuel 68, 1507-1521.

De Souza-Santos, M.L., 2004. Solid Fuels Combustion and Gasification. Marcell Dekker, New York.

Deng, Z., Xiao, R., Jin, B., Huang, H., Shen, L., Song, Q., Li, Q., 2008. Computational fluid dynamics modeling of coal gasification in a pressurized spout fluid bed. Energy & Fuels 22, 1560-1569.

Desrosiers, R., 1981. Thermodynamics of gas-char reactions., in: Reed, T.B. (Ed.), Biomass Gasification - Principles and Technology. Park Ridge, New York, pp. 119-153.

Di Blasi, C., 1996. Kinetic and heat transfer control in the slow and flash pyrolysis of solids. Ind. Eng. Chem. Res. 35, 37-46.

Di Blasi, C., 1998a. Comparison of semi global mechanisms for primary pyrolysis of lignocellulosic fuels. Journal of Analytical and Applied Pyrolysis 47, 43-64.

Di Blasi, C., 1998b. Multiphase moisture transfer in the high temperature drying of wood particles. Chemical Engineering Science 53, 353-366.

Di Blasi, C., 2000. Dynamic behaviour of stratified downdraft gasifiers. Chemical Engineering Science 55, 2931-2944.

Di Blasi, C., 2008. Modeling chemical and physical processes of wood and biomass pyrolysis. Progress in Energy and Combustion Science 34, 47-90.

Di Blasi, C., Branca, C., Santoro, A., Gonzalez Hernandez, E., 2001. Pyrolytic behavior and products of some wood varieties. Combustion and Flame 124, 165-177.

Dornburg, V., Faaij, A.P.C., 2001. Efficiency and economy of wood-fired biomass energy systems in relation to scale regarding heat and power generation using combustion and gasification technologies. Biomass and Bioenergy 21, 91-108.

Du, W., Bao, X., Xu, J., Wei, W., 2006. Computational fluid dynamics (CFD) modeling of spouted bed: Assessment of drag coefficient correlations. Chemical Engineering Science 61, 1401-1420.

Dupont, C., Nocquet, T., Da Costa Jr, J.A., Verne-Tournon, C., 2011. Kinetic modelling of steam gasification of various woody biomass chars: Influence of inorganic elements. Bioresource Technology 102, 9743-9748.

Ebeling, J.M., Jenkins, B.M., 1985. Physical and chemical properties of biomass fuels. Transactions of the American Society of Agricultural Engineers 28, 898-902.

Enwald, H., Peirano, E., Almstedt, A.E., 1996. Eulerian two-phase flow theory applied to fluidization. International Journal of Multiphase Flow 22, 21-66.

Epstein, N., Grace, J.R., 1997. Spouting of particulate solids, Handbook of Powder Science and Technology, 2nd ed. Chapman & Hall, New York.

Fiaschi, D., Michelini, M., 2001. A two-phase one-dimensional biomass gasification kinetics model. Biomass and Bioenergy 21, 121-132.

Fletcher, D.F., Haynes, B.S., Christo, F.C., Joseph, S.D., 2000. A CFD based combustion model of an entrained flow biomass gasifier. Applied Mathematical Modelling 24, 165-182.

Font, R., A. Marcilla, E. Verdu, Devesa., J., 1989. Chemicals from almond shells by pyrolysis in fiuidized bed, in: G. L- Ferrero, K. Maniatis, A. Buekens, Bridgwater, A.V. (Eds.), Pyrolysis and Gasification. Elsevier Applied Science, London, UK, pp. 230-237.

Franco, C., Pinto, F., Gulyurtlu, I., Cabrita, I., 2003. The study of reactions influencing the biomass steam gasification process. Fuel 82, 835-842.

Fushimi, C., Araki, K., Yamaguchi, Y., Tsutsumi, A., 2003. Effect of heating rate on steam gasification of biomass. 1. Reactivity of char. Industrial & Engineering Chemistry Research 42, 3922-3928.

Galgano, A., Di Blasi, C., 2004. Modeling the propagation of drying and decomposition fronts in wood. Combustion and Flame 139, 16-27.

Garcı´a. L. , M. L. Salvador, J. Arauzo, Bilbao, R., 1999. Catalytic Steam Gasification of Pine Sawdust. Effect of Catalyst Weight/Biomass Flow Rate and Steam/Biomass Ratios on Gas Production and Composition. Energy and Fuels 13.

Gao, K., Wu, J., Wang, Y., Zhang, D.-k., 2006. Bubble dynamics and its effect on the performance of a jet fluidised bed gasifier simulated using CFD. Fuel 85, 1221-1231.

GEK, 03May 2011. Gasifier Experimenters Kit (GEK).[Online]. Accessed Retrived on 03rd May 2011, Available:http://www.gekgasifier.com/gasification-basics/gasifier-types/

Gibilaro, L.G., 2001. "Fluidization Dynamics", 1st edition ed. Butterworth-Heinemann; 1st edition (November 21, 2001)

Gidaspow, D., 1994. Multiphase Flow and Fluidization: Continuum and Kinetic Theory Descriptions. Academic Press (21 Feb 1994).

Gidaspow, D., Bezburuah, R., Ding., J., 1992. Hydrodynamics of circulating fluidized beds, kinetic theory approach. Fluidization VII, Proceedings of the Seventh Engineering Foundation Conference on Fluidization, 75–82.

Gil, J., Aznar, M.P., Caballero, M.A., Francés, E., Corella, J., 1997. Biomass Gasification in Fluidized Bed at Pilot Scale with Steam−Oxygen Mixtures. Product Distribution for Very Different Operating Conditions. Energy & Fuels 11, 1109-1118.

Gil, J., Corella, J., Aznar, M.P., Caballero, M.A., 1999. Biomass gasification in atmospheric and bubbling fluidized bed: Effect of the type of gasifying agent on the product distribution. Biomass and Bioenergy 17, 389-403.

Giltrap, D.L., McKibbin, R., Barnes, G.R.G., 2003. A steady state model of gas-char reactions in a downdraft biomass gasifier. Solar Energy 74, 85-91.

Gómez-Barea, A., Leckner, B., Ollero, P., Fernández-Baco, C., Salvador, L., 2006. Reduction of Physical Effects during Reactivity Tests in Fluidized Bed. Industrial & Engineering Chemistry Research 45, 7344-7350.

Gómez-Barea, A., Ollero, P., Leckner, B., 2007. Mass transport effects during measurements of gas-solid reaction kinetics in a fluidised bed. Chemical Engineering Science 62, 1477-1493.

Gräbner, M., Ogriseck, S., Meyer, B., 2007. Numerical simulation of coal gasification at circulating fluidised bed conditions. Fuel Processing Technology 88, 948-958.

Graboski, M., 1981. Kinetics of char gasification reactions, in: Reed, T.B. (Ed.), Biomass Gasification - Principles and Technology. Park Ridge, New York, pp. 154-182.

Grace, J.R., 1990. High velocity fluidized bed reactors. Chemical Engineering Science 45, 1953-1966.

Grace, J.R., Taghipour, F., 2004. Verification and validation of CFD models and dynamic similarity for fluidized beds. Powder Technology 139, 99-110.

Gray, M.R., Corcoran, W.H., Gavalas, G.R., 1985. Pyrolysis of a wood derived material - Effects of moisture and ash content. Industrial & Engineering Chemistry Process Design and Development 24, 646-651.

Guo, B., Li, D., Cheng, C., Lü, Z.-a., Shen, Y., 2001. Simulation of biomass gasification with a hybrid neural network model. Bioresource Technology 76, 77-83.

Gururajan, V.S., P.K.Agarwal, J.B.Agnew, 1992. Mathematical modelling of fluidized bed coal gasifiers. Trans IChem E 70, 211-238.

Herguido, J., Corella, J., Gonzalez-Saiz, J., 1992. Steam gasification of lignocellulosic residues in a fluidized bed at a small pilot scale. Effect of the type of feedstock. Industrial & Engineering Chemistry Research 31, 1274-1282.

Hajek, M., Judd, M.R., 1995. Use of neural networks in modelling the interactions between gas analysers at coal gasifiers. Fuel 74, 1347-1351.

Higman, C., Van der Burgt, M., 2003. Gasification. Elsevier.

Hobbs, M.L., Radulovic, P.T., Smoot, L.D., 1993. Combustion and gasification of coals in fixed-beds. Progress in Energy and Combustion Science 19, 505-586.

Hofbauer, H., Veronik, G., Fleck, T., Rauch, R., MacKinger, H., Fercher, E., 1997. The FICFB - gasification process. Developments in Thermochemical Biomass conversion 2, 1016-1025.

Hofbauer, H., Reinhard, R., Klaus, B., Reinhard, K., Christian, A., 2002. Biomass CHP Plant Güssing – A Success Story, Expert Meeting on Pyrolysis and Gasification of Biomass and Waste. Renet-Austria, Vienna, Stasbourg, France.

Hon, D.N.-S., Shiraishi., N., 2001. Wood and Cellulosic Chemistry in: David N.-S. Hon, N.S. (Ed.), 2nd Edition ed. CRC Press, Marcel Dekker, New York.

Ishida, M., Wen, C.Y., 1971. Comparison of zone reaction model and unreacted core shrinking model in solid-gas reactions--I Isothermal analysis. Chemical Engineering Science 26, 1031-1041.

Janse, A.M.C., de Jonge, H.G., Prins, W., van Swaaij, W.P.M., 1998. Combustion kinetics of char obtained by flash pyrolysis of pine wood. Industrial & Engineering Chemistry Research 37, 3909-3918.

Janse, A.M.C., Westerhout, R.W.J., Prins, W., 2000. Modelling of flash pyrolysis of single wood particle. Chemical Engineering and Processing 39, 239-252.

Jarungthammachote, S., Dutta, A., 2007. Thermodynamic equilibrium model and second law analysis of a downdraft waste gasifier. Energy (Oxford) 32, 1660-1669.

Jarungthammachote, S., Dutta, A., 2008. Equilibrium modeling of gasification: Gibbs free energy minimization approach and its application to spouted bed and spout-fluid bed gasifiers. Energy Conversion and Management 49, 1345-1356.

Jayah, T.H., Aye, L., Fuller, R.J., Stewart, D.F., 2003. Computer simulation of a downdraft wood gasifier for tea drying. Biomass and Bioenergy 25, 459-469.

Kim, Y.J., Lee, J.M., Kim, S.D., 2000. Modeling of coal gasification in an internally circulating fluidized bed reactor with draught tube. Fuel 79, 69-77.

Klass, D.L., 1998. Biomass for Renewable Energy, Fuels, and Chemicals. Academic Press, San Diego.

Knoef, H., 2000. Inventory of biomass gasifier manufacturers and installations, Final Report to European. Commission, Contract DIS/1734/98-NL,. University of Twente, Enschede.

Kunii, D., Levenspiel, O., 1991. Fluidization Engineering, Second Edition ed. Butterworth-Heinemann.

Lee, J.M., Kim, Y.J., Lee, W.J., Kim, S.D., 1998. Coal gasification kinetics derived from pyrolysis in a fluidized-bed reactor. Energy 23, 475-488.

Levenspiel, O., 1999. Chemical Reaction Engineering (3rd Edition). John Wiley & Sons.

Li, X., Grace, J.R., Watkinson, A.P., Lim, C.J., Ergüdenler, A., 2001. Equilibrium modeling of gasification: A free energy minimization approach and its application to a circulating fluidized bed coal gasifier. Fuel 80, 195-207.

Li, X.T., Grace, J.R., Lim, C.J., Watkinson, A.P., Chen, H.P., Kim, J.R., 2004. Biomass gasification in a circulating fluidized bed. Biomass and Bioenergy 26, 171-193.

Liu, H., Gibbs, B.M., 2003. Modeling NH3 and HCN emissions from biomass circulating fluidized bed gasifiers. Fuel 82, 1591-1604.

Luo, C.-H., Aoki, K., Uemiya, S., Kojima, T., 1998. Numerical modeling of a jetting fluidized bed gasifier and the comparison with the experimental data. Fuel Processing Technology 55, 193–218.

Luo, C., Watanabe, T., Nakamura, M., Uemiya, S., Kojima, T., 2001. Gasification kinetics of coal chars carbonized under rapid and slow heating conditions at elevated temperatures. Journal of Energy Resources Technology 123, 21-26.

Lv, P., Chang, J., Wang, T., Wu, C., Tsubaki, N., 2004a. A kinetic study on biomass fast catalytic pyrolysis. Energy & Fuels 18, 1865-1869.

Lv, P.M., Xiong, Z.H., Chang, J., Wu, C.Z., Chen, Y., Zhu, J.X., 2004b. An experimental study on biomass air–steam gasification in a fluidized bed. Bioresource Technology 95, 95-101.

Macak, J., Malecha, J., 1978. Mathematical model for the gasification of coal under pressure. Industrial & Engineering Chemistry Process Design and Development 17, 92-98.

Maniatis, K., A V. Bridgwater, Buekens., A., 1989. Fluidized bed gasification of wood: Performance of a demonstration plant., in: G. L- Ferrero, K. Maniatis, A. Buekens,

Bridgwater, A.V. (Eds.), Pyrolysis and Gasification. Elsevier Applied Science, London, UK, pp. 274-281.

Matsui, I., Kunii, D., Furusawa, T., 1987. Study of char gasification by carbon dioxide. 1. Kinetic study by thermogravimetric analysis. Industrial & Engineering Chemistry Research 26, 91-95.

Melgar, A., Pe´rez, J.F., Laget, H., Horillo, A., 2007. Thermochemical equilibrium modelling of a gasifying process. Energy Conversion and Management 48, 59–67.

Miller, R.S., Bellan, J., 1997. A generalized biomass pyrolysis model based on superimposed cellulose, hemicellulose and lignin kinetics. Combustion Science and Technology 126, 97 - 137.

Mohan, D., Pittman, C.U., Steele, P.H., 2006. Pyrolysis of wood/biomass for bio-oil: A critical review. Energy & Fuels 20, 848-889.

Murakami, T., Xu, G., Suda, T., Matsuzawa, Y., Tani, H., Fujimori, T., 2007. Some process fundamentals of biomass gasification in dual fluidized bed. Fuel 86, 244-255.

Nikoo, M.B., Mahinpey, N., 2008. Simulation of biomass gasification in fluidized bed reactor using ASPEN PLUS. Biomass and Bioenergy 32, 1245-1254.

Narvaez, I., Orio, A., Aznar, M.P., Corella, J., 1996. Biomass Gasification with Air in an Atmospheric Bubbling Fluidized Bed. Effect of Six Operational Variables on the Quality of Produced Raw Gas. Industrial and Engineering Chemistry 35, 2110-2120.

NETL, 2012. Texaco Entrained Flow Gasifier.(Online). Retrived on 27thJanuary 2012, Available:http://www.netl.doe.gov/technologies/coalpower/gasification/pubs/photo.html

Nemtsov, D.A., Zabaniotou, A., 2008. Mathematical modelling and simulation approaches of agricultural residues air gasification in a bubbling fluidized bed reactor. Chemical Engineering Journal 143, 10-31.

Nordgreen, T., Liliedahl, T., Sjöström, K., 2006. Elemental Iron as a tar breakdown catalyst in conjunction with atmospheric fluidized bed gasification of biomass: A thermodynamic study. Energy & Fuels 20, 890-895.

Oevermann, M., Gerber, S., Behrendt, F., 2008. Euler-Euler and Euler-Lagrange modeling of wood gasification in fluidized beds. Proceedings of 9th Circulating Fluidized Bed Technology;.

Ollero, P., Serrera, A., Arjona, R., Alcantarilla, S., 2003. The CO2 gasification kinetics of olive residue. Biomass and Bioenergy 24, 151-161.

Overend, R.P., T.A.Milne, L.K.Mudge, 1985. Fundamentals of Thermochemical Biomass Conversion. Elsevier Applied Science Publishers.

Papadikis, K., Bridgwater, A.V., Gu, S., 2008. CFD modelling of the fast pyrolysis of biomass in fluidised bed reactors, Part A: Eulerian computation of momentum transport in bubbling fluidised beds. Chemical Engineering Science 63, 4218-4227.

Papadikis, K., Gu, S., Bridgwater, A.V., Gerhauser, H., 2009. Application of CFD to model fast pyrolysis of biomass. Fuel Processing Technology 90, 504-512.

Petersen, I., Werther, J., 2005a. Experimental investigation and modeling of gasification of sewage sludge in the circulating fluidized bed. Chemical Engineering and Processing 44, 717-736.

Petersen, I., Werther, J., 2005b. Three-dimensional modeling of a circulating fluidized bed gasifier for sewage sludge. Chemical Engineering Science 60, 4469-4484.

Prasad, B.V.R.K., Kuester, J.L., 1988. Process Analysis of a Dual Fluidized Bed Biomass Gasification System. Industrial & Engineering Chemistry Research 27, 304-310.

Prins, M.J., Ptasinski, K.J., J. J. G. Janssen, F., 2003. Thermodynamics of gas-char reactions: first and second law analysis. Chemical Engineering Science 58, 1003-1011.

Prins, M.J., Ptasinski, K.J., Janssen, F.J.J.G., 2007. From coal to biomass gasification: Comparison of thermodynamic efficiency. Energy 32, 1248-1259.

Pröll, T., Hofbauer, H., 2008. H2 rich syngas by selective CO2 removal from biomass gasification in a dual fluidized bed system — Process modelling approach. Fuel Processing Technology 89, 1207-1217.

Ptasinski, K.J., 2008. Thermodynamic efficiency of biomass gasification and biofuels conversion. Biofuels, Bioproducts and Biorefining 2, 239-253.

Ramin Radmanesh, Chaouki, J., Guy, C., 2006. Biomass gasification in a bubbling fluidized bed reactor: Experiments and modeling. AIChE Journal 52, 4258-4272.

Rapagnà, S., Jand, N., Kiennemann, A., Foscolo, P.U., 2000. Steam gasification of biomass in a fluidised bed of olivine particles. Biomass and Bioenergy 19, 187-197.

Ravelli, S., Perdichizzi, A., Barigozzi, G., 2008. Description, applications and numerical modelling of bubbling fluidized bed combustion in waste-to-energy plants. Progress in Energy and Combustion Science 34, 224-253.

Reed, T.B., 1981. Biomass Gasification: Principles and Technology. Noyes Publications

Reman, G.H., 1955. Effect of gas and solid mixing in fluidized beds on chemical reactions., Chemistry & Industry, London, pp. 46-51.

Rezaiyan, J., Cheremisinoff, N.P., 2005. Gasification Technologies - A Primer for Engineers and Scientists. CRC Press Taylor & Francis Group.

Ross, D.P., Yan, H.-m., Zhang, D.-k., 2004. Modelling of a laboratory-scale bubbling fluidised-bed gasifier with feeds of both char and propane. Fuel 83, 1979-1990.

Rowell, R.M., 2005. Handbook of Wood Chemistry and Wood Composites. CRC Press, Boca Raton, Florida.

Ruggiero, M., Manfrida, G., 1999. An equilibrium model for biomass gasification processes. Renewable Energy 16, 1106-1109.

Rutherford, J., 2006. Heat and power applications of advanced biomass gasifiers in New Zealand's wood industry., Chemical and Process Engineering. University of Canterbury, Christchurch.

Sadaka, S.S., Ghaly, A.E., Sabbah, M.A., 2002. Two phase biomass air-steam gasification model for fluidized bed reactors: Part I--model development. Biomass and Bioenergy 22, 439-462.

Saw, W., McKinnon, H., Gilmour, I. and Pang, S. 2011. Production of hydrogen-rich syngas from steam gasification of blend of biosolids and wood using a dual fluidised bed gasifier. Fuel (2011), doi:10.1016/j.fuel.2011.08.047

Schuster, G., Löffler, G., Weigl, K., Hofbauer, H., 2001. Biomass steam gasification - An extensive parametric modeling study. Bioresource Technology 77, 71-79.

Scott, S.A., Davidson, J.F., Dennis, J.S., Fennell, P.S., Hayhurst, A.N., 2005. The rate of gasification by CO2 of chars from waste. Proceedings of the Combustion Institute 30, 2151-2159.

Serdar, Y., 2004. Pyrolysis of biomass to produce fuels and chemical feedstocks. Energy Conversion and Management 45, 651-671.

Sharma, A.K., 2008. Equilibrium and kinetic modeling of char reduction reactions in a downdraft biomass gasifier: A comparison. Solar Energy 82, 918-928.

Sheng, C., Azevedo, J.L.T., 2005. Estimating the higher heating value of biomass fuels from basic analysis data. Biomass and Bioenergy 28, 499-507.

Smith, J.M., Van Ness, H.C., Abbott, M.M., 2001. Introduction to Chemical Engineering Thermodynamics, Sixth ed. ed. McGraw-Hill International, Singapore.

Smoot, L., Smith, P., 1985. Coal Combustion and Gasification. Plenum Press, New York.

Syamlal, M., O'Brien, T.J., 1989. Computer simulation of bubbles in a fluidized bed. AIChE Symp. Series 85, 22-31.

Speight, J.G., 2011. The Biofuels Handbook. Royal Society of Chemistry, Cambridge.

Thunman, H., Niklasson, F., Johnsson, F., Leckner, B., 2001. Composition of volatile gases and thermochemical properties of wood for modeling of fixed or fluidized beds. Energy & Fuels 15, 1488-1497.

Thurner, F., Mann, U., 1981. Kinetic investigation of wood pyrolysis. Industrial & Engineering Chemistry Process Design and Development 20, 482-488.

Toomey, R.D., Johnstone, H.F., 1952. Gaseous fluidization of solid particles. Chemical Engineering Progress 48, 220-226.

Tsui, H., Wu, C.-H., 2003. Operating concept of circulating fluidized bed gasifier from the kinetic point of view. Powder Technology 132, 167-183.

Van Wachem, B.G.M., Schouten, J.C., van den Bleek, C.M., Krishna, R., Sinclair, J.L., 2001. Comparative analysis of CFD models of dense gas–solid systems. AIChE Journal 47, 1035-1051.

Wagenaar, M., Prins, W., Vanswaaij, W.P.M., 1993. Flash pyrolysis kinetics of pine wood. Fuel Processing Technology 36, 291-298.

Waldheim, L., Nilsson, T., 2001. Heating value of gases from biomass gasification, in: IEA-Bioenergy (Ed.), Task 20 -Thermal Gasification of Biomass. TPS Termiska Processer AB, p. 60.

Walker Jr, P.L., Rusinko Jr, F., Austin, L.G., 1959. Gas reactions of carbon, in: D.D. Eley, P.W.S., Paul, B.W. (Eds.), Advances in Catalysis. Academic Press, pp. 133-221.

Wang, Y., Kinoshita, C.M., 1993. Kinetic model of biomass gasification. Solar Energy 51, 19-25.

Wang, Y., Yan, L., 2008. CFD studies on biomass thermochemical conversion. International Journal of Molecular Sciences 9, 1108-1130.

Wen, C.-Y., Yu, Y.H., 1966. Mechanics of fluidization. Chem. Eng. Prog. Symp.Series 62, 100-111.Wen, C.Y., 1968. Non catalytic heterogeneous solid-fluid reaction models. Industrial & Engineering Chemistry 60, 34-54.

Westbrook, C., Dryer, F., 1984. Chemical kinetic modeling of hydrocarbon combustion. Progress Energy Combust Science 10, 1-57.

Wurzenberger, J.C., Wallner, S., Raupenstrauch, H., Khinast, J.G., 2002. Thermal conversion of biomass: Comprehensive reactor and particle modeling. AIChE Journal 48, 2398-2411.

Xu, G., Murakami, T., Suda, T., Matsuzaw, Y., Tani, H., 2009. Two-stage dual fluidized bed gasification: Its conception and application to biomass. Fuel Processing Technology 90, 137-144.

Xu, Q., Pang, S. and Levi, T. 2011a. Reaction kinetics and producer gas compositions of steam gasification of coal and biomass blend chars, part 1: Experimental investigation. *Chemical Engineering Science,* 66: 2141-2148.

Xu, Q., Pang, S. and Levi, T. 2011b. Reaction kinetics and producer gas compositions of steam gasification of coal and biomass blend chars, part 2: Mathematical modelling and model validation. *Chemical Engineering Science*, 66: 2232-2240.

Xiao, G., Ni, M.-j., Chi, Y., Jin, B.-s., Xiao, R., Zhong, Z.-p., Huang, Y.-j., 2009. Gasification characteristics of MSW and an ANN prediction model. Waste Management 29, 240-244.

Yan, H.-m., Heidenreich, C., Zhang, D.-k., 1998. Mathematical modelling of a bubbling fluidised-bed coal gasifier and the significance of 'net flow'. Fuel 77, 1067-1079.

Yoon, H., Wei, J., Denn, M.M., 1978. A model for moving-bed coal gasification reactors. AIChE Journal 24, 885-903.

Zainal, Z.A., Ali, R., Lean, C.H., Seetharamu, K.N., 2001. Prediction of performance of a downdraft gasifier using equilibrium modeling for different biomass materrials. Energy Conversion and Management 42, 1499-1515.

Chapter 3

One Dimensional Modelling of Biomass Gasification in Dual Fluidized Bed Gasifier

This chapter presents a 1D model for simulation of biomass gasification in a BFB gasifier which was the key part of the DFB gasifier system. In this chapter, the biomass gasification process was described as two a stage process: initial pyrolysis process followed by a gasification process in the BFB gasifier. The final gas composition of the produced fuel gas was affected by both processes. The model developed in this study included the kinetics in the pyrolysis and gasification reactions, equations for mass and energy transfer, and the equations for quantification of hydrodynamics. The main objective of the model was to calculate the gas composition at different operating conditions. Governing hydrodynamic equations for a bubbling bed and kinetic expressions for the gasification process were adopted from the literature. In addition the model incorporated two phase theory of gases and solids including the emulsion phase and the bubble phase. In the mass and energy conservation equations, inter-phase exchanges were also considered. Finally the numerical methods for solving the proposed model were described. A set of 14 highly non-linear partial differential equations (PDEs) were developed that describes the mass balances (5 Equations for the emulsion phase and the bubble phase each and a material balance equation for the solid char) and three energy balances (one for the solid char, bubble and emulsion phase). These PDEs were solved using 'pdepe' solver function from the PDE modules of Matlab software with properly defined initial and boundary conditions.

3.1 Introduction

The objective of this part of study was to develop a 1D mathematical model to predict producer gas composition and profiles in biomass gasification in a BFB gasifier under known operation conditions and then to examine the sensitivity of gasifier performance. The focus in this chapter was to develop the reaction models, and the mass and the energy balance equations. The reaction model incorporated the pyrolysis reaction kinetics and the gasification reaction kinetics. Later in chapter 6, the developed model was validated with

experimental data and, after the validation; the model was used to optimize the biomass gasification operation and to improve the gasifier design for producing producer gas with high calorific values.

Mathematical modelling of the fluidized bed biomass gasification process with steam as the gasification agent is a complex process, as properties of the biomass and the gas composition vary significantly through the bed in the gasifier. The reaction kinetics modelling requires a thorough understanding of both the hydrodynamics and the chemical reactions taking place inside the gasifier. Moreover numerical technique is needed to solve the developed model which involved a set of highly nonlinear differential equations. In the biomass gasification, a fundamental consideration is that the chemical energy of solid fuel and input gasification agent was converted into both thermal and chemical energy of the producer gas. As the chemical energy contained within the producer gas is a function of its chemical composition, the chemical composition of the producer gas determines its quality as a fuel. Producer gas with high concentrations of combustible gas species such as H_2, CO and CH_4 will have high calorific value which is the target for the gasification optimization. Reaction kinetics models can have varying levels of complexity depending on the number of dimensions in which flow is considered to occur, and the accuracy of heterogeneous and homogenous reaction rates in the model. Therefore this part of work was to develop a simple 1D flow pattern of a plug flow gasifier model on the reaction aspects of gasification. In the next chapter a detailed study on hydrodynamics model to understand the flow phenomenon in the BFB will be presented.

Figure 3.1 shows the DFB gasification system with steam as the gasification agent. The system consists of two columns, one being the CFB combustion reactor on the left hand side and the other BFB gasification reactor on the right hand side. In the CFB chamber, the solid char was combusted to supply heat to heat up the circulating bed material to a temperature in a range of 750 - 850°C. At the top of this chamber, the hot bed material and the flue gas were separated in a cyclone, and the hot bed material then drops to the BFB chamber to supply heat for the steam gasification of the biomass. The biomass was introduced into the BFB chamber at a given height from the bottom and this was done through a mechanically driven screw feeder. The biomass used was Radiata pine wood pellets, each having dimensions of about 1 cm long and 0.5 cm in diameter. The main positive feature of biomass wood pellets was that they were consistent and nearly uniform in shape which provides good mechanical flow characteristics. Once being fed to the gasifier, the biomass was quickly mixed with the

bed material, and was almost instantaneously heated up to the bed temperature (650 - 800°C). The steam was blown through the bed of solid particles from the bottom of the BFB chamber at a sufficient velocity to keep the particles in a state of suspension; it takes a fraction of a second before contacting with the biomass. As a result of this process, the biomass was pyrolysed very fast, resulting in a component mixture with a relatively large amount of gaseous materials (such as CO_2, CO, H_2, CH_4) and less quantity of char, tar and moisture. Further the gasification and the tar-conversion reactions occurred in the gas phase. However, in the developed model the tar conversion was neglected considering the low tar concentration and its slow reactions. In this chapter, a mathematical model to simulate the biomass steam gasification process in the BFB chamber in the DFB gasification system was developed as shown in Fig. 3.2. In the model, the initial pyrolysis reactions and the gasification reactions were considered and were modeled separately based on the reactions kinetics. The gasification operation conditions and biomass properties for the simulation are given in Table 3.1.

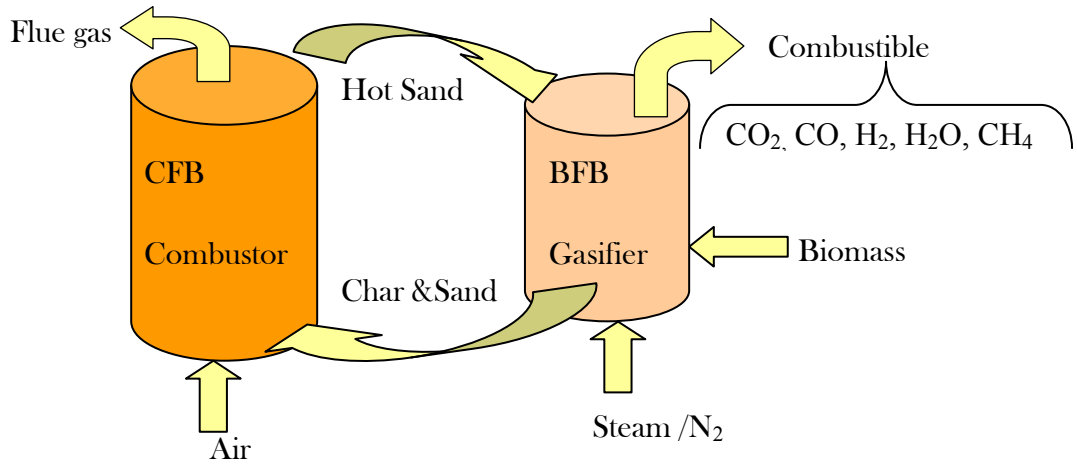

Figure 3.1: Sketch of the DFB gasification system with steam as gasification agent.

Table 3.1: Values of gasification operating conditions and biomass properties in the modelling of the biomass gasification in a BFB gasifier

Bed diameter (m)	0.02
Bed height (m)	0.2
BFB height (m)	2
Operating Pressure (Pa)	1.01×10^{5}
Operating bed temperature range (K)	953 to 1053
Biomass feed rate (kg/h)	15
Steam feed rate ranges (kg/h)	5 to 12.5
S/B ratio range	0.33 to 0.84
Pressure drop between CFB and BFB, ΔP_{mf} (Pa)	3.58×10^{3}
Particle size of bed material (m)	2.75×10^{-4}
Particle size of char (m)	2.00×10^{-3}
Terminal Velocity (m/s)	0.64
Superficial gas velocity (m/s)	0.22-0.56
Minimum fluidization velocity (m/s)	0.23
Biomass moisture content (%)	0-20
Bulk density of sand (kg/m^3)	1.60×10^{3}
Bulk density of biomass (kg/m^3)	3.60×10^{2}
Bulk density of char (kg/m^3)	1.08×10^{2}
Mass of sand in the BFB, m_{sand} (kg)	12
Circulation of sand in the BFB, $\dot{m}_{sand}$ (kg/h)	7.00×10^{2}
Fuel ultimate analysis [(c)]:	
C (% daf)	50.54
H (% daf)	7.08
O (% daf)	41.11

Note: [(c)] *(Nikoo and Mahinpey, 2008)*.

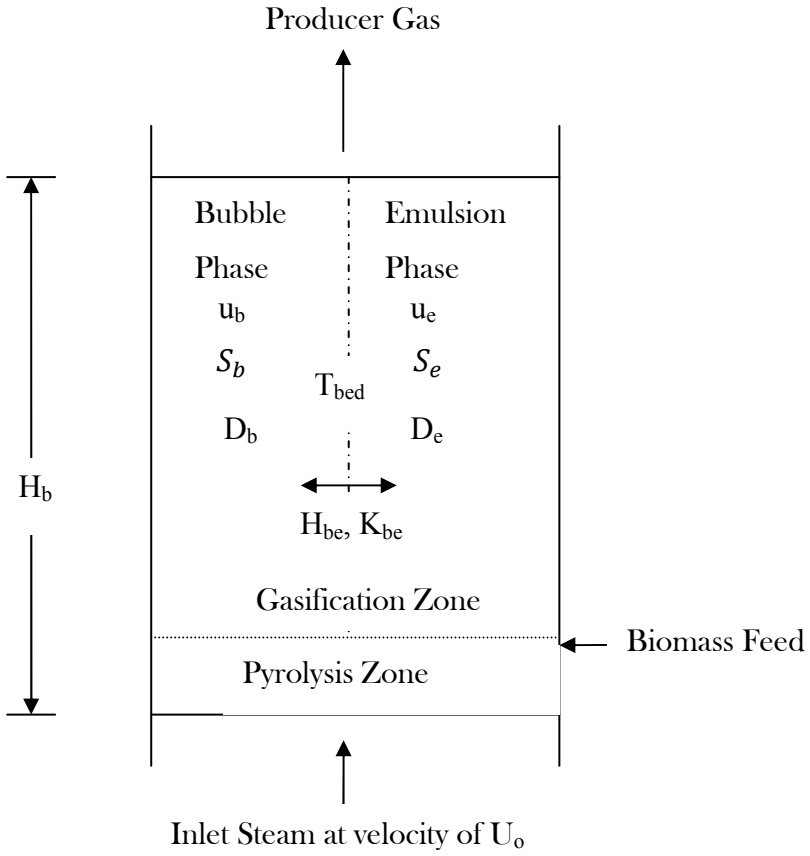

Figure 3.2: Illustration of steam gasification processes of biomass in a BFB.

3.2 Mathematical modelling of the biomass steam gasification

In a general gasifier, the overall gasification process can be divided into four zones or four processes: drying zone, pyrolysis zone, oxidation zone and reduction or gasification zone. However, in the steam gasification process, the oxidation reaction may not occur.

To develop the gasification model in a fluidized bed, chemical formula of biomass was defined as $CH_aO_b$where, a and b are the H/C and O/C mole ratio, respectively. In the initial stage of pyrolysis under high temperatures, the biomass was decomposed to form char, volatile gases and tar, while in the following gasification stage, reactions occur among the gasification agent (steam), volatile gases and char evolved from the first stage. The initial stage occurs in the pyrolysis zone at the bottom of the gasifier filled with bed material as shown in Figure 3.2. This stage is very fast within a fraction of a second *(Radmanesh et al., 2006)* inside the fluidized bed, however this pyrolysis process always occurs at the inlet of the feed when the biomass was first in contact with hot bed material.

3.2.1 Stage 1: Pyrolysis model

In the initial pyrolysis, the biomass was firstly decomposed which involves break-up of the molecular chains of cellulose, hemicelluloses and lignin. Then reactions occur among the decomposed products. A number of approaches have been reported to model this very complicated process although most were based on empirical observations. *Di Blasi* (2008) proposed a simple two-stage semi-global first order reaction kinetics models, based on the Broido-Shafizadeh decomposition mechanism, as shown in Figure.3.3.

During the thermal degradation under the operating and feed conditions as specified in the Table 3.1 for a BFB gasifier, volatiles gases, tar and char were formed initially in the pyrolysis reactions. This pyrolysis reaction kinetics was given by k_1, k_2 and k_3, respectively, according to *Chan et al. (1985)*. Following this in the pyrolysis process, some tar was cracked to form volatile gases (k_4) according to *Graham et al. (1994)* and to form char by repolymerisation (k_5) as described by *Chan et al.(1985)*. Using the above pyrolysis model as shown in Figure 3.3, the predicted product yields from the pyrolysis as a function of operation temperature were in close agreement with experimental data (*Di Blasi, 2008)*. In the biomass gasification model in this study, the reaction kinetics constants derived from *Di Blasi(2008)* were employed for the pyrolysis reactions which use Arrhenius reaction kinetics. The values of these parameters are listed in Table 3.2 for woody biomass.

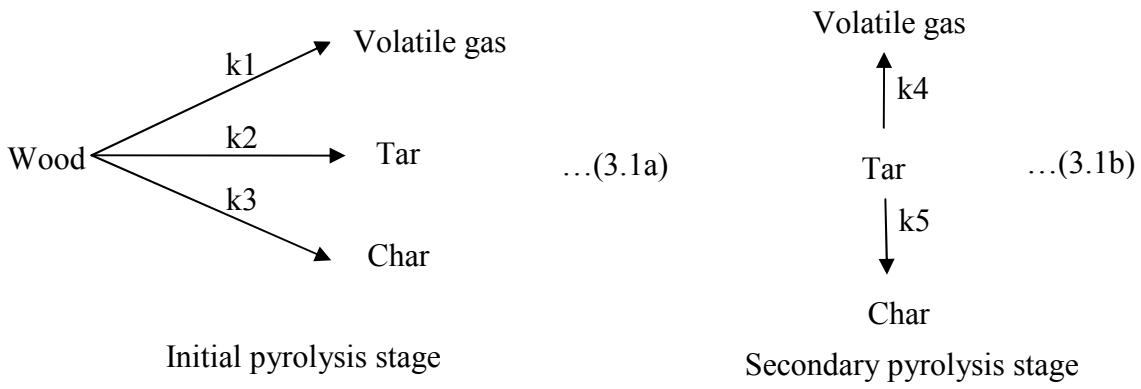

Figure 3.3: Broido-Shafizadeh model of pyrolysis of wood particles (Di Blasi, 2008).

Table 3.2: Arrhenius reaction kinetics for pyrolysis model for woody biomass *(Chan et al., 1985; Graham et al., 1994)*.

Reactions	Pre-exponential factor k_{0j} [1/s]	Activation Energy E_{Aj} [kJ/mol]
Wood → Volatile gas[(a)]	1.30×10^8	140
Wood → Tar[(a)]	2.00×10^8	133
Wood → Char[(a)]	1.08×10^7	121
Tar → Volatile gas [(b)]	1.10×10^6	100.8
Tar → Char [(a)]	1.48×10^6	144

Note: [(a)]*(Chan et al., 1985)* ,[(b)]*(Graham et al., 1994)*

In the pyrolysis reactions of biomass, some reactions are endothermic and the others are exothermic *(Bilbao et al., 1993; Di Blasi, 2002)*. For example, the primary char formation is an exothermic process, whereas tar formation and vaporization is an endothermic process *(Milosavljevic et al., 1996; Rath et al., 2003)*. In the secondary pyrolysis stage, the tar cracking is weakly exothermic process *(Di Blasi, 1994)*.

From the reaction network kinetics described in Figure 3.2, five reactions were involved. The rates of formation of char, gas and tar in the wood pyrolysis were given as follows:

$$\frac{\partial M_{wood}}{\partial t} = -(k_1 + k_2 + k_3)M_{wood} \tag{3.2}$$

$$\frac{\partial M_{char}}{\partial t} = k_3 M_{wood} + k_5 M_{tar} \tag{3.3}$$

$$\frac{\partial M_{tar}}{\partial t} = k_2 M_{wood} - k_4 M_{tar} - k_5 M_{tar} \tag{3.4}$$

$$\frac{\partial M_{volatile}}{\partial t} = k_1 M_{wood} + k_4 M_{tar} \tag{3.5}$$

where M_{wood} is the mass of woody biomass [kg], M_{char} is the mass of char [kg], M_{tar} is the mass of tar [kg] and $M_{volatile}$is the mass of gas [kg]. k_j is the rate constants of Arrhenius type reactions and were defined as:

$$k_j = k_{0j} exp\left(-E_{Aj}/(RT)\right) \tag{3.6}$$

in which k_{0j} is pre-exponential factor of the reaction *j*, E_{Aj} is the activation energy of the reaction *j*, R is the gas constant and T is the operating temperature. Using the values of

kinetic rate constants of *Chan et al.(1985) and Graham et al. (1994)* as given in Table 3.2*,* the above kinetic model was solved to predict the proportions of gas, tar and char as a function of pyrolysis temperature over time. As the pyrolysis reaction proceeds almost instantaneously at high temperatures and completes within a fraction of a second (at relatively faster rate), the temperature required in the Equation (3.6) was assumed to be equal to the operating temperature. Therefore, under the conditions of biomass gasification, the biomass fuels are likely to remain in the bed most of the pyrolysis time due to lower superficial velocity. The reaction time constant for overall pyrolysis is given as

$$\tau_p = \frac{1}{\frac{1}{k_{01}exp(E_{A1}/RT)}+\frac{1}{k_2exp(E_{A2}/RT)}+\frac{1}{k_3exp(E_{A3}/RT)}} \quad (3.7)$$

The volatiles formed from Broido-Shafizadeh decomposition mechanism of biomass particles were only the total gas and thus the individual gas composition was not known. For this reason, the above kinetics model was not suitable for the modeling of the overall gasification process.

The decomposition of volatile gases from the pyrolysis can also be modelled by other two different approaches, namely (i) non stoichiometric thermodynamic equilibrium model and (ii) an empirical function of product distribution based on experimental results obtained from pyrolysis of woody biomass in the BFB reactor.

3.2.1.a Non Stoichiometric Equilibrium Model for initial pyrolysis

In this research work, a simple equilibrium model was integrated with the biomass decomposition kinetics model to predict the product composition and the gas composition under the ideal equilibrium conditions. *Schuster et al. (2001),* who developed an equilibrium model for biomass steam gasification in a fluidized bed gasifier, concluded that although the accuracy of the equilibrium model was acceptable in some cases, the thermodynamic equilibrium may not be achieved, mainly due to the short reaction time and relatively low operation temperatures *(Bridgwater, 1995)*.

In the equilibrium model it was assumed that the volatile gases behave ideally and all reactions were at thermodynamic equilibrium at the end of the process. The volatile gases formed from the initial biomass decomposition reach equilibrium during the flow through the

char bed assuming that the pressure in the char bed was constant atmospheric pressure. As described in Chapter 2, the resistance to heat conduction and mass diffusion inside the char particles was not accounted in this model as the reactions proceed adiabatically. Perfect mixing and uniform temperature were assumed in the gasifier bed although different hydrodynamics were observed in practice, depending on the design of the gasifier. The tar and char formed in the initial biomass decomposition were assumed to be inactive compared to gases.

The non-stoichiometric equilibrium model was based on the fact that at equilibrium, the Gibbs free energy of the system is minimal for a specified temperature and pressure. The generalized reaction of biomass with air and steam as shown in Equation (2.15) earlier in Chapter 2 was modified for initial pyrolysis assuming that the biomass was thermally decomposed at high temperature (Equation 3.8) while the tar and char from the pyrolysis remained inactive.

$$[N_{wood}CH_aO_b] \xrightarrow{\Delta hightemp} \begin{bmatrix} N_{CO}CO + N_{CO_2}CO_2 + N_{H_2}H_2 + N_{CH_4}CH_4 \\ +N_{H_2O}H_2O + N_{CH_{0.2}O_{0.13}}CH_{0.2}O_{0.13} \end{bmatrix} \quad (3.8)$$

The quantities on the right hand sides of Equation (3.8) such as $N_{CO}, N_{CO_2}, N_{H_2}, N_{H_2O}$ *and* N_{CH_4} were the number of moles of the producer gas species. These producer gas species were unknown and required five equations to get them solved. Those equations were generated using mass/mole balance and the equilibrium constant relationships from the possible reactions involving these gas species. The molecular formula for char used in the model was $CH_{0.2}O_{0.13}$*(Corella and Sanz, 2005)*. The quantities of tar formed at the operating temperatures were significantly low and hence they were not included in the equilibrium model. Now considering the global pyrolysis reaction as in Equation (3.8), balances of carbon, hydrogen and oxygen were formulated as the following three equations:

Carbon Balance:

$$f_1 = 0 = N_{wood} - \left(N_{CO} + N_{CO_2} + N_{CH_4} + N_{CH_{0.2}O_{0.13}}\right) \quad (3.9)$$

Hydrogen Balance:

$$f_2 = 0 = aN_{wood} - \left(2N_{H_2O} + 2N_{H_2} + 4N_{CH_4} + 0.2N_{CH_{0.2}O_{0.13}}\right) \quad (3.10)$$

Oxygen Balance:

$$f_3 = 0 = bN_{wood} - \left(N_{H_2O} + N_{CO} + 2N_{CO_2} + 0.13N_{CH_{0.2}O_{0.13}}\right) \quad (3.11)$$

The non-stoichiometric equilibrium model does not need any particular reaction mechanism. According to Duhem's theorem the equilibrium state is completely determined by specifying any two independent variables, for a closed system formed initially from given masses of particular chemical species. The usual problem is to find the composition of the system that reaches equilibrium from an initial state of fixed amounts of reacting species when temperature and pressure are specified *(Smith et al., 2001)*. From the initial biomass decomposition, various products are formed and multiple reactions exists in the following pyrolysis.

In the modelling of the gas composition of each species of CO, CO_2, CH_4, H_2, H_2O, the required values of element number of gas species *k* (A_k) were determined from the initial numbers of moles which come directly from chemical formulas of the species. Using these values, a set of five equations for each species CO, CO_2, CH_4 , H_2, H_2O were formed to minimise the free energy at equilibrium as given below in Equation (3.12) *(Smith et al., 2001)*:

$$Componenti: \quad f_i = 0 = \frac{\Delta G_i^{\circ}}{RT} + ln\frac{N_i}{\sum_i N_i} + \frac{\sum_k \lambda_k a_{ik}}{RT} \quad (3.12)$$

where the subscript i of the function f_i ranges from 4 to 8 for the species components CO, CO_2, CH_4 , H_2, and H_2O . ΔG_i° is the standard Gibbs energy changes for formation of species *i* [kJ/kg]; a_{ik} is the number of atoms of *k* per molecule of species *i* and N_i is the number of moles of species *i* [mol] estimated from *Smith et al. (2001)*. λ_k is the unknown lagrange multiplier for each elements C, H and O. The values for lagrange multiplier will be evaluated in the model although they don't have any physical significance, but were included for the completeness to solve the equations.

Along with the five equations for each of individual gas species formed from Equation (3.12) and the three material balance Equations $(3.9 - 3.11)$ for the components of wood namely carbon, hydrogen and oxygen were solved simultaneously using '*fsolve'* solver in Matlab. The eight unknowns namely the five individual gas composition and three unknown lagrange multiplier for each elements C, H and O were found. The *fsolv*e solver attempts to solve those Equations $(3.9 - 3.12)$ of the form $f_i(x) = 0$, where f_i and x can be vectors or matrices. To solve these simultaneous equations using the *fsolve* solver function, *fsolve* solver takes in the set of nonlinear equations and appropriate guess values of unknown variables N_i

as input arguments to the calling function *fsolve*. The output arguments for these functions were the solved variables, function variable f_i and an '*exitflag'* which tell whether the solution was converged or not. The convergence criterion for the *fsolve* solver was that the maximum absolute value of the changes in the molar fractions for all species was less than a pre-set upper limit. Typically the value of f_i tends to 1×10^{-6} or lesser to ensure good accuracy and convergence.

The simulation results of the gas composition for initial pyrolysis from the non stoichiometric equilibrium model for the temperatures from 680 to 780°C were compared with the experimental data. From the model simulation results, the concentrations (molar fractions) of CO and H_2 increased with the operating temperature with CO concentration changing from 48.6% (mol/mol) at 680°C to 52.2% (mol/mol) at 780°C with an uncertainty of ±10% (mol/mol). In the same temperature range, the corresponding H_2 concentration also increased slightly from 35.4% to 36.8% (mol/mol), however the uncertainty predicted was very high ranging ±20% (mol/mol). With the operating temperature increase in the same range, the CO_2 concentration decreased from 2.6% to 0.2% (mol/mol) and the concentration of CH_4 decreased slightly from 12.3% to 10.8% (mol/mol). Again the uncertainty for CO_2 and CH_4 were foreseen to be higher at ±20% (mol/mol) and ±2% (mol/mol) in the operating temperatures 680 to 780^{o}C respectively. Here the uncertainty was measured as standard error. The standard error (SE) for the measured values was calculated from the ratio of standard deviation and the square root of number of sample data. Thus simulation result deviated largely for CO, CO_2 and H_2 with the experimental data and hence an empirical model was developed for the initial pyrolysis in the next section.

3.2.1.b Development of a product distribution function for initial pyrolysis

In the current work, the pyrolysis zone is considered to exist in bottom of the gasifier where the fed biomass is first in contact with hot bed material and steam. The biomass pyrolysis reactions are given as follows:

$$[N_{wood}CH_{1.44}O_{0.66}] \xrightarrow{\substack{\Delta high \\ temp}} \left[\begin{cases} Mgas\ (Volatiles) \xrightarrow{\Delta} (N_{CO}CO, N_{CO_2}CO_2, N_{H_2}H_2, N_{CH_4}CH_4) \\ \qquad\qquad + M_{tar}(tar) \\ \qquad\qquad + M_{char}(char) \end{cases} \right] \tag{3.13}$$

In the above reaction, the volatile gas mainly contains gaseous species of $CO, CO_2, H_2\ and\ CH_4$ which yields and compositions can be calculated as a function of temperature using correlation fitted from the experimental results conducted during this research work. The composition of gaseous species, i, is given as y_i in mole fraction. The operation temperature was considered to be the dominant factor for the gas yield and gas composition based on experimental results. This can be explained by the fact that the pyrolysis reaction is very fast in a fraction of second and hence influence of steam feed has the least influence.

In the experiments, the reactor must be preheated to 770°C in the start-up stage operation to achieve gasification process. At start-up stage, air is introduced to both CFB and BFB in order to fluidize bed material in the appropriate fluidization régime. The high CFB fluidizing rate allows the bed material to be pneumatically transferred to the BFB, and circulate through the system. Fluidizing air is also injected into the chute and siphon transition regions to maintain bed material circulation. Later LPG is fed to the both CFB and BFB in similar proportion as air, heating the bed material and reactor. In general the start-up period lasts 4-5 hours, during which time bed material circulation, temperatures and reactor oxygen content are monitored in order to minimize the possibility of 'hot spots' developing within the reactor which could lead to bed material agglomeration. Once circulation is steady LPG injection is gradually increased and heat-up becomes stable, with a slight increase in heating rate usually observed around 650°C.

In the experimentation for the initial pyrolysis of wood pellets, nitrogen was used as the fluidization agent thus the gasification reactions between the volatile gases and steam were eliminated. Pine wood pellets are fed to the BFB after the reaching steady state, entering 300mm from the base of the gasification column, where it devolatilises and begins endothermic pyrolysis reactions. During the steady-state operation number of gas samples is taken every 5minutes. Gas samples were collected from the top of the BFB chamber using a 50ml solid phase extraction column (SPE column) which contains 3ml amino normal phase to absorb the tars. The gas samples collected were analyzed using an Agilent 3000C Micro Gas Chromatograph (Micro GC) which was calibrated with a specified mixture of producer gas components. The yield of each gas species as a function of operating temperature T for H_2, CO, CH_4 and CO is shown in Figure 3.4. The experimental results show that in the initial pyrolysis, H_2 yield increases while the other components of CO, CH_4 and CO_2 decreases with the temperature. From these results, a correlation of product gas distribution as a function of

temperature was developed as in Equation ($3.14\,a, b$), where the values for parameters of $m_{0,i}$ and $b_{0,i}$ for different species along with its R^2 value are shown in Table 3.3 for the feedstock of pine wood pellets. The correlation coefficient (R^2) of the proposed correlation and the experimental results were 0.89, 0.94, 0.93 and 0.85, respectively, for H_2, CO, CH_4 and CO_2 (Figures 3.4a to 3.4d)

$$y_i = m_{0,i} \times T^{b_{0,i}} \qquad (3.14a)$$

or in the linear form as, $\quad log_{10}(y_i) = log_{10}(m_{0,i}) + b_{0,i} \times log_{10}(T) \qquad (3.14b)$

Table 3.3: Values of parameters of $m_{0,i}$ and $b_{0,i}$ in fitted correlation for prediction of product gas composition for initial pyrolysis of pine wood pellets in a BFB.

i (species)	$m_{0,i}$	$b_{0,i}$	R^2 $value$
H_2	1.3353×10^{-16}	5.72682	0.89
CO	1.8006×10^{7}	-1.87095	0.94
CO_2	2.4808×10^{3}	-0.69559	0.85
CH_4	4.4313×10^{5}	-1.49449	0.93
H_2O	Based on initial biomass moisture content		

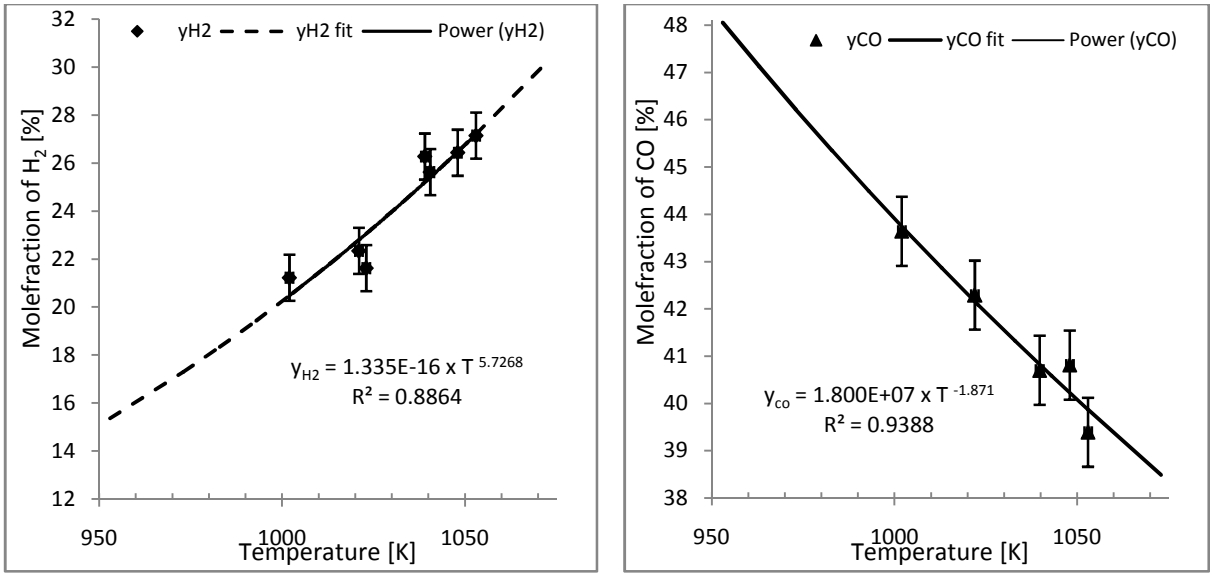

(a) H_2 (b) CO

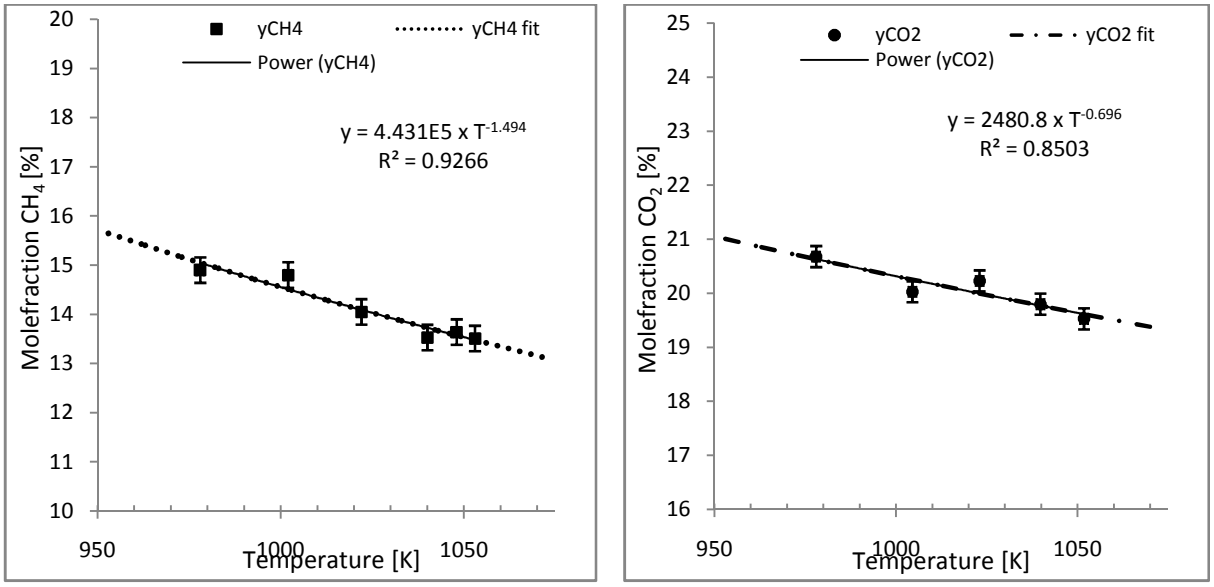

(c) CH_4 (d) CO_2

Figure 3.4: Experimental results and fitted correlation predictions of gas product composition in initial pyrolysis of pine wood pellets at different reaction temperatures.

Table 3.4: Gasification reactions in the second stage of biomass gasification process in a BFB gasifier. The changes in enthalpy at minimum Gibbs energy (ΔH_r) were calculated from *Perry et al. (1997)*.

Reactions	*Equations*	ΔH_r $[kJ/mol]$	
Steam Gasification Type I	$C + H_2O \overset{K_{eq\,6a}}{\Longleftrightarrow} CO + H_2$	138.33	$(3.15a)$
Steam Gasification Type II	$C + 2H_2O \overset{K_{eq\,6b}}{\Longleftrightarrow} CO_2 + 2H_2$	105.44	$(3.15b)$
Water Gas Shift reaction	$CO + H_2O \overset{K_{eq\,7}}{\Longleftrightarrow} CO_2 + H_2$	-30.86	(3.16)
Methanation reaction	$C + 2H_2 \overset{K_{eq\,8}}{\Longleftrightarrow} CH_4$	-93.8	(3.17)
Bouduard reaction	$C + CO_2 \overset{K_{eq\,9}}{\Longleftrightarrow} 2CO$	170.45	(3.18)
Steam Methane Reforming reaction	$CH_4 + H_2O \overset{K_{eq\,10}}{\Longleftrightarrow} CO + 3H_2$	232.78	(3.19)

3.2.2. Stage 2: Biomass Gasification model

In the second stage of gasification following the initial pyrolysis, reactions occur among the gasification agent (steam), volatile gases and char evolved from the initial stage of pyrolysis. It was assumed that the tars were not involved in the reactions during the gasification. For the reactions the char was assumed to be elemental carbon. These gasification reactions as listed in Table 3.4 are named, respectively, as Steam Gasification reaction (Equation 3.15 a,b), Water Gas-Shift reaction (Equation 3.16), Methanation reaction (Equation 3.17), Bouduard reaction (Equation 3.18) *(Wang and Kinoshita, 1993)*, and Steam Methane Reforming reaction (Equation 3.19) *(Yan et al., 1998)*. These reactions take place simultaneously although the reaction rates were different and vary with operation conditions. Detailed overview of these reactions is described earlier in Chapter 2. The second type of Steam Gasification reaction in Equation $(3.15b)$ has significant contribution to the gasification process when excessive steam is used. The CO_2 formed by this reaction could be consumed by the Bouduard reaction (Equation 3.18). However, the Steam Gasification reaction (3.15b) may be regarded as the combination of Water Gas-Shift reaction (Equation 3.16) and the Steam Gasification reaction type I (Equation 3.15a).

The kinetics for the above gasification reactions (Equations 3.15 to 3.19) were assumed to have Arrhenius type temperature dependence as given by *Wang and Kinoshita (1993)*. These kinetic functions are given in Equations (3.20) to (3.24) corresponding to reactions (3.15a), (3.16) to (3.19) which are represented in the modelling by subscript j varying from 1 to 5 in constant k_{0j} and in activation energy (E_{Aj}). The values for k_{0j} and E_{Aj} are given in Table 3.5 which are cited from *Wang and Kinoshita (1993)*.

$$r_1 = k_{01} exp\left(\frac{-E_{A1}}{RT}\right)\left([H_2O] - \frac{[CO].[H_2]}{K_{eq\,6}}\right) \tag{3.20}$$

$$r_2 = k_{02} exp\left(\frac{-E_{A2}}{RT}\right)\left([CO].[H_2O] - \frac{[CO_2][H_2]}{K_{eq\,7}}\right) \tag{3.21}$$

$$r_3 = k_{03} exp\left(\frac{-E_{A3}}{RT}\right)\left([H_2]^2 - \frac{[CH_4]}{K_{eq\,8}}\right) \tag{3.22}$$

$$r_4 = k_{04} exp\left(\frac{-E_{A4}}{RT}\right)\left([CO_2] - \frac{[CO]^2}{K_{eq\,9}}\right) \tag{3.23}$$

$$r_5 = k_{05} exp\left(\frac{-E_{A5}}{RT}\right)\left([CH_4].[H_2O] - \frac{[CO][H_2]^3}{K_{eq\,10}}\right) \tag{3.24}$$

The equilibrium constants K_{eqj} in the above equations are a function of temperature and standard Gibbs energy only and can be calculated from Equation (3.25) *(Perry et al., 1997).*

$$-RT\left[ln\left(K_{eqj}\right)\right] = \Delta G_i^{\circ} or -\left[ln\left(K_{eqj}\right)\right] = \Delta G_i^{\circ}/RT \quad (3.25)$$

where, ΔG_i° is the standard Gibbs energy at any temperature and its values are derived using the method described in *Modell and Reid (1974) and Smith et al. (2001).*

The standard property change of reactions such as ΔH_i° and ΔG_i° vary with temperature at the equilibrium condition by the following equations *(Perry et al., 1997; Smith et al., 2001)*:

$$\frac{\Delta H_i^{\circ}}{R} = \frac{J_j}{R} + (\Delta A)T + \frac{\Delta B}{2}T^2 + \frac{\Delta C}{3}T^3 - \frac{\Delta D}{T} \quad (3.26)$$

$$\Delta G_i^{\circ} = J_j - RT\left((\Delta A)lnT + \frac{\Delta B}{2}T + \frac{\Delta C}{6}T^2 + \frac{\Delta D}{2T^2} + I_j\right) \quad (3.27)$$

where, $J_j$and I_j are constants for reaction *j*. The constants J_j and I_j are determined using the Equation (3.26)and (3.27)at standard temperature of 298.15 K respectively. The values of ΔH_i° corresponds to $\Delta H_{f_i,298}^{\circ}$, ΔG_i° corresponds to $\Delta G_{f_i,298}^{\circ}$ and the values of *A, B ,C* and *D* are given in *Perry et al. (1997)* and listed in Table 3.6. The values of *ΔA, ΔB, ΔC, ΔD* for any reaction is determined by the product of stoichiometric coefficient and the data of heat capacity *A, B, C, D* respectively such that for $\Delta A = \sum_{j=1}^{7} \nu_{ij} A_j$, $\Delta B = \sum_{j=1}^{7} \nu_{ij} B_j$, $\Delta C = \sum_{j=1}^{7} \nu_{ij} C_j$, and $\Delta D = \sum_{j=1}^{7} \nu_{ij} D_j$.

Table 3.5: Values of reaction kinetic constants and activation energy for the chemical reactions (3.15-3.19) *(Macak and Malecha, 1978; Wang and Kinoshita, 1993).*

Reaction *j*	k_{0j} (1/s)	E_{Aj} (kJ/mol)
$C + H_2O \overset{K_{eq\,6a}}{\Longleftrightarrow} CO + H_2$(Reaction 3.15a)[(d)]	1.517×10^{4}	121.62
$CO + H_2O \overset{K_{eq\,7}}{\Longleftrightarrow} CO_2 + H_2$(Reaction 3.16)[(e)]	2.780×10^{3}*(f)*	12.56
$C + 2H_2 \overset{K_{eq\,8}}{\Longleftrightarrow} CH_4$(Reaction 3.17)[(d)]	4.189×10^{-3}	19.21
$C + CO_2 \overset{K_{eq\,9}}{\Longleftrightarrow} 2CO$ (Reaction 3.18)[(d)]	3.616×10^{1}	77.39
$CH_4 + H_2O \overset{K_{eq\,10}}{\Longleftrightarrow} CO + 3H_2$ (Reaction 3.19)[(d)]	7.301×10^{-2}	36.15

Note: [(d)]*(Wang and Kinoshita, 1993),* [*(e)*]*(Macak and Malecha, 1978)* [*(f)*]*kmol/m^{3}s*

Table 3.6: Heat of formation of species *i* at 25°C, Gibbs energy of formation of species *i* at 25°C and heat capacity constants A,B, C and D *(Perry et al., 1997)*

Species	$\Delta H^{\circ}_{f_i,298}$ $(kJ/kmol)$	$\Delta G^{\circ}_{f_i,298}$ $(kJ/kmol)$	T_{max} [K]	A	10^3 B	10^6 C	10^{-5} D
H_2	0	0	3000	3.249	0.422	-	0.083
CO	-110525	-137169	2500	3.376	0.557	-	-0.031
CO_2	-393509	-394359	2000	5.457	1.047	-	-1.157
H_2O	-241818	-228572	2000	3.470	1.450	-	0.121
CH_4	-74520	-50460	1500	1.702	9.081	-2.164	-
C	0	0	2000	1.771	0.771	-	-0.867
N_2	0	0	2000	3.280	0.593	-	0.040

3.3 Mass and energy balance equations

3.3.1 Mass balance

From the above description, the pyrolysis reactions and gasification reactions were affected by temperature. In addition, the gas species diffuse within the gasifier if a gradient exist. Therefore, the producer gas yield and gas composition are also a function of temperature. Furthermore, temperatures of gases and bed material within a gasifier change along the gasifier height which, in turn, will affect the gas composition. In order to predict the temperature profile and to predict the gas composition profile within the gasifier, the heat and mass transfer processes involved in the fluidized bed need to be included in the model. This section will focus on establishment of heat and mass balance equations.

The bubbling process of gas through solids in a fluidized bed was described in *Kunii and Levenspiel(1991)* in which two phase flow regimes were proposed. In the model developed in this study, it was assumed that the fluidized bed gasifier consists of particle-lean bubble phase and particle-rich emulsion phase. In the particle-lean bubble phase the gas flows in excess of the minimum fluidization velocity, in the form of large bubbles and thus the solids

are not in good contact with the gas. In the particle-rich emulsion phase the gas velocity through the bed was at the minimum fluidization velocity.

Therefore, it was assumed that the heterogeneous reactions (reactions between gases and solid char) were insignificant, thus ignored in the bubble phase. Under this condition only Water Gas-Shift reaction and Methane Reforming reaction occurred. However, in the emulsion phase in which the solids and the gaseous fluids were mixed uniformly without any elutriation, both the homogenous and the heterogeneous phase reactions possibly occurred. The volume fraction of the emulsion phase was assumed to be constant, equivalent to that in the incipient fluidization. The model also considers the interphase heat and mass transfer of particles and gases.

In the BFB gasifier shown in Figure 3.2, the cross-sectional area is *S* and the axial position is represented by z measured from the bottom of the gasifier. The gases formed in the gasifier were assumed to follow the Ideal Gas Law. Over a short height of the gasifier,Δz, continuity equation can be established based on the mass balance for all materials flowing through this small volume element. In this way, the mass continuity differential equation can be developed as follows *(Levenspiel, 1999; Missen et al., 1999; Tosun, 2002)*

$$\begin{bmatrix} Rate\ of\ mass \\ accumulation \\ of species(i) \\ in\ the\ control \\ volume \end{bmatrix} = -\begin{bmatrix} Net\ rate\ of\ mass \\ change\ for \\ species(i)\ in\ the \\ control\ volume \\ by\ convective \\ gas\ flow \end{bmatrix} - \begin{bmatrix} Net\ rate\ of \\ mass\ change \\ for\ species(i) \\ in\ the\ control \\ volume\ by \\ diffusion \end{bmatrix} + \begin{bmatrix} Rate\ of\ production \\ of\ species(i)\ by \\ chemical\ reactions \\ in\ the\ control \\ volume \end{bmatrix}$$

The first two terms on the right hand side of the above equation were defined over space interval. *Kunii and Levenspiel (1991)*, who was the first to propose the two phase concept, introduced a new term called the net exchange rate of species between the bubble and emulsion phases. By including this new term, the mass balance for the bubble phase over the control volume can be derived as follows.

$$\begin{bmatrix} Rate\ of\ mass \\ accumulation \\ of species(i) \\ in\ the\ bubble \\ phase\ control \\ volume \end{bmatrix} = -\begin{bmatrix} Net\ rate\ of \\ mass\ change \\ for\ species(i) \\ in\ the\ bubble \\ phase\ \ control \\ volume\ by \\ convective \\ gas\ flow \end{bmatrix} - \begin{bmatrix} Net\ rate\ of \\ mass\ change \\ for\ species(i) \\ in\ the\ bubble \\ control\ volume \\ by \\ diffusion \end{bmatrix} - \begin{bmatrix} Net\ exhange \\ rate \\ of species(i) \\ between \\ bubble\ and \\ emulsion \\ phase\ in\ the \\ control \\ volume \end{bmatrix} + \begin{bmatrix} Rate\ of \\ production \\ of\ species(i) \\ by\ chemical \\ reactions\ in \\ the\ bubble \\ phase \\ control\ volume \end{bmatrix}$$

Mathematical expressions of each term have been developed as follows. The rate of mass accumulation of species (*i*) in the bubble phase control volume can be described as:

$$\frac{\partial}{\partial t}(S_b \Delta z\, C_{ib}) \tag{3.28}$$

where S_b is the cross-sectional area of the bubble phase region in the BFB, which is calculated as the product of reactor cross sectional area (S) andthe volume fraction of the bubble phase (ε_b). C_{ib} is the concentration of the species (*i*) in the bubble phase.

The net rate of mass change for species (*i*) over the bubble phase control volume by convection can be described as:

$$u_b S_b C_{ib}|_{z+\Delta z} - u_b S_b C_{ib}|_z \tag{3.29}$$

where u_b is the bubble velocity an important parameter in the fluidized bed model and is expressed as a function of superficial gas velocity gas u_0, velocity at minimum fluidization condition u_{mf} and rise velocity of single bubble relative to emulsion solids u_{br}*(Davidson et al., 1985; Kunii and Levenspiel, 1991).*

$$u_b = u_0 - u_{mf} + u_{br} \tag{3.30}$$

The expression for the rise velocity of single bubble relative to emulsion solids u_{br} *(Davidson et al., 1985),* the gas velocity at minimum fluidization condition u_{mf} and Archimedes number Ar respectively were provided by *Cui and Grace,(2007)* as follows

$$u_{br} = 0.711\sqrt{(\mathrm{g}d_b)} \tag{3.31}$$

$$u_{mf} = \frac{\mu_g\left[27.2^2 + 0.0408Ar\right]^{0.5}}{d_p \rho_g} - 27.2 \tag{3.32}$$

The minimum fluidization velocity correlation of binary mixtures of solids with different particle sizes, especially the mixtures of biomass particles with bed of particles is given by *Zhong et al., (2008)* as follows

$$u_{mf,mixture} = u_{mf,s}\left(\frac{u_{mf,b}}{u_{mf,s}}\right)^{{x_b}^2} \tag{3.33}$$

where, $u_{mf,s}$ and $u_{mf,b}$ are the minimum fluidization velocity of small particle and large particle respectively and x_b mass fraction of larger particle.

Archimedes number, $Ar = \frac{d_p^3 \rho_g (\rho_s - \rho_g) g}{\mu_g{}^2}$ (3.34)

where d_p is the particle diameter, ρ_g *and* ρ_s is the average densities of the gas and solids species respectively and μ_g is the average viscosity of gas species.

In the expression(3.31), d_b is the average bubble diameter which is expressed as a function of height of the reactor in the fluidized bed *(Kunii and Levenspiel, 1991; Mori and Wen, 1975):*

$$d_b(z) = d_{bm} - (d_{bm} - d_{b0})\exp(-0.3z/d_t) \quad (3.35)$$

where d_{bm} is the maximum bubble diameter and d_{b0} is the minimum bubble diameter. These are defined as

$$d_{bm} = 1.64\left(S(u_0 - u_{mf})\right)^{0.4} \quad (3.36)$$

and $d_{b0} = 0.872\left[\frac{S(u_0 - u_{mf})}{n_d}\right]^{0.4}$ (3.37)

In the above calculationn_d is the number of holes in the distributor.

The net rate of mass change by diffusion for species *(i)* in the bubble phase control volume can be described as

$$\left\{-S_b D_{ib} \frac{\partial C_{ib}}{\partial z}\Big|_{z+\Delta z}\right\} - \left\{-S_b D_{ib} \frac{\partial C_{ib}}{\partial z}\Big|_{z}\right\} \quad (3.38)$$

where D_{ib} is the diffusion coefficient of species *(i)* with respect to total gas mixture in the bubble phase which depicts the plug flow.The values of diffusion coefficients $D_{ib}$of species *(i)* introduced in this model had been estimated by the method of *Fairbanks and Wilke, (1950)* who used the term of effective diffusion coefficients species *(i)* with respect to total gas mixture.

$$D_{ib} = \frac{1 - y_{b_i}}{\frac{y_{b_i}}{\sum_{k \neq i} D_{b\,ik}}} \quad (3.39)$$

In the above equation, y_{b_i} is the mole fraction of species *(i)* in bubble phase and $D_{b\,ik}$ is the binary gas phase diffusion coefficient of species *(i)* with respect to each component of the species *(k)* in the bubble phase. An empirical correlation for the binary gas phase diffusion coefficients of species developed by *Fuller et al. (1966)* that gives the smallest standard deviation, using a nonlinear least-squares analysis have been used in this model

$$D_{b\,ik} = \frac{10^{-7} T^{1.75} \left(\frac{1}{Mw_i} + \frac{1}{Mw_j}\right)^{0.5}}{P\left[(V_i)^{\frac{1}{3}} + (V_j)^{\frac{1}{3}}\right]^2} \quad (3.40)$$

where Mw_i and $Mw_k$is the molecular weight of species *i* and *k*. V_i is the diffusion volume for species *i*, as given in Table 3.7

Table 3.7: Diffusion volume of gas species (Fuller et al., 1966)

Species *i* (and/or) *k*	diffusion volume for species *i or k*
H_2	7.07
CO	18.9
CO_2	26.9
H_2O	12.7
CH_4	24.4

The net exchange rate of species *(i)* between bubble phase and emulsion phase in the control volume can be described as:

$$S_b \Delta z K_{be} (C_{ib} - C_{ie}) \quad (3.41)$$

In which K_{be} is the inter phase mass transfer coefficient, estimated from the expression given by *Kunii and Levenspiel, (1991).*

According to *Davidson's theory* as defined by *Kunii and Levenspiel, (1991)* there exists an intermediate phase between the bubble and emulsion phase. The inter phase mass transfer coefficient depends on the emulsion side mass transfer coefficient K_{ce} and bubble side mass transfer coefficient K_{bc} as given by

$$\frac{1}{K_{be}} = \frac{1}{K_{bc}} + \frac{1}{K_{ce}} \quad (3.42)$$

where $K_{ce} = 6.77 \left(\frac{D_{ie} \varepsilon_{mf} u_{br}}{d_b^3}\right)^{0.5}$; $K_{bc} = \frac{4.5 u_{mf}}{d_b} + \left(\frac{5.85\, {D_{ib}}^{1/2} g^{1/4}}{d_b^{5/4}}\right)$

In the above equation the void fraction at minimum fluidization condition is estimated from the expression, $\varepsilon_{mf} = 0.4025 + 603.7 \times d_p$asspecified by *Abrahamsen and Geldart, (1980).* The rate of production of species *(i)* by chemical reactions in the bubble phase control volume can be given as

$$S_b \Delta z\, R_{ib} \quad (3.43)$$

where $R_{ib} = \sum_{j=1}^{5} \nu_{ij} r_{jb}$.

Finally the overall material balance in the bubble phase within the control volume can be written as follows by introducing Equations $(3.28), (3.29), (3.38)$, (3.41)and (3.43)into the bubble phase mass balance equation. Dividing both sides of the expression by $S\Delta z$ and letting $\Delta z \to 0$, the following differential equation can be obtained:

$$\frac{\partial(\varepsilon_b C_{ib})}{\partial t} = -\frac{\partial(u_b \varepsilon_b C_{ib})}{\partial z} + \frac{\partial}{\partial z}\left(D_{ib}\varepsilon_b \frac{\partial C_{ib}}{\partial z}\right) - K_{be}\varepsilon_b(C_{ib} - C_{ie}) + \varepsilon_b R_{ib} \qquad (3.44)$$

In a similar way, the mass balance equation for the emulsion phases can also be derived as Equation (3.44). In the derivation, it was considered that the particle-rich emulsion phase has a volume fraction $\varepsilon_e = 1 - \varepsilon_b$. Note that in the emulsion phase, the gas flows at the minimum fluidization velocity. Therefore, the gas volume fraction over the emulsion region can have the gas volume fraction at minimum fluidization, ε_{mf}. Accordingly, the particle volume fraction over the emulsion phase region is $1 - \varepsilon_{mf}$ *(Kunii and Levenspiel, 1991)*.

Similarly for the gases in the emulsion phase, we have

$$\frac{\partial}{\partial t}\left(S_e \varepsilon_{mf} \Delta z\, C_{ie}\right) = -\left(u_e S_e \varepsilon_{mf} C_{ie}\Big|_{z+\Delta z} - u_e S_e \varepsilon_{mf} C_{ie}\Big|_{z}\right) - \left(\left\{-S_e D_{ie}\varepsilon_{mf}\frac{\partial C_{ie}}{\partial z}\Big|_{z+\Delta z}\right\} - \left\{-S_e D_{ie}\varepsilon_{mf}\frac{\partial C_{ie}}{\partial z}\Big|_{z}\right\}\right) + S_b \Delta z K_{be}(C_{ib} - C_{ie}) + \left(\sum_{j=1}^{5}\nu_{ij} r_{je}\right)\varepsilon_{mf} S_e \Delta z \qquad (3.45)$$

where S_e is the cross-sectional area of emulsion phase region given as $S \times \varepsilon_e$. $D_{ie}$is the diffusion coefficient in the emulsion phase of species *(i)* with respect to total gas mixture which depicts the mixed flow. The values of $D_{ie}$was estimated similar to that of $D_{ib}$from Equations $(3.39 - 3.40)$. $C_{ie}$is the concentration of the species in the emulsion phase, ε_e is the volume fraction of the emulsion phase and u_e is the emulsion velocity.Again dividing both sides of the above expression by $S\varepsilon_{mf}\Delta z$ and letting $\Delta z \to 0$, the following differential equations can be obtained:

$$\frac{\partial(\varepsilon_e C_{ie})}{\partial t} = -\frac{\partial(u_e \varepsilon_e C_{ie})}{\partial z} + \frac{\partial}{\partial z}\left(D_{ie}\varepsilon_e \frac{\partial C_{ie}}{\partial z}\right) + \frac{\varepsilon_b}{\varepsilon_{mf}} K_{be}(C_{ib} - C_{ie}) + \varepsilon_e R_{ie} \qquad (3.46)$$

where $R_{ie} = \sum_{j=1}^{5} \nu_{ij} r_{je}$

In both the bubble and the emulsion phases, the changing rate of species *i* were influenced by the interphase mass transfer coefficient K_{be}. In the fluidized bed gasifier, the interphase transfer was enhanced as a result of mixing of the gases and the solids with circulation of bed

materials. Since the bed material acts as an inert solid in the bed, the concentrations of the solid species from the biomass gasification in the emulsion phase C_{cs} (kg of *char* /kg of inert bed material) is defined as relative weight fraction of solid species with respect to the mean average inert bed material hold up in the BFB during steady state operation whose total weight is defined as M_{sand}.

Mass balance of char

The material balance of the solid char in the fluidized bed can be specified as follows.

$$M_{sand}\left(\frac{\partial C_{cs}}{\partial t}+\frac{\partial(u_e C_{cs})}{\partial z}\right)=(W_{in}-W_{out})+M_{sand}D_{sr}\frac{\partial^2 C_{cs}}{\partial z^2}+R_{cs} \qquad (3.47)$$

The first term on the right hand side W_{in} is the rate of char into the gasification process after the initial pyrolysis which is obtained from Equation (3.3), W_{out} is the rate of char out of the gasification process which is given as the ratio of mass of char in the bed and the mean residence time of sand $\alpha\frac{M_{sand}C_{cs}}{\tau}$.

In this model the transportation of generated biomass chars out of the BFB was taken into account by considering the circulation of sand between the BFB and CFB. In the above equation, the mean residence time of the sand τ was provided as ratio of mean average inert bed material holdup termed as M_{sand}in the BFB during steady state operation and the solids circulation rate termed as $\dot{M}_{sand}$, ie, $\tau=\frac{M_{sand}}{\dot{M}_{sand}}$.The term $\alpha$was defined as the carryover factor of the specified material, whose value was related to as the ratio of actual mass flow rate of a specific solid particle through the chute over the theoretical mass flow corresponding to the solids circulation rate. The density of biomass char particles were so low compared with the inert bed material and hence they buoyant on the top of the bed. The value of $\alpha$for biomass char was related to as the ratio of density of the biomass char and the density of inert bed material and therefore αvalue was set as 0.1.

The second term on the right hand side in the above equation corresponds to axial dispersion of solids.

The third term on the right hand side in the above equation, R_{cs} is the rate of generation (or consumption) of solid char species in the emulsion phase can be given in this model as

$$R_{cs} = \sum_{j=1}^{5}\left(M_{w_c}\nu_{cj}r_{je}\right)\left(\frac{V_{gas,e}\,.\varepsilon_{mf}}{V_{gas,e}\left(1-\varepsilon_{mf}\right)}\right)\left(\frac{M_{sand}}{\rho_{sand}}+\frac{M_{sand}C_{cs}}{\rho_c}\right). \quad (3.48)$$

where, M_{w_c} molecular weight of char ($CH_{0.2}O_{0.13}$) which is defined as 14.2 kg/kmol *(Corella and Sanz, 2005)*; r_{je} is the reaction rate of the j^{th} chemical reaction; C_{cs} is the weight fraction of char with respect to the inert bed material; ρ_c is the density of char; ρ_{sand} is the density of the inert bed material, sand in this study; M_{sand} is the total weight of the inert bed material, sand. $\left(\frac{V_{gas,e}.\varepsilon_{mf}}{V_{gas,e}\left(1-\varepsilon_{mf}\right)}\right)$ is the ratio of volume of gas in emulsion phase to that of particles in emulsion phase and $V_{gas,e}$is the total gas volume of the emulsion phase in the entire bed.

3.3.2 Energy balance

In a similar way to mass balance, energy balance and heat transfer equations can also be developed for the individual species of gases and solids in the gasifier. The general energy balance equation for the control volume of bubble phase and emulsion phase can be developed according to the conservation of energy developed by *Luyben (1996),Moran et al. (2011) and Welty et al.(2008)*.

$$\begin{bmatrix} Rate\ of \\ accumulation \\ of\ energy \\ within \\ element \\ of \\ control \\ volume \end{bmatrix} = \begin{bmatrix} Net\ rate \\ of\ addition \\ of\ heat\ to \\ the\ control \\ volume \\ from\ its \\ surrounding \end{bmatrix} - \begin{bmatrix} Net\ rate \\ of\ work \\ done\ by \\ the\ control \\ volume \\ on\ its \\ surrounding \end{bmatrix} - \begin{bmatrix} net\ rate\ of\ energy \\ (internal, \\ kinetic, \\ and\ potential) \\ flow\ into \\ element\ of \\ volume\ by \\ convection \\ and/or \\ diffusion \end{bmatrix}$$

There was no energy transfer by work and hence the second term on the right hand side in the above equation becomes zero, and not included in the energy balance equation for bubble and emulsion phase. Applying the above energy balance equation to emulsion phase for a control volume and rearranging the equation, the following equations (3.49) was proposed. The first four term of Equation (3.49) relates the net rate of addition of heat; by heat of reaction, conduction, heat exchange from inert solids (sand) circulation and net heat exchange rates between the bubble and emulsion phase. The last two terms of Equation (3.49) relates net

energy flow into the emulsion phase control volume by convection and diffusion respectively.

$$\begin{bmatrix} Rate\ of\ energy\ accumulation\ within\ the\ control\ volume \end{bmatrix} = \begin{bmatrix} Rate\ of\ energy\ generation\ by\ chemical\ reaction\ within\ control\ volume \end{bmatrix} + \begin{bmatrix} Net\ rate\ of\ energy\ change\ in\ the\ control\ volume\ by\ conduction \end{bmatrix} + \begin{bmatrix} Net\ heat\ exchange\ rate\ by\ the\ bed\ materials\ and\ char\ particles \end{bmatrix} + \begin{bmatrix} Net\ heat\ exhange\ rate\ for\ species(i)\ between\ bubble\ and\ emulsion\ phases\ in\ the\ control\ volume \end{bmatrix} - \begin{bmatrix} Net\ rate\ of\ energy\ change\ for\ species(i)\ over\ the\ control\ volume\ by\ convective\ gas\ flow \end{bmatrix} - \begin{bmatrix} Net\ rate\ of\ energy\ change\ for\ species(i)\ in\ the\ control\ volume\ by\ diffusion \end{bmatrix} \quad (3.49)$$

In the above equation, the energy accumulation in the emulsion phase control volume can be described, separately, for the homogenous and heterogeneous phases as follows:

$$\left\{\varepsilon_{mf}\Delta z\sum_{i=1}^{5}\frac{\partial(S_e C_{ie} Cp_{e,i} T_e)}{\partial t}\right\}_{homo} + \left\{\left(1-\varepsilon_{mf}\right)\Delta z\sum_{i=1}^{2}\frac{\partial(S_e C_{ie} Cp_{e,i} T_e)}{\partial t}\right\}_{hetero} \quad (3.50)$$

In the above equation, $Cp_{e,i}$ is the specific heat of species *(i)* at a specified emulsion phase temperature T_e in the emulsion phase, which is a function of temperature and expressed by an empirical relationship as follows *(Perry et al., 1997).* The constants of heat capacities such as A, B, C and D for each gas species *i* as well as carbon (char) are given in Table 3.6. The specific heat of inert bed material, sand, is Cp_{sand} which can be determined by a correlation given by *Hemingway, (1987).*

$$Cp_{e,i} = R\times\left(A + B\frac{(T_e+T_0)}{2} + \frac{C}{3}\left(4\left(\frac{T_e+T_0}{2}\right)^2 - T_e T_0\right) + \frac{D}{T_e T_0}\right. \quad (3.51)$$

$$Cp_{sand} = \left(57.9588 + 9.33019\times10^{-3}T_e + 1834713/{T_e}^2\right)\times10^3/Mw_{sand} \quad (3.52)$$

where, Mw_{sand} is the molecular weight of sand.

The net energy change for species *(i)* in the emulsion phase control volume by convective gas flow for the homogenous and heterogeneous phases can be quantified as follows:

$$\varepsilon_{mf}\left\{S_e\sum_{i=1}^{5}u_eC_{ie}\Delta H_{ie}\Big|_{z+\Delta z}-S_e\sum_{i=1}^{5}u_eC_{ie}\Delta H_{ie}\Big|_{z}\right\}_{homo}$$
$$+\left(1-\varepsilon_{mf}\right)\left\{S_e\sum_{i=1}^{2}u_eC_{ie}\Delta H_{ie}\Big|_{z+\Delta z}-S_e\sum_{i=1}^{2}u_eC_{ie}\Delta H_{ie}\Big|_{z}\right\}_{hetero} \quad (3.53)$$

The net energy change for species *(i)* in the emulsion phase control volume by diffusion for the homogenous and heterogeneous phases:

$$-D_{ie}\varepsilon_{mf}\left\{S_e\sum_{i=1}^{5}H_{ie}\frac{\partial C_{ie}}{\partial z}\Big|_{z+\Delta z}-S_e\sum_{i=1}^{5}H_{ie}\frac{\partial C_{ie}}{\partial z}\Big|_{z}\right\}_{homo}-D_{ie}\left(1-\right.$$
$$\left.\varepsilon_{mf}\right)\left\{S_e\sum_{i=1}^{2}H_{ie}\frac{\partial C_{ie}}{\partial z}\Big|_{z+\Delta z}-S_e\sum_{i=1}^{2}H_{ie}\frac{\partial C_{ie}}{\partial z}\Big|_{z}\right\}_{hetero} \quad (3.54)$$

where H_{ie} is the species i specific enthalpy in the emulsion phase represented as $H_{ie}=H_{298,i}^{0}+Cp_{e,i}T_e$.

The heat generated by the chemical reactions can be calculated by:

$$S_e\Delta Z\varepsilon_{mf}\sum_{i=1}^{5}R_{ie}H_{ie}+R_{cs}H_c \quad (3.55)$$

in which $H_c\left(\frac{kJ}{kg}\right)$ is the mass specific enthalpy of char and can be represented as $H_c=\frac{1}{M_{w_c}}\left(H_{298,c}^{0}+Cp_{e,c}T_e\right)$.

The heat exchange between the bubble and emulsion phases can be described as:

$$S_b\Delta zH_{be}(T_b-T_e) \quad (3.56)$$

where, $T_b$and T_e are the temperatures of bubble and emulsion phase. H_{be} is the inter phase volumetric heat transfer coefficient between the bubble phase and emulsion phase, estimated from the expression given by *Kunii and Levenspiel (1991).* The inter phase volumetric heat transfer coefficient depends on the emulsion side volumetric heat transfer coefficient H_{ce} and bubble side volumetric heat transfer coefficient H_{bc} as given by

$$\frac{1}{H_{be}}=\frac{1}{H_{bc}}+\frac{1}{H_{ce}} \quad (3.57)$$

$$H_{ce}=6.78\left(\frac{\varepsilon_{mf}\lambda_g\rho_gCp_{e,g}u_b}{Mw_gd_b^3}\right)^{0.5}\ and H_{bc}=\left(\frac{4.5\left(u_{mf}\rho_gCp_{b,g}\right)}{Mw_gd_b}\right)+\frac{5.85\left(\left(\frac{\lambda_g\rho_gCp_{b,g}}{Mw_g}\right)^{1/2}g^{1/4}\right)}{d_b^{5/4}}$$

where $Cp_{e,g}$ and $Cp_{b,g}$ are the average specific heats of gas species *(i)*, respectively, in the emulsion phase and in the bubble phase, using mass weighted averaging procedure as $Cp_{e,g} = \sum_{i=1}^{5} y_{ie} Cp_{e,i}$ and $Cp_{b,g} = \sum_{i=1}^{5} y_{ib} Cp_{b,i}$

The gas density ρ_g can be assumed to obey the ideal gas law as

$$\rho_g = \frac{P}{RT \sum_{i=1}^{5} (y_{ib}/Mw_i)} \tag{3.58}$$

The gas thermal conductivity λ_g was also estimated using mass weighted average procedure as

$$\lambda_g = \sum_{i=1}^{5} y_{ie}\, \lambda_{g,i} \tag{3.59}$$

where, $\lambda_{g,i}$ is the thermal conductivity of gases is polynomial in temperature and can be described by the following equation described by *Rohsenow et al., (1998).*

The net rate of energy change in the emulsion phase control volume by conduction

$$\left\{S_e \varepsilon_{mf} {\lambda_s}^* \frac{\partial T_e}{\partial z}\Big|_{z+\Delta z}\right\} - \left\{S_e \varepsilon_{mf} {\lambda_s}^* \frac{\partial T_e}{\partial z}\Big|_{z}\right\} \tag{3.60}$$

where ${\lambda_s}^*$ is the thermal conductivity of solids estimated from the expression represented by *Di Blasi, (2004)*

$${\lambda_s}^* = \varepsilon_b \lambda_{rg} + \varepsilon_b \frac{\lambda_s}{\left[\frac{\lambda_s}{(d_p \lambda_{rs})} + 1.43(1 - 1.2\varepsilon_b)\right]} \tag{3.61}$$

$$\lambda_s = 0.0013 + 0.05(T_e/1000) + 0.63(T_e/1000)^2 \tag{3.62}$$

$$\lambda_{rg} = 4\sigma 0.05 {T_b}^3 \quad \text{and} \quad \lambda_{rs} = 4\sigma 0.85 {T_e}^3 \tag{3.63}$$

where σ is the Stefan Boltzmann constant.

The net heat transfer rate to the gases by the circulating bed of sand and char can be characterized as:

$$\left(H_{sand}\dot{M}_{sand}\right)\Big|_{z+\Delta z} + \left(H_c \dot{M}_c\right)\Big|_{z+\Delta z} - \left(H_{sand}\dot{M}_{sand}\right)\Big|_{z} + \left(H_c \dot{M}_c\right)\Big|_{z} \tag{3.64}$$

where $\dot{M}_{sand}$ and $\dot{M}_c$ are the mass circulation rates of sand and char.

Finally the total energy balance in the emulsion phase within the control volume can be written by substituting the terms from Equations $(3.50), (3.53) - (3.56), (3.60)$ and

(3.64)in Equation (3.49). Dividing both the sides of the expression by $S\varepsilon_{mf}\Delta z$ and letting $\Delta z \to 0$, the differential form of the energy balance equations can be derived as follows:

$$\left\{\sum_{i=1}^{5}\frac{\partial\left(\varepsilon_e C_{ie} Cp_{e,i} T_e\right)}{\partial t}\right\}_{homo} + \left\{\frac{\left(1-\varepsilon_{mf}\right)}{\varepsilon_{mf}}\sum_{i=1}^{2}\frac{\partial\left(\varepsilon_e C_{ie} Cp_{e,i} T_e\right)}{\partial t}\right\}_{hetero}$$
$$= -\left(\frac{\partial}{\partial z}\sum_{i=1}^{5}(\varepsilon_e u_e C_{ie}\Delta H_{ie})_{homo} + \frac{\left(1-\varepsilon_{mf}\right)}{\varepsilon_{mf}}\frac{\partial}{\partial z}\sum_{i=1}^{2}(\varepsilon_e u_e C_{ie}\Delta H_{ie})_{hetero}\right)$$
$$+ D_{ie}\left(\frac{\partial}{\partial z}\left(\varepsilon_e\sum_{i=1}^{5}H_{ie}\frac{\partial C_{ie}}{\partial z}\right)_{homo}\right.$$
$$\left.+\frac{\left(1-\varepsilon_{mf}\right)}{\varepsilon_{mf}}\frac{\partial}{\partial z}\left(\varepsilon_e\sum_{i=1}^{2}H_{ie}\frac{\partial C_{ie}}{\partial z}\right)_{hetero}\right) + \left\{\varepsilon_e\sum_{i=1}^{5}R_{ie}H_{ie} + \frac{1}{\varepsilon_{mf}V_r}R_{cs}H_c\right\}$$
$$+ \varepsilon_e{\lambda_s}^*\frac{\partial}{\partial z}\left(\frac{\partial T_e}{\partial z}\right) + \frac{\varepsilon_b}{\varepsilon_{mf}}H_{be}(T_b - T_e) + \frac{1}{\varepsilon_{mf}S}\frac{\partial\left(H_{sand}\dot{M}_{sand} + H_c\dot{M}_c\right)}{\partial z} \tag{3.65}$$

For the bubble phase, a similar procedure to the emulsion phase energy balance equation can be employed to derive the energy balance equation; however, the contribution of heat conduction by the bed material and the char were ignored as the gases exist as large bubbles at the minimum fluidization gas velocity thus the heat transfer between the solid and gas was insignificant. In this way, the energy balance equation for the bubble phase is:

$$\sum_{i=1}^{5}\frac{\partial\left(\varepsilon_b C_{ib} Cp_{b,i} T_b\right)}{\partial t}$$
$$= -\frac{\partial}{\partial z}\sum_{i=1}^{5}(\varepsilon_b u_b C_{ib}\Delta H_{ib}) + D_{ib}\frac{\partial}{\partial z}\left(\varepsilon_b\sum_{i=1}^{5}H_{ib}\frac{\partial C_{ib}}{\partial z}\right) + \varepsilon_b\sum_{i=1}^{5}R_{ib}H_{ib}$$
$$+ \varepsilon_b\lambda_g\frac{\partial}{\partial z}\left(\frac{\partial T_b}{\partial z}\right) - \varepsilon_b H_{be}(T_b - T_e)$$

(3.66)

where H_{be} is the inter-phase volumetric heat transfer coefficient between bubble phase and emulsion phases which is the same as that in the emulsion phase energy balance analysis. ε_b is the volume fraction of the bubble phase, C_{ib} and C_{ie} are the concentrations of i^{th} species in the bubble and the emulsion phases, respectively. Cp_b and Cp_e are specific heat of the gas mixture in the bubble phase and the emulsion phase, respectively. R_{ib} and R_{ie} are the rates of generation of i^{th} species in the bubble and the emulsion phases, respectively. The bubble and

the emulsion phase superficial velocities, u_b and u_e, can be determined from hydrodynamic relationship involved in the gasifier which are presented in the next section.

Energy balance of char

The temperature of inert bed material particles are related to gas temperature and the temperature of char particles. The char particle temperature can be determined by the energy balance equation:

$$\frac{M_{sand}\partial(C_{cs}Cp_{char}T_{char})}{\partial t} = -M_{char}\frac{\partial(C_{cs}u_s\Delta H_c)}{\partial z} + M_{sand}D_{sr}\frac{\partial}{\partial z}\left(H_c\frac{\partial C_{cs}}{\partial z}\right) + R_{cs}H_c + v_{char}\lambda_s\frac{\partial^2 T_{char}}{\partial z^2} + h_{conv}A(T_{bed} - T_{char}) + \sigma_{rad}\varepsilon_{rad}A\left({T_{bed}}^4 - {T_{char}}^4\right) \quad (3.67)$$

The term on the left hand side is the energy accumulation of char. The first term on right hand side is char energy change by convective heat flow, the second term is energy by dispersion of solids in axial direction; the third term forms the heat generated by the chemical reactions; the fourth term is the energy by conduction; the fifth term forms the energy by convective heat transfer and the sixth term is energy by radiation.

The fluid dynamics of a fluidized bed are complex because of the interactions of particles and gas.The effects of solids mixing is considered using the axial solids dispersion coefficient is given by *Niklasson et al., (2002)* as

$$D_{sr} = 3/16 \times \frac{\varepsilon_b}{(1-\varepsilon_b)}\frac{u_{mf\times d_b}}{\varepsilon_{mf}} \quad (3.68)$$

Convective heat transfer coefficient of individual particles in the BFB is taken from correlations of *Gunn(1978)*. This correlation is valid for range of volume fraction (0-0.65). Convective heat transfer coefficient of individual particles in the BFB, $h_{conv} = \frac{Nu\lambda_s}{d_p}$ where the Nusslet Nu number correlations of *Gunn(1978)* is given as

$$Nu = (7 - 10\varepsilon_b + 5{\varepsilon_b}^2)\left(1 + 0.7{Re_p}^{0.2}Pr^{1/3}\right) + (1.33 - 2.4\varepsilon_b + 1.2{\varepsilon_b}^2){Re_p}^{0.7}Pr^{1/3} \quad (3.69)$$

3.4 Hydrodynamic relationships

In the biomass gasification in a BFB gasifier, controlling the gas velocity in an appropriate range is important to achieve required fluidization and minimize the pressure drop. In addition, heat and mass transfer rates are also related to the fluidization characteristics of the bed. Therefore, understanding and quantitatively description of the hydrodynamics of the gas-solid fluidization within the gasifier is important. Figure 3.5 shows the pressure drop as a function of gas superficial velocity over a bed of granular solid materials with a gas stream flowing through it (*Kunii and Levenspiel, 1991)*. When the superficial gas velocity is lower than the minimum fluidization velocity (u_{mf}), the bed remains to be stationary and the solids movement are not observed. In this case, the pressure drop increases linearly with the gas velocity. As the velocity is increased to reach the minimum fluidization velocity, the pressure drop across the bed also reaches the maximum value of ΔP_{mf} where the particles begin to separate and be fluidized. The maximum pressure drop (ΔP_{mf}) in the gasifier filled with granular bed materials can be determined by Ergun's correlation as a function of superficial minimum fluidization velocity and bed porosity *(Téllez et al., 1999).*

$$\Delta P_{mf} = \frac{150\mu_g(1-\varepsilon_b)^2}{d_p^2{\varepsilon_b}^3}u_{mf} + \frac{1.75\rho_g(1-\varepsilon_b)}{d_p{\varepsilon_b}^3}u_{mf}^2 \tag{3.70}$$

In order to derive the expression for $\frac{du_0}{dz}$, used in the PDEs of Equations$(3.44, 3.46, 3.65\ and\ 3.66)$, the Ideal Gas Law $\mathrm{P = CRT}$ and the maximum pressure drop (ΔP_{mf}) Equation (3.70) for the bubble phase were second order differentiated with respect to z,

$$\frac{d^2p}{dz^2} = \frac{150\mu_g(1-\varepsilon_b)^2}{d_p^2{\varepsilon_b}^3}\frac{du_0}{dz} + \frac{1.75\rho_g(1-\varepsilon_b)}{d_p\varepsilon^3}2u_0\frac{du_0}{dz} \tag{3.71}$$

$$\frac{d^2p}{dz^2} = R\left(C_{ib}\frac{d^2T_b}{dz^2} + T_b\frac{d^2C_{ib}}{dz^2} + 2\frac{dT_b}{dz}\frac{dC_{ib}}{dz}\right) \tag{3.72}$$

From Equation $(3.71)$and (3.72)we can derive an expression for $\frac{du_0}{dz}$, obtained as given below

$$\frac{du_0}{dz} = \frac{R\left(C_{ib}\frac{d^2T_b}{dz^2}+T_b\frac{d^2C_{ib}}{dz^2}+\frac{2dT_bdC_{ib}}{dz\ dz}\right)}{\left(\frac{150\mu_g(1-\varepsilon_b)^2}{d_p^2{\varepsilon_b}^3}+\frac{1.75\rho_g(1-\varepsilon_b)}{d_p\varepsilon^3}2u_0\right)} \tag{3.73}$$

In the hydrodynamics model developed in this thesis, the particle properties (e.g. particle diameter, solid density) were assumed to be the same as that of the bed material. The bed material is much smaller and denser than those of the feedstock and chars. In addition, the feedstock and the chars account for 5-10 wt% of the total bed materials, and thus the inert bed material plays a major role in the BFB.

However, considering the behaviour (i.e, heat and mass transfer) of the char particles in the bed, the average value of the mixture of biomass char particles and bed material will be considered.

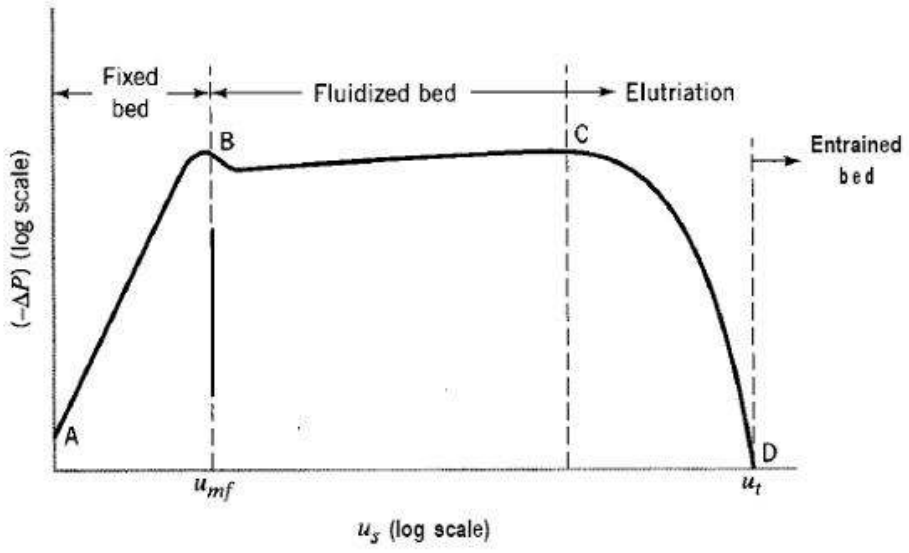

Figure 3.5: Pressure drop verses as a function of gas superficial velocity for uniform sized particles in the fluidized bed gasifier *(Kunii and Levenspiel, 1991)*.

When the superficial gas velocity is further increased, the terminal velocity is reached when the bed material elutriation occurs and some of the bed materials are carried away from the gasifier. The bed can be operated safely in a range of superficial gas velocities between the minimum fluidization velocity and the terminal velocity of the particles. In this study, bubbling bed flow regime is required and the hydrodynamics in this regime are determined from models published in literature *(Gidaspow, 1994; Huilin et al., 2003; Kunii and Levenspiel, 1991; Mori and Wen, 1975; Téllez et al., 1999)*. The results of the hydrodynamics of the BFB were used in the biomass gasification model. Property variables of the gases and

the solid involved in the hydrodynamic model equations are interrelated through hydrodynamics of the bubble phenomena which is summarized in Table 3.8.

In the biomass gasifier, determination of the minimum fluidization velocity u_{mf} was critical both for the modelling and for the gasification operation. The heat and mass transfer coefficients between the bubble phase and the emulsion phase were related to the minimum fluidization gas velocity, mass fractions of the bed materials and the bubble diameter and other bubble properties. Due to the irregular shape and size of the biomass particles, the minimum fluidization velocity varies significantly as shown in *Cui and Grace (2007)* who proposed separate correlations for spherical and angular particles. *Mori and Wen (1975)* proposed a correlation to calculate the bubble diameter, d_b, as shown in Table 3.8.

Table 3.8: Hydrodynamics parameters used in the modelling of fluidized bed gasifier.

Parameters	Equations	References
Minimum fluidization velocity, $u_{mf}(m/s)$	$u_{mf} = \frac{\mu_g[27.2^2 + 0.0408Ar]^{0.5}}{d_p \rho_g} - 27.2$	*(Cui and Grace, 2007)*
Archimedes number, Ar	$Ar = \frac{d_p^3 \rho_g (\rho_s - \rho_g) g}{{\mu_g}^2}$	*(Cui and Grace, 2007)*
bubble diameter, $d_b(m)$	$d_b = d_{bm} - (d_{bm} - d_{b0}) exp(0.3Z/d_t)$ where $d_{bm} = 1.64\left(S(u - u_{mf})\right)^{0.4}$ and $d_{b0} = 0.872\left[\frac{A(u-u_{mf})}{n_d}\right]^{0.4}$	*(Kunii and Levenspiel, 1991; Mori and Wen, 1975)*
bubble velocity $u_b(m/s)$	$u_{br} = 0.711\sqrt{(g d_b)}$ $u_b = u_0 - u_{mf} + u_{br}$	*(Davidson et al., 1985)*
Bubble fraction	$\varepsilon_b = \frac{u_0 - u_{mf}}{u_b - u_{mf}}$	*(Kunii and Levenspiel, 1991)*
emulsion velocity $u_e(m/s)$	$u_e = \frac{u_{mf}}{(1 - \varepsilon_b)}$	*(Davidson et al., 1985)*
Inter phase mass transfer coefficient, $K_{be}\left(\frac{1}{s}\right)$	$\frac{1}{K_{be}} = \frac{1}{K_{bc}} + \frac{1}{K_{ce}}$; $K_{ce} = 6.77\left(\frac{D\varepsilon_{mf}u_{br}}{d_b^3}\right)^{0.5}$ and $K_{bc} = \frac{4.5u_{mf}}{d_b} + \left(\frac{5.85\, D^{1/2} g^{1/4}}{d_b^{5/4}}\right)$	*(Kunii and Levenspiel, 1991)*
Inter phase volumetric heat transfer coefficient, $H_{be}\left(\frac{kW}{m^3 K}\right)$	$\frac{1}{H_{be}} = \frac{1}{H_{bc}} + \frac{1}{H_{ce}}$; $H_{ce} = 6.78\left(\frac{\varepsilon_{mf}\lambda_g \rho_g C_{P,g} u_b}{d_b^3}\right)^{0.5}$	*(Kunii and Levenspiel, 1991)*

$$H_{bc} = \left(\frac{4.5\left(u_{mf}\rho_g C_{P,g}\right)}{d_b}\right) + \frac{5.85\left(\left(\lambda_g \rho_g C_{P,g}\right)^{1/2} g^{1/4}\right)}{d_b^{5/4}}$$

Pressure gradient at minimum fluidization condition (Pa)	$\Delta P_{mf} = \frac{150\mu_g\left(1-\varepsilon_{mf}\right)^2}{d_p^2 {\varepsilon_{mf}}^3} u_{mf} + \frac{1.75\rho_g\left(1-\varepsilon_{mf}\right)}{d_p {\varepsilon_{mf}}^3} u_{mf}^2$	*(Téllez et al., 1999)*
Terminal velocity, $u_t(m/s)$	$u_t = \sqrt{\frac{4gd_p\left(\rho_s-\rho_g\right)}{3\rho_g C_D}}$	*(Cui and Grace, 2007)*
Drag co-efficient, $C_D(-)$	$C_D = \frac{24}{Re_s}(1+0.15Re_s^{0.687})$	*(Gidaspow, 1994)*
Effective density, $\rho_{eff}\left(\frac{kg}{m^3}\right)$	$\rho_{eff} = \frac{M_{char}\rho_{char} + M_{bed}\rho_{bed}}{M_{char}+M_{bed}}$	*(Zhong et al., 2008)*

3.5 Solving the gasification model using a numerical method

3.5.1. Initial and boundary conditions

The developed biomass gasification model presented in previous sections consists of a series of 14 PDEs and solving these equations requires defined initial conditions (ICs) and boundary conditions (BCs) as well as a numerical method to be employed. The initial conditions include mass of biomass, mass of steam, concentrations of major producer gas species and material temperatures within the gasifier at the starting time (*t=0*).

In principle, if a differential equation is of order 'n', then to solve the differential equation we need to know the values of 'n' constants from the initial and boundary conditions. So based on the degree of the differential equations the required number of constants values are to be known in order to solve the problem. For dealing with second order partial differential equations, boundary conditions specify the variables or its derivatives or a combination of both. For any given problem, the boundary conditions must be specified over the enclosing boundaries or over perimeter of the modelled region.

In the BFB gasifier model, the boundary conditions were those at the inlet (bottom) and the outlet (top) of the BFB gasifier. In this model three different types of boundary conditions

were used at inlet and outlet of the gasifier for different parameters. At the inlet, the concentration of the gas species for both the emulsion and bubble phase used Robin type boundary condition, while for the temperatures; simple Dirichlet boundary conditions were used. At the exit, for all the parameters Neumann Boundary Condition was used. The boundary conditions at the steam inlet of the gasifier (*z = 0; t > 0*):

For the bubble phase,

Concentration of the gas species, $C_{ib} - \frac{\varepsilon_b D_{ib}}{u_b}\frac{\partial C_{ib}}{\partial z} = \varepsilon_b C_{i0} \quad where, i = 1,2..5$

Temperature, $T_b = T_{in}$

For the emulsion phase,

Concentration of the gas species, $C_{ie} - \frac{\varepsilon_e D_{ie}}{u_e}\frac{\partial C_{ie}}{\partial z} = \varepsilon_e C_{i0} \quad where, i = 1,2..5$

Temperature, $T_e = T_{in}$

Solids concentration, $C_{cs} - \frac{\varepsilon_b D_{sr}}{u_s}\frac{\partial C_{cs}}{\partial z} = \frac{C_{c0}}{Msand}$

Temperature, $T_{char} = T_{in}$

The boundary conditions at the producer gas exit of the gasifier ($Z = H_b$; $t > 0$):

For the bubble phase,

Concentration of the gas species, $\frac{\partial C_{ib}}{\partial z} = 0 \quad where, i = 1,2..5$

Temperature, $\frac{\partial T_b}{\partial z} = 0$

For the emulsion phase,

Concentration of the gas species, $\frac{\partial C_{ie}}{\partial z} = 0 \quad where, i = 1,2..5$

Temperature, $\frac{\partial T_e}{\partial z} = 0$

Solids, $\frac{\partial C_{ks}}{\partial z} = 0$

Temperature, $\frac{\partial T_{char}}{\partial z} = 0$

The initial concentrations of product species for the gasification reactions in the BFB gasifier were set to be those determined from the initial pyrolysis. The initial temperature of the bubble phase (T_b) and that of the emulsion phase (T_e) were the same as the bed temperature.

3.5.2. Numerical method for solving the developed model

A set of 14 highly non-linear PDEs that describe the mass balances (5 Equations for the bubble phase (3.44), 5 Equations for the emulsion phase (3.46) and a solid char Equation (3.47)) and energy balances (three Equations (3.65 − 3.67) for the 2 phases and solid char) needed to be solved for the simulation of the gasifier. The simultaneous solution of these parabolic PDEs yields the transient concentration distribution of different species and the temperature in the gasifier. Using the values of initial condition and the boundary conditions as described in Section 3.5.1, the proposed unsteady state gasification model had been solved. In the simulation, the biomass bed in the gasifier was fluidized by the injected steam, which is a known parameter, at a given S/B ratio. The fluidization condition was checked to stay with the bubbling fluidization regime. The details of the input parameters used for computation at the operating conditions are presented in Table 3.1 and a detailed flow diagram for the computational procedure of the numerical methods used is shown in Figure 3.6.

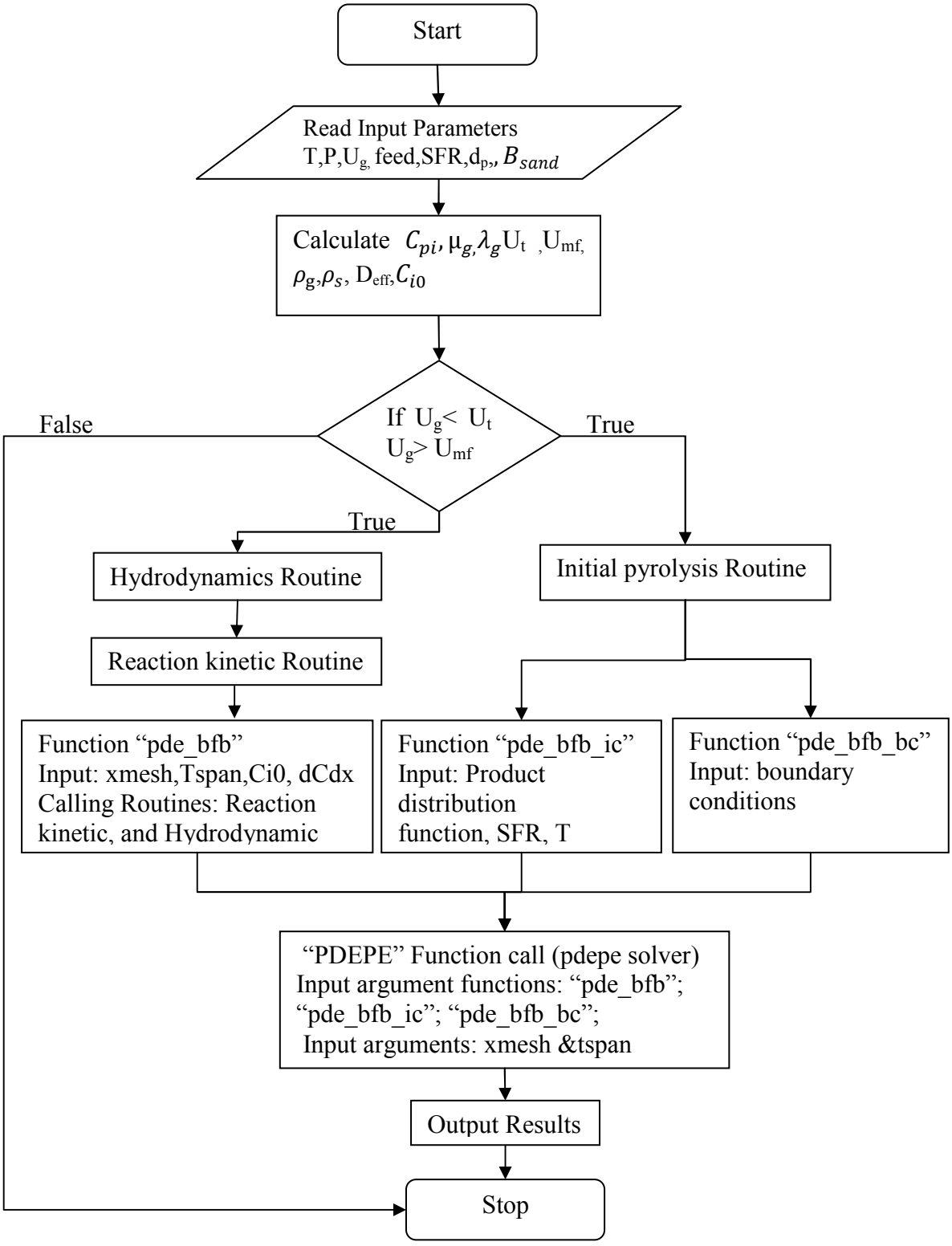

Figure 3.6: Flow diagram of the computational method

In this calculation procedure the model contains three modules to be evaluated: the initial pyrolysis distribution function routine, the hydrodynamic routine for the hydrodynamic closures for the model and the reaction kinetics routines that involve both emulsion and bubble phase before the nonlinear PDEs were solved. In the simulation, the PDEs $(3.44, 3.46, 3.47, 3.65, 3.66\ and\ 3.67)$ with the nonlinear boundary and initial conditions were coupled and solved using the solver function of the MATLAB Partial Differential Equation toolbox called the 'pdepe' solver. The MATLAB 'pdepe' solver solves initial-boundary value problems for systems of parabolic PDEs in the one space variable z and time t of the form shown in Equation (3.74).The 'pdepe' solver firstly converts the PDEs to Ordinary differential Equations ODEs using a second-order accurate spatial discretization based on a fixed set of nodes specified by the user.

$$c\left(x,t,u,\frac{\partial u}{\partial x}\right)\frac{\partial u}{\partial t}=\frac{\partial}{\partial x}\left(x\,f\left(x,t,u,\frac{\partial u}{\partial x}\right)\right)+s\left(x,t,u,\frac{\partial u}{\partial x}\right) \qquad (3.74)$$

In Equation(3.74), $f\left(x,t,u,\frac{\partial u}{\partial x}\right)$ is a flux term and $s\left(x,t,u,\frac{\partial u}{\partial x}\right)$ is a source term. The coupling of the partial derivatives with respect to time is restricted to multiplication by a diagonal matrix $c\left(x,t,u,\frac{\partial u}{\partial x}\right)$. These three terms were computed by the function 'pde_bfb'. Using the Equation (3.74), 14 nonlinear PDEs were formed and solved simultaneously and the terms '*c', 'f', 's'* corresponding the PDEs were formed as vectors.

In the Equation (3.74) the unknown variable 'u' specified is a vector variable, whose length will be equal to the no of unknown variable. In this model, there are six unknown variables for the emulsion phase (one temperature variable T_e from Eq.(3.66) and five concentrations variables $C_{ie}\ where\ i = 1,2..5$ in Eq.(3.46)) and another six unknown variables for the bubble phase (one temperature variable T_b in Eq.(3.65) and five concentrations variables $C_{ib}\ where\ i = 1,2..5$ in Eq.(3.44)); and one temperature variable T_{char} from Eq.(3.67) one unknown variable C_{cs} in Eq.(3.47); so the vector variable 'u' have a total size of 14 represented as, u(1),u(2),...u(14).

In this model the input arguments for the'pdepe' solver are 'function variables' such as 'pde_bfb_ic', 'pde_bfb_bc' and 'pde_bfb' and two vector variables that is represented by 'xmesh' and 'tspan'. The 'pde_bfb_ic' function variable input represents the initial condition, the function 'pde_bfb_bc'acts as function variable for the boundary conditions, while the function 'pde_bfb' in the 'pdepe' solver is a handle to a function that defines the

components(c, f, s) of the PDE for all the 14 nonlinear PDEs. These functions as input arguments for the 'pdepe' solver are represented in the flow diagram (Figure 3.6). The xmesh is a vector (x_0, x_1, ...,x_n) specifying the points at which a numerical solution is requested for every value in tspan. The elements of xmesh satisfy the condition $x_0 < x_1 < ... < x_n$ and in this model it is defined with the mesh size of 0.02m along with the integral length from zero (initial value) to two (final value).The tspan is a vector (t_0, t_1, ...,t_f) specifying the points at which a solution is requested for every value in xmesh. The elements of tspan satisfy the condition$t_0 < t_1 < ... < t_f$. The tspan defines the time step of 3.6s from zero seconds (initial time step) to 40mins (final time step). In addition, the test for converge of solution of the model of the PDEs; the pdepe solver function has an optional parameter input which defines the relative and absolute tolerance value of the solution variables. In this model the relative and absolute tolerance for the measure of accuracy was set to about $10^{-4}$and 10^{-6}, respectively, which showed a corresponding relative error of 0.01% and the convergence of the solution has been achieved within the range of set values.

3.5.3. Selected simulation results

A selective simulation was carried out on the developed model at about 780^{o}C and a S/B ratio of about 0.53 using the conditions as presented in Table 3.1. As discussed in Section 3.2, the concentrations of the product species from the pyrolysis were used as initial conditions for the subsequent gasification reactions. Therefore, the pyrolysis was simulated first and the predicted results of gas product compositions for operating temperature of 780^{o}C from the product distribution function (Equation 3.14a) contains 27.2% H_2, 39.8% CO, 19.6% CO_2 and 13.5% CH_4 (mol/mol). These results were in close agreement with our experimental measurements. The trend of the above gas compositions was also in consistent with previous studies of Wei and his colleagues carried out pyrolysis experiment for four different kinds of biomass including pine sawdust from 500^{o}C to 800^{o}C *(Wei et al., 2006)*. The model predicted gas composition from the present study was also in close agreement with the experimental results of Wei *et al.* (2006) for pyrolysis of pine sawdust at operation temperatures from 700 to 800^{o}C. These results are shown in Table 3.9.

The simulation results of product gas composition from the second stage of the gasification process at the top of the gasifier are shown in Figure 3.7 over different time intervals for the same operating conditions. However, the modelling results for gasification have noticeable

discrepancies from the experimental values. The model predictions were in close agreement with the experimental data for CO, CH_4 with discrepancies of less than 2% (mol/mol) compared to the experimental data. The discrepancies in the gas concentration for $H_2$and CO_2 were less than 7.5% (mol/mol) and 8 % (mol/mol), respectively. For both experimental and simulation results the H_2 content increased and CO_2, CO and CH_4contents decreased as the operating temperature increased from 680 to 780°C. For the effect of steam-to-biomass ratio, the modelling results also showed similar trends as those of the experimental data.

From the Figure 3.7, it was found that the CO concentration is higher at about 35.7 mol/mol % (dry basis) but decreases from the overall pyrolysis concentration. The concentration of $H_2$and CO_2wereincreased to about 28.3mol% from its corresponding pyrolysis product of 27.1mol/mol% (dry basis) for H_2 and that of CO_2 concentration from19.6% to 23 mol/mol% (dry basis).The concentrations of CH_4decreased marginally with respect to the pyrolysis products, with concentration of CH_4changing from 13.5% to 13.1 mol/mol% (dry basis).*Franco et al., (2003)* investigated three different biomass including pine wood for temperature of 800^{o}C whilst varying a steam/biomass ratio from 0.4 to 0.85 wt/wt and their findings were very close to our model as seen in Table 3.9.

Table 3.9: Comparison between the model predicted and experimental measured gas composition from biomass pyrolysis and biomass gasification under operating temperature of 780^{o}C and S/B ratio of 0.53

Species	Model prediction mole fraction [mol/mol %]		CAPE Experiment mole fraction [mol/mol %]		Experiment from literature [mol/mol%]	
	Pyrolysis	Gasification at S/B=0.53	Pyrolysis	Gasification at S/B=0.53	Pyrolysis# 700-800^{o}C	Gasification+ at S/B (0.5-0.8), 800^{o}C
H_2	27.16	28.3	27.14	36	24-29	21 – 35
CO	39.81	35.7	39.39	37.3	43-49	47 – 40
CO_2	19.57	23	19.95	14.2	14-16	11.6 – 16
CH_4	13.46	13.1	13.47	11.57	9-11	16 –10.5

 # (Wei et al., 2006)+ (Franco et al., 2003)

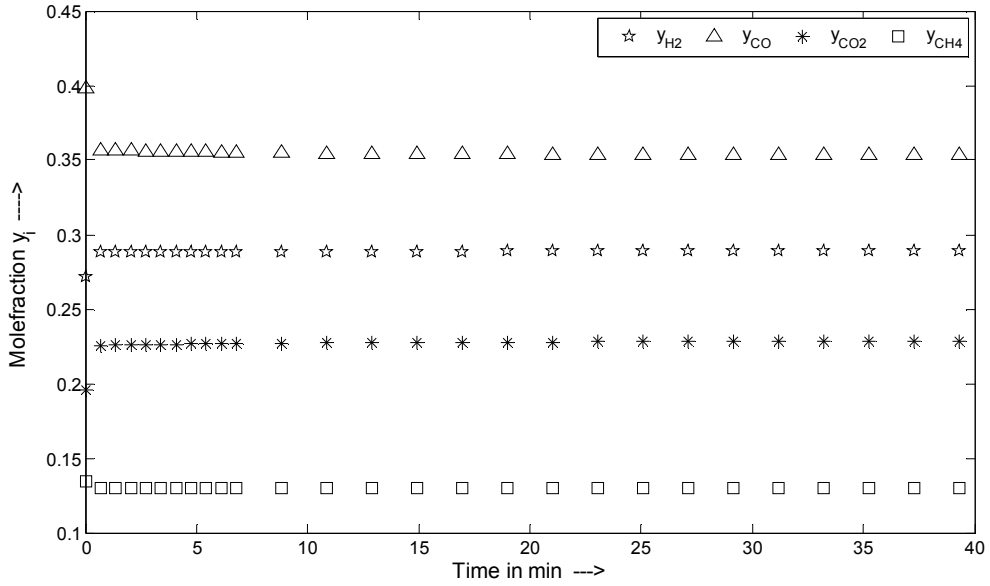

Figure 3.7: The predicted producer gas composition from biomass gasification at the top of the fluidized bed gasifier operating at 780^{o}C, 1 atmospheric pressure and S/B ratio of 0.53.

Later in Chapter 6 the developed one dimensional model will be validated by comparison of the simulation results with the experimental data for the biomass gasification in the temperature range from 680 to 780°C and S/B ratio between 0.33 and 0.84. After the validation the model was used to examine the effects of operation variables including steam/biomass ratio and gasification temperatures.

3.6 Conclusion

In this chapter, a 1D mathematical model was developed to simulate the biomass gasification process in a BFB gasifier with steam as gasification agent. The gasification process consists of initial pyrolysis reactions and subsequent gasification reactions. The initial pyrolysis process was also divided into two stage reactions with the first stage being biomass decomposition and the second stage being reactions of tars to form gases and char. These reactions were simulated to predict the yields of gases, char and tar as well as gaseous species in the product gas. The results from the pyrolysis were used as initial conditions for the subsequent gasification modelling which considered the reactions among char, gases from pyrolysis and gasification agent, steam in this case.

The gasification model developed also included heat and mass transfer processes with the gasifier to quantify the temperature profile and the gas concentration profile within the gasifier. The pyrolysis reactions and the gasification reactions were affected by reaction temperature and the gas species will diffuse within the gasifier, therefore, the gas yield and composition were a function of location of the gasifier under given operation conditions. In order to simulate the heat and mass transfer process, hydrodynamics were also needed. In this model developed, two flow phases were considered (emulsion and bubble phase) and published hydrodynamics correlations were adopted. However, more detailed hydrodynamics of the gas-solid flow in the gasifier will be analyzed in Chapter 4 and a 2D gasification model considering the variation both along the gasifier height and radius were taken into account.

The proposed model had been solved using a numerical method with defined boundary and initial conditions. Selected simulation results were presented. The model will be validated using experimental data in Chapter 6.

3.7 References

Abrahamsen, A.R., Geldart, D., 1980. Behaviour of gas-fluidized beds of fine powders part I. Homogeneous expansion. Powder Technology 26, 35-46.

Bilbao, R., Millera, A., Murillo, M.B., 1993. Temperature Profiles and Weight-Loss in the Thermal-Decomposition of Large Spherical Wood Particles. Industrial & Engineering Chemistry Research 32, 1811-1817.

Bridgwater, A.V., 1995. The technical and economic feasibility of biomass gasification for power generation. Fuel 74, 631-653.

Chan, W.R., Kelbon, M., Krieger, B.B., 1985. Modelling and experimental verification of physical and chemical process during pyrolysis of a large biomass particle. Fuel 64, 1505-1515.

Cui, H., Grace, J.R., 2007. Fluidization of biomass particles: A review of experimental multiphase flow aspects. Chemical Engineering Science 62, 45-55.

Corella, J., Sanz, A., 2005. Modeling circulating fluidized bed biomass gasifiers. A pseudo-rigorous model for stationary state. Fuel Processing Technology 86, 1021–1053.

Davidson, J.F., Clift, R., Harrison, D., 1985. Fluidization. Orlando : Academic Press, London

Di Blasi, C., 1994. Numerical simulation of cellulose pyrolysis. Biomass and Bioenergy 7, 87-98.

Di Blasi, C., 2002. Modeling intra- and extra-particle processes of wood fast pyrolysis. AIChE Journal 48, 2386-2397.

Di Blasi, C., 2004. Modeling wood gasification in a countercurrent fixed-bed reactor. AIChE Journal 50, 2306-2319.

Di Blasi, C., 2008. Modeling chemical and physical processes of wood and biomass pyrolysis. Progress in Energy and Combustion Science 34, 47-90.

Fairbanks, D.F., Wilke, C.R., 1950. Diffusion Coefficients in Multicomponent Gas Mixtures. Industrial & Engineering Chemistry 42, 471-475.

Franco, C., Pinto, F., Gulyurtlu, I., Cabrita, I., 2003. The study of reactions influencing the biomass steam gasification process. Fuel 82, 835-842.

Fuller, E.N., Schettler, P.D., Giddings, J.C., 1966. New method for prediction of binary gas-phase diffusion coefficients. Industrial & Engineering Chemistry 58, 18-27.

Gidaspow, D., 1994. Multiphase Flow and Fluidization: Continuum and Kinetic Theory Descriptions. Academic Press (21 Feb 1994).

Graham, R.G., Bergougnou, M.A., Freel, B.A., 1994. The kinetics of vapour-phase cellulose fast pyrolysis reactions. Biomass and Bioenergy 7, 33-47.

Gunn, D.J., 1978. Transfer of Heat or Mass to Particles in Fixed and Fluidized-Beds. International Journal of Heat and Mass Transfer 21, 467-476.

Hemingway, B.S., 1987. Quartz: Heat capacities from 340 to 1000 K and revised values for the thermodynamic properties. American Mineralogist 72, 273-279.

Huilin, L., Gidaspow, D., Bouillard, J., Wentie, L., 2003. Hydrodynamic simulation of gas-solid flow in a riser using kinetic theory of granular flow. Chemical Engineering Journal 95, 1-13.

Kunii, D., Levenspiel, O., 1991. Fluidization Engineering, Second Edition ed. Butterworth-Heinemann.

Levenspiel, O., 1999. Chemical Reaction Engineering (3rd Edition). John Wiley & Sons.

Luyben, W.L., 1996. Process Modelling, Simulation, and Control for Chemical Engineers. McGraw-Hill Publisbing Company.

Macak, J., Malecha, J., 1978. Mathematical model for the gasification of coal under pressure. Industrial & Engineering Chemistry Process Design and Development 17, 92-98.

Melaaen, M.C., 1996. Numerical analysis of heat and mass transfer in drying and pyrolysis of porous media. Numerical Heat Transfer, Part A: Applications 29, 331-355.

Milosavljevic, I., Oja, V., Suuberg, E.M., 1996. Thermal effects in cellulose pyrolysis: Relationship to char formation. Industrial and Engineering Chemistry Research 35, 653-662.

Missen, R.W., Mims, C.A., Saville, B.A., 1999. Introduction to chemical reaction engineering and kinetics. John Wiley & Sons, Inc.

Modell, M., Reid, R.C., 1974. Thermodynamics and its Applications. Prentice-Hall, Englewood Cliffs, N. J.

Moran, M.J., Shapiro, H.N., Boettner, D.D., Bailey, M.B., 2011. Fundamentals of Engineering Thermodynamics, 7th ed. Wiley.

Mori, S., Wen, C.Y., 1975. Estimation of bubble diameter in gaseous fluidized beds. AIChE Journal 21, 109-115.

Niklasson, F., Thunman, H., Johnsson, F., Leckner, B., 2002. Estimation of Solids Mixing in a Fluidized-Bed Combustor. Ind. Eng. Chem. Res. 41, 4663-4673.

Nikoo, M.B., Mahinpey, N., 2008. Simulation of biomass gasification in fluidized bed reactor using ASPEN PLUS. Biomass and Bioenergy 32, 1245-1254.

Perry, R.H., Green, D.W., Maloney, J.O., 1997. Perry's Chemical Engineers' Handbook. McGraw-Hill, New York.

Radmanesh, R., Courbariaux, Y., Chaouki, J., Guy, C., 2006. A unified lumped approach in kinetic modeling of biomass pyrolysis. Fuel 85, 1211-1220.

Rath, J., Wolfinger, M.G., Steiner, G., Krammer, G., Barontini, F., Cozzani, V., 2003. Heat of wood pyrolysis. Fuel 82, 81-91.

Rohsenow, W., Hartnett, J., Cho, Y., 1998. Handbook of heat transfer. McGraw-Hill Professional; 3 edition

Schuster, G., Löffler, G., Weigl, K., Hofbauer, H., 2001. Biomass steam gasification - An extensive parametric modeling study. Bioresource Technology 77, 71-79.

Smith, J.M., Van Ness, H.C., Abbott, M.M., 2001. Introduction to Chemical Engineering Thermodynamics, Sixth ed. ed. McGraw-Hill International, Singapore.

Téllez, C., Menéndez, M., Santamaría, J., 1999. Simulation of an inert membrane reactor for the oxidative dehydrogenation of butane. Chemical Engineering Science 54, 2917-2925.

Tosun, I., 2002. Modeling in Transport Phenomena - A Conceptual Approach. Elsevier Science B.V.

Wang, Y., Kinoshita, C.M., 1993. Kinetic model of biomass gasification. Solar Energy 51, 19-25.

Wei, L., Xu, S., Zhang, L., Zhang, H., Liu, C., Zhu, H., Liu, S., 2006. Characteristics of fast pyrolysis of biomass in a free fall reactor. Fuel Processing Technology 87, 863-871.

Welty, J.R., Wicks, C.E., Wilson, R.E., Rorrer, G.L., 2008. Fundamentals of Momentum, Heat, and Mass Transfer, 5th ed. John Wiley & Sons, Inc.

Yan, H.-m., Heidenreich, C., Zhang, D.-k., 1998. Mathematical modelling of a bubbling fluidised-bed coal gasifier and the significance of 'net flow'. Fuel 77, 1067-1079.

Zhong, W., Jin, B., Zhang, Y., Wang, X., Xiao, R., 2008. Fluidization of Biomass Particles in a Gas−Solid Fluidized Bed. Energy & Fuels 22, 4170-4176.

Chapter 4

A hydrodynamics model for flows in the BFB

In this study a mathematical Eulerian-Eulerian granular kinetic model was developed to simulate 2D flows in the BFB of sand using steam as the fluidization agent. This model was then extended into 3D to understand the hydrodynamic characteristics in the BFB gasifier.

For simulation of the gas-solid flows in the DFB gasifier system, complete mixing of gas-solids phase laminar flow model was proposed and numerically solved. It was assumed there were no chemical reactions involved within the bed. Conservation of mass and momentum equations for the gas and the solid phases were used to compute the hydrodynamics of flows in BFB for core-annular flow regimes. The principal input into the model was feed stream while the solid circulating bed material inside the bed uses a semi empirical viscosity relationship and particle-gas interaction drag force. The model predicts the dynamics of flow of solid particles and the gas feed streams, particle bed pressure and the gas pressure.

4.1 Introduction

Fluidized beds are the most widely used type of gasifiers for pyrolysis and gasification, as they offer a number of advantages, such as high heat transfer rates and good temperature control. In general, a fluidized bed is a vertical, tubular column/vessel in which a bed of solids are fluidized with a continuous stream of gas normally injected from the bottom. Multiphase BFB gasifiers are extensively used in the petrochemical and biochemical industries and in recent years, for more complex reaction systems. Although fluidized bed technology has been used in commercial plants in coal and biomass combustion, there are a number of areas for better understanding in biomass gasification such as scale-up, erosion, agglomeration and de-fluidization. *Gidaspow et al. (1992)* suggests that with understanding of the hydrodynamic theory of fluidized bed and accurately modelling, the risk associated with these issues can be reduced.

In a fluidized bed the gas-solid system exhibits a range of fluidization behaviour from stationary to aggressive turbulence which depends mainly on the superficial gas velocity. The hydrodynamics of fluidized beds had been widely investigated, both experimentally and theoretically, towards the quantification of particle–particle, fluid–particle and particle–bubble interactions, flow structure and flow regime. The existing hydrodynamic theory with equations describing these phenomena has been verified by experiments only for small scale plants by various authors. Extensive work on the design of such reactor columns had been reported in the literature *(Kersten et al., 2003a; Kersten et al., 2003b; Shah, 1979)*. Most of the past modelling of the BFB gasifiers was based on empirical correlations fitted from experiments. Even though these correlations fit the data well, they were restricted to a narrow range of operating parameters. However investigation on a large scale plants does not necessarily reflect the desired characteristics as verified by the small scale plant.

In the past modelling of complex flow behaviour in a fluidized bed was approached mostly by experimental measurements and analytical analysis, rather than numerical simulation due to huge computation time and lack of validation. With the advancement in technology and rapid development of super computers over the decades, numerical simulation (multi-dimensional CFD modelling) has become the most promising technique to predict the flow behaviour in the gas-solid fluidized beds quickly and accurately and hence had been used in this work. On the other hand the complex hydrodynamics of the fluidized bed gasifiers were not well understood and hence CFD modelling had been promoted as a useful tool for understanding multiphase flows in the gasifiers. By means of the CFD models, new design can be modelled ensuring time and cost effective solutions. This reduces the cost of building and testing different sizes of rigs for the purpose of scale up.

This chapter gives a brief overview on the fluidized bed hydrodynamic model and discusses the CFD modelling in the gas-solid particle fluidized beds. Finally the method used to solve the governing equations involved in the CFD simulations were be described.

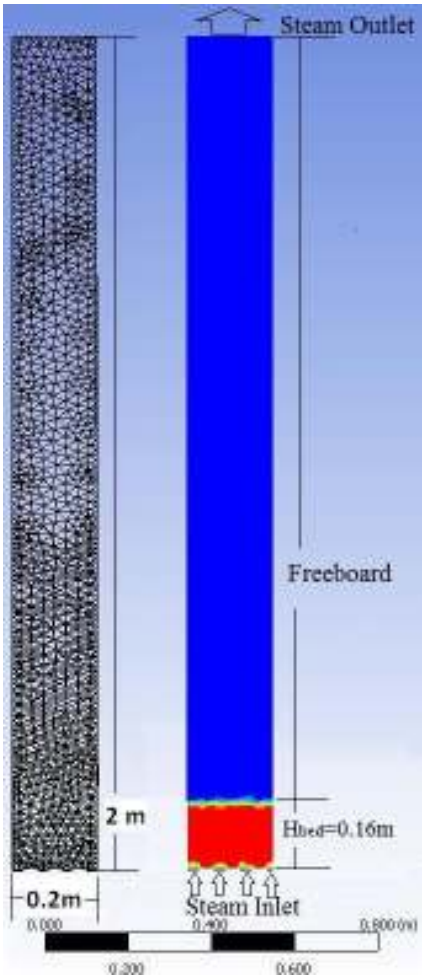

Figure 4.1: Schematic diagram of the BFB gasification gasifier with mesh grid.

4.2. Hydrodynamic model and numerical procedure

In the current study the momentum transport from the fluidizing gas to a solid particle for the BFB (i.e., hydrodynamic model) was developed based on the schematic diagram as shown in Figure 4.1. The principle of conservation of mass and momentum presented in the hydrodynamic model were related to the pressure drop in the system, several interphase drag coefficient functions and granular properties which were published by different authors *(Gidaspow et al., 1992; Syamlal and O'Brien, 1989; Wen and Yu, 1966)*. The flow, mixing, segregation and attrition phenomenon of particulate systems of granular particles plays an important role in the fluidized bed. They are characterized by the mean square of particle velocity fluctuations, which is directly related to the so-called granular temperature Θ_s. For the Eulerian model, the conservation of the kinetic energy of the moving particles was described by the granular temperature, Θs while the solid-phase shear and bulk viscosities

were obtained by applying the kinetic theory of granular flow (KTGF) available in ANSYS Fluent *(ANSYS FLUENT12.0., 2009)*. The ANSYS Fluent solution provides options to select appropriate correlations that suit the model domain where the properties such as velocity, pressure and the volume fraction of gas and solids were determined.
In this model the following assumptions are made:

1) No heat and mass transfer between the gases and solids and no chemical reactions involved;
2) Constant input flux of gas streams at isothermal condition;
3) Fixed amount of solid particles in the BFB as seen in Figure 4.1;
4) Both solid and gas phases have constant densities and gas viscosity was constant at a given operating temperature;
5) Solid particle viscosity was assumed to be a constant based on KTGF *(Gidaspow et al., 1992)*.

4.2.1 Continuity equation

The principle of general mass conservation or the continuity equations is based on that fact that all the mass flow rates into the control volume (CV) are equal to the sum of all mass flow rates out of the CV and the rate of change of mass within the CV. The above principle can be applied to individual flow components or to the overall flow stream. The mass conversion equations or the continuity equations for gas and solid flows in the cold model fluidized beds are given below according to *Gibilaro (2001) and Papadikis et al (2008).* The phases are able to interpenetrate and the sum of all volume fractions in each computational cell is unity:

a) Gas phase

$$\frac{\partial}{\partial t}\left(\varepsilon_g \rho_g\right) + \nabla.\left(\varepsilon_g \rho_g \vec{v}_g\right) = 0 \qquad (4.1)$$

b) Solid phase

$$\frac{\partial}{\partial t}\left(\varepsilon_s \rho_s\right) + \nabla.\left(\varepsilon_s \rho_s \vec{v}_s\right) = 0 \qquad (4.2)$$

where ρ_g, ρ_sstand for density(kg/m^3), $\vec{v}_g, \vec{v}_s$for velocity $(m/s)$and $\varepsilon_g, \varepsilon_s$for volume fraction. The subscript $g\ and\ s$, respectively, refers to gas and solid phase.

4.2.2 Momentum equation

Unlike the 1D model described in Chapter 3 where the fluidization dynamics were described by empirical and semi-empirical correlations, in this CFD model the fluidization behaviour is described by the momentum equations. Momentum is a vector quantity that possesses the directional properties of the phases and the corresponding magnitude involved in the CV (gasifier). Like the mass conservation, momentum can also be conserved in the CV. The conservation of momentum of flows is defined by Newton's second law of motion in the fluidized bed. The momentum conservation equations are established according to *Gibilaro (2001)* by considering the forces that act on the fluid mass of the system, the momentum carried into and out of the systems. In addition, inter phase momentum transfer term is also included in the momentum conservation equation based on *Navier Stokes* equations *(Papadikis et al., 2008)*.

a) Gas phase

$$\frac{\partial}{\partial t}\left(\varepsilon_g \rho_g \vec{v}_g\right) + \nabla.\left(\varepsilon_g \rho_g \vec{v}_g \vec{v}_g\right) = -\nabla \varepsilon_g P_g + \varepsilon_g \rho_g g + \beta\left(\vec{v}_s - \vec{v}_g\right) + \nabla \varepsilon_g \vec{T}_g + \nabla \varepsilon_s \vec{T}_s \qquad (4.3)$$

b) Solid phase

$$\frac{\partial}{\partial t}\left(\varepsilon_s \rho_s \vec{v}_s\right) + \nabla.\left(\varepsilon_s \rho_s \vec{v}_s \vec{v}_s\right) = -\nabla \varepsilon_s P_s + \varepsilon_s \rho_s g + \beta\left(\vec{v}_g - \vec{v}_s\right) - \nabla \varepsilon_s \vec{T}_s \qquad (4.4)$$

The terms on the right-hand side of momentum Equations $(4.3 - 4.4)$ are pressure drop, gravity, fluid particulate interphase drag forces, and an additional force called the phase viscous stress tensors, respectively. The term $\nabla \varepsilon_s \vec{T}_s$ in Equation (4.3) represents the shear force on the particles due to local strain in the fluid. P_g is the gas pressure (Pa) and P_s is the solids pressure (Pa). According to the closure principles of governing equations, fluid particulate interphase drag coefficient, β, is discussed in details in the following section. The additional forces represented by viscous stress tensors, $\nabla \vec{T}_g$ and $\nabla \vec{T}_s$, need to be obtained from the basic fluid-field variables.

The equation of state of the gas was assumed to be the ideal gas law where solid phase was considered incompressible

$$P_g = \rho_g R T \qquad (4.5)$$

where R stands for universal gas constant $(kJ/(kmol.K))$ and T is the temperature (K).

However, the gas phase was compressible and its behaviour can be modelled as a Newtonian fluid without considering the effect of its turbulence on the gas viscosity. The gas stress tensor $\vec{T}_g$can then be determined by

$$\vec{T}_g = 2\varepsilon_g \mu_g \vec{\tau}_g \tag{4.6}$$

The solid stress tensor, $\vec{T}_s$ is calculated from the solid pressure $P_s(Pa)$, solid bulk viscosity ξ_s (kg/ms), and solid shear viscosity $\mu_s(kg/ms)$ as given in Equation (4.7). *(Papadikis et al., 2008)*

$$\vec{T}_s = (\xi_s \nabla . \vec{v}_s) I + 2\mu_s \vec{\tau}_s \tag{4.7}$$

where the tensor $\tau_i (i = g, s)$ is given by *Papadikis et al (2008)* as

$$\tau_i = \frac{1}{2}[\nabla \vec{v}_i + (\nabla \vec{v}_i)^T] - \frac{1}{3}(\nabla . \vec{v}_i) I \tag{4.8}$$

The above approach is also called the Eulerian-Eulerian model. In order to solve the above model, the fluid particulate interphase drag coefficient (β), the solid bulk viscosity (ξ_s) and the solid shear viscosity (μ_s) need to be determined from various models which will be discussed in the following sections. The solids properties such as solids pressure, solid bulk viscosity and solid shear viscosity are described later in Section 4.2.4 in details.

4.2.3 Fluid particulate interphase drag coefficients

In the solid-gas flow, gravity and drag are reported to be the dominant forces for the majority of flows with granular particles as the solid phase. However, for very dense flow, the frictional stresses became more important *(Schouten et al., 2001)*. For relatively small particles with densities being much larger than the density of the continuous gas phase, the fluid particulate interphase drag force is dominant over the other forces such as lift and virtual mass *(Ranade, 2002)*. As mentioned in the above section (Equations 4.3 and 4.4), the fluid particulate interphase drag force is represented by the drag coefficient, β. *Wen and Yu (1966)* modelled the fluid particulate interphase drag coefficient, which was valid for only dilute systems. A modified model proposed by *Gidaspow et al. (1992)* combined the *Ergun Equation (Gidaspow, 1994)* coefficients with the model of *Wen and Yu (1966)* for fluid particulate interphase drag coefficient which holds good for dense fluidized beds. The fluid

particulate interphase drag coefficients developed by *Gidaspow et al.(1992)* is represented in Equation(4.9).

$$\beta = \begin{cases} \frac{3}{4} C_D \frac{\varepsilon_s \varepsilon_g \rho_g |\vec{v}_s - \vec{v}_g|}{d_p} \varepsilon_g^{-2.65} & for \varepsilon_g > 0.80 \\ 150 \frac{\varepsilon_s (1-\varepsilon_g) \mu_g}{\varepsilon_g d_p^2} + 1.75 \rho_g \varepsilon_s \frac{|\vec{v}_s - \vec{v}_g|}{d_p} & for \varepsilon_g \leq 0.85 \end{cases} \quad (4.9)$$

However, for the continuously CFB gasifiers the coefficient model developed by *Gidaspow et al., (1992)* shows higher errors compared to a solid shear stress model proposed by *Syamlal and O'Brien (1989)* which arises from particle momentum exchange due to collision. In that case the model for fluid particulate interphase drag coefficient considering solid shear stress developed by *Syamlal and O'Brien (1989)* is more appropriate, and this model is given in Equation(4.10).

$$\beta = \frac{3}{4} \frac{\varepsilon_s \varepsilon_g \rho_g |\vec{v}_s - \vec{v}_g|}{v_{r,s}^2 d_p} C_D \left(\frac{Re_s}{v_{r,s}} \right) \quad (4.10)$$

where C_D is the drag coefficient that is derived by Dalla Valle as cited in *Syamlal and O'Brien (1989)* and is determined from relative Reynolds number, Re_s between the gas and solid phases, and the terminal velocity for the solid phase, $v_{r,s}$. The terminal velocity for the solid phase is, in turn, related to the relative Reynolds and gas phase fraction (ε_g) *(Garside and Al-Dibouni, 1977)*:

$$v_{r,s} = 0.5\left(A - 0.06Re_s + \sqrt{(0.06Re_s)^2 + 0.12Re_s(2B - A) + A^2}\right) \quad (4.11)$$

where $$A = \varepsilon_g^{4.14}; \quad (4.12)$$

$$B = \begin{cases} 0.8\varepsilon_g^{1.28} & for\ \varepsilon_g \leq 0.85 \\ \varepsilon_g^{2.65} & for\ \varepsilon_g > 0.85 \end{cases} \quad (4.13)$$

Finally the drag coefficient and the Reynolds number of the particles are given as follows

$$C_D = \left(0.63 + \frac{4.8}{\sqrt{Re_s / v_{r,s}}}\right)^2 \quad (4.14)$$

$$Re_s = \frac{\rho_g \varepsilon_g |\vec{v}_s - \vec{v}_g| d_s}{\mu_g} \quad (4.15)$$

In which μ_g is the gas viscosity (kg/ms) and d_p is the diameter of the particles of solid phase (m).

Depending on the problem domain constraints one of the two fluid particulate interphase drag coefficients were used our model. In the hydrodynamic model for the BFB, the fluid particulate interphase drag coefficient was calculated using Equation (4.9). On the other hand when modelling the DFB (which consists of the BFB and CFB) to understand the solids transfer between the beds, the fluid particulate interphase drag coefficients was treated with the model developed *by Syamlal and O'Brien (1989)* using Equation (4.10) which is more appropriate for CFB.

4.2.4 Kinetic theory of granular flow (KTGF)

In this model, the interaction between flow fields of the gas phase and solid phase generates stresses due to the impact of particles to particles were considered. Analogy to the kinetic theory of dense gases for the description of kinetic energy of gas molecules, the KTGF was developed to model the fluctuation of solid velocity and its variations due to gas flow causing the particles impact *(Lun et al., 1984)*. All the granular phase properties, such as the solids pressure, the solids shear stress, the solids shear viscosity and the solid bulk viscosity were expressed in terms of the granular temperature. In this approach, the average kinetic energy represented by granular temperature of the solid phase (Θ_s) was computed by solving the conservation of kinetic theory of granular Equation (4.16) for the randomly moving particles. In order to solve the fluctuating energy equation, we need to specify the collisional energy dissipation, γ_s, due to inelastic collisions of the particles and the diffusion coefficient for the granular conductivity, κ_s. The solid viscosity such as the solid shear viscosity, the solid bulk viscosity and the solids pressure can then be computed as a function of granular temperature at any time and position. The conservation of the kinetic energy of the moving particles can be described by the granular temperature, Θs *(Papadikis et al 2008)*:

$$\frac{3}{2}\left[\frac{\partial}{\partial t}(\varepsilon_s\rho_s\Theta_s) + \nabla.(\varepsilon_s\rho_s\vec{v}_s\Theta_s)\right] = \vec{T}_s : \nabla\vec{v}_s + \nabla.(\kappa_s\nabla\Theta_s) - \gamma_s \qquad (4.16)$$

The first term on the right-hand side is the production of fluctuating energy by the effective solid shear stresses. The second term is the diffusive flux of granular energy due to the gradient of granular temperature with κ_s describing the diffusion coefficient. The third term is the dissipation energy due to the inelastic collision of particles.

The diffusion coefficient for granular energy has been derived by *Syamlal et al. (1993)* as follows:

$$\kappa_s = \frac{15 d_s \varepsilon_s \rho_s \sqrt{\Theta_s \pi}}{4(41-33\eta)} \left[1 + \frac{12}{5}\eta^2(4\eta - 3) g_0 \varepsilon_s + \frac{16}{15\pi}(41 - 33\eta)\eta g_0 \varepsilon_s\right] \qquad (4.17)$$

where $\eta = \frac{1}{2}(1+e_{ss})$,$\Theta_s$ is the granular temperature(m^2/s^2), $g_0$the radial distribution is function and e_{ss} is the restitution coefficient of particles. For the restitution coefficient, different values were presented, from 0.8 to 1, in the literature *(Petersen and Werther, 2005)*. In this work, a restitution coefficient value of 0.9 was used which was reported for the average granular diameter of 275μm in the literature *(Enwald et al., 1996)* while the same average diameter of 275μm was used in the gasifier experiment as well.

The collisional dissipation of energy (γ_s) represents the rate of energy dissipation within the solid phase due to collision between particles. This term is represented by the expression derived by *Lun et al. (1984).*

$$\gamma_s = \frac{12(1-e_{ss}^2) g_0}{d_s \sqrt{\pi}} \rho_s {\varepsilon_s}^2 \Theta_s^{3/2} \qquad (4.18)$$

Once the granular temperature is known, the solid pressure and its gradient can be determined. For granular solid flow in the fluidized bed with the compressible gas as fluidization agent, the solids volume fraction is always less than its maximum solids packing value. The solids pressure (P_s) and its gradient (∇P_s) can be calculated by accounting for kinetic motion and normal stresses arising from collisions between individual solid particles.

$$P_s = \rho_s \varepsilon_s \Theta_s + 2\rho_s(1 + e_{ss}) g_0 {\varepsilon_s}^2 \Theta_s \qquad (4.19)$$

In the Equation (4.19) the first term of the solids pressure is the kinetic term and the second term is due to particle collisions.

The solids stress tensor contains the solid shear viscosity, μ_s and the solid bulk viscosity, ξ_s arising from particle momentum exchange due to translation and collision. A frictional component of viscosity can also be included to account for the viscous-plastic transition that occurs when particles of a solid phase reach the maximum solid volume fraction. Several authors such as *Gidaspow et al., (1992) and Syamlal and O'Brien (1989)* have developed expressions for the solid shear viscosity,μ_s, as a function of granular temperature as given in Equation (4.20). In this model the first term of right-hand side of the equation accounts for the kinetics *(Syamlal and O'Brien, 1989)* and the second term accounts the collision term was taken from *Gidaspow et al., (1992) and Syamlal and O'Brien (1989)*.

$$\mu_s = \frac{\varepsilon_s \rho_s d_s \sqrt{\theta_s \pi}}{6(3-e_{ss})} \left[1 + \frac{2}{5}(1 + e_{ss})(3e_{ss} - 1) g_0 \varepsilon_s\right] + \frac{4}{5}\varepsilon_s^2 \rho_s d_s g_0 (1 + e_{ss}) \sqrt{\frac{\theta_s}{\pi}} \qquad (4.20)$$

The solid bulk viscosity, ξ_s, derived from *Lun et al.(1984)*, accounts for the resistance of the granular particles to compression and expansion.

$$\xi_s = \frac{4}{3}\varepsilon_s^2 \rho_s d_s g_0 (1 + e_{ss}) \sqrt{\frac{\theta_s}{\pi}} \tag{4.21}$$

The radial distribution function, g_0 is a correction factor that modifies the probability of collisions between particles when the solid granular phase becomes dense. It's a function that governs the transition from the "compressible" condition with $\varepsilon_s < \varepsilon_{s,max}$ where the spacing between the solid particles can continue to decrease, to the "incompressible" condition with $\varepsilon_s = \varepsilon_{s,max}$where no further decrease in the spacing can occur.

$$g_0 = \left[1 - \left(\frac{\varepsilon_s}{\varepsilon_{s,max}}\right)^{1/3}\right]^{-1} \tag{4.22}$$

4.3 Simulation of the fluidized bed hydrodynamics

In this study the hydrodynamics simulation was carried out firstly for 2D BFB gasifier and then the simulation was extended to 3D for the integrated system called DFB gasification system with a BFB gasifier and a CFB gasifier.

In the 2D simulation, the hydrodynamic simulation of BFB gasifier has been done where the gasifier bed was filled with bed material (normally sand) to certain height and was fluidized with the fluidization agent such as air or steam. As the gas flows through the bed material, two phase mixture was formed with unique characteristics. The solids expand first and then may flow along with the further increase in the gas velocity.

In the 3D simulation of the integrated system, a continuous circulation of bed materials from CFB to the top of the BFB was incorporated in the DFB gasification system. In the DFB gasifier system, the bed expansions in the BFB gasifier were retarded with the circulating bed of sand coming from the top of CFB gasifier. It has become increasingly more important to develop a fundamental model to predict the mixing characteristics in such gasifiers. In recent times, use of models based on the fundamental governing equations to predict the flow characteristics in BFB gasifiers and other multiphase reactors is gaining momentum *(Huilin et al., 2003; Neri and Gidaspow, 2000; Syamlal and O'Brien, 2003).* The simulation parameters required for solving the differential equations for the fluid and particulate phases

are shown in Table 4.1. Based on these discussions two different scenarios are simulated as described in the following sections.

Case 1:

2D simulation was conducted for the BFB gasifier of 2m tall and 0.2m inner diameter (I.D.) as shown in Figure 4.1. In this case the BFB was filled with the bed material to a height of 0.16m which holds 8 kg of bed material and the rest space of the BFB gasifier above the bed was called freeboard zone. The steam was fed from bottom to fluidize the bed. The velocity of the steam was critical and was maintained below the terminal velocity but above the minimum fluidization velocity to keep the bed fluidized in the bubbling fluidization regime. In this simulation, the steam inlet structure is designed as a multi-perforated plate to study the mix behaviour of the solids in the BFB.

Case 2:

3Dsimulation was then conducted for the DFB system which consists of two gasifier columns: the CFB gasifier and the BFB gasifier as shown in Figure 4.2(a). The CFB was 3.7m tall and 0.1m I.D while the BFB was 2m tall and 0.2m I.D. Initially the CFB is filled with the bed material to a height of 0.96m which corresponds to 12kg of sand bed. Both the gasifiers were designed with eight distributor tubes of0.12m in height above the support plate, each being 18mm in inner diameter to fluidize the bed material. The distributor tubes were positioned in such a way that forms a heptagon shaped network when the centre of the tubes were connected along with one additional tube at the centre as shown in Figure 4.2(b). The BFB was positioned at 0.3m above the CFB and 0.4m apart, both being connected at the bottom and the top. The bottoms of both gasifiers were connected by a chute, designed to provide uniform flow of bed material along with the char particles in the practical biomass gasifier under the influence gravity from BFB to CFB. The chute was inclined at an angle of 30° from the CFB whose length and diameter were 0.3m and 0.06m, respectively, as shown in Figure 4.1(a). To prevent back flow of bed materials from CFB due to pressure difference between the beds, an additional stream of chute fluidizing air/steam was injected via chute inlet valves. In addition to the primary air distributors at the base, the CFB was also designed with secondary air injected at a height of 0.25m from the base to uplift the bed materials and

carryover to air-solid mixture to the top of CFB gasifier. The mixture of air and bed material flows out of the CFB gasifier from the top to a cyclone in which the air and bed materials were separated. The bed materials were returned to the BFB gasifier and the air exits to the ambient.

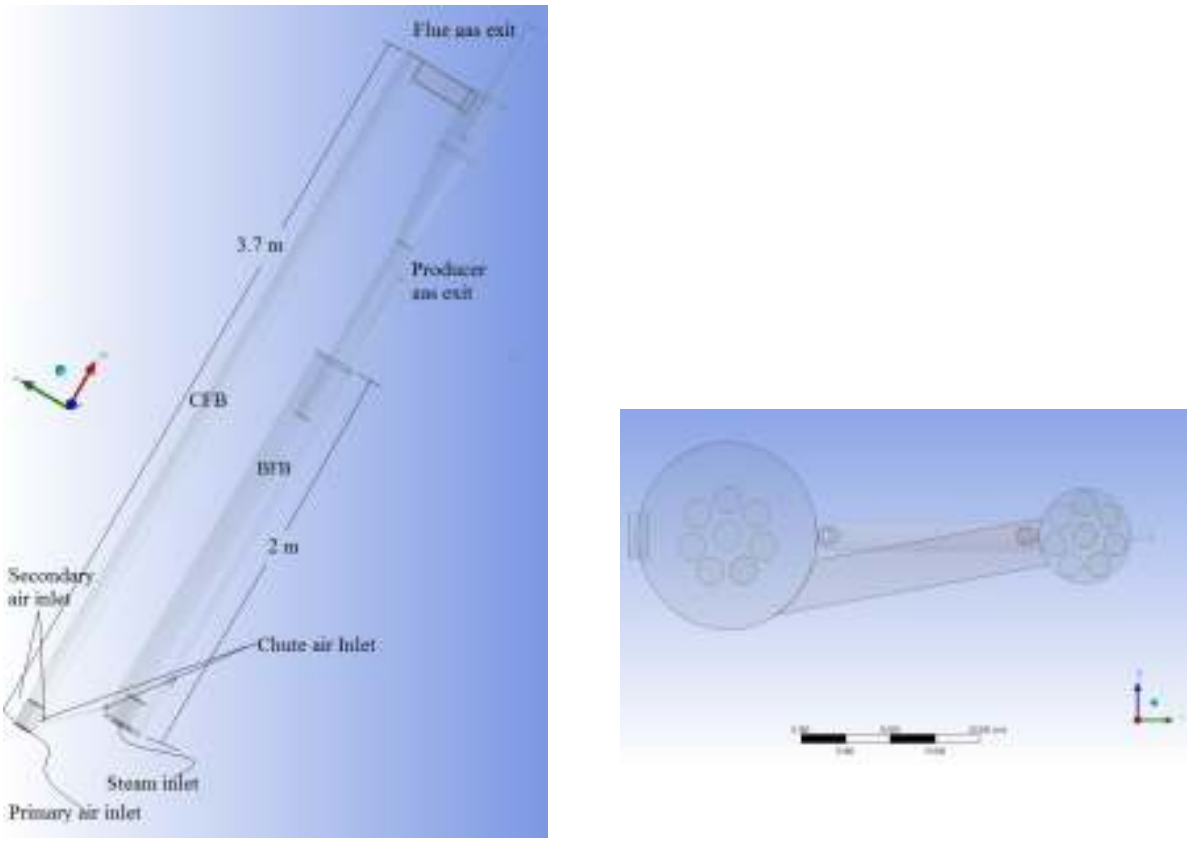

(a) isomeric view (b) top view

Figure 4.2: DFB gasification system with steam as gasification agent and circulating bed material.

Table 4.1: Simulation parameters in this modelling

Property	Value	Comment
Superficial velocity, $U_0(m/s)$	1 ; 0.45	2D; 3D model
density, $\rho_g, \rho_s(kg/m^3)$	0.353; 1600	$gas\ (steam); solid(sand)$
Gas viscosity, $\mu_g(kg/ms)$	2.44×10^{-5}	$Steam$
Mean solids particle diameter,d_s	275 μm	$Uniform\ distribution$
Initial solids packing, ε_s	0.53	$fixed\ value$

maximum particle packing, $\varepsilon_{s,max}$	0.63	
Height (m)	3.70 ; 2.07	$CFB; BFB$
Width (m)	0.1 ; 0.2	$CFB; BFB$
Height of solids (m)	0.96	CFB
Solver type	$Phase\ Coupled$ SIMPLE	Solver
Restitution coefficient, e_{ss}	0.9	$Value\ in\ literature$
Convergence criteria	10^{-3}	$Specified$
Time step (s)	0.01	$Specified$
Maximum number of iterations	20	$Specified$
Discretization scheme	First order upwind	$Specified$
Under relaxation factors		
$Pressure, P$	0.3	
$Momentum, m$	0.7	Solution control value
$Granular\ temperature, \Theta_s$	0.2	
$Volume\ fraction, \varepsilon$	0.2	

4.4 Discretization method used in CFD

For numerical simulation of the gas-solid flow in a fluidized bed gasifier using the CFD tool, the key issue was the selection of the discretization method and then to create a set of non-linear equations of mass (species), momentum and energy balances that approximate a mathematical model to provide solutions. The selection of suitable discretization methods for CFD depends mainly on the conservative property. The solution for a conservative scheme discretization method imposes a constraint on the solution error basedonly on the conservative quantities over the solution domain. While the error due to non-conservative schemes can be contributed both by the discretization errors and the iteration errors. However, non-conservative schemes discretization approximation such as the finite element method (FEM) introduces errors which decrease as the grid size is refined and increase appreciably on relatively coarse grids. Hence in most of the CFD modelling packages, the

conservative scheme of finite volume method (FVM) method is commonly used including *ANSYS FLUENT* which is employed in the present study. In some cases, FEM may be more stable than the FVM approach, it needs extreme care of the choice of the approximations and requires more memory than FVM *(Ptasinski, 2008)*.

A FVM discretization is based upon an integral form of the PDE to be solved where the computational domain is discretized into finite number of CVs instead of finite element (as in FEM).For every CV the governing equations for the solution variables (e.g., u, v, w, p and T) are solved one after another sequentially or simultaneously. The computational node for each CV to be calculated lies at the centre of the CV and interpolation method is used to express variable values at the CV surface in terms of the nodal values. This method works by converting the CV integrals to surface integrals (divergence theorem) which can be evaluated as fluxes at the cell walls.

4.5. Approaches for numerical calculations of multiphase flows

In general, the CFD models for the gas-solid flow can be divided into two groups, the Lagrangian-Eulerian models and the Eulerian-Eulerian models. The Lagrangian-Eulerian modelling approach describes the solid phase at particle level as discrete and the gas phase as a continuum. On the other hand, an Eulerian-Eulerian model considers the overall behaviour of the solid particles and regards the gas and solid as two homogenous fluids penetrating into each other. For modelling the combustion and the gasification of solid fuels, the Lagrangian-Eulerian approach requires a robust CFD framework and tracking of large number of particles which were computationally demanding. Thus this approach is mostly limited to a dilute solid in the gas phase in which case the solid particles interactions are not intensive or can be neglected *(Fletcher et al., 2000; Lu et al., 2008)*. This limitation contravenes the gas solid phase interactions in the fluidized bed model, and therefore, the Eulerian-Eulerian is used in this work.

The Eulerian-Eulerian model approach (commonly known as Eulerian model) was based on the inter penetrating continua, in which the concept of phase volume fraction was introduced and conservation law was applied to each of these phases as a separate continuum (field) as described in Sections 4.2.1 and 4.2.2.The constitutive relations were obtained from empirical information, or, in the case of granular flows, by application of kinetic theory. The volume fractions for each phase were assumed to be continuous functions of space and time and their

total sum is equal to one. The multiphase Eulerian model has been designated with the fluid phase as primary phase and a number of secondary phases with at least one secondary phase as particle or granular. This model incorporates any combination of gas, solids and liquid phases and does not distinguish between the fluid-fluid and the fluid-solid (granular) multiphase flows. Though the Eulerian model was multiphase model, the number of secondary phases was limited to one or two depending on memory of the computer as convergence of too many phases becomes difficult. Even with sufficiently larger memory available for complex multiphase flows, the solution was limited by convergence behaviour. For the proposed model in the present study for gas-solid (two phase) system, *two-fluid* Eulerian model approach was employed with the gas phase as the primary phase and the particulate or granular phase as the secondary phase, each phase being treated as a continuum. Due to the continuum representation of the particle phase and the high particle concentrations in the gas-solid fluidized beds, the particle-particle interactions cannot be neglected and the Eulerian models require an additional closure laws to describe the rheology of particles. Moreover, the solid phase has similar properties to a continuous fluid phase. In most recent continuum models, constitutive equations, the viscous forces and the solid pressure of the particulate phase were described as a function of the so called granular temperature *(Gidaspow, 1994)*. Eulerian models predicted well the bubble formation and the distribution of time-averaged solids concentration in BFBs. Therefore, the Eulerian model has shown its suitability for modelling dense gas-solid fluidized bed gasifiers. The Eulerian-Eulerian model approach in *ANSYS FLUENT* is facilitated by the built in Eulerian model.

4.6 Solving the hydrodynamics model using a numerical method

4.6.1 Initial and Boundary conditions

The definition of appropriate initial and boundary conditions were required for solving the proposed mode. For the initial conditions, different flow conditions were implemented and used in the simulations. Initially, the bed was filled with the bed material to a certain height and there were no motions for both the gas and the particles in the fluidized bed and the velocities of both phases were assumed to be zero. In ANSYS Fluent, for the two-fluid Eulerian model, initial and boundary conditions can be provided, separately, for the gas phase, the solid phase and the mixture phase.

At the start of the simulation (initial conditions at t = 0), the axial superficial gas velocity, $\vec{v}_g$, within the static bed height $h_0$and the particle concentration in the freeboard region were set to zero.

The gas at the inlet position, which was at the bed bottom, was assumed to be uniform plug-flow and the normal velocity of particles was set at zero. At the outlet, the top of the gasifier, atmospheric pressure was prescribed for the mixture phase. The specification of appropriate boundary conditions at the wall was also important. At the wall, no slip flow occurs for both the gas phase and the solid phase where the corresponding gas tangential and normal velocities were set to zero. The boundary conditions vary for Case1 and Case 2 and the details for both cases are given in Table 4.2 (Case 1) and in Table 4.3 (Case 2), respectively.

Case 1

The geometry for Case 1 model was relatively simple, which was generated using ANSYSWorkbench12.1. For the 2D model, a fine hexahedral mesh was generated with automatic patch conforming/sweeping method, generating a total of 12006 nodes and 5469 elements with the element size of 0.0125m as shown in Figure 4.1.

Table 4.2: Boundary conditions for the case 1 simulation of the BFB gasifier.

Position	Mixture phase	Gas phase	Solid phase (sand)
Pressure outlet at the exit of BFB	$P = P_{out}$	-	-
Velocity inlet for BFB at the bottom	-	$\vec{v}_g = v_{g,bfb,primary} = 0.4\ m/s$	$\vec{v}_s = 0$
Walls	No slip boundary condition for both phases. (ie, zero velocity)		

Case 2

The 3D simulations in Case 2 assume that there was no biomass fed to the system and no chemical reactions occur in the system. For the DFB gasification system, a fine hexahedral mesh was generated with automatic patch conforming/sweeping method, generating a total of 105703nodes and 373941elements with a minimum mesh size of 0.0006m as shown in Figure 4.3.

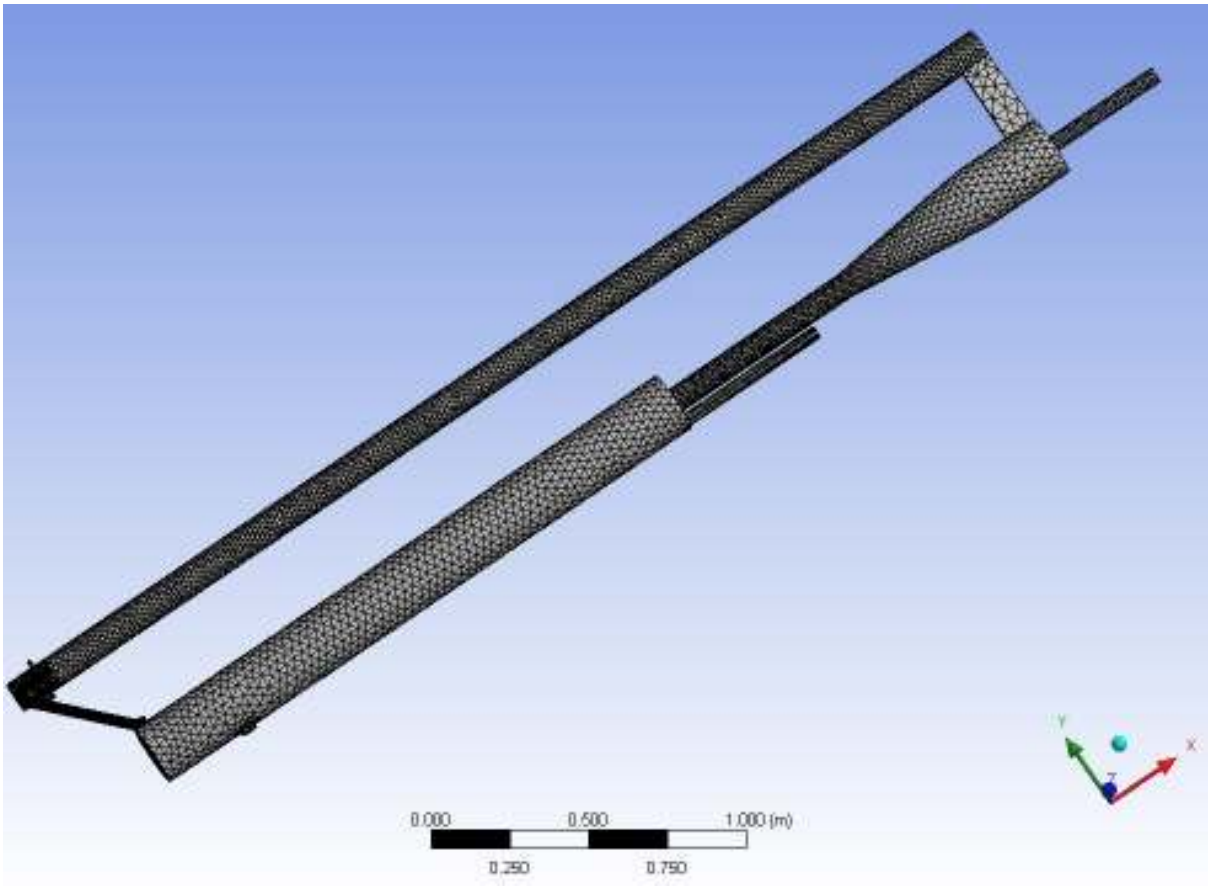

Figure 4.3: The DFB gasification system with the mesh grid.

Table 4.3: Boundary condition for the simulation of the DFB gasifier.

Position	Mixture phase	Gas phase	Solids- Sand
Pressure outlet at the exit of CFB	$P = P_{out}$	-	-
Pressure outlet at the exit of BFB	$P = P_{out}$	-	-
Velocity inlet for CFB at the bottom	-	$\vec{v}_g = v_{g,cfb,primary} = 6.35\ m/s$	$\vec{v}_s = 0$
Velocity inlet for BFB at the bottom	-	$\vec{v}_g = v_{g,bfb,primary} = 0.4\ m/s$	$\vec{v}_s = 0$
Secondary velocity inlet for CFB at the bottom & above the chute outlet	-	$\vec{v}_g = v_{g,cfb,secondary} = 33.83\ m/s$	$\vec{v}_s = 0$
Chute velocity inlet at both ends of CFB & BFB	-	$\vec{v}_g = v_{g,chute} = 1.8\ m/s$	$\vec{v}_s = 0$
Wall	No slip boundary condition for both phases. (ie, zero velocity)		

4.6.2. Numerical method for solving the developed model

The CFD modelling and simulation were performed using ANSYS Workbench 12.1, which was an interactive platform tool where project workflow can be customized by selecting the required analysis system. The ANSYS Workbench 12.1 contains built-in toolboxes or can be individually built by selecting the required components from the component systems on to the project schematic interface. The advantage of using the ANSYS Workbench 12.1 was that it allows working within one integrated interface from building the geometry through the solution process, to post-processing and final output. This enables higher compatibility and increases the speed of the computation. In the simulation of this study, the object was built using the Fluid Flow (FLUENT) analysis system which consists of five components: geometry, mesh, fluent-setup, solutions and results. The ANSYS FLUENT provides sophisticated graphical user interfaces (GUI) to specify the problem domain with input parameters, solving the PDE equations and to examine the results. Hence all codes contain three main elements:

1. Pre-processing.
2. Solver and
3. Post-processing.

The modelling process of hydrodynamics model in the BFB using the CFD tool is shown as flow diagram in Figure 4.4.

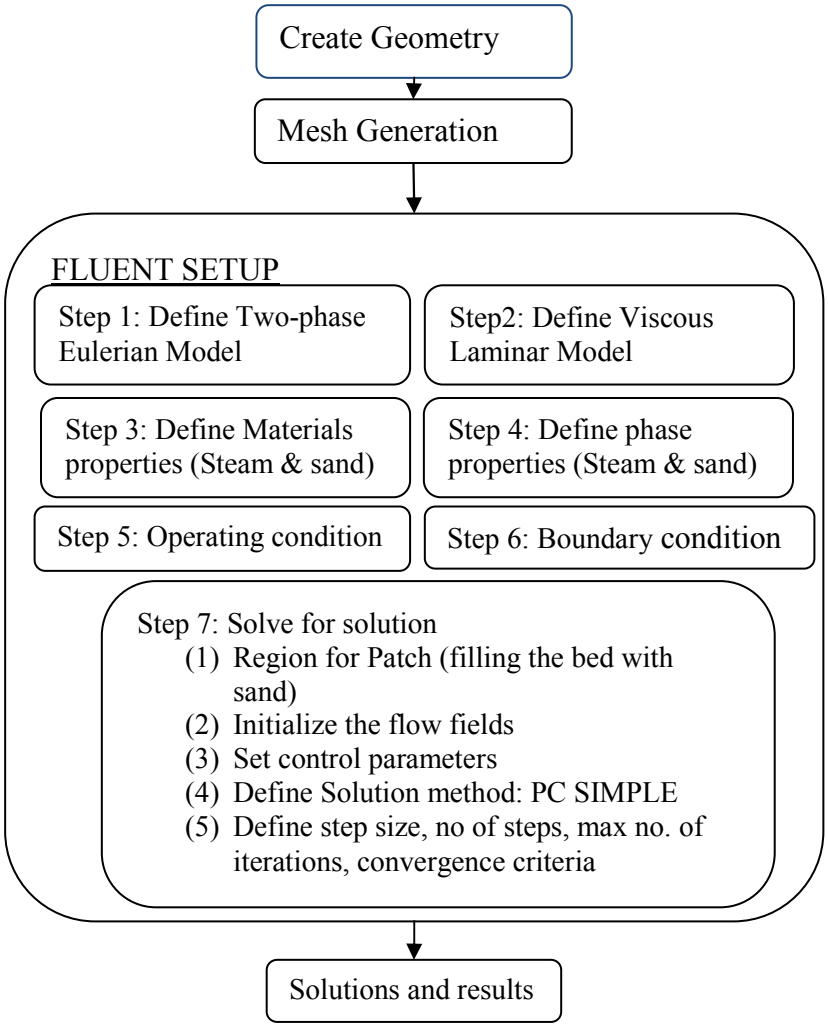

Figure 4.4: Flow diagram of the fluidization modelling process in BFB using CFD tools.

4.6.2.1. *Pre-Processing*

Pre-processing was the first step in building and analysing a flow model which consists of defining the problem domain, input of a flow problem by means of GUI and subsequent transformation of this input into a form suitable for the use by the solver. The main steps and considerations for the Pre-processing are:

- The basic step for the simulation was to define the geometry of the design problem using the Computer Aided Design tool of ANSYS Workbench12.1.
- Grid/Mesh generation: For the Eulerian multiphase model, which has a large number of highly coupled transport equations, computational time and space were be high. Hence the mesh sizing plays a vital role. The larger mesh size induces greater error propagation and deviations from the solution. On the other hand if very fine mesh size

was used, the accuracy of the solution was reached but the computational time and space requirement increased. Both the accuracy of the solution and its cost in terms of necessary computer hardware and calculation time were dependent on the fineness of the grid. ANSYS Workbench Mesh has built-in mesh generators called automatic patch confirming or sweeping methods, which performs meshing automatically when solving the problem using a hexahedral mesh. Unlike the tetrahedral or triangular meshes, the hexahedral mesh approach reduces the density of the mesh keeping the number of nodes the same while decreasing the computation time substantially. ANSYS Workbench Mesh has solution adaptive meshing capability which will automatically refine the grid in areas of rapid variation to improve accuracy wherever needed.

- Defining the properties of gas, solid and their mixture, and the problem description were done in the built-in library of ANSYS FLUENT 12.1 where the elements selections of physical or chemical phenomena that need to be modelled were included. Appropriate boundary conditions were identified at cells, which match the system boundary conditions. The solution of a flow problem (velocity, pressure, temperature etc.) was defined at nodes inside each cell. The drag coefficient between the gas phase and solid phase was calculated using the model proposed by *Syamlal and O'Brien (1989)*. The granular properties such as the solid shear viscosity, the solids pressure and the radial distribution were also given by the model proposed by *Syamlal and O'Brien (1989)* while the solid bulk viscosity was provided by the *Lun et al.(1984)*model.

4.6.2.2. *Solver*

The ANSYS FLUENT 12.1 has built-in models for solving the PDEs of the mass and momentum balances. In order to solve the nonlinear-coupled PDEs of multiphase flow problems with the addition of several features such as the kinetic theory described in Section 4.2, the pressure-based solver provides the solution tool with the Phase Coupled SIMPLE (PC SIMPLE) solver in the FLUENT package of ANSYS workbench 12.1.In the pressure-based approach, the pressure field was obtained by solving a pressure or pressure correction equation which was obtained by manipulating the continuity and momentum equations.

In PC SIMPLE solver, the momentum of each phase were solved and then coupled by the phases in a segregated fashion. Fluxes were re-enacted at the faces of the CV and then a pressure correction equation was built based on total continuity. The coefficients of the pressure correction equations came from the coupled per phase momentum equations. This PCSIMPLE solver was robust and simple, and significantly improves the convergence speed; however, the memory requirement for the coupled algorithm was more.

The solution process involves iterations where in the entire set of governing equations were solved repeatedly until the solution converges. For the discretization of all conservation equations (momentum, continuity, energy, volume fraction), a first-order upwind scheme was used with the time step of 0.01s where gradients and derivatives were evaluated through the least-square method. The restitution coefficient between the solid particles was chosen as 0.9. The first-order upwind scheme provides stability for the discretization of the pressure-correction equation, and gives good results for the solid-gas flows in the fluidized beds. The solution controls were given by the under relaxation factors. The simulation parameters required for solving the differential equations for the fluid and particulate phases are listed in Table 4.1.

4.6.2.3 *Post-Processing*

Finally the results of the model simulation were processed with the data visualization tools of ANSYS FLUENT which has full post-processing capabilities such as domain geometry and grid display, vector plots, contour plots of different properties.

4.7 Results

Figures 4.5-4.8 show the distribution of solids fractions, velocity vector of solid fractions, pressure at different time from time t = 0 to 60 min. The idea here is to show the interactions between the solids and gas phase in the BFB, which keeps changing in position over elapsed time. The particle tracks may be predicted using the discrete phase model (DPM), however, including the DPM in the 2D gasification model with hydrodynamics and reactions is very complex and computing time can be extensive. These complications and constraints on available computational resources may restrict the number of particles considered in DPM simulations.

Figure 4.5 shows the results of solid fraction distributions at different elapsed time from 2Dsimulation of the BFB gasifier fluidized with superficial steam at a velocity of 1m/s and operation temperature of 700^{o} C. The system chosen for the simulation was a greywacke sand (d_P = 275µm, ρ_p=1600kg/m^3) which belongs to the Geldart type B powder classification. In the simulation, the model proposed by *Syamlal and O'Brien (1989)* was used for the fluid particulate interphase drag force coefficient.

From the simulation results, it can be seen that when the superficial gas velocity exceeds the minimum fluidization velocity, spontaneous formation of tiny bubble starts at the inlet position which rises through the fluidized bed, therefore direct particle–particle interactions should be included in the momentum balance equation. The bubbles start to grow due to entrained gas and were coalesced with other bubbles over the time as seen from Figure 4.5. Due to the increase in bubble diameter the bubbles rise faster, thus increasing the level of the bed. The eruption of bubbles in the bed can be observed as the time elapse. The solid circulation pattern was one of the important hydrodynamic characteristics, which indicates directly the solid mixing and the rates of heat and mass transfer in the gas-solid fluidized bed. The results can also be used to examine the mixing performance of multi-perforated inlet steam.

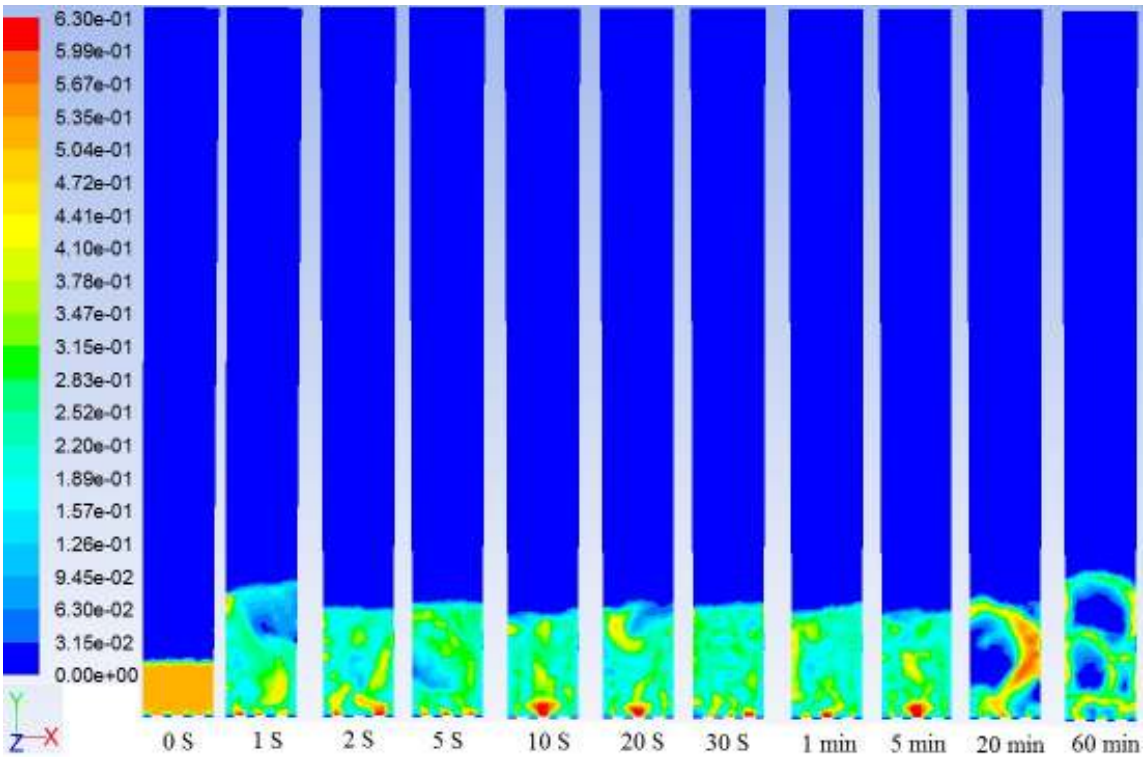

Figure 4.5: Solid fractions distribution from the 2D simulation of the BFB gasifier simulation using Syamlal and O'Brien (1989) drag law at different elapsed time with steam superficial velocity of 1m/s and at operation temperature of 700^{o}C.

Figure 4.6 shows the velocity vector distribution corresponding to the solid fractions of Figure 4.5 from the 2Dsimulation of the BFB gasifier. It was found that when simulating with a single perforated inlet stream, the solids flow turns around gradually so that particles eventually reach a flow pattern ascending at the centre and descending near the walls. With perforated inlets at the BFB base, the flow behaviour in Figure 4.6 is characterized by non-periodic formation of bubbles in the bed, though the circular patterns were still observed. Such portions of bubbles enhance the particles under going up and down motion, thus favouring a strong particle recirculation all over the bed.

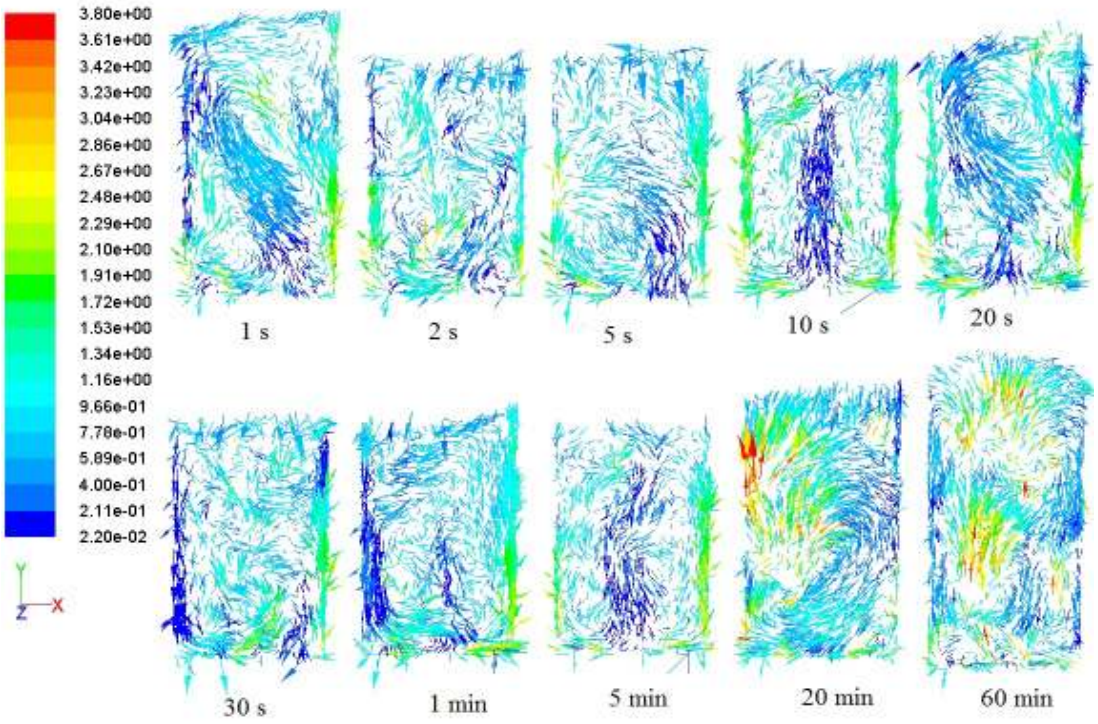

Figure 4.6: Velocity vector of solid fraction from the 2D simulation of the BFB gasifier using Syamlal and O'Brien (1989) drag law at different elapsed time with steam superficial velocity of 1m/s and at operation temperature of 700^{o}C.

Another similar 2D simulation to the above was also conducted for the hydrodynamics in the BFB gasifier but the model proposed by *Gidaspow et.al, (1992)* was instead used for the solid

particulate interphase drag force coefficient and the results are shown in Figure 4.7. It can be seen that the results using both of these interphase drag force models are consistent and illustrate the similar behaviour in terms of solid distribution in the bed. However, according to the work of *Behjat et al. (2008)*, the simulation results using the model of *Syamlal and O'Brien (1989)* gave better agreement with the experimental data than using the model of *Gidaspow et.al, (1992)*.

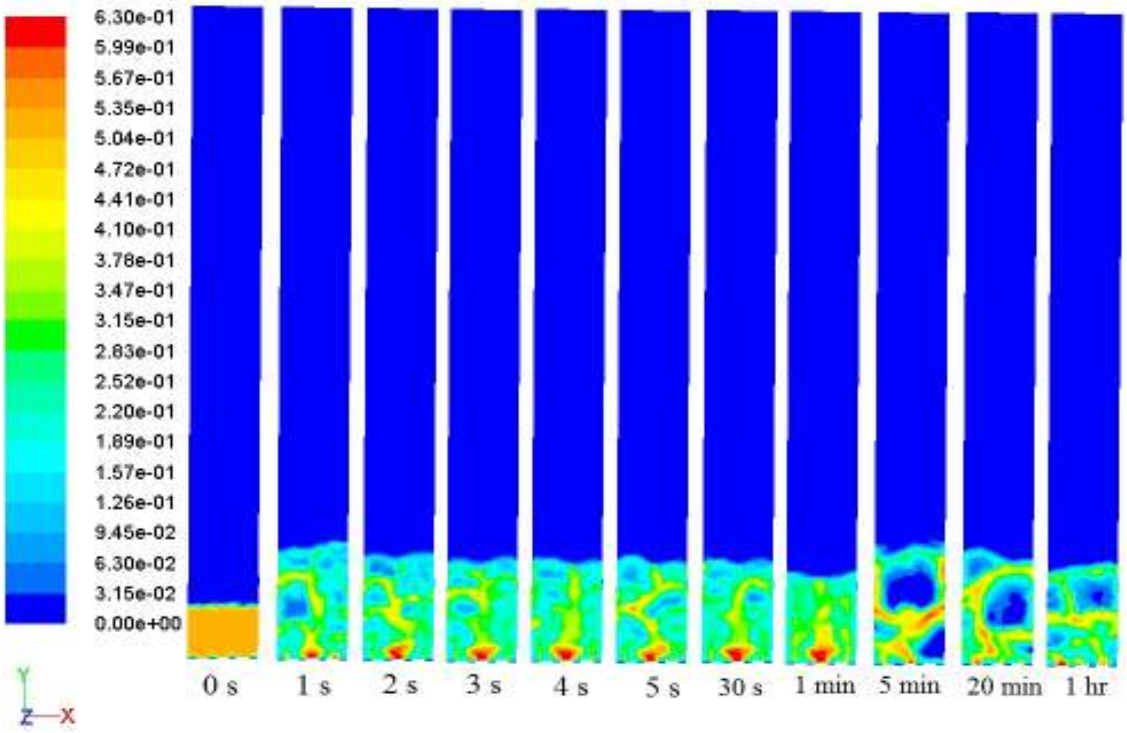

Figure 4.7: Solid fractions distribution from the 2D simulation of the BFB gasifier simulation using Gidaspow et.al, (1992) drag law at different elapsed time with steam superficial velocity of 1m/s and at operation temperature of 700^{o}C.

Figure 4.8 shows the 2D simulation results for relative static pressure distribution of the mixed gas phase and solid phase in the BFB gasifier using the solid particulate interphase drag force law developed by *Syamlal and O'Brien (1989)* at operation temperature of 700^{o} C while the superficial velocity of steam is maintained at 1m/s. From the simulation results, it was found that the overall pressure at the base of the BFB was high and towards the outlet the pressure tends to be close to atmospheric pressure. As described earlier in Chapter 2 during fluidization stage the pressure difference in the BFB gasifier remains constant with increase

in velocity above the minimum fluidization velocity. The 2D simulation results as shown in Figure 4.8 are consistent with the conclusion drawn from the literature review.

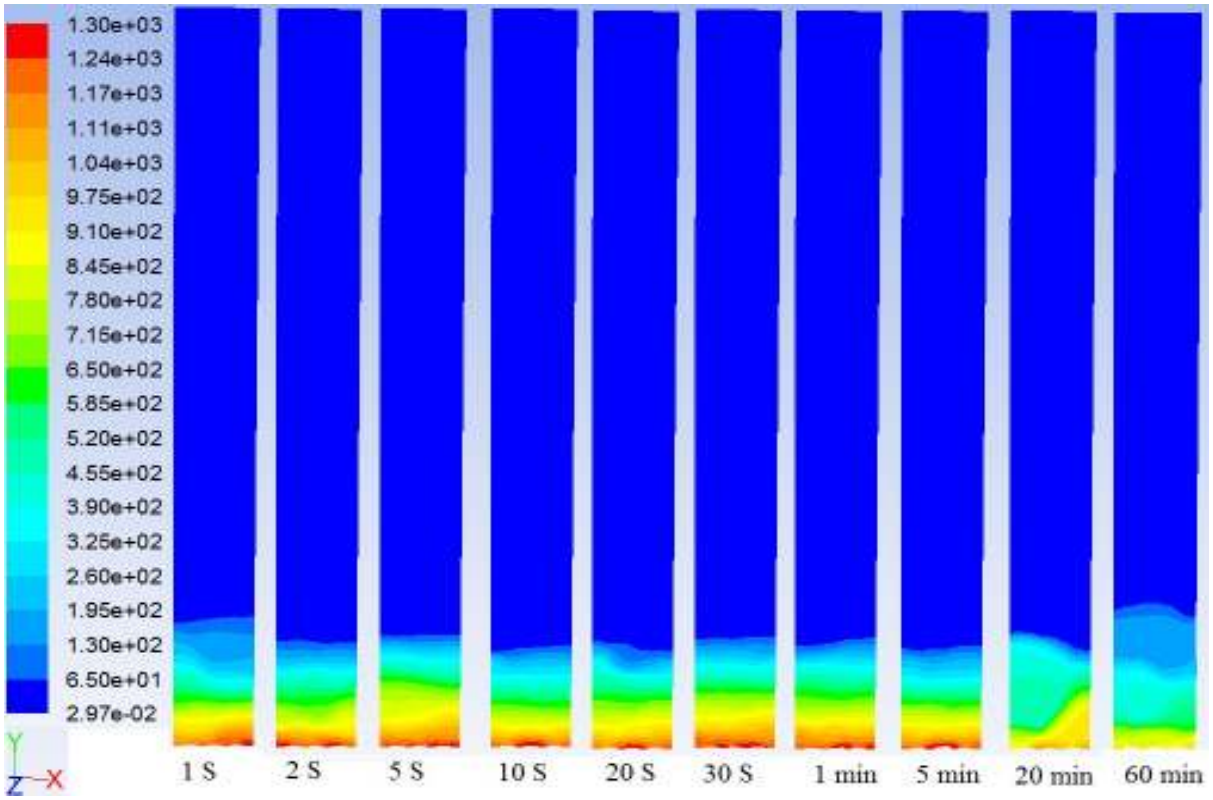

Figure 4.8: Relative static pressure distribution of the mixture from the 2D simulation of the BFB gasifier using Syamlal and O'Brien (1989) drag law at different elapsed time with steam superficial velocity of 1m/s and at operation temperature of 700^{o}C.

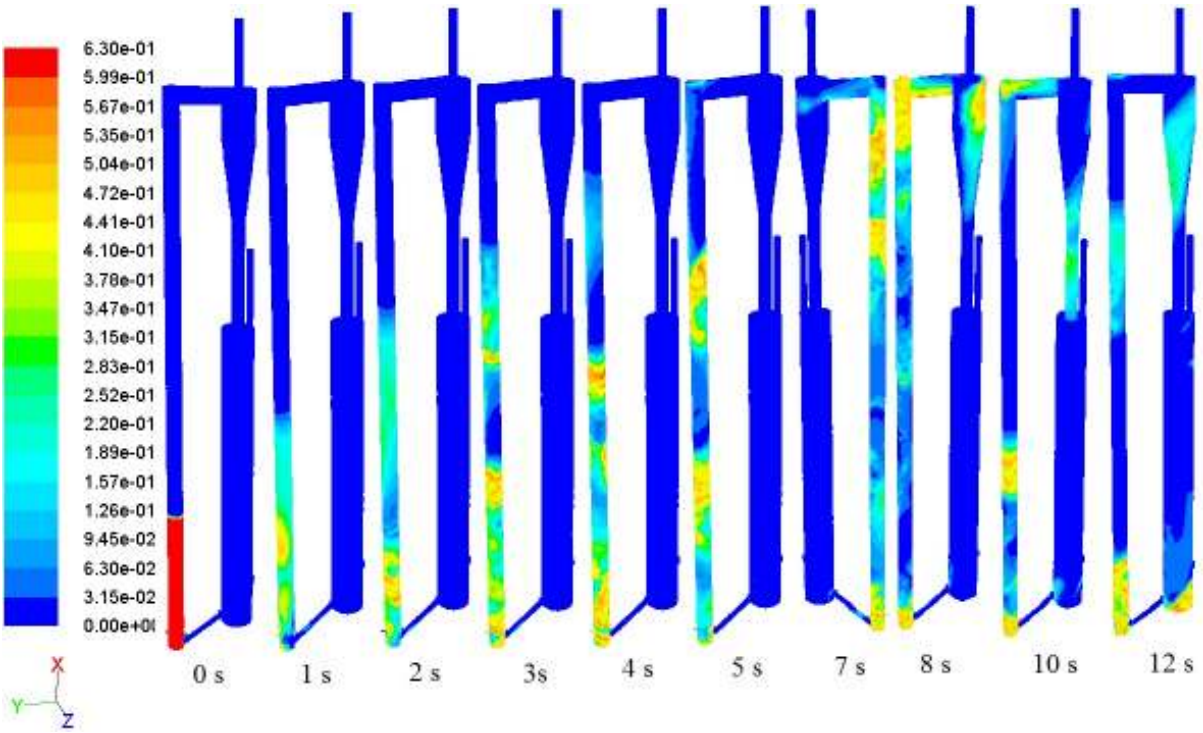

Figure 4.9: Volume fraction of sand in the DFB gasifier at different time steps.

Figure 4.9 shows the 3D simulation results on the distribution of solid bed material fraction through the DFB gasifier at different elapsed time. As the bed inventory was 12-15 kg in the gasifier, which was too low to sustain steady state continuous flow in circulating around the DFB system. The solid flow pattern changed with time up to 12 s from the start. As described in Section 4.3, the CFB gasifier was initially filled with the bed material. The other initial and boundary conditions used in the 3D simulation are given in Table 4.3. The primary and the secondary air velocities applied to the CFB are 6.35 m/s and 33.83 m/s, respectively. The air velocity in the chute was maintained at 1.8 m/s to provide continuous transfer of bed material which induces pressure difference across the chute. The steam velocity in the BFB was maintained at 0.4 m/s which was just enough to keep the bed bubbling and bed material continuous mixing. In this 3D simulation of flow hydrodynamics, the biomass feeding was not considered.

In the CFB gasifier the bed materials were lifted above the chute opening due to the velocity of the primary air from the bottom. While at the base of the bed the gravitational force and drag force exerted to the solids by the air flowing from the chute were lower than those exerted to the solid by the primary air flow along the heights of the CFB gasifier. This induces the expansion of the bed which was further lifted by the secondary air flow. As a result, the bed collapses and moves towards the top of the CFB. While in the CFB gasifier the

uplift superficial velocity of the solid and gases were influenced only by the drag and gravitational forces.

The velocity vector profile of both the solid phase and the gas phase in the CFB gasifier is shown in Figure 4.10. At the bottom of the bed in the CFB gasifier turbulence mixing occurs due to the primary air and the in flowing bed materials from the chute. Along the height of the CFB gasifier the influence of the upward force by the primary and secondary air flow was predominant over the gravitational and drag forces. The upward forces on the particle were more along one side of the CFB gasifier towards the wall due to the air and bed material flowing from the chute and lesser on the other side where only a small portion of gases and solids fall down, which can be seen in velocity profile of both solids and gases in Figure 4.10.

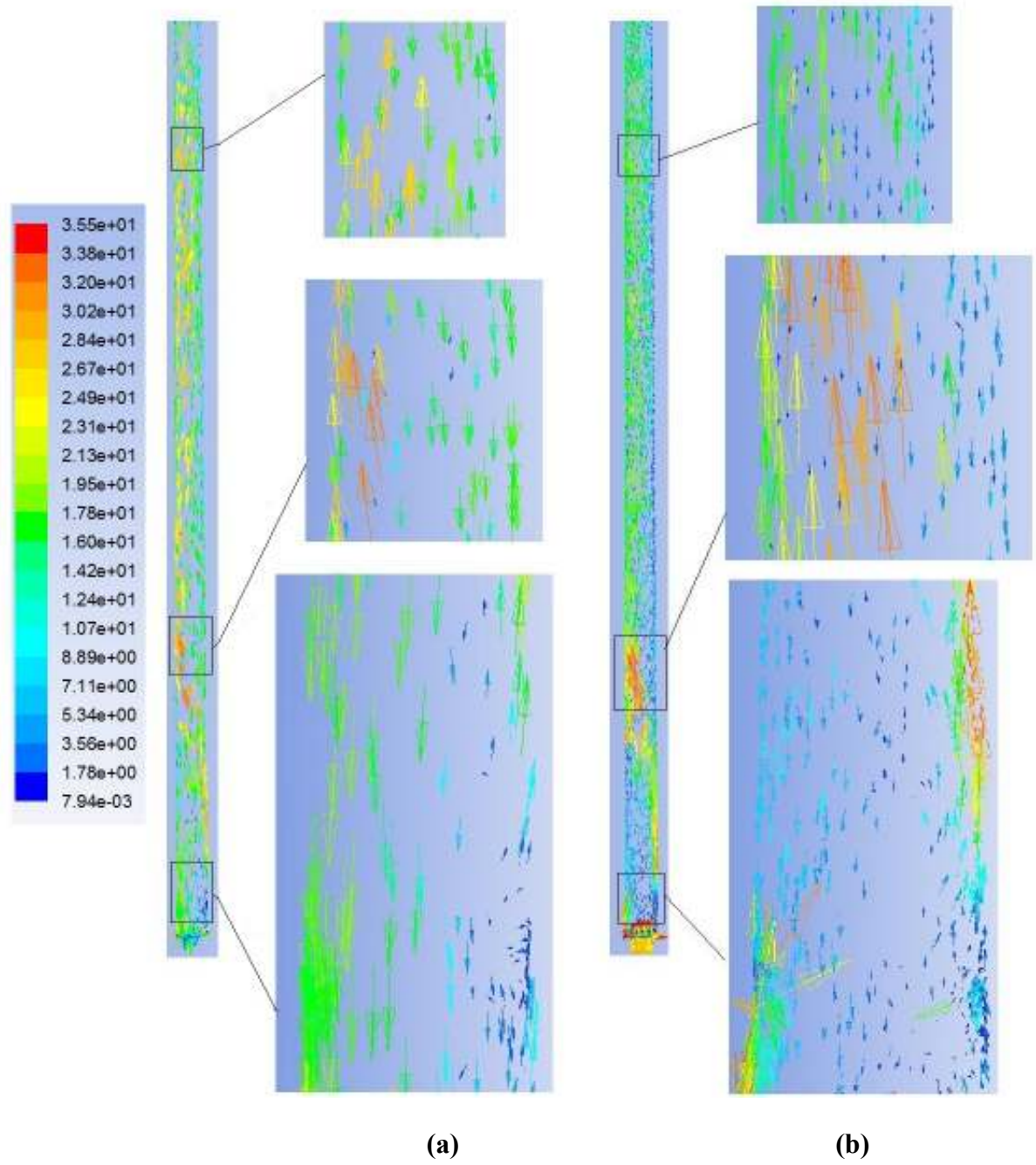

Figure 4.10: Velocity vector profile in the CFB gasifier (a) solids (b) gases.

The velocity vector profile of both the solid phase and the gas phase in the BFB gasifier is shown in Figure 4.11 which was influenced by the motion of the particles carried out from the CFB gasifier. In the BFB gasifier, at the bottom of the bed near the steam inlet and opening of the chute, more turbulence has been observed and hence there will be good mixing. The static bed height in the BFB gasifier was less than that in the CFB gasifier due to

the lower steam superficial velocity which was nearly equal to minimum fluidizing velocity. In addition, a small proportion part of steam in the BFB gasifier flows to the CFB gasifier through the chute. Along the height of the BFB gasifier the velocity of the falling solid particles were highly influenced by gravity and drag force while the upward motion of the solid particles due to superficial velocity was less as seen in Figure 4.11a. In Figure 4.11b, the upward motion of the steam was virtually parallel to the axis along the gasifier height while at the bottom full turbulence was observed due to impact with the bed materials.

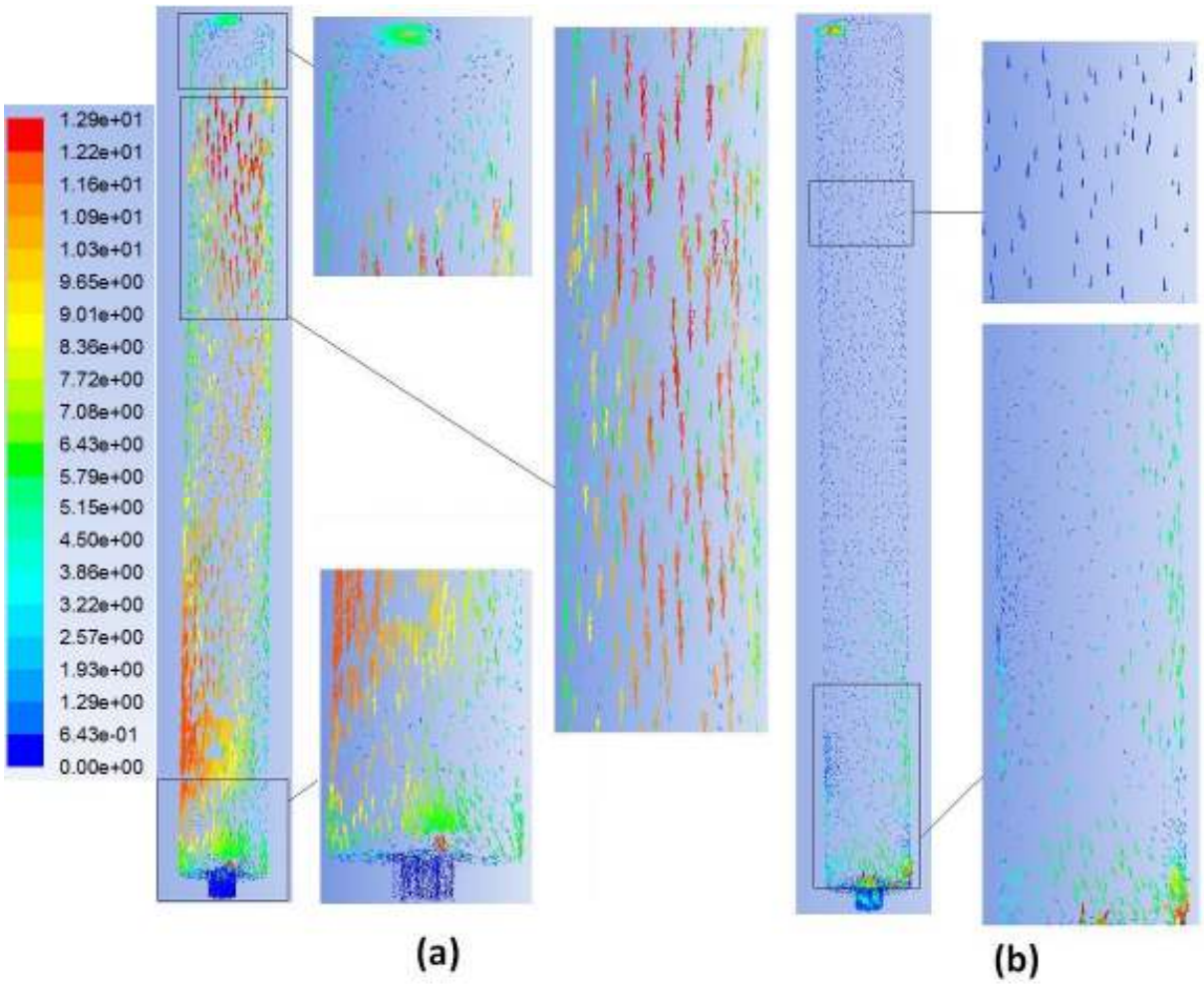

Figure 4.11: Velocity vector profile in the BFB gasifier: (a) Solids (b) Gases.

Figure 4.12 shows the effects of granular temperature or granular kinetic energy over time in correspondence to solids flow pattern as presented in Figure 4.9. The value of granular kinetic energy is strongly related to the shear stress due to the solids pressure and the granular conductivity (or solid viscosity). Initially the granular temperatures were denser at the bottom

of the CFB gasifier and at the chute which was occupied with the bed material and thus the shear stress were greater. With constant superficial velocity the high granular kinetic energy at the base promotes the bed expansion and rising up. The granular temperature was high where the bed was dense and vice versa. This trend can be seen with different time step in comparison with the results shown in Figure 4.9 for the volume fraction of the bed. This behaviour was explained in KTGF (Equation 4.16)and the result was also consistent with experimental observations by *Gibilaro (2001)* and *Gidaspow (1994)*. The value of the granular temperature varies between 0.03 to 0.09 (m^2/s^2)signifying highly fluctuating nature of the flow over time and with position of the gasifier.

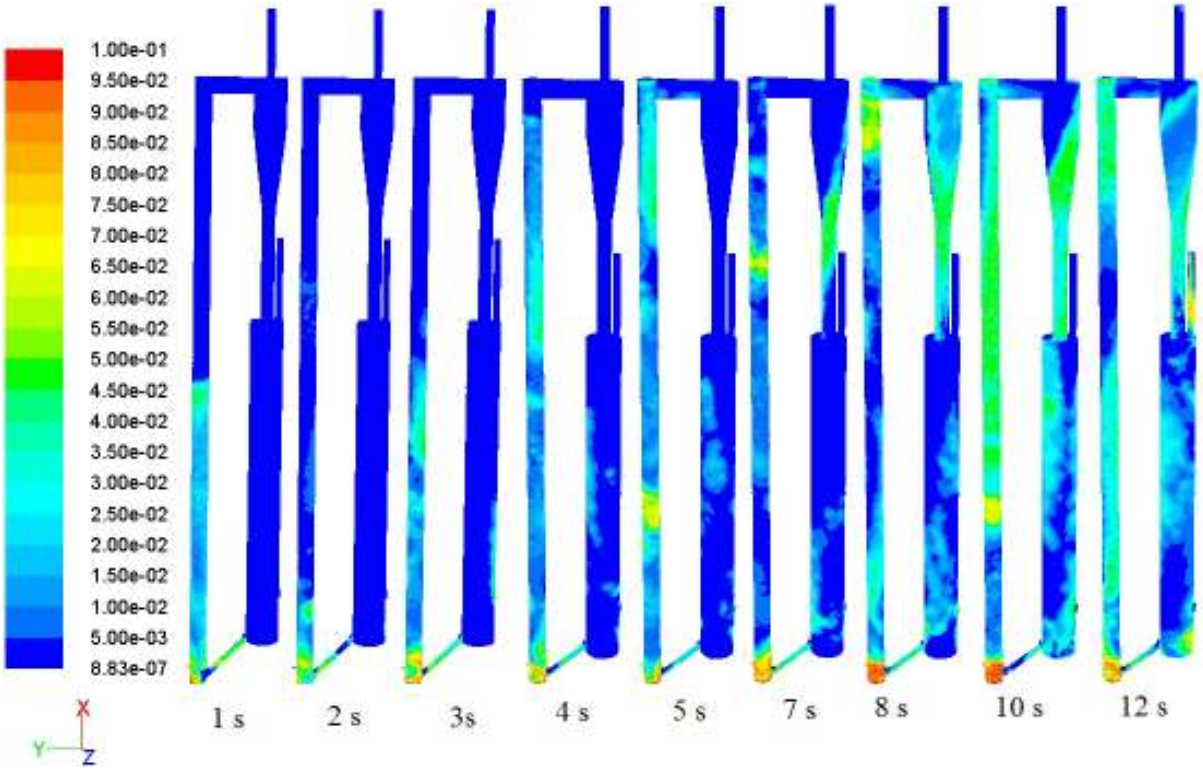

Figure 4.12: Granular temperature of sand in the DFB gasifier at different time steps.

Figure 4.13 shows the relative static pressure of the gas-solid mixture along the heights of BFB gasifier (Figure 4.13a) and of CFB gasifier (Figure 4.13b) at different elapsed time. The pressure at the base of both gasifiers was high and it decreases along the height of the gasifiers although the trends for the decrease are different between these two gasifiers. The pressure in the BFB gasifier drops sharply in a short height from the base and then decreases only slightly towards the BFB gasifier top. On the opposite of the BFB gasifier, the pressure

in the CFB gasifier drops gradually from the base toward the top. The simulation results of the pressure in both the gasifiers are consistent with the experimental data under the same operation conditions *(Das et al., 2008; Kaiser et al., 2003)*. The minimum fluidization pressure calculated for fluidized bed under the same experimental conditions was about 2.5KPa to keep the bed in fluidized conditions.

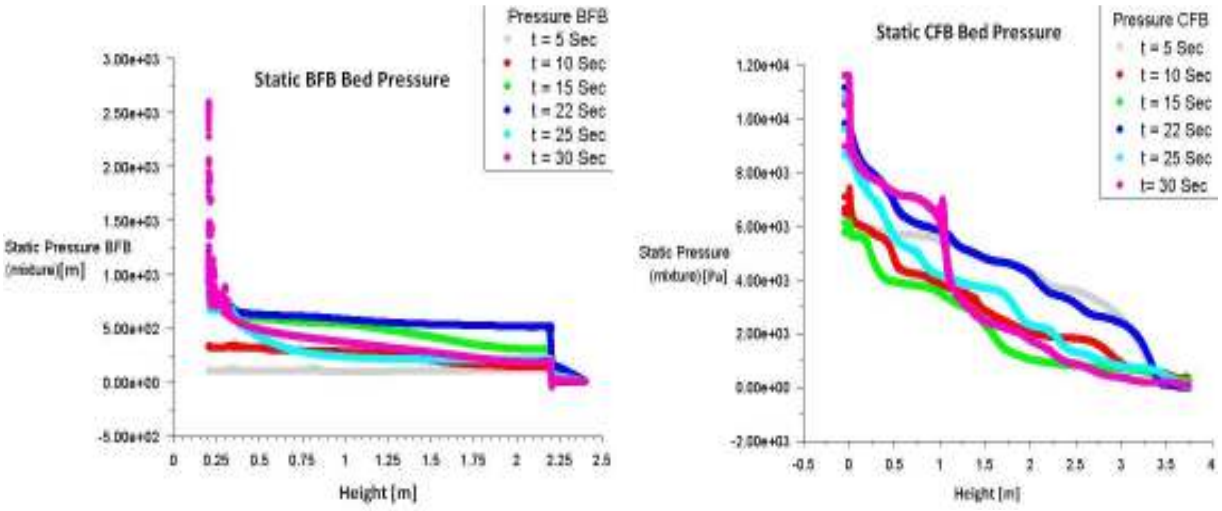

(a) **(b)**

Figure 4.13: The simulated relative static pressure of mixed gas and solids in the BFB gasifier (a) and in the CFB gasifier (b) at different elapsed time.

4.8 Conclusion

Gas–solid dispersed flow in the DFB gasification system is complex, involving multiple modes of momentum transfer and mass transfer. In the present work, a hydrodynamic model has been proposed based on the Eulerian-Eulerian model in which constitutive equations are established for the gas phase, the solid phase and the mixed gas-solid phase. Interphase drag forces are included by introducing fluid particulate interphase drag force coefficient which is modelled by different models. The interaction between the solids particle owing to the gas flow causes the fluctuations of solid particles and the energy associated with this process called the granular temperature are solved using the KTGF model. The varying granular temperature are used to compute the solids properties such as solid shear viscosity, solid bulk viscosity and the solids pressure involved in the momentum transfer.

The model was numerically solved using CFD software tool (ANSYS FLUENT 12.1) for simulation of two scenarios, Case 1 for the BFB gasifier only (2D simulation) and Case 2 for

the integrated CFB gasifier with the BFB gasifier (3D simulation). The latter is also called DFB gasification system. In the simulations, the chemical reactions and biomass feed are not included thus assuming constant temperature through both gasifiers.

Effects of various interactions on the overall hydrodynamics of gasifier have been studied in the fully developed region of DFB gasifier. In the 3D simulation the upward force caused by the superficial velocity of the primary and secondary air flow dominates the gas–solids drag force and the gravitational force on the CFB gasifier while in the BFB gasifier the governing factors are the solid gas drag force and gravitational force as the steam superficial velocity is nearly equal to minimum fluidizing velocity.

The 2D CFD model for gas and solid phases of BFB gasifier indicates good solid mixing behaviour with steam superficial velocity above the minimum fluidization velocity where the model predicted the dynamics of flow of solid particles and the gas feed streams, particle bed pressure and the gas pressure. The next stage of this work (in Chapter 5) involves the extension of the developed hydrodynamics model of BFB gasifier (2D model) with the conservation of mass (species), momentum equations for gas and solid phases and energy balances integrated with the gasification reaction kinetics model developed in Chapter 3.

4.9 References

ANSYS FLUENT12.0., 2009. Theory Guide. ANSYS, Inc.

Behjat, Y., Shahhosseini, S., Hashemabadi, S.H., 2008. CFD modeling of hydrodynamic and heat transfer in fluidized bed reactors. International Communications in Heat and Mass Transfer 35, 357-368.

Das, M., Meikap, B.C., Saha, R.K., 2008. Voidage and Pressure Profile Characteristics of Sand−Iron Ore−Coal−FCC Single-Particle Systems in the Riser of a Pilot Plant Circulating Fluidized Bed. Industrial & Engineering Chemistry Research 47, 4018-4024.

Enwald, H., Peirano, E., Almstedt, A.E., 1996. Eulerian two-phase flow theory applied to fluidization. International Journal of Multiphase Flow 22, 21-66.

Fletcher, D.F., Haynes, B.S., Christo, F.C., Joseph, S.D., 2000. A CFD based combustion model of an entrained flow biomass gasifier. Applied Mathematical Modelling 24, 165-182.

Garside, J., Al-Dibouni, M.R., 1977. Velocity-Voidage Relationships for Fluidization and Sedimentation in Solid-Liquid Systems. Industrial & Engineering Chemistry Process Design and Development 16, 206-214.

Gibilaro, L.G., 2001. "Fluidization Dynamics", 1st edition ed. Butterworth-Heinemann; 1st edition (November 21, 2001)

Gidaspow, D., 1994. Multiphase Flow and Fluidization: Continuum and Kinetic Theory Descriptions. Academic Press (21 Feb 1994).

Gidaspow, D., Bezburuah, R., Ding., J., 1992. Hydrodynamics of circulating fluidized beds, kinetic theory approach. Fluidization VII, Proceedings of the Seventh Engineering Foundation Conference on Fluidization, 75–82.

Huilin, L., Gidaspow, D., Bouillard, J., Wentie, L., 2003. Hydrodynamic simulation of gas-solid flow in a riser using kinetic theory of granular flow. Chemical Engineering Journal 95, 1-13.

Kaiser, S., Loffler, G., Bosch, K., Hofbauer, H., 2003. Hydrodynamics of a dual fluidized bed gasi'er. Part II: simulation of solid circulation rate, pressure loop and stability. Chemical Engineering Science 58, 4215-4223.

Kersten, S.R.A., Prins, W., van der Drift, A., van Swaaij, W.P.M., 2003a. Experimental fact-finding in CFB biomass gasification for ECN's 500 kW(th) pilot plant. Industrial & Engineering Chemistry Research 42, 6755-6764.

Kersten, S.R.A., Prins, W., van der Drift, B., van Swaaij, W.P.M., 2003b. Principles of a novel multistage circulating fluidized bed reactor for biomass gasification. Chemical Engineering Science 58, 725-731.

Lu, J., Yu, L., Zhang, X.P., Zhang, S.J., Dai, W.B., 2008. Hydrogen Production from a Fluidized-bed Coal Gasifier with In Situ Fixation of CO2–Part I: Numerical Model. Chemical Engineering & Technology 31, 197-207.

Lun, C.K.K., Savage, S.B., Jeffrey, D.J., Chepurniy, N., 1984. Kinetic Theories for Granular Flow: Inelastic Particles in Couette Flow and Slightly Inelastic Particles in a General Flow Field. Journal of Fluid Mechanics 140, 223-256.

Neri, A., Gidaspow, D., 2000. Riser Hydrodynamics: Simulation using Kinetic Theory. AIChE Journal 46, 52-67.

Papadikis, K., Bridgwater, A.V., Gu, S., 2008. CFD modelling of the fast pyrolysis of biomass in fluidised bed reactors, Part A: Eulerian computation of momentum transport in bubbling fluidised beds. Chemical Engineering Science 63, 4218-4227.

Petersen, I., Werther, J., 2005. Experimental investigation and modeling of gasification of sewage sludge in the circulating fluidized bed. Chemical Engineering and Processing 44, 717-736.

Ptasinski, K.J., 2008. Thermodynamic efficiency of biomass gasification and biofuels conversion. Biofuels, Bioproducts and Biorefining 2, 239-253.

Ranade, V.V., 2002. Computational Flow Modeling for Chemical Reactor Engineering. Academic Press New York.

Schouten, J.C., Krishna, R., Sinclair, J.L., 2001. Comparative analysis of CFD models of dense gas-solid systems. American Institute of Chemical Engineers. AIChE Journal 47, 1035-1035.

Shah, Y.T., 1979. Gas-Liquid-Solid Reactor Design. McGraw Hill, New York.

Syamlal, M., O'Brien, T.J., 1989. Computer simulation of bubbles in a fluidized bed. AIChE Symp. Series 85, 22-31.

Syamlal, M., Rogers, W., O'Brien, T.J., 1993. MFIX Documentation Theory Guide. U.S. Department of Energy, Morgantown Energy Technology Center, Morgantown, West Virginia.

Syamlal, M., O'Brien, T.J., 2003. Fluid dynamic simulation of O-3 decomposition in a bubbling fluidized bed. AIChE Journal 49, 2793-2801.

Wen, C.-Y., Yu, Y.H., 1966. Mechanics of fluidization. Chem. Eng. Prog. Symp.Series 62, 100-111.

Chapter 5

Two Dimensional Modelling of Biomass Gasification in a BFB Gasifier

This chapter presents the developed 2D model of biomass steam gasification in the BFB, considering the reaction kinetics involved and the mass, energy and momentum transfer equations as well as fluid hydrodynamics. In this model numerical methods (conservation of mass, momentum and energy) were used to predict the gas distribution within the gasifier. In this 2D steam-biomass gasification model, the laminar finite-rate reaction model was adopted to describe the chemical kinetics using Arrhenius kinetic expressions. For the simulation of fluid hydrodynamics, the laminar viscous model was compared with the $k-\varepsilon$ turbulence viscous model, where both of these viscous models were coupled with the finite-rate reaction model for species. This was done to study the effects of turbulence on the steam-biomass gasification product distribution. In this 2D model, the laminar viscous model was used at low S/B ratio where the flow regime is laminar, while the $k-\varepsilon$ turbulence viscous model was used at higher S/B ratio where the flow regime was turbulent.

5.1 Introduction

The objective of this part of study was to develop a2D modelling within the framework of the commercial CFD ANSYS FLUENT 12.1 package to simulate the biomass-steam gasification processes in a BFB gasifier. This was done by integrating the hydrodynamics described in Chapter 4, the reaction kinetics (as described in Chapter 3) and balances of mass, energy and momentum. In this 2D model, the distribution of biomass gasification variables can be predicted in directions along the gasifier height and along the gasifier radius. Another difference between the 2D models and the 1D model presented in Chapter 3 is that the hydrodynamics were dealt in detail in the 2D model. In this 2D model the feed of biomass was from one side of the BFB gasifier at a height of 0.3m from the bottom, while the BFB filled with bed material enhance the heat transfer and mixing which was not quantified in the 1D model. However in the 1D model, the gasification agent and biomass were fed together at the inlet from the bottom of the bed and the bed material contributed sensible heat.

The momentum equation was explicitly solved with constitutive relations and closure laws were adopted in the 2D model, whereas in the 1D model, the hydrodynamic behaviour was described by semi-empirical relations. In addition, in this 2D model two fluid phases of gas and solids were considered, where the solid phase is modelled by the finite volume Eulerian granular model (i.e. KTGF model). The model also takes into account the heat transfer, momentum exchange and mass transfer both within each phase and between the two phases. The mass transfer was due to the heterogeneous chemical reactions. The momentum exchange was due to the drag between gas phase and solid phase. The reaction kinetics in this model was facilitated with Arrhenius kinetics using the ANSYS FLUENT's laminar finite-rate reaction model. In addition to these governing transport equations, the turbulence-chemistry model was used in the simulation of the BFB gasifier to describe the coupling of reaction finite-rate reaction model and turbulent flow along with the $k-\varepsilon$ *turbulence viscous model*. It is a complicated but essential model for the reliable simulation of transport and reaction phenomena in the gasifier *(Chejne and Hernandez, 2002; Guo et al., 2003)*.

5.2 Development of the 2D mathematical model

Although the KTGF model based on the two-fluid method (TFM) has given a reasonable accuracy for prediction of dense gas–solid flows*(Gao et al., 2009; Huilin et al., 2003; Ibsen et al., 2000),* modelling when there are complicated chemical reactions is much more difficult because of the complex mechanism of heat transfer and solid mixing. Hence, careful consideration has to be given to the solution of equations with large numbers of energy and species transport equations and to the nonlinear source terms of complicated chemical reactions. It is clear from the literature review that no models have been found which integrated the two phase flow with complex gasification processes in the BFB.

In order to ensure good convergence and acceptable computational time, the following assumptions and simplifications were made in development of the 2D model for simulation of biomass steam gasification in the BFB gasifier:

1. In the 2D model, the gasification process and fluid flow occur within the rectangular section consisting of the gasifier top, the gasifier bottom and the two inner walls.
2. Two phases of fluids were considered to be gas and solid. The KTGF was used in transport equations to describe the particle collisions and fluctuations in the bed. The

frictional stress models and other interaction forces such as lift force, and virtual mass force were not taken into account by TFM.

3. The impact of particles collision was not affected by the operating temperature. Hence, both the exothermic and endothermic reactions have no impact on the fluctuation of solid velocity and do not have a rise in the temperature of granular.
4. The solid phase was dense at the bottom of the bed and hence was treated as continuous in this region of the bed, where the mean free path of thermal radiation between the solid particles was much smaller than the solid particles, thus limiting the contribution of radiative heat transfer *(Ranade, 2002)*.
5. The gas phase was assumed to be continuous in the gasifier and hence the interpenetrating and mixing between the solids and gas were allowed to exist at the bottom of the bed.
6. In the freeboard of the gasifier (space above the bed), the thermal radiation heat transfer in the gas was negligible *(De Souza-Santos, 1989)*.
7. The particles in the bed were inelastic, spherical and uniform in size.
8. In the same way as in the 1D modelling (Chapter 3), the tar content of the biomass gasification was not considered as constitutive specie and was assumed to be inactive.

5.2.1 Continuity equation

The general mass conservation or the continuity equations (as in Equation 4.1 *and* 4.2) described earlier in Chapter 4 for gas and solid flows in fluidized beds was modified. The gasification gas phase changes also included and their reactions kinetics were described in Chapter 3. These modified continuity equations are given below and these are similar in form to Equations (3.44) and (3.46) presented in Chapter 3, respectively *(ANSYS FLUENT12.0., 2009, Gibilaro, 2001)*. In these equations the gas (a) and solid (b) phases are able to interpenetrate into each other and the sum of all volume fractions in each computational cell is unity:

a) Gas phase

$$\frac{\partial}{\partial t}\left(\varepsilon_g \rho_g\right) + \nabla.\left(\varepsilon_g \rho_g \vec{v}_g\right) = -S_{sg} \tag{5.1}$$

b) Solid phase

$$\frac{\partial}{\partial t}\left(\varepsilon_s \rho_s\right) + \nabla.\left(\varepsilon_s \rho_s \vec{v}_s\right) = S_{sg} \tag{5.2}$$

where ρ_g, ρ_sstands for the density (kg/m^3), $\vec{v}_g, \vec{v}_s$ for the velocity (m/s) and $\varepsilon_g, \varepsilon_s$for the volume fraction of gas phase (with subscript of g) and solid phase (with subscript of s), respectively. When the continuity equations are used in heterogeneous reaction, there are mass, momentum and heat exchanges between the gas phase and the solid phase. In the present work, the source term S_{sg}on the right hand side of Equations (5.1 and 5.2) was due to the conversion process where the char generated from the initial pyrolysis reacted with devolatilization products and with steam, thus the solid phase of the reacted char was changed into the gas phase which can be quantified by the mass source term *(Syamlal and O'Brien, 2003)*:

$$S_{sg} = \sum_{j=1}^{5}\left(M_{w_c}\nu_{cj}r_j\right) \tag{5.3}$$

For the gas phase density, a mixture of ideal gas was assumed *(ANSYS FLUENT12.0., 2009)*

$$\rho_g = \frac{P_g}{RT\sum_{\mathrm{i=1}}^{\mathrm{n}}\frac{Y_i}{M_{wi}}} \tag{5.4}$$

where $P_g\ (kPa)$, $T(K), Y_i(kg/kg)$, $M_{w_i}(kg/kmol)$ are the gas pressure, the gas mixture mean temperature, the mass fraction and the molecular weight for each species, respectively, while the solid phase density was assumed to be constant.

5.2.2 Momentum equation

In this 2D BFB model, the basic momentum conservation equations were the same as for the model presented in hydrodynamics model in Chapter 4.The modified momentum balance equations were proposed based on Newton's second law of motion that states the momentum change rate equalled the sum of all forces acting on the domain. The momentum with a gas-solid fluidized bed arises from different forces accountable in the momentum conservation equation such as viscous forces, body forces due to gravity, solids pressure forces, static pressure forces, and drag forces *(Syamlal and O'Brien, 2003)*.

a) Gas phase

$$\frac{\partial}{\partial t}\left(\varepsilon_g\rho_g\vec{v}_g\right) + \nabla.\left(\varepsilon_g\rho_g\vec{v}_g\vec{v}_g\right) = -\nabla\varepsilon_g P_g + \varepsilon_g\rho_g g + \beta\left(\vec{v}_s - \vec{v}_g\right) + \nabla\varepsilon_g\vec{T}_g + \nabla\varepsilon_s\vec{T}_s - S_{sg}\vec{v}_g \tag{5.5}$$

b) Solid phase

$$\frac{\partial}{\partial t}(\varepsilon_s \rho_s \vec{v}_s) + \nabla.(\varepsilon_s \rho_s \vec{v}_s \vec{v}_s) = -\nabla \varepsilon_s P_s + \varepsilon_s \rho_s g + \beta(\vec{v}_g - \vec{v}_s)$$

$$-\nabla \varepsilon_s \vec{T}_s + S_{sg} \vec{v}_s \quad (5.6)$$

In the above equations, the terms on the left-hand side represent temporal and spatial transport momentum change rates. The terms on the right-hand side of the equations are pressure drop $\nabla \varepsilon_g P_g$ for the gas phase momentum equation (5.5), the solids pressure forces $\nabla \varepsilon_s P_s$ for the particulate phase momentum equation (5.6), the body force due to gravity ($\varepsilon_s \rho_s g$), the fluid particulate interphase drag forces $\beta(\vec{v}_s - \vec{v}_g)$, and an additional force called the phase viscous stress tensors $\nabla \vec{T}_g, \nabla \vec{T}_s$, respectively. The interpenetrating continua of solid phase directs the solids pressure $P_s$in the particulate phase which represents the solid phase normal forces arising from collisions of individual solid particles. The stress term $\vec{T}_g$ in Equation (5.5) represents the shear stress tensor in the gas phase. In the solids phase the momentum equation (5.6) $\vec{T}_s$ represents the shear stress tensor due to the collision among the particles.

According to the closure principles of governing equations, fluid particulate interphase drag coefficient, β, and the additional forces, $\nabla \vec{T}_g$ and $\nabla \vec{T}_s$, need to be obtained from the basic fluid-field variables and the KTGF which describes the gas-particle collision resulting from random granular motions were discussed in detailed in Chapter 4.

5.2.3 Conservation of energy

In the 2D model developed in this study, the conservation of energy was considered for each phases (gas and solid) as described by *ANSYS FLUENT12.0., (2009)*. The energy equation takes into account the heat transfer between the phases, thermal conductivity within the phases, viscous dissipation and a term describing the work of expansion of void space.

(a) Gas phase

$$\frac{\partial}{\partial t}(\varepsilon_g \rho_g H_g) + \nabla.(\varepsilon_g \rho_g \vec{u}_g H_g) = \frac{\partial \varepsilon_g P_g}{\partial t} + \vec{T}_g : \nabla \varepsilon_g \vec{u}_g - \nabla \cdot \varepsilon_g \vec{q}_g + S + Q_{gs} \quad (5.7)$$

(b) Solid phase

$$\frac{\partial}{\partial t}(\varepsilon_s \rho_s H_s) + \nabla.(\varepsilon_s \rho_s \vec{u}_s H_s) = \frac{\partial \varepsilon_s P_s}{\partial t} + \vec{T}_s : \nabla \varepsilon_s \vec{u}_s - \nabla \cdot \varepsilon_s \vec{q}_s - S - Q_{gs} \qquad (5.8)$$

where, H_s and H_g are the specific enthalpies of the solid and gas phases (kJ/kg); $\vec{q}_s$and $\vec{q}_g$ were the heat fluxes for solid and gas phase, respectively. The fourth term in Equation (5.7) and (5.8), S is the source term, which accounts for sources of energy due to heat generated or consumed with chemical reactions as a result of enthalpy change which can be expressed in Equation (5.9).

$$S = S_{sg} H_g \qquad (5.9)$$

The specific enthalpy $H_g$in the gas phase represented as

$$H_g = \sum_{i=1}^{n} Y_{i,g} H_i \qquad (5.10)$$

where $H_i(kJ/kg)$is the enthalpy for each chemical species *i* in the mixture of the gas released from solid phase to the gas phase and considers both thermal and chemical enthalpy *and* $Y_{i,g}$ is the local mass fraction of species, i, in gas phase *(Perry et al., 1997)*.

$$H_i = \int_{T_0=298K}^{T} C_{p,i} dT + H_{298,i}^{0} \qquad (5.11)$$

The specific enthalpy of the solid phases $H_s$is represented as

$$H_s = \sum_{i=1}^{n} Y_{i,s} H_i \qquad (5.12)$$

The constants of heat capacities such as A, B, C and D for each gas species *i* as well as carbon (char) are given in Table 3.6.

The heat exchange between phases can be expressed as a function of temperature difference between the phases in consistency with the local balance conditions as follows *(Kunii and Levenspiel, 1991)*,

$$Q_{gs} = h_{gs}(T_g - T_s) \qquad (5.13)$$

where $h_{gs}(W/m^3 \cdot K)$ is the heat transfer coefficient between the phases which is related to the Nusselt number of the solid phase*(ANSYS FLUENT12.0., 2009; Kawi et al., 2007)* and is given by

$$h_{gs} = \frac{6\lambda_g \varepsilon_s \varepsilon_g Nu_s}{d_p^2} \qquad (5.14)$$

For a system of granular flow the correlation of Nusselt number, Nu_s, is given by *Gunn (1978)* suitable for the void fraction of the bed ranging from 0.35 to 0.65 and the Reynolds number up to 10^5.

$$Nu_s = \left(7 - 10\varepsilon_g + 5\varepsilon_g^2\right)\left(1 + 0.7Re_s^{0.2}Pr^{1/3}\right) + \left(1.33 - 2.4\varepsilon_g + 1.2\varepsilon_g^2\right)Re_s^{0.7}Pr^{1/3} \quad (5.15)$$

5.2.4 Gas turbulent model

In the gas-solid flow in the BFB biomass gasifier, the flows can be either laminar or turbulent and determination of the flow regime was important as the hydrodynamics and transfer processes can be significantly different between the two flow regimes. The flow regime was determined based on the Reynolds numbers which was a function of superficial gas velocity. In previous studies of *Patil et al. (2005a, b)*, the simulation of biomass gasification in the BFB gasifier using KTGF reaction showed a close agreement between the predicted results and the experimental data in the laminar flow regime. The laminar flow hydrodynamics model equations were discussed earlier in Chapter 4, however, at high flow velocities, hydrodynamics equations describing the turbulent flow regime were necessary. Strong turbulence flows in both phases exist in the BFB gasifier with high steam-biomass ratio and need to be adequately modelled.

In the present work, the turbulent mixing and chemical kinetic rates had been considered in both the heterogeneous and homogeneous reactions. The turbulence behaviour for gas solid mixture in this work had been modelled by turbulent viscosity models in which the turbulent viscosity for the momentum balance equation was obtained from two quantities namely turbulence kinetic energy$k$and turbulence dissipation rateε. It was found that the transport equations using the standard $k-\varepsilon$ mixture turbulence model represents a single mixture phase and were less computationally intensive than the standard $k-\varepsilon$ per-phase turbulence model and the standard $k-\varepsilon$dispersed turbulence model. In this model, standard $k-\varepsilon$ mixture turbulence model approach of turbulence in multiphase flows was taken in consideration. The particle-particle interactions, based on the kinetic theories of non-uniform dense gases used mixture properties and mixture velocities to capture important features of the turbulent flow.

Transport equations of k and ε(Equations 5.16 and 5.17) were used for closure of conservation equations as follows *(ANSYS FLUENT12.0., 2009)* :

$$\frac{\partial}{\partial t}(\rho_m k) + \nabla \cdot (\rho_m \vec{v}_m k) = \nabla \cdot \left(\frac{\mu_{t,m}}{\sigma_k} \nabla k\right) + G_{k,m} - \rho_m \varepsilon \tag{5.16}$$

$$\frac{\partial}{\partial t}(\rho_m \varepsilon) + \nabla \cdot (\rho_m \vec{v}_m \varepsilon) = \nabla \cdot \left(\frac{\mu_{t,m}}{\sigma_\varepsilon} \nabla \varepsilon\right) + \frac{\varepsilon}{k}\left(C_{1\varepsilon} G_{k,m} - C_{2\varepsilon} \rho_m \varepsilon\right) \tag{5.17}$$

where, the production of turbulence kinetic energy, $G_{k,m}$ is given in Equations (5.18).

$$G_{k,m} = \mu_{t,m}(\nabla \vec{v}_m + (\nabla \vec{v}_m)^T) : \nabla \vec{v}_m \tag{5.18}$$

Solving for the values of k and ε from Equations (5.16) and (5.17), we can model the turbulent viscosity of the mixture, $\mu_{t,m}$as *(ANSYS FLUENT12.0., 2009)*:

$$\mu_{t,m} = \rho_m C_\mu \frac{k^2}{\varepsilon} \tag{5.19}$$

The constants $C_{1\varepsilon}, C_{2\varepsilon}, C_\mu, \sigma_k, and\ \sigma_\varepsilon$ in these equations use the default values from *Launder and Spalding (1972)* with values defined as $C_{1\varepsilon} = 1.44,\ C_{2\varepsilon} = 1.92,\ C_\mu = 0.09, \sigma_k = 1.0, and\ \sigma_\varepsilon = 1.3$.

The gas stress tensor $\vec{T}_g$ applied in the gas phase momentum Equation (5.7) then replaces the laminar viscosity Equation (4.6) in Chapter 4by turbulent viscosity of the mixture, $\mu_{t,m}$as follows *(ANSYS FLUENT12.0., 2009)*

$$\vec{T}_g = \varepsilon_g \mu_{t,m}[\nabla \vec{v}_m + (\nabla \vec{v}_m)^T] - \frac{2}{3}\varepsilon_g \mu_{t,m}(\nabla . \vec{v}_m) \tag{5.20}$$

5.2.5 Conservation equation for chemical species

The species transport, as described in Chapter 3, had been applied to the 2D biomass gasification model and the conservation equations for chemical species in multiphase flows had been solved using ANSYS FLUENT12.1. For the gas phase, the local mass fraction of each species, $Y_{i,g}$, was predicted through the solution of a convection diffusion equation for the i^{th} species. The generalized conservation equation for chemical species (as in Equations 3.44 and 3.46 in Chapter 3), when being applied to a multiphase mixture, can be represented in the following form *(ANSYS FLUENT12.0., 2009)*:

$$\frac{\partial}{\partial t}\left(\varepsilon_g \rho_g Y_{i,g}\right) + \nabla . \left(\varepsilon_g \rho_g \vec{v}_g Y_{i,g}\right) = \nabla . \varepsilon_g \overrightarrow{J_\iota^g} + \beta\left(Y_{i,g} - Y_{i,s}\right) + \varepsilon_g R_{i,g} \tag{5.21}$$

$$\frac{\partial}{\partial t}\left(\varepsilon_s \rho_s Y_{i,s}\right) + \nabla.\left(\varepsilon_s \rho_s \vec{v}_s Y_{i,s}\right) = \nabla.\varepsilon_s \vec{J_\iota}^{s} - \beta\left(Y_{i,g} - Y_{i,s}\right) + \varepsilon_s R_{i,s} \quad (5.22)$$

where $R_{i,g}$and $R_{i,s}$ are the production rates of the i^{th} species in each phase by homogeneous or heterogeneous reactions. $\vec{J_\iota}^{g}$ and $\vec{J_\iota}^{S}$ are the diffusion fluxes of i^{th} species, which arise due to gradients of concentration and temperature for gas phase and solid phase, respectively. The sum of all reactions at each phase and total mass transfer between the phases must be zero. The sum of weight fraction of all chemical species at each phase must be one. The sum of volume fraction of each phase must also be one. The volume fraction occupied by one phase cannot be occupied by other phase.

In the species transport equations of the gas phase, mass diffusion coefficients were used to calculate the diffusion flux of chemical species in the turbulent flow using a modified version of Fick's law as in Equation (5.23) *and* (5.24)*(Guha, 2008)*

$$\vec{J_\iota}^{g} = -\left(\rho D_{i,m} + D_{turb}\right)\nabla Y_{i,g} \quad (5.23)$$

$$\vec{J_\iota}^{s} = -\left(\rho D_{i,m} + D_{turb}\right)\nabla Y_{i,s} \quad (5.24)$$

where $D_{turb}(m^2/s)$is the turbulent diffusivity defined as ratio of turbulent viscosity of the mixture, $\mu_{t,m}$ and turbulent Schmidt number Sc_t. The default turbulent Schmidt number Sc_t 0.7 is used in the model.$D_{i,m}(m^2/s)$ is the diffusion coefficient of species *(i)* in the mixture in this model have been estimated by the method of *Fairbanks and Wilke, (1950)* and *Fuller et al. (1966)* and as discussed earlier in Equations (3.39 *and* 3.40) in Chapter 3.

$$D_{ib} = \frac{1-Y_{i,g}}{\sum_{j\neq i}\frac{Y_{i,g}}{D_{bij}}} \quad (3.39)$$

$$D_{b\,ik} = \frac{10^{-7}T^{1.75}\left(\frac{1}{Mw_i}+\frac{1}{Mw_k}\right)^{0.5}}{P\left[(V_i)^{\frac{1}{3}}+(V_k)^{\frac{1}{3}}\right]^2} \quad (3.40)$$

where Mw_i and $Mw_k$is the molecular weight of species *i* and *k*. $V_i$is the diffusion volume for species *i*, as given in Table 3.7

5.2.6 Biomass gasification reaction model

The biomass-steam gasification processes in the BFB gasifier can be divided into two stages following the short biomass drying process: the initial devolatilization (initial pyrolysis of biomass to char, volatile gases and tar) and the subsequent gasification reactions. The biomass drying was considered as instantaneous process in the feeding zone according to experimental results *(Chejne and Hernandez, 2002)*, and it was thus ignored in the modelling. The pyrolytic process of the biomass was assumed to be completed in the feeding zone as discussed earlier in Equation (3.13) (Chapter 3).

$$[N_{wood}CH_{1.44}O_{0.66}] \xrightarrow[temp]{\Delta high} \left[\begin{cases} Mgas\ (Volatiles) \xrightarrow{\Delta} (N_{CO}CO, N_{CO_2}CO_2, N_{H_2}H_2, N_{CH_4}CH_4) \\ M_{tar}(tar) \\ M_{char}(char) \end{cases} \right] \quad (3.13)$$

The correlation of pyrolysis products as a function of operating temperature was fitted from the experimental results conducted in the 100 kW DFB gasifier in this study (Equation 3.14a). Once the drying and initial pyrolysis processes had been completed, the char particle was gasified with steam. The resultant volatile gases reacts with chars and the gasification agent (steam in this study) according to the heterogeneous and homogeneous chemical reactions described by the Arrhenius kinetic rates. The reaction scheme for steam-biomass gasification is summarized in Table 5.1 including both the initial pyrolysis and the subsequent gasification reactions as discussed in detail in Chapter 3.

Table 5.1: Reactions, kinetic constants and activation energy for the chemical reactions.

No.	Chemical Reaction j	A_j (1/s)	E_{Aj}E (kJ/mol)	References
1	$\text{Biomass} \xrightarrow{K_1} \text{Volatiles}$	1.30×10^8	140	*(Chan et al., 1985)*
2	$\text{Biomass} \xrightarrow{K_2} \text{Tar}$	2.00×10^8	133	*(Chan et al., 1985)*
3	$\text{Biomass} \xrightarrow{K_3} \text{Char}$	1.08×10^7	121	*(Chan et al., 1985)*
4	$\text{Tar} \xrightarrow{K_4} \text{Volatiles}$	1.10×10^6	100.8	*(Graham et al., 1994)*
5	$\text{Tar} \xrightarrow{K_5} \text{Char}$	1.48×10^6	144	*(Chan et al., 1985)*

6	$C + H_2O \overset{K_{eq\ 6a}}{\Longleftrightarrow} CO + H_2$	1.517×10^{4}	121.62	*(Wang and Kinoshita, 1993)*
7	$CO + H_2O \overset{K_{eq\ 7}}{\Longleftrightarrow} CO_2 + H_2$	$2.780\times10^{3(f)}$	12.56	*(Macak and Malecha, 1978)*
8	$C + 2H_2 \overset{K_{eq\ 8}}{\Longleftrightarrow} CH_4$	4.189×10^{-3}	19.21	*(Wang and Kinoshita, 1993)*
9	$C + CO_2 \overset{K_{eq\ 9}}{\Longleftrightarrow} 2CO$	3.616×10^{1}	77.39	*(Wang and Kinoshita, 1993)*
10	$CH_4 + H_2O \overset{K_{eq\ 10}}{\Longleftrightarrow} CO + 3H_2$	7.301×10^{-2}	36.15	*(Wang and Kinoshita, 1993)*

(f) kmol/m³s

In the developed 2D biomass gasification model, the reaction kinetics were computed using the FLUENT's built-in laminar finite-rate reaction model. At lower S/B ratio, where the flow was always laminar, the laminar finite-rate reaction model computes the chemical source terms using Arrhenius expressions ignoring the effects of turbulent fluctuations. For the turbulent flow, the flow was provided by gas turbulent model and the turbulent chemistry in FLUENT was provided by the eddy dissipation model which was based on the turbulent mixing rate. However in the latter case, the mixing rate tends to dominate the reaction rate only when there were one or two reactions in the system *(ANSYS FLUENT 12.0., 2009)*. Therefore, if every reaction was regarded as turbulent, the solution of the species transport equations based on the turbulent eddy-dissipation model becomes numerically incorrect involving multiple reactions, because in this way every reaction involved has the turbulent rate. Hence in this model, the gasification reaction mechanisms in turbulent flow are also based on Arrhenius rates, which differ for each reaction. Thus the FLUENT's built-in laminar finite-rate reaction model were used for both the laminar and turbulent flow.

The net source of chemical species, *i*, due to reaction was computed as the sum of the Arrhenius reaction sources over the $N_R$reactions that the species participate in as defined in *ANSYS FLUENT12.0., (2009)*:

$$R_i = M_{w,i} \sum_{i=1}^{N_R} \hat{R}_i \tag{5.25}$$

$$\hat{R}_i = \left(v_{i,j}^{p} - v_{i,j}^{r}\right)\left(k_{f,j} \prod_{i=1}^{N} [C_i]^{v_{i,j}^{r}} - k_{b,j} \prod_{i=1}^{N} [C_i]^{v_{i,j}^{p}}\right) \tag{5.26}$$

where, $M_{w,i}$is the molecular weight of species *i*, $\hat{R}_i$ is the Arrhenius molar rate of creation/consumption of species *i* in reaction *j*, *N* is the number of chemical species in the system, $v_{i,j}^{p}$ and $v_{i,j}^{s}$ are the stoichiometric coefficients for species *i* in products (*p*) and in

reactants (s) with reaction j, $k_{f,j}$ and $k_{b,j}$ are the forward and backward rate constants for reaction j,$C_i$is molar concentration of species i ($kmol/m^3$).

5.3 Domain for the modelling of biomass gasification in a BFB gasifier

The domain for the 2D model for biomass gasification in a BFB gasifier was a rectangular section of 2m high (along gasifier height) and 0.2m wide (along internal diameter of the gasifier) as shown in schematic diagram using ANSYS Workbench (Figure 5.1). The BFB gasifier was initially filled with sand (bed material) maintained at operating temperature to a height of 0.16m, where the total volume fraction of solids was patched as 0.53 *(Chejne and Hernandez, 2002)* and the remaining space of the BFB gasifier above the sand bed was called freeboard zone. For the particles used in this work, the maximum particle packing $\varepsilon_{s,max}$ was set to 0.63 *(Enwald et al., 1996)*. A fine tetrahedron mesh was generated with patch independent mesh method, generating a total of 18668 nodes and 8881 elements.

In this model the design of a single plate with perforated holes was mounted at the gasifier bottom thus allowing steam flowing upwards from the bottom to fluidize the bed. The superficial steam velocity at the inlet was determined from inlet condition and used as the inlet boundary condition. In addition the pressure at the outlet position was assumed to be atmospheric pressure which was also taken as the outlet boundary condition. A zero gradient condition was used for the turbulent kinetic energy at the walls. The no-slip wall condition was used for both the gas and solid phases.

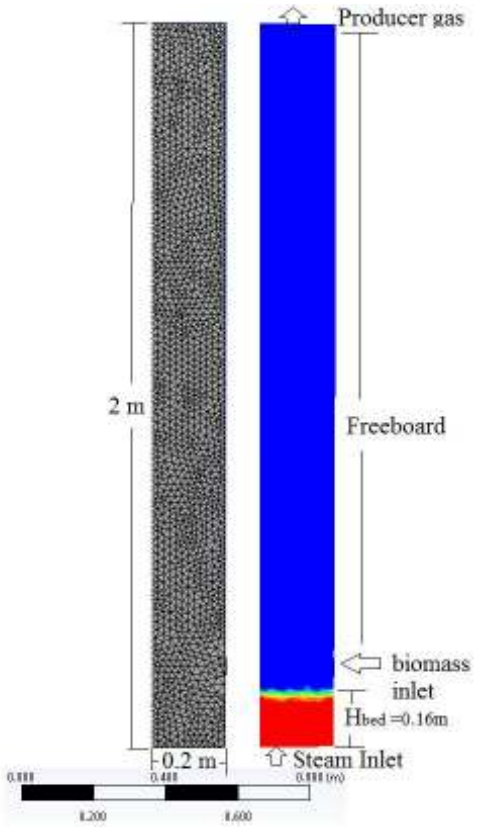

Figure 5.1: Schematic diagram of the BFB gasification system with the mesh grid in the 2D modelling of biomass gasification in a BFB gasifier.

The biomass was continuously fed from a height of 0.2m through the side of the BFB. As the BFB was maintained at high temperature, instantaneous devolatilization of biomass to char, volatile gases and tar occurs at the operating temperature ranging from 680 to 800^{o}C at the feed point as discussed earlier in Chapter 3. Hence the products distribution prediction from the initial pyrolysis model will be used for initial conditions for subsequent gasification modelling, and this can be determined by $y_i = m_{0,i} \times T^{b_{0,i}}$ (Equation 3.14a).

5.4 Numerical procedures and considerations

The procedure for solving the developed 2D model for biomass steam gasification in the BFB using the CFD tool is shown as flow diagram in Figure 5.2.

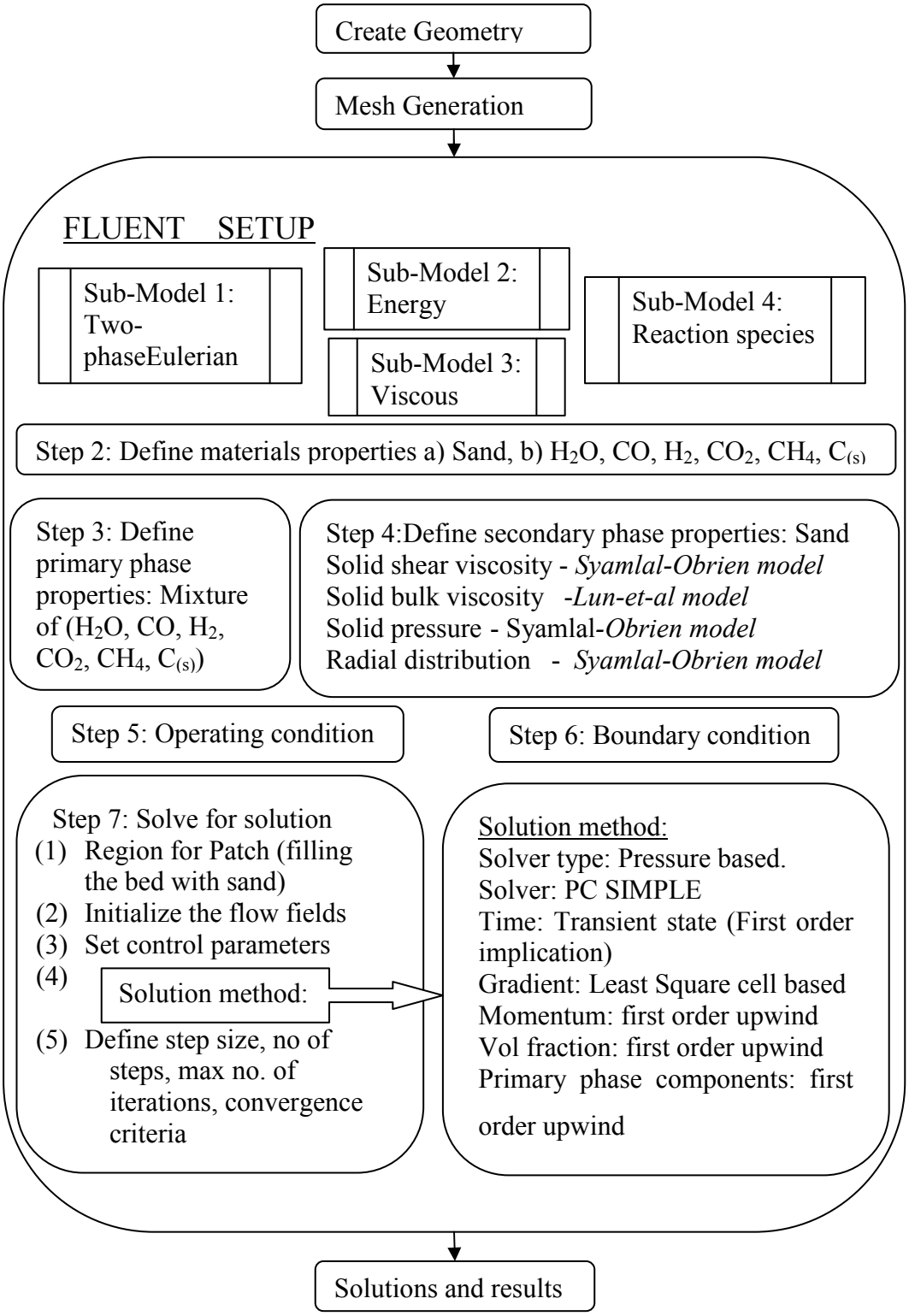

Figure 5.2: Flow diagram of the procedure for solving the 2D model for biomass steam gasification in the BFB using CFD tools.

Table 5.2: Simulation parameters in the 2D modelling of biomass steam gasification in the BFB gasifier.

Property	Value / model	Comment / Reference
BFB dimension (m)	$2.07; 0.2$	$Height; Width$
Height of solids (m)	0.16	BFB
Superficial gas velocity, $U_0(m/s)$	$0.2 - 0.8$	$steam$
Operating temperature, $T(K)$	$953 - 1053$	
Operating pressure, $P(Pa)$	1.01×10^5	
Density,$\rho(kg/m^3)$	1600; *incompressible ideal gas*	$solid\ (sand); gas\ mixture$
Specific heat , $C_p(J/\text{kg} - \text{K})$	$830; mixing\ law$	$solid\ (sand); gas\ mixture$
Thermal conductivity, $\lambda(W/\text{m} - \text{K})$	$0.242; kinetic\ theory$	$solid\ (sand); gas\ mixture$
Gas viscosity $(\text{kg}/m - \text{s})$	$mass\ weighted\ mixing\ law$	$gas\ mixture$
Mean solids particle diameter, d_s	$275\ \mu m$	$Uniform\ distribution$
solids packing, ε_s, $\varepsilon_{s,max}(-)$	$0.53; 0.63$	$initial; maximum$
Restitution coefficient, $e_{ss}(-)$	0.9	$Value\ in\ literature$
Solid shear viscosity $(\text{kg}/m - \text{s})$	*Syamlal-Obrien*	*(Syamlal and O'Brien, 1989)*
Solid bulk viscosity $(\text{kg}/m - \text{s})$	*Lun-et-al*	*(Lun et al., 1984)*
Solid pressure (Pa)	*Syamlal-Obrien*	*(Syamlal and O'Brien, 1989)*
Radial distribution $(-)$	*Syamlal-Obrien*	*(Syamlal and O'Brien, 1989)*
Solver type	$Phase\ Coupled$ SIMPLE	$Solver$
Convergence criteria	10^{-3}	$Specified$
Time steps	10^{-3}	$Specified$
Maximum number of iterations	20	$Specified$
Discretization scheme	*First order upwind*	$Specified\ for\ all\ fields$
Under-relaxation factors		
Pressure, P	0.3	
Momentum, M	0.7	$Solution\ control\ value$
Granular temperature, Θs	0.2	
Volume fraction, ε	0.2	

The 2D geometry of the BFB and its mesh generation were developed in a similar way to that for simulation of flow hydrodynamics as described in Chapter 4. The non-linear partial differential equations (PDEs) of multiphase flow problems integrated with the transfer processes and reaction equations described earlier were numerically solved using PC

SIMPLE solver algorithm based on FVM using ANSYS FLUENT 12.1 package. The ANSYS FLUENT 12.1 has built-in models for solving the PDEs of the mass, momentum and energy balances. Based on this, four sub-models, namely the two phase Eulerian model, the energy model, the viscous model and the species model, were chosen as shown in Figure 5.2. The two phase Eulerian model was selected with the gas phase mixture constituting CO, CO_2, CH_4, H_2, H_2O, $C_{(s)}$ and N_2 as primary phase and the sand particles as the secondary phase which were granular with granular properties being specified in Table 5.2. At low S/B ratio the flow regime was laminar and hence the laminar model was used for the viscous model while at higher S/B ratio the flow regime tends to transition and turbulent flow where the standard $k-\varepsilon$mixture turbulence model was chosen for the viscous model. For the species reactions in the bed the laminar finite-rate model was selected.

In solving the developed 2D model, the most vital part in the model setup was to define the species and their physical properties through the material components defined in the Materials task page. These properties of the gas species used in the model were adapted from *Smith et al. (2001)*. The pressure drop inside the bed doesn't significantly change and hence the density of gas mixture was determined following incompressible ideal gas law. It was assumed to depend only on the operating pressure and not the local relative pressure field as in Equation 5.4. The composition-dependent specific heat capacity for the gas mixture used the mixing-law, and that of viscosity of the gas mixture follows the mass weighted mixing law, while the thermal conductivity of gas mixture was calculated using the kinetic theory. The drag coefficient between the gas phase and solid phase was determined using correlations proposed by *Syamlal and O'Brien (1989)*. The restitution coefficient between the solid particles was chosen as 0.9. The heat transfer coefficient between the gas phase and solid phase was determined using the method proposed by *Gunn (1978).*

The developed 2D model was solved using transient-state pressure based solver, with first-order discretization schemes where the gradients and its derivatives were evaluated through the least-square method. In addition to the conservation equations (momentum, continuity, energy, and volume fraction), the granular temperature, the turbulent kinetic energy, the turbulent kinetic energy dissipation rate and the mass fractions of all the chemical species involved in the gasification processes were also discretized by using the first-order upwind scheme. This scheme provides stability for the discretization of the pressure-correction equation, and gave good results for most the gas-solid flow system. In this discretization scheme, quantities at the cell faces were determined by assuming that the cell-centre values

represent an average value and hold throughout the entire cell; the face quantities were identical to the cell quantities. Thus when first-order upwinding was selected, the current face value was taken equal to the cell-centre value of the upstream cell in the N-1 iteration. The solution controls were given by the under relaxation factors as shown in Table 5.2. The simulation parameters required for solving the differential equations for the fluid and particulate phases and the closure principles of governing the transport equations were also listed in Table 5.2.

It has been aware that obtaining a converging solution in a reacting flow in TFM can be difficult when a multiple reaction species coupled with corresponding non-linear conservative equations. If the influence of the chemical reactions on the gas–solid flow system was strong, then coupling between the mass/momentum balances and the species transport equations would also be strong. To improve the convergence in such a case, initial simulation was done using the cold flow where the momentum, energy, and mass balance were solved without chemical reactions, possibly including the species. Furthermore, in order to increase the convergence and to stabilize the solution, under-relaxation factors were introduced which were significant parameters of a numerical scheme. Hence the under-relaxation factor for pressure, momentum, granular temperature and volume fractions were reduced resulting in the decrease of the residual and by reducing the time step. For a good convergence smaller time steps were required and hence in solving this proposed model, the time step was set as 10^{-3}s with maximum number of iterations set as 20 which gave a convergence criterion of 10^{-3}, while the residuals of the species, velocity components and the volume fraction falls in the range of $10^{-3} - 10^{-4}$.

5.5 Selected simulation results

A selective simulation for the biomass steam gasification in a BFB gasifier using the developed 2D model had been carried out under the same operating condition as used in the 1D model as discussed earlier in Chapter 3 (operation temperature of 780^{o}C and steam/biomass ratio of 0.53). The results of average gas concentration in the producer gas at the gas exit predicted from the 1D and 2D model simulations and those obtained from biomass steam gasification experiments are presented in Table 5.3 for comparison. In the Table 5.3 the descriptor ‘Wet’ refers to the producer gas containing steam while the

descriptor 'Dry' refers to the moisture free producer gas. The gas concentration profiles both along the gasifier height and the radius predicted from the 2D model are shown in Figure 5.3.

Table 5.3: Results of average gas concentrations of the producer gas at the gas exit predicted from the 1D model and the 2D model and those measured from biomass gasification experiments under operating temperature of 780°C, 1 atmospheric pressure and S/B ratio of 0.53.

Species	CAPE Experiment mole fraction (mol %)		Model prediction, mole fraction (mol %)							
			1D Model		2D Model					
					Average at the exit		Bed centre at the exit		Average valuetaken from radial axis (0.025 to 0.2m)	
	Wet	Dry	Wet	Dry	Wet	Dry	Wet	Dry	Wet	Dry
CO	28.7	37.3	28.6	35.7	24.2	34.0	23.0	32.3	26.7	36.1
H_2	27.7	36.0	22.6	28.2	22.4	31.2	22.8	32.1	22.0	30.7
CO_2	10.9	14.2	18.4	23.0	16.1	22.5	16.6	23.4	15.7	21.3
CH_4	8.9	11.6	10.5	13.1	8.8	12.3	8.6	12.1	9.3	12.6
H_2O	23.8	n/a	20.0	n/a	28.4	n/a	25.3	n/a	22.3	n/a

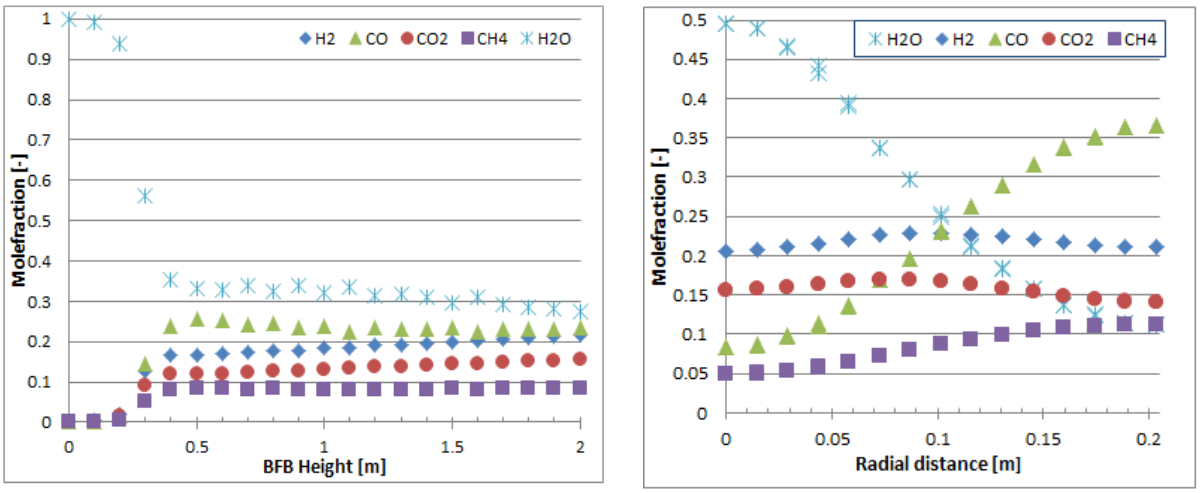

(a) (b)

Figure 5.3: Profiles of gas concentration of the producer gas (wet basis) at the centre-line of the bed along the gasifier height (a) and gasifier radius at the gasifier exit corresponding to z = 2m(b) from biomass steam gasification in the BFB gasifier under operating temperature of 780°C, 1 atmospheric pressure and S/B ratio of 0.53.

From the results presented in Table 5.3, it can be seen that the average concentrations of CO_2 and H_2O from the model simulations were higher while that of the CO and H_2 from the same simulations were less compared to the experimental values. The average concentration of the CH_4 at the exit agrees closely to that of the 1D model and the experimental results. The modelling results for 2D model gasification have noticeable discrepancies from the experimental values especially for H_2 andCO_2. The model predictions were in close agreement with the experimental data for CO, $CH_4$with discrepancies of less than 3.3% (mol/mol) and 0.7 % (mol/mol) respectively compared to the experimental data. The discrepancies in the gas concentration for H_2 and CO_2 were less than 4.8% (mol/mol) and 8.3 % (mol/mol), respectively. However, it was surprising to see that the 1D model results and average 2D model simulation results were closely in agreement on dry basis and show small discrepancy with the experimental results. In addition, the 1D model predicts the CO concentration about 1.5% lower than experimental value on dry basis whereas the 2D model predicts the CO concentration of about 3.3% lower than the experimental data.

In case of 1D model, considering the biomass feed along with the gasification agent (steam) the mixing process, initial pyrolysis and the gasification reaction processes occurs instantaneously at the bottom feed inlet where the contact time for the feed biomass inside the BFB is slightly higher compared with the 2D model in which case the feed enters one side of the BFB at a height of 0.2m. These results in 1D model to be slightly varied with that the 2D model. From Figure 5.3, the gas composition variations can be observed from the 2D model simulation. In 2D model the concentration of H_2O is mainly present at the bottom of the bed until 0.25m. The heterogeneous and homogenous reactions of initial pyrolysis products with the gasification agent occurs at elevated position above the BFB gasifier bed as seen in Figure 5.3a. From Figure 5.3, it can be seen that due to the very fast release of volatile gases and the high volatile content in the biomass fuel, the gas distribution and the steam distribution are not uniform both along the radius direction and along the reactor height. It is also found that the lateral feed of biomass inducesthe steam to move towards one side of the spatial co-ordinate, where the mixing and gasification reaction occurring is less compared to the spatial co-ordinate near the feed. Consequently, the gasification reaction along the radial co-ordinates varied significantly, resulting in uneven producer gas composition at the exit of BFB reactor.As a result the concentration of H_2O varies widely in the radial direction of BFB and along the height of the bed with the concentration of H_2O varying from 50 to 10 mol% at the exit. This effect is shown in Figure 5.3b. Therefore, the gasification behaviour of biomass

gasification in a BFB gasifier is strongly affected by the gas-solid mixing, gas and solid flows, and the chemical reactions involved. Hence in the 2D model the average concentration of the gas species computed ignoring the concentration near the wall, which shows the trend closely to that of 1D model. Though the 1D model provides more accurate gas concentration, the 2D model design was useful in finding the average gas composition of producer gas in the spatial coordinates. To further improve the reliability of the model, the species concentration profile and the fluid dynamics characteristics within the gasifier need to be validated in the future which requires advanced experimental setup.

5.6 Conclusion

In this chapter, a 2D model has developed for simulation of biomass steam gasification in a BFB gasifier which can be used to predict the producer gas composition at the gasifier exit, and the distributions of gas composition along the gasifier height and gasifier radius. The 2D model developed includes constitutive equations of mass (species), momentum and energy balances for the gas phase, the solid phase and the mixed gas-solid phase in incorporation with KTGF (as described in Chapter 4) and gasification reaction kinetics determined by Arrhenius kinetics (as described in Chapter 3).

The 2D model considers the turbulence flow at higher S/B ratio and hence the gas-solid mixing in the BFB is considered by employing the turbulence-chemistry model with coupling the built-in finite-rate reaction model and the $k-\varepsilon$ turbulence viscous model. On the other hand at low S/B ratio, the flow regime of the gas solid system tends to be laminar profile in which case the viscous model, are modelled with simple laminar viscous model while coupling with the finite-rate reaction model. In ANSYS FLUENT the finite-rate reaction model is facilitated by Arrhenius kinetic expressions. The product distribution function for the pyrolysis processes is adapted from the 1D model and used as initial feed concentration for the biomass.

The proposed model has been solved using a numerical method with defined boundary and initial conditions. Selected simulation results are presented. The model will be validated using experimental data in Chapter 6.

5.7 References

ANSYS FLUENT12.0., 2009. Theory Guide. ANSYS, Inc.

Chan, W.R., Kelbon, M., Krieger, B.B., 1985. Modelling and experimental verification of physical and chemical process during pyrolysis of a large biomass particle. Fuel 64, 1505-1515.

Chejne, F., Hernandez, J.P., 2002. Modelling and simulation of coal gasification process in fluidised bed. Fuel 81, 1687-1702.

De Souza-Santos, M.L., 1989. Comprehensive modelling and simulation of fluidized bed boilers and gasifiers. Fuel 68, 1507-1521.

Enwald, H., Peirano, E., Almstedt, A.E., 1996. Eulerian two-phase flow theory applied to fluidization. International Journal of Multiphase Flow 22, 21-66.

Fairbanks, D.F., Wilke, C.R., 1950. Diffusion Coefficients in Multicomponent Gas Mixtures. Industrial & Engineering Chemistry 42, 471-475.

Fuller, E.N., Schettler, P.D., Giddings, J.C., 1966. New method for prediction of binary gas-phase diffusion coefficients. Industrial & Engineering Chemistry 58, 18-27.

Gao, J., Lan, X., Fan, Y., Chang, J., Wang, G., Lu, C., Xu, C., 2009. CFD Modeling and Validation of the Turbulent Fluidized Bed of FCC Particles. AIChE Journal 55.

Gibilaro, L.G., 2001. "Fluidization Dynamics", 1st edition ed. Butterworth-Heinemann; 1st edition (November 21, 2001)

Graham, R.G., Bergougnou, M.A., Freel, B.A., 1994. The kinetics of vapour-phase cellulose fast pyrolysis reactions. Biomass and Bioenergy 7, 33-47.

Guha, A., 2008. Transport and Deposition of Particles in Turbulent and Laminar Flow. Annual Review of Fluid Mechanics 40, 311-341.

Gunn, D.J., 1978. Transfer of Heat or Mass to Particles in Fixed and Fluidized-Beds. International Journal of Heat and Mass Transfer 21, 467-476.

Guo, Y.C., Chan, C.K., Lau, K.S., 2003. Numerical studies of pulverized coal combustion in a tubular coal combustor with slanted oxygen jet☆. Fuel 82, 893-907.

Huilin, L., Gidaspow, D., Bouillard, J., Wentie, L., 2003. Hydrodynamic simulation of gas-solid flow in a riser using kinetic theory of granular flow. Chemical Engineering Journal 95, 1-13.

Ibsen, C.H., Solberg, T., Hjertager, B.H., 2000. A Study of Dilute to Dense Flow in a Circulating Fluidized Bed, International Symposium on Multiphase Flow and Transport Phenomena, Antalya, Turkey.

Kawi, O.S.A.E., Atwani, E.F., Abdelmonemi, S.A., Abdallai, A.M., Elshazly, K.M., 2007. Hydrodynamic and Thermal Modelling of Gas–Particle Flow in Fluidized Beds. International Journal of Chemical Reactor Engineering 5.

Kunii, D., Levenspiel, O., 1991. Fluidization Engineering, Second Edition ed. Butterworth-Heinemann.

Launder, B.E., Spalding, D.B., 1972. Lectures in Mathematical Models of Turbulence. Academic Press, London; New York.

Lun, C.K.K., Savage, S.B., Jeffrey, D.J., Chepurniy, N., 1984. Kinetic Theories for Granular Flow: Inelastic Particles in Couette Flow and Slightly Inelastic Particles in a General Flow Field. Journal of Fluid Mechanics 140, 223-256.

Macak, J., Malecha, J., 1978. Mathematical model for the gasification of coal under pressure. Industrial & Engineering Chemistry Process Design and Development 17, 92-98.

Melaaen, M.C., 1996. Numerical analysis of heat and mass transfer in drying and pyrolysis of porous media. Numerical Heat Transfer, Part A: Applications 29, 331-355.

Patil, D.J., van Sint Annaland, M., Kuipers, J.A.M., 2005a. Critical comparison of hydrodynamic models for gas–solid fluidized beds—Part I : bubbling gas–solid fluidized beds operated with a jet. Chemical Engineering Science 60, 57-72.

Patil, D.J., van Sint Annaland, M., Kuipers, J.A.M., 2005b. Critical comparison of hydrodynamic models for gas–solid fluidized beds—Part II: freely bubbling gas–solid fluidized beds. Chemical Engineering Science 60, 73-84.

Perry, R.H., Green, D.W., Maloney, J.O., 1997. Perry's Chemical Engineers' Handbook. McGraw-Hill, New York.

Ranade, V.V., 2002. Computational Flow Modeling for Chemical Reactor Engineering. Academic Press New York.

Syamlal, M., O'Brien, T.J., 1989. Computer simulation of bubbles in a fluidized bed. AIChE Symp. Series 85, 22-31.

Syamlal, M., O'Brien, T.J., 2003. Fluid dynamic simulation of O-3 decomposition in a bubbling fluidized bed. AIChE Journal 49, 2793-2801.

Wang, Y., Kinoshita, C.M., 1993. Kinetic model of biomass gasification. Solar Energy 51, 19-25.

Chapter 6

Model validation and application for parameter sensitivity analysis

This chapter includes experimental validation of the developed 1D reaction kinetic model for BFB gasifier (presented in Chapter 3) and the extended 2D CFD model (presented in Chapter 5). Comparison of the simulation results with the measured data from experiments performed at the CAPE gasifier was made. The effects of operating parameters on the model such as temperature, steam/biomass ratio were examined.

6.1 Simulation and validation of the developed 1D biomass gasification model

In this study, two sets of experiments were conducted: the first set was for the validation of overall biomass gasification models and the second set was only for the validation of the initial pyrolysis model.

6.1.1 Experiments for validation of gasification models

In order to validate the developed biomass gasification models, a series of experiments were conducted at the 100 kW DFB gasifier in the Department of Chemical and Process Engineering, University of Canterbury. Figure 6.1 shows the image of the gasifier with its flow diagram as shown in Figure 3.1.

The DFB gasifier consisting of CFB and BFB was constructed using refractory material to handle temperature of up to 1200^{o}C. At the start up, air was blown into the CFB and BFB beds from a 50 HP Rootes blower and air compressor at a rate of 700-800 L/min and 80-100 L/min, respectively. In the initial heat-up period, liquefied petroleum gas (LPG) was supplied to CFB at a flow rate of 40 L/min and to BFB at a flow rate of 41 L/min from a LPG bottle that heated up the gasifiers as well as the bed material. Before the experiment, 12 kg of greywacke sand was fed into the CFB and BFB gasifiers which have a bulk density of 1600 kg/m^3 with the majority of the particle sizes ranging from 180μm to 355μm. The size distribution of the greywacke bed material is shown in Figure 6.2.

Figure 6.1: Image of the 100 kW DFB gasification systems with steam as gasification agent.

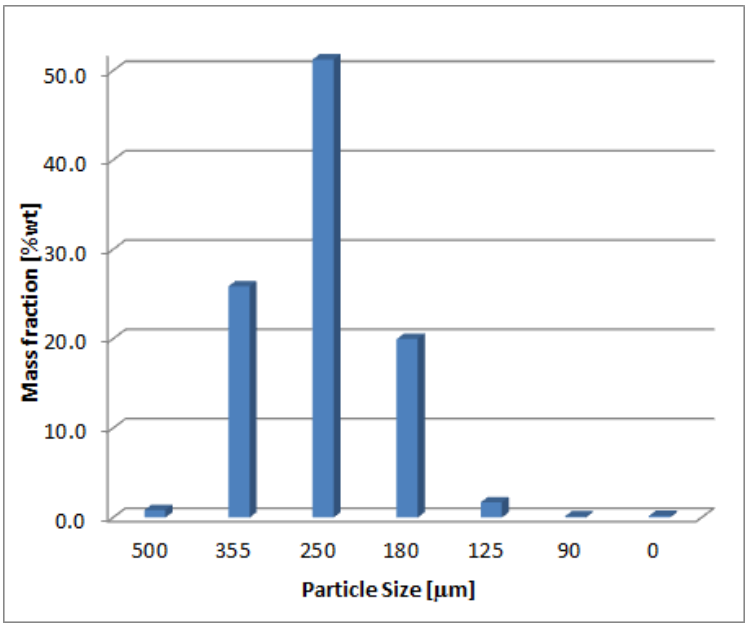

Figure 6.2: Particle size distribution of greywacke sand used in the biomass-steam gasification experiments in the 100 kW DFB gasifier.

To achieve the required gasification temperature in the BFB, the CFB was preheated about 100^{o}C higher than that of preset BFB bed temperature. The start-up phase lasted about 4-5

hours during which period the plant was monitored for bed material circulation, temperatures and gasifier oxygen content in order to maintain a stable state condition. Once the preset temperatures were achieved and the system operation was stable, the supply of air to the BFB gasifier was switched to steam then the DFB gasifiers was fine-tuned to re-gain stable operation by controlling the LPG flow rates to the CFB while the LPG flow to the BFB was turned off. After the system was stable with the steam feed to the BFB, pellets of *Pinus Radiata* sawdust were fed to the BFB gasifier with feeding rate of 15 kg/h at a height of 0.2m from the base of the gasifier where instantaneous pyrolysis occurred. The chars formed over time were circulated along with the bed materials through the chute at the bottom of the BFB gasifier to the CFB gasifier where complete combustion occurred and the bed materials were heated up. At this stage the LPG feeding rate was reduced to maintain the required operating temperature. The heated bed materials were carried up by the flue gas in the CFB gasifier and then separated in a cyclone. The bed materials were then returned back to the BFB to provide sufficient heat for the overall endothermic gasification reactions.

During the steady state operation of the gasifier experiments, samples were taken every 20 minutes and at the same time operating parameters were measured. The data were averaged for each hour and the average values will be used as one run for model validation. In most cases, the gasifying operations were limited to 3-4 hours in each experiment due to a number of limiting factors such as bed material elutriation or agglomeration. A total of five gasifier experiments were conducted with a constant biomass feeding rate of 15kg/h. In the first two experiments the operating temperature was varied from 680 to 780^{o}C at constant steam flow rate of 8kg/h (S/B ratio of 0.53), while in the remaining experiments the operating temperature was maintained constant at 710^{o}C and the steam flow rate was increased from 5 kg/h to 12.6 kg/h with the S/B ratio increasing from 0.33 to 0.84. Gas samples were collected at the top of the BFB gasifier using a double-syringe device as described by *Bull, (2008)* and were analysed using a 3000A Micro GC. At the same time when the gas samples were taken, the gasifier operating parameters such as BFB bed temperature, BFB bed pressure, air flows to the CFB and steam flows to the BFB were recorded. The BFB bed temperature were measured at four different positions of the BFB namely such that (i) inlet, (ii) outlet, (iii) and (iv)at a height 0.2 m and 1m from the base of the BFB respectively. The pressure drop of the BFB bed was measured with a pressure gauge located near the bottom of BFB which connects the bottom of the BFB to the biomass feed port in BFB. The primary air supply to the bottom of the CFB and BFB (during the heat up stage) was measured using rotameters

while the steam flow to the BFB after the heat up stage was through steam flow meter. The air flow to the BFB was progressively reduced to zero while the steam flow was increased. The details in experimental conditions and results were described in Table 6.1.

Table 6.1: The experimental operating conditions and the composition of the producer gas.

Experiment	1			2				3			4				5		
Run	1	2	3	4	5	6	7	8	9	10	11	12	13	14	15	16	17
Biomass feeding rate (kg/h)	15	15	15	15	15	15	15	15	15	15	15	15	15	15	15	15	15
Steam flow rate in BFB (kg/h)	8	8	8	8	8	8	8	5	5.8	6.5	7.4	8.2	9	9.8	10.6	11.4	12.6
Primary air flow in CFB (L/min)	775	775	775	775	775	775	775	775	775	775	775	775	775	775	775	775	775
Helium flow (L/min)	6.5	5.72	4.9	4.9	6.5	6.5	6.4	5.72	5.72	5.72	5.72	5.72	5.72	5.72	5.72	5.72	5.72
BFB bed pressure (kPa)	3.9	3.9	4.0	4.1	4.3	4.7	5.1	3.7	3.9	4.5	4.5	4.6	4.6	4.7	6.0	6.1	6.6
BFB bed temperature T_{bed}(^{o}C)	680	696	708	730	741	758	780	710	710	710	710	710	710	710	710	710	710
Steam/biomass ratio (kg/kg)	0.53	0.53	0.53	0.53	0.53	0.53	0.53	0.33	0.39	0.43	0.49	0.55	0.60	0.65	0.71	0.76	0.84
Producer gas composition at exit (dry N_2 free basis mol/mol %)																	
H_2	20.2	20.1	25.6	25.4	26.9	28.8	35.6	23.9	29.3	30.4	28.8	31.4	30.4	31.0	30.9	31.0	31.4
CO	39.1	40.7	38.9	38.8	37.4	36.7	36.9	43.4	36.4	34.4	34.4	32.6	33.4	32.0	33.1	32.2	32.3
CO_2	23.1	22.3	18.1	18.6	18.2	18.1	14.1	14.7	17.8	19.2	21.1	20.9	21.1	22.0	20.8	21.7	21.4
CH_4	15.2	14.9	15.7	15.4	15.2	14.4	11.5	16.1	14.5	13.9	13.7	13.2	13.4	13.1	13.5	13.4	13.4
He	2.4	2.1	1.7	1.78	2.26	1.96	1.9	2.0	1.92	1.9	1.88	1.85	1.84	1.82	1.75	1.72	1.7
Dry producer gas calculated (tar free)																	
Volume flow rate(m^3/h)	14.5	14.7	15.6	14.9	15.5	17.9	18.2	15.4	16.1	16.2	16.4	16.7	16.8	17	17.7	18	18.2
mass flow rate (kg/h)	15.3	15.6	15.8	16.4	17.0	18.2	18.5	14.9	15	15.2	15.9	15.7	16	16.2	16.7	17.1	17.2
H_2O at the exit (mol/mol %)	39.1	38.2	35.5	34.9	31.8	24.9	23.7	29.0	30.7	32.1	32.8	35.5	37.0	38.3	38.2	38.5	43.1

6.1.2 Experiments for validation of the initial pyrolysis

To validate the developed model for initial pyrolysis in the biomass steam gasification, a series of experiments were conducted with nitrogen gas being used as fluidization agent to the BFB gasifier instead of steam. Thus only pyrolytic products such as char, tar, pyrolysis gases (mainly CO, CO_2, H_2 and CH_4) occurred when the biomass pellets were fed. The moisture in the biomass pellets used is about 8 wt%, which will be vaporized into water vapours on instantaneous drying at high temperature inside the gasifier *(Bridgwater, 2003; Corella and Sanz, 2005; Garcia et al., 1998).*During the experiments, nine sets of sample data were measured with the operating parameters as described in Table 6.2. In the experiments, the gasifier was firstly heated up using LPG to preset target temperatures in the same way as described in the gasification experiments using air as the fluidization agent in both the CFB and the BFB gasifiers. Once the target temperature was achieved, nitrogen was introduced into the BFB gasifier as the fluidization agent. Under this inert condition of nitrogen fluidization in BFB, the biomass pellets were fed in and the gas samples were collected at the top the BFB gasifier for analysis using a 3000A Micro GC.

Table 6.2: The experimental operating conditions and the composition of the initial pyrolysis gas.

Run	1	2	3	4	5	6	7	8	9
Biomass feeding rate (kg/h)	15	15	15	15	15	15	15	15	15
N_2 flow rate in BFB (L/min)	89	89	87	89.8	89.8	87	87	87	87
Primary air flow in CFB (L/min)	775	775	775	763	763	768	768	763	804
BFB bed pressure (kPa)	6.2	6.3	6.6	4.4	4.6	4.7	4.8	6.8	6.6
BFB bed temperature $T_{bed}(^oC)$	705	729	734	748	750	766	768	775	787
Gas composition at exit (N_2 and H_20 free basis mol/mol %)									
H_2	22.7	21.2	26.6	22.3	21.6	26.3	25.6	26.4	27.1
CO	41.7	43.6	40.4	40.8	43.8	38.9	42.6	40.8	39.4
CO_2	20.7	20.3	19.7	23.2	20.3	21.6	18.1	19.1	20
CH_4	14.9	14.8	13.4	13.7	14.4	13.3	13.8	13.6	13.5

The process of biomass pyrolysis has been investigated in previous studies *(Garcia et al., 1998; Lv et al., 2004; Wang et al., 2005a, b)*, however, the reported gas compositions from

the pyrolysis vary significantly with biomass type and pyrolysis conditions. As discussed in Chapter 3, the concentrations of the product species from the pyrolysis were used as initial conditions for the subsequent gasification reactions. Therefore, the pyrolysis was simulated first. From sensitivity studies in the current work, it was found that the initial gas compositions from the pyrolysis have significant effect on the gasification process. Therefore the initial gas compositions prior to the gasification was determined from the rate kinetic Equations $(3.2 - 3.5)$ followed by the production distribution Equation $(3.14a)$. The results from simulation of the initial pyrolysis of biomass were given in Table 6.3 in comparison with the experimental values for operation temperature ranging from 680 to 787°C. Using the values of Arrhenius kinetic rate constants from the Table 3.3, the above kinetic model was solved to predict the proportions of gas, tar and char as a function of pyrolysis time (as in Equation (3.07).

Table 6.3: Model predicted concentrations of product species from initial pyrolysis at different temperatures using rate Equations (3.2-3.5) coupled with the production distribution Equation (3.14) along with the experimental results.

T (^{o}C)	680	705	729	734	748	750	766	768	775	787
Mass fraction from rate kinetic Equations $(3.2 - 3.5)$(wt %)										
Char	16.54	16.01	15.53	15.44	15.19	15.15	14.88	14.84	14.73	14.54
Tar	2.07	0.43	0.06	0.04	8×10^{-3}	6×10^{-3}	5×10^{-3}	8×10^{-4}	2×10^{-4}	5×10^{-5}
Volatiles	81.39	83.57	84.41	84.52	84.81	84.84	85.12	85.16	85.27	85.46
Pyrolysis production distribution using Equation (3.13) (mol/mol %)										
H_2	15.4	17.9	20.6	21.3	23.0	23.2	25.3	25.5	26.5	28.1
CO	48.0	46.1	44.2	43.8	42.6	42.4	41.0	40.9	40.2	39.2
CO_2	21.0	20.8	20.5	20.4	20.2	20.2	19.9	19.8	19.7	19.4
CH_4	15.6	15.2	14.6	14.5	14.2	14.2	13.8	13.8	13.6	13.3
Experimental pyrolysis gas composition at exit (N_2 and H_20 free basis mol/mol %)										
H_2	n/a	22.7	21.2	26.6	22.3	21.6	26.3	25.6	26.4	27.1
CO	n/a	41.7	43.6	40.4	40.8	43.8	38.9	42.6	40.8	39.4
CO_2	n/a	20.7	20.3	19.7	23.2	20.3	21.6	18.1	19.1	20
CH_4	n/a	14.9	14.8	13.4	13.7	14.4	13.3	13.8	13.6	13.5

The instant pyrolysis reaction of the biomass particles ceased in less than 1s as superficial velocity was 0.4 m/s. At operation temperature of 680°C, the wood particles were decomposed completely into char, tar and volatile gases in about 0.4s from the point when the wood particles had reached the operation temperature. This time was reduced to 0.1s at the operation temperature of 780°C. By this time the char formation was complete and remains at about 16 wt% of the feed wood particles. With the pyrolysis process continuing, some tars were converted into hydrocarbon gases and thus the volatile gases concentration increases and tar concentration decreases. These results are shown in Figure.6.3.

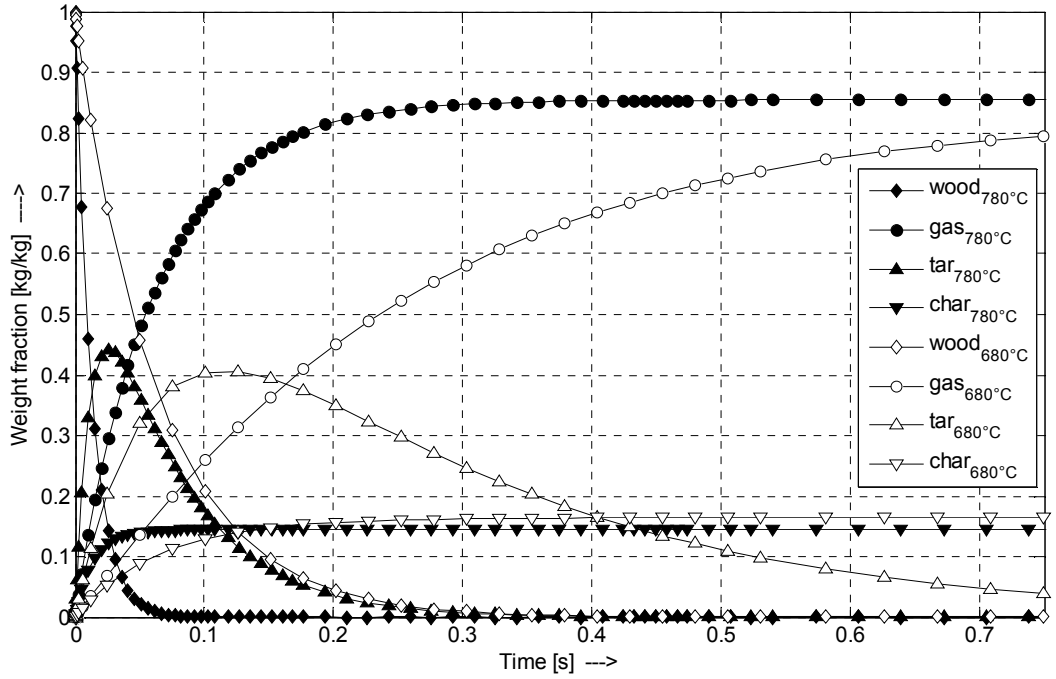

Figure 6.3: Mass fraction of wood decomposition by initial pyrolysis over time predicted from the kinetic model using Chan's and Graham's coefficients.

From Figure 6.3, it can be seen that all the pyrolysis products remain constant in less than 1s of thermal degradation. However, in the practical gasification process, with the wood particles falling down from the feed point in the gasification reactor, steam was injected and flows upwards in contact with the biomass. The pyrolysis reactions ceased at relative faster rate and the subsequent gasification reactions and mixing took place simultaneously when the steam fed into the gasifier was in contact with the product gases from the initial pyrolysis.

The experimental data had been used for comparison with the model simulation results of the gas composition in the initial pyrolysis for temperatures from 680 to 780°C. The results are shown in Figure 6.4. From the model simulation results, the concentrations (molar fractions) of CO and CO_2 decreased with the gasification temperature. The CO_2 concentration changing slightly from 21% (mol/mol) at 680°C to 19.6% (mol/mol) at 780°C with an uncertainty (measured as standard error) of ±0.6% (mol/mol) . The standard error (SE) for the measured values was calculated from the ratio of standard deviation and the square root of number of sample data. In the same temperature range, the corresponding CO concentration decreased from 48% to 39.9% (mol/mol) where the uncertainty predicted was ±0.8% (mol/mol). With the operating temperature increased in the same range, the H_2 concentration increased from 15.4% to 27.2% (mol/mol) and the concentration of CH_4 decreased slightly from 15.6% to 13.1% (mol/mol). The uncertainty for H_2 was foreseen to be higher at ±1.0% (mol/mol), while the error for CH_4 was lower at ±0.3% (mol/mol) in the operating temperatures 680 to 780^{o}C. The correlation coefficient (R^2) of the proposed correlation Equation ($3.14b$) and the experimental results were found to be 0.89, 0.94, 0.93 and 0.85, respectively, for H_2, CO, CH_4 and CO_2. The value (R^2) close to one was a rough indicator of the goodness of fit. However the uncertainties in the slope and intercept were much better for judging the quality of the fit. The uncertainties of slope for H_2, CO, CH_4 and CO_2 were found to be 16%, -14%,-14% and 24% respectively and the uncertainties of intercepts for H_2, CO, CH_4 and CO_2 were found to be -17%, 11%,11% and 14% respectively. The uncertainties in the slope and intercept were not as good as the (R^2) might have indicated. However, a better statistical test of the goodness of fit is to use the Fisher F-statistic *(Patnaik, 2004)*. The F-statistic is the ratio of the variance in the data explained by the linear expression divided by the variance unexplained by the model. The F-statistic value is given in Equation 6.1.

$$F-statistic = \frac{varianceexplained}{varianceunexplained} = \frac{regressionss/v_1}{residualss/v_2} = \frac{(\sum(\hat{y}_i - y_{av})^2)/v_1}{(\sum(y_i - \hat{y}_i)^2)/v_2} \qquad (6.1)$$

The F-statistic under the null hypothesis, that the data is a random scatter of points with zero slopes. The critical values of the F statistic are listed in *Patnaik (2004)*. The F-critical value at 95% confidence interval for 9 data points were 5.59. However the F-statistic values for the H_2, CO, CH_4 and CO_2 were found to be 39, 46, 50.5 and 17 respectively using the Equation 6.1. The F-statistic values were much greater than F-critical value and the null hypothesis failed and the linear expression developed was significant. Thus the simulation results were in close agreement with the experimental data.

The trend of the above predicted gas compositions is also consistent with previous studies of *Lv et al. (2004)* who conducted pyrolysis experiments using pine sawdust in the fluidized bed rector at operating temperature of 700°C. Their experimental results show that the pyrolysis gas products under inert condition consist of about 52 % CO, 16.2 % H_2, 15.4 % CH_4 and 9.7% CO_2 (mol/mol) *(Lv et al., 2004)*. It can be observed that their experimental data are in close agreement for H_2 and CH_4 while the CO_2 concentration is slightly under-predicted and CO concentration is slightly over-predicted compared with our model.

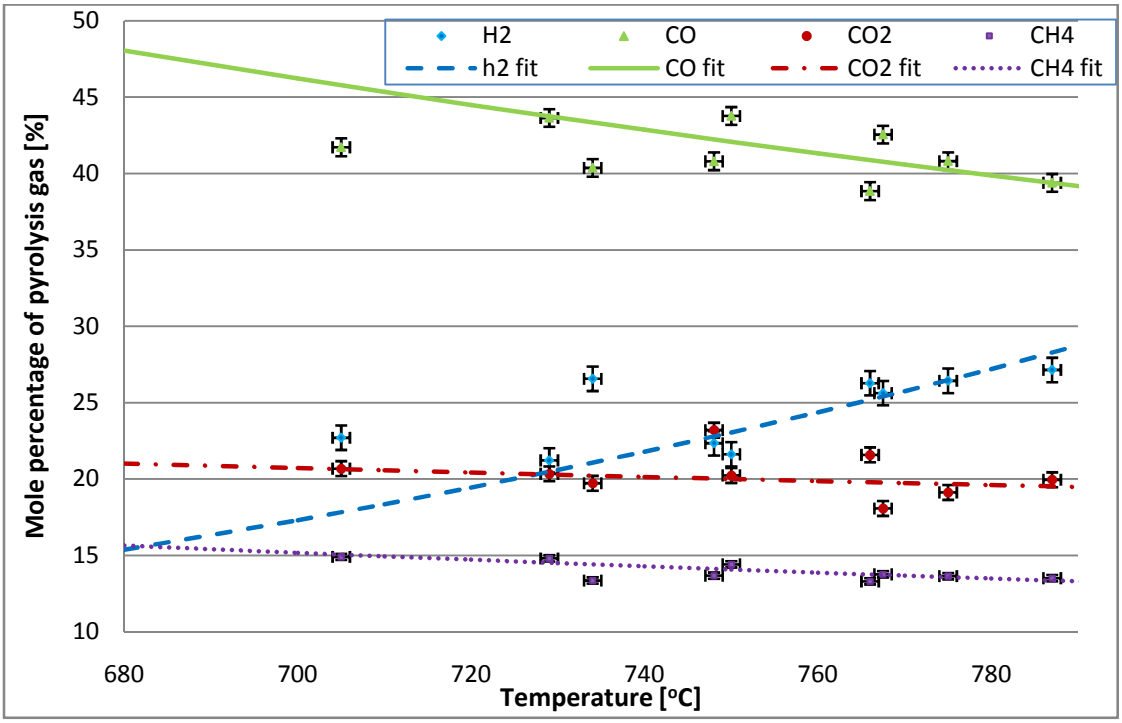

Figure 6.4: Gas composition (molar fraction) in initial pyrolysis of biomass at the top of the BFB gasifier at different reaction temperatures with constant pressure of 1 atm.

6.1.3 Experimental validation of the 1D gasification model

By using the gas composition and the char yield from the pyrolysis model as the initial conditions for the modelling of gasification reactions, the developed 1D biomass steam gasification model had been solved. The simulation results were compared with experimental data obtained from the experiments described in Section 6.1.1 as shown in Figure 6.5 for operation temperature from 680 to 780°C and operating pressure of 1 atm with constant S/B ratio of 0.53.

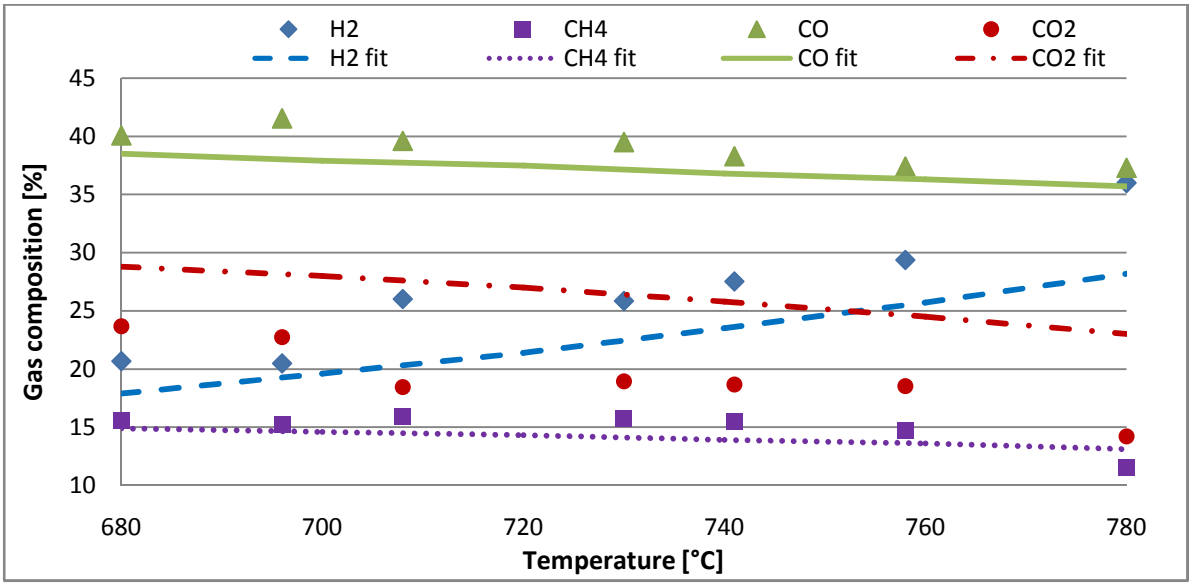

Figure 6.5: Model predicted and experimentally measured producer gas compositions for steam gasification of wood pellets at operating temperatures from 680 to 780°C; operating pressure of 1 atm with a constant S/B ratio of 0.53 and a biomass feeding rate of 15 kg_{dry}/h.

In the experiments, the gas samples were measured three times in each run and the data in Figure 6.5 are the average values over the three measurements in each run. It was noticed in the experiments that the operation temperature changed within a range of ±20°C from the set point thus the actual temperature at the measurement point was used in the plot. In the meantime, the developed model was run to predict the producer gas composition at 40 minutes from the start of the gasification, as shown in lines in Figure 6.5. However the model reaches steady state in less than 5 minutes. It was found from the producer gas composition for the temperature ranges from 680-780°C that the CH_4 composition was the lowest while the CO concentration was the highest among gas components. From the comparison, the model predictions were in close agreement with the experimental data for CO, CH_4 with discrepancies of less than 2% (mol/mol) compared to the experimental data. The discrepancies in the gas concentration for H_2 and CO_2 were less than 4.5% (mol/mol) and 8 % (mol/mol) respectively. For both experimental and simulation results the H_2 increases and CO_2,CO and CH_4 decreases markedly as the operating temperature increases from 680 to 780°C.

The gasification reactions in the developed model have been analysed and the reaction kinetics were examined to better understand the gas formation and its composition at different operation temperatures.

Figure 6.6 shows the gas species formed by the major reactions involved in gasification process at one atmospheric pressure with different operating temperatures at constant S/B ratio of 0.53. For illustrative purpose, the basis (i.e., initial concentrations) for the above reactions considered was from the products of initial pyrolysis. The endothermic reactions (Equations 3.15, 3.18 and 3.19) favoured, the forward reactions with more H_2 and CO with the increase in operating temperature from 701 to 780°C as seen in Figure 6.6a, 6.6c and 6.6e. The exothermic Methanation reaction (Equation 3.17) had the equilibrium constant K_c ranging from 0.16 to 0.056 in the operating temperature range; therefore, increasing operation temperature favoured the reverse reaction and produces more reactant gas of H_2 as seen in Figure 6.6i and 6.6j. On the other hand, the exothermic Water Gas-Shift reaction (Equation 3.16) had its equilibrium constant K_c ranging from 1.8 to 1.18 for the operating temperature range, favoured products with more CO_2 and H_2at lower operating temperature and consequently the CO_2 and H_2 content decreases as the operating temperature was increased producing more CO and H_2O as shown in Figure 6.6g. Both Methanation reaction (Equation 3.17) and Steam Methane Reforming reaction (Equation 3.19) produce H_2 and CO, respectively, with the consumption of formed methane due to initial pyrolysis reaction. Hence the methane concentration remains almost constant over the range of operating temperatures examined.

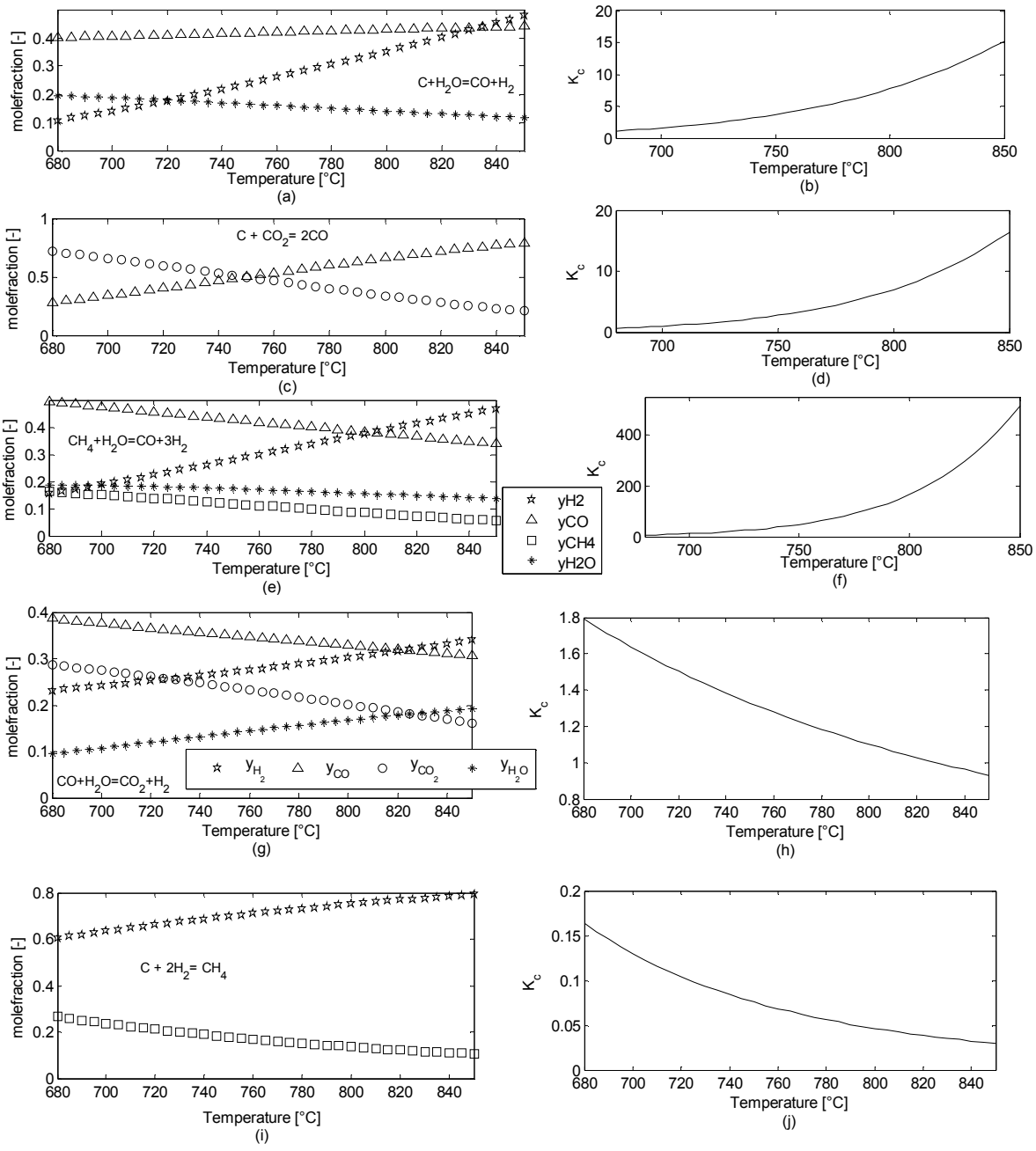

Figure 6.6: The gas composition with different operating temperatures for various reactions occurring in the gasifier at 1 atmospheric pressure.

Figure 6.7 shows the gas species formed by the major reactions involved in gasification process at one atmospheric pressure with different S/B ratio at constant operating temperature of 710^{o}C. It is evident from Figure 6.7 that increase in steam content drives the Steam Gasification Reaction (Equation 3.15), Steam Methane Reforming reaction (Equation 3.19) and the Water Gas-Shift reaction (Equation 3.16) in the forward direction producing more H_2 and CO_2, respectively, at a given temperature. However, the increase in steam content also

increases the CO content, which is ultimately consumed by the endothermic Bouduard reaction (Equation 3.18) whose equilibrium constant K_c decreases favouring reverse reaction producing more CO_2.

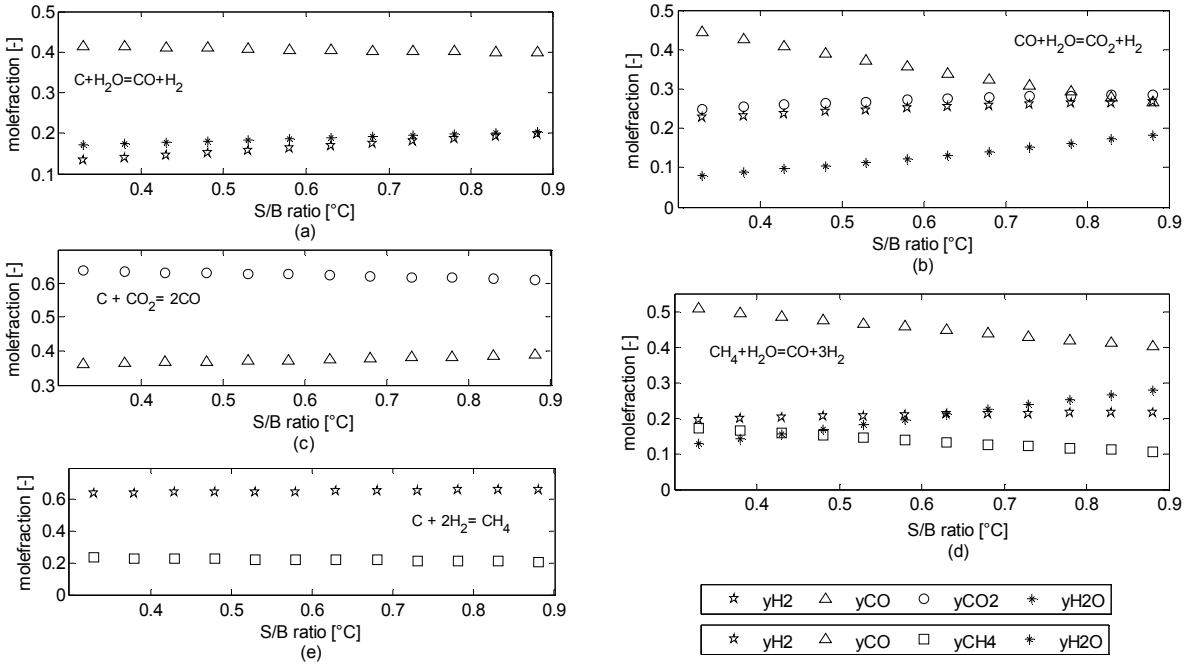

Figure 6.7: The gas composition with different S/B ratio for various reactions occurring in the gasifier at 1 atmospheric pressure and 710^{o}C.

6.2 Application of the 1D model for sensitivity analysis

6.2.1 Influence of temperature on the producer gas composition

As discussed previously in Chapter 3, the biomass gasification consists of two stages, an initial pyrolysis stage followed by the gasification stage. In the initial pyrolysis stage, the biomass was decomposed into volatiles, char and tar, therefore, the initial gas compositions of CO_2, CO, H_2, CH_4 in the producer gas vary with the pyrolysis temperature and the moisture content in the biomass. The net contribution of H_2O in the producer gas from the biomass steam gasification process was from the excessive feed steam reacting with the volatile products of initial pyrolysis in subsequent gasification reactions such as Steam Gasification reaction, Water Gas-Shift reaction and Steam Methane Reforming reaction. For the given S/B ratio, the moisture content (H_2O) in the producer gas decreases with the gasification temperature, for example decreasing from 27% (mol/mol) at operating

temperature 680°C to 20% (mol/mol) at 780°C. This is because the Steam Gasification reaction type I (Equation3.15a) had equilibrium constant K_c of 1.13 at 680°C and increased to 5.77 at 780^{o}C which favours consumption of H_2O at elevated temperatures, producing CO and H_2. Similarly, the equilibrium constant K_c for Steam Methane Reforming reaction (Equation 3.19) increased from 6.9 to 102.7 for the operating temperature range, and as a result the rate of Steam Methane Reforming reaction (Equation3.19)also increased which also favoured forward reactions with the consumption of H_2OOn the other hand, the exothermic Water Gas-Shift reaction (Equation 3.16) favoured forward reaction at relatively lower temperatures forming more H_2 and CO_2. However, while at higher temperatures, the equilibrium constant K_c reduces and eventually the reaction rate was reduced and the consumption of H_2O reduced. Hence the overall effect of increase in operating temperature decreased the moisture content of the producer gas.

On the opposite trend, the concentration of CH_4 decreases from about 14.9% to 13.1% (mol/mol) on dry basis when the gasification temperature was increased from 680 to 780°C as seen in Figure 6.5. From previous studies of *Gil et al. (1999),* it is found that at lower temperatures, the pyrolysis of biomass produces more methane and some hydrocarbons are not cracked into hydrogen and carbon molecules. At the relatively lower temperatures, the equilibrium constant K_c for exothermic Methanation reaction (Equation 3.17) was lower than 1 and decreased further at higher temperature and for the endothermic Steam Methane Reforming reaction (Equation 3.19) they were lower than at higher temperatures; therefore, the composition of CH_4 was higher at lower temperatures. With increase in operation temperature, the pyrolysis process produces less CH_4 and more CH_4 was consumed due to the increase in the rates of both Methanation reaction and Steam Methane Reforming reaction. Hence the overall CH_4 composition drops as the operating temperature increases from 680 to 780°C.

The CO concentration decreased slightly from 38.5% to 35.7% (mol/mol) with operating temperature increasing from 680°C to 780°C as seen in Figure 6.5. With increase in the operating temperature, the initial pyrolysis produced less CO and more H_2 and hydrocarbons. In the subsequent gasification reactions, the Bouduard reaction (Equation 3.18), Steam Gasification reaction type I (Equation3.15a) and the Steam Methane Reforming reaction (Equation3.19) shifted towards the product side producing more CO. However, with the increase in operation temperature, the equilibrium constant K_c of exothermic Water Gas-Shift

reaction was 1.18 at 680°C and decreased to 0.8 at 780°C which favours consuming more CO and H_2O. Therefore, the overall concentration of CO decreases with the temperature increasing from 680°C to 780°C.

From Figure 6.5, it is found that the H_2 concentration increased by about 10.3% (mol/mol) on dry basis with temperature from 17.9% at 680°C to 28.2% at 780°C. With increase in operation temperature, the initial pyrolysis produces more hydrogen. In the subsequent gasification reactions, the endothermic Steam Gasification reaction (Equation3.15a) favoured forward reaction, producing more CO and H_2. The slow Steam Methane Reforming reaction (Equation3.19) also favoured forward reactions producing three moles of H_2 and a mole of CO consuming one mole of CH_4 and one mole of H_2O. As discussed before the Methanation reaction also favoured H_2. Therefore the H_2 concentration increase with the operation temperature in the temperature range examined.

The concentration of CO_2 changes from 28.8% to 23 % (mol/mol) in the operating range from 680°C to 780°C. However, with temperature increasing, type I Steam Gasification reaction was more active than type II Steam Gasification reaction, thus the CO_2 content decreases at higher temperatures. While the equilibrium constant K_c for Bouduard reaction in Equation (3.18) was about 0.63, the temperature around this equilibrium constant enhances the reverse reaction forming more CO_2 by consuming CO. However as the operating temperature increased, the equilibrium constant K_c also increased to 4.9 close to 780°C, the Bouduard reaction shifts towards the product direction and more CO_2 was consumed.

By considering all of the above reactions, the net effect was that with operation temperature increasing from 680 to 780°C, the composition of CH_4 and CO decreased slightly while H_2 concentration increased more significantly and the content of CO_2 was decreased significantly. In the same time, CO content decreases by about 2.8% (mol/mol) while CO_2 content decreases by about 5.8 % (mol/mol) on dry basis in the same temperature range.

6.2.2 Effects of steam to biomass(S/B) ratio

The model was also used to investigate the effect of S/B ratio in a wider range from 0.33 to 0.84 on the producer gas composition for steam gasification of wood pellets at 710°C and the results are shown in Figure 6.8in which experimental data were also presented for comparison. From the gasification reactions, it was known that the increase in S/B ratio

favoured the forward reaction of the fast exothermic Water Gas-Shift reaction (Equation 3.16), thus producing more CO_2 and H_2 by consuming more CO and H_2O. Hence with increase in S/B ratio from 0.33 to 0.84, the CO concentration decreased from 40.2% to 33.8% (mol/mol) and that of H_2 increases from 24.4% to 30% (mol/mol) as seen from Figure 6.8.

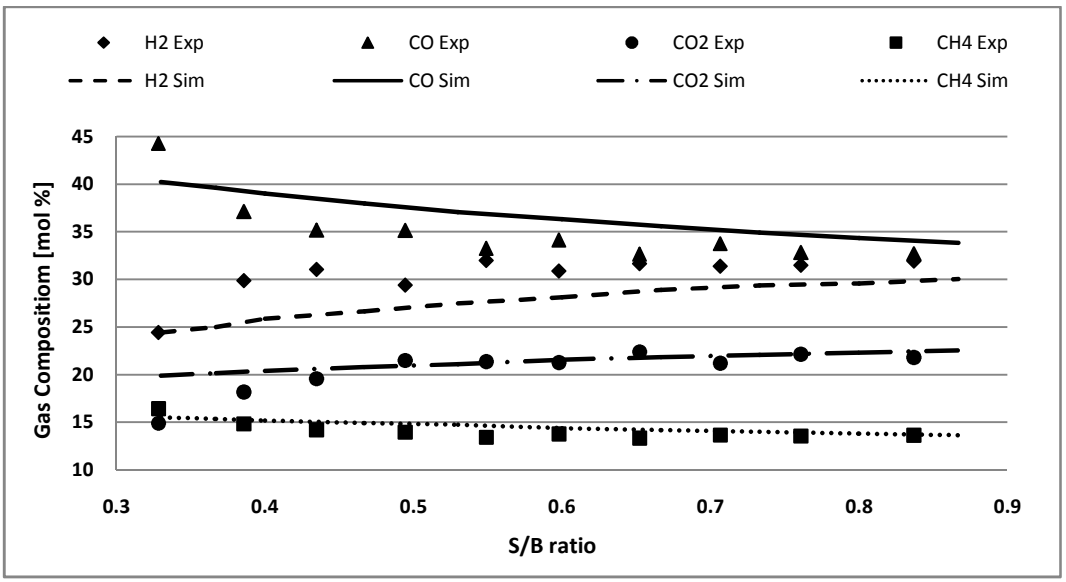

Figure 6.8: Plot of the dry producer gas composition from experiments and from model simulation for steam gasification of wood pellets at operating temperature of 710°C and 1atmospheric pressure with S/B ratio ranging from 0.33to 0.84 at a constant biomass feeding rate of 15 kg_{dry}/h.

As the S/B ratio increased, the steam content also increased which promoted the Steam Gasification Reaction (Equation $3.15a$) that produced more H_2 and CO_2. Simultaneously, some CO_2 was consumed in the Bouduard reaction with carbon (Equation3.18), producing CO, but the reaction rate was very slow compared with the Steam Gasification reaction. Hence overall CO_2 increases moderately from 19.9% to 22.6% (mol/mol) with the same range of S/B ratio as seen in Figure 6.8.

With increase in the S/B ratio, the Steam Methane Reforming reaction (Equation3.19) favoured the forward reaction producing more H_2 and CO by consuming more CH_4. At the same time more CH_4 was generated from the initial pyrolysis and the net consequence was that with increase in S/B ratio from 0.33 to 0.84, the CH_4 concentration in the producer gas

decreased slightly from 15.5% to 13.6% (mol/mol). Considering all of the above reactions (Equations 3.15 to3.17and 3.19), the effects with increasing the S/B ratio favoured the production of H_2 molecules as seen in Figure 6.8. These results are in close agreement with previous published experimental observations *(Franco et al., 2003; Rapagnà et al., 2000)*.

On the other hand the increase in S/B ratio decreased the bed temperature based on the model simulation results. Figure 6.9 shows the temperature profiles along the BFB gasifier operated at two different temperatures over a wide range of S/B ratios from 0.33 to 0.84 with a feeding rate of woody biomass 15 kg_{dry}/h. As the S/B ratio was increased the temperature drops faster both in the bed and in the freeboard space along the height of the BFB gasifier. This temperature drop in the bed, in turn, has influences on the gasification reactions thus the gas composition.

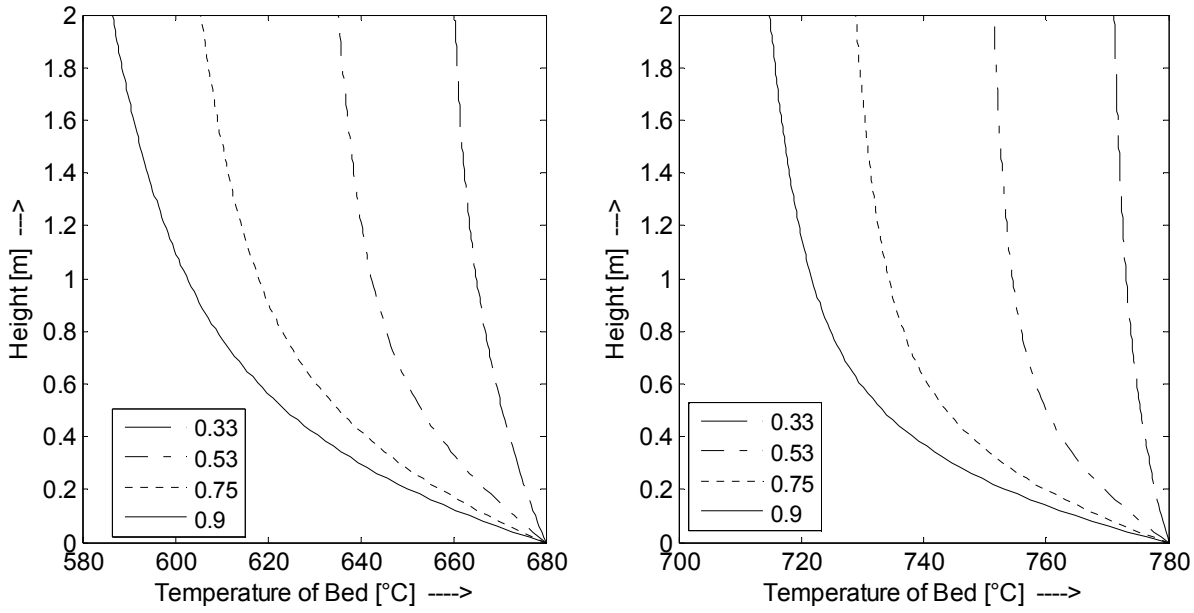

Figure 6.9: Temperature profiles along the BFB gasifier with various S/B ratios at a constant biomass feeding rate of 15 kg dry/h at 1 atmospheric pressure and operation temperature of (a) 680^{o}C and (b) 780^{o}C.

6.2.3 Analysis of emulsion and bubble phases in the BFB gasifier

In this study the model had been developed based on the dual flow regime as bubble phase and emulsion phase. The effect of producer gas composition in the BFB gasifier had been investigated for two different operating temperatures at a constant S/B ratio of 0.53, pressure at 1 atm and woody biomass feeding rate of 15 kg_{dry}/h. The simulation results are shown in Figure 6.10. In the bottom zone of the bed the emulsion phase reactions were dominant and the interphase mass transfer coefficient from bubble to emulsion phase K_{be}(1/s) was higher due to large fractions of bed materials in that zone. Hence the composition of the individual gases in the bubble phase decreased while that of the emulsion phase gases increased as seen in Figures 6.10(a) and 6.10(b). Along the height of the bed, the fractions of bed materials decreased and hence the interphase mass transfer coefficient also decreases. As a result, the influence of bubble phase reactions became more influential than that of the emulsion phase reactions towards the production of the producer gas composition.

In the bubble phase only exothermic Water Gas-Shift reaction (Equation3.16) and endothermic Steam Methane Reforming reaction (Equation3.19) were considered. When operated in the temperature range 680^{o}C to 780^{o}C, the endothermic Steam Methane Reforming reaction favoured forward reaction producing more of H_2 and CO while the exothermic reaction produces more CO along the BFB gasifier. At low operating temperature (680^{o}C) initial pyrolysis produced high concentration of CO as this was seen in the bubble phase. However at high operating temperature (780^{o}C) the initial pyrolysis produced more H_2 and relatively less CO.

In the emulsion phase all the reactions (Equations 3.15 to 3.19) were involved and hence the effect of operation temperature is the same as discussed in Section 6.2.1 and the changes of gas composition with the CFB gasifier height is also shown in Figure 6.10.

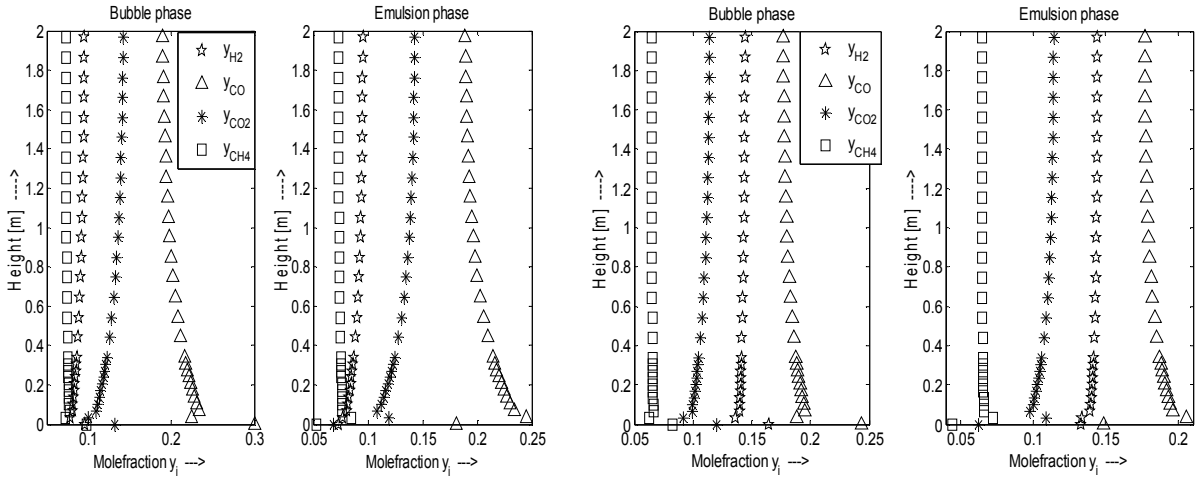

(a) (b)

Figure 6.10: Model predicted dry producer gas composition along the BFB gasifier height showing both bubble phase and emulsion phase gases for steam gasification of wood pellets at operating temperatures (a) 680 °C and (b) 780 °C with a constant S/B ratio of 0.53,1 atmospheric pressure and a biomass feeding rate of 15 kg_{dry}/h.

The gas composition profiles in both bubble phase and emulsion phases were further examined for different S/B ratios. The model predicted gas composition profiles in the biomass steam gasification in the CFB gasifier at operation temperature of 710°C are shown in Figure 6.11(a) for S/B ratio of 0.4 and in Figure 6.11(b) for S/B ratio of 0.8 at constant woody biomass feeding rate of 15 kg_{dry}/h. As discussed before for varying temperature condition in the bubble and the emulsion phases, a similar effect was also observed for the varying S/B ratio. In the bottom zone of the bed, the emulsion phase reactions were dominant due to the bed material leading to higher interphase mass transfer coefficient between the bubble and emulsion phase and this effect changes along the height of the BFB gasifier. The concentration of individual gas species decreased in the bubble phase and increases in the emulsion phase. In the freeboard space, the bubble phase reactions began to dominate and hence the gas concentration starts to increase in bubble phase.

From previous discussion, it is known that at 710^{o}C the initial pyrolysis produced more CO and a less amount of CO_2, H_2 and CH_4 with higher S/B ratio. In the subsequent gasification process, the increase in S/B ratio in the same operating temperature favours forward Steam Methane Reforming reaction producing more H_2 while consuming CH_4 and H_2O. On the other hand the Water Gas-Shift reaction consumes CO and H_2O producing H_2 and CO_2.

These effects can be seen in the bubble phase of Figure 6.12. In the emulsion phase, the reactions consist of both homogeneous and heterogeneous reactions. In addition to the effects seen in bubble phase, the enhanced Steam Gasification reaction contributed to the high concentration of H_2 at higher S/B ratio.

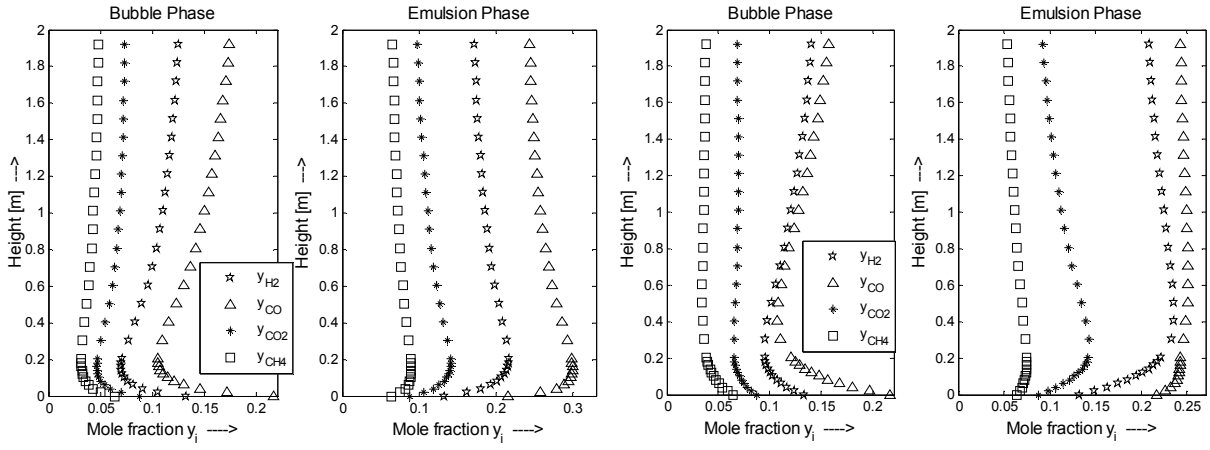

(a) (b)

Figure 6.11: Model predicted gas composition profiles along the height of the BFB gasifier in steam gasification of wood pellets at operating temperature and pressure of 710°C, 1 atmospheric and at a constant biomass feeding rate of 15 kg_{dry}/h with S/B ratio (a) 0.4 and (b) 0.8.

6.2.4 Char conversion along the BFB gasifier: Influence of temperature and S/B ratio.

The developed 1D model had also been used to examine the conversion of chars which were formed from the initial pyrolysis of woody biomass. The model predicted char conversion profiles and remaining chars along the height of the gasifier are shown in Figure 6.12 for different operating temperature and S/B ratios.

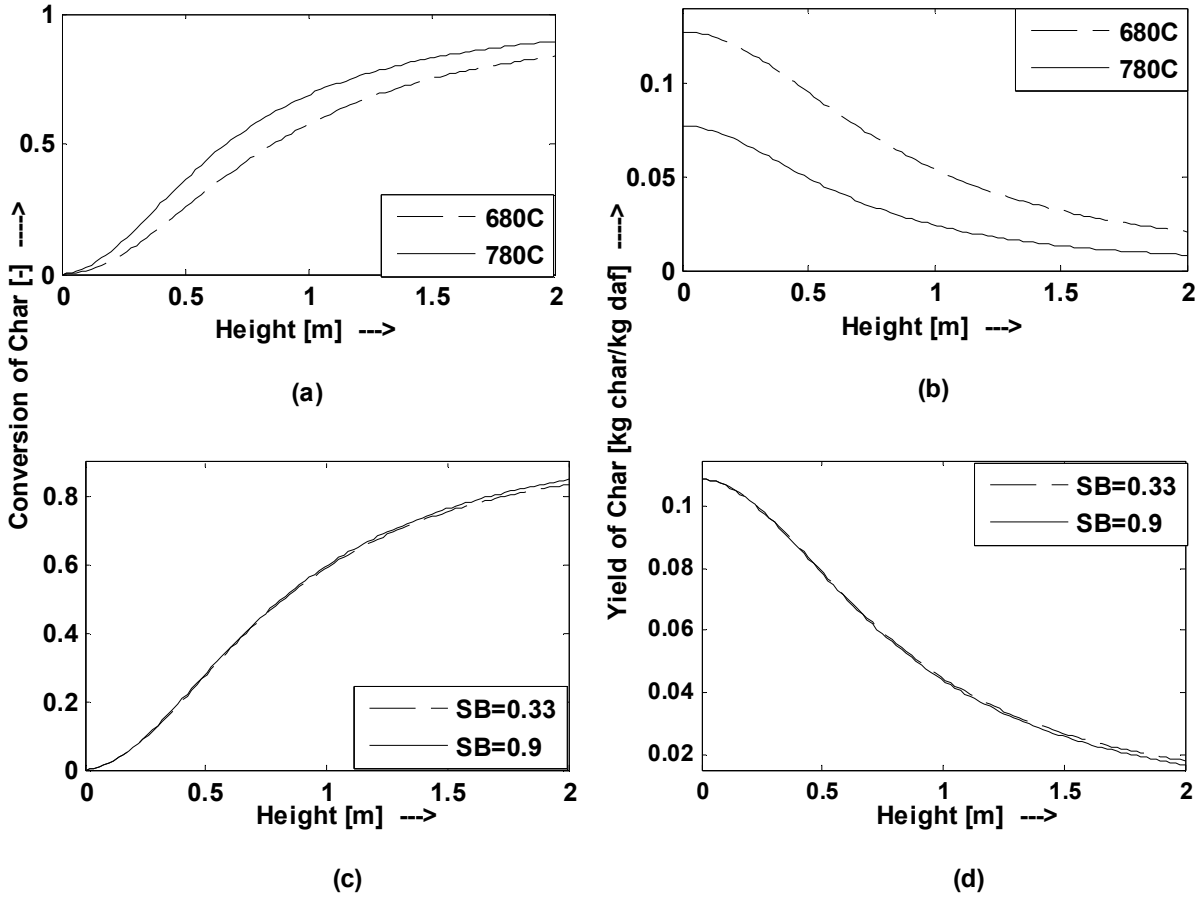

Figure 6.12: Model predicted char conversion profiles and remaining chars in the biomass gasification along the height of the BFB gasifier with fixed biomass feeding rate of 15 kg_{dry}/h and 1 atmospheric pressure: Effect of operation temperature on the char conversion (a) and remaining char (b) at constant S/B ratio 0.53; Effect of S/B ratio on char conversion (c) and remaining char (d) at operation temperature of 710°C.

It was known that the yield of char from the initial pyrolysis of woody biomass decreases as the operating temperature increases. At an operating temperature of about 680^{o}C the yield of char was about 12.72 wt % of feed and that for temperature of 780^{o}C was reduced to about 7.71wt % of the feed as shown at the bottom zone of the BFB gasifier. Along the height of the BFB gasifier, the char content decreases as it was converted during the gasification process and eventually 80-90 % conversion of char was achieved at the top of the BFB gasifier. At higher operating temperatures, the char conversion rate along the height of the BFB bed increased due to forward reactions of Steam Gasification reaction (Equation3.15) and Bouduard reaction (Equation3.18). However, the exothermic Methanation reaction

(Equation3.17), whose equilibrium constant K_c ranges between 0.16 and 0.056, favoured reverse reaction forming char and H_2. On the other hand, the S/B ratio did not show any noticeable influence on the char conversion. The increase in S/B ratio increased the rate of Steam Gasification reaction while consuming more char; however the bed temperature decreases as discussed in Section 6.2.2 and forward rate of Bouduard reaction gradually decreased. Hence the change in S/B ratio had less influence on char conversion.

6.2.5 Effect of solid mixing

The behavior of the solid mixing is studied from the solids dispersion coefficient. The solid dispersion coefficient D_{sr} depends on the bubble fraction and bubble diameter in the bed. The solid dispersion coefficient is plotted against the excess gas velocity multiplied by the height of the bed $x(u_g - u_{mf})$, giving a quantity of the same dimension as the dispersion coefficient in Figure 6.13a.

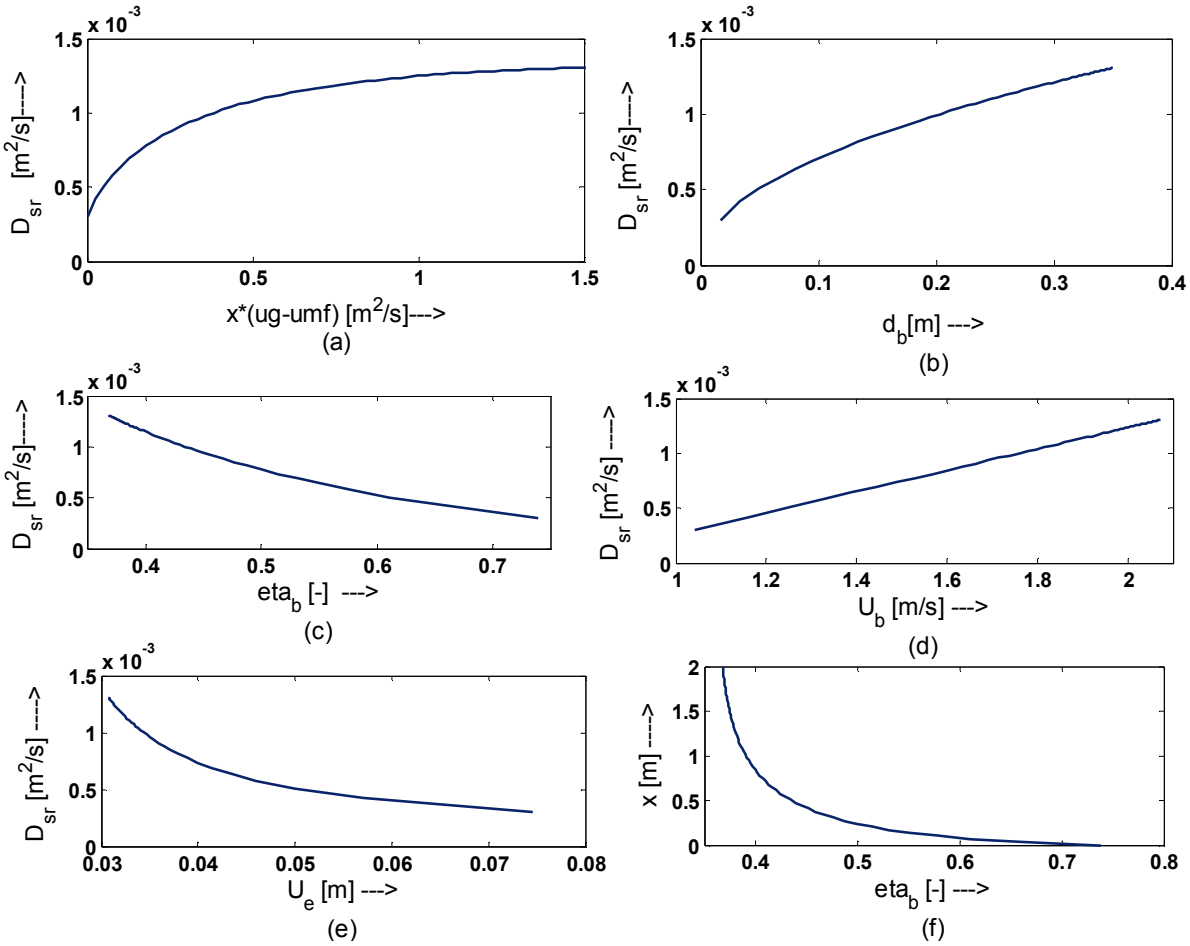

Figure 6.13: Model predicted solid dispersion coefficient D_{sr} versus following parameters (a) excess gas velocity multiplied by the height of the BFB (b) bubble diameter (c) bubble

fraction (d) bubble velocity (e) emulsion velocity and (f) bubble fraction vs height of the BFB.

The solid dispersion coefficient is also plotted against the bubble diameter, bubble fraction, bubble velocity and emulsion velocity as in Figure 6.13 (b) to 6.13 (e). Fig. 6.13 shows that solid dispersion coefficients increase with the height of the BFB, because the bubble diameter increases with the height of the BFB. Similar trend is observed from the experiments with the bubbling bed at atmospheric pressure, whose computed axial solid dispersion coefficients agree with the measured data *(Niklasson et al., 2002)*.The bubble velocity at the bottom of the BFB is lower and hence the solid dispersion coefficient is lower thus the solid mixing is affected. Along the height of the BFB the bubble fraction decreases (Figure 6.13 f) and hence the bubble velocity and solid dispersion coefficient increases. However the along the height of the BFB the solid dispersion coefficient increases, but the solids fraction is less. It can be seen that the solid dispersion coefficient increases as the emulsion velocity decreases (as in Figure 6.13 e) due to the fact that the emulsion velocity decreasing along the height.

6.2.6 High heating value of the producer gas

The calorific value of the producer gas from the biomass gasification was determined by the composition of the individual gas species such as CO, CH_4 and H_2. The HHV of the dry producer gas at the standard state can be estimated by the following equation *(Li et al., 2004)* which was derived based on the heat of combustion of different gases.

$$HHV_{dry\ producer\ gas} = \frac{(12.75*[H_2]+12.63*[CO]+39.82*[CH_4])}{100} \qquad MJ/Nm^3 \qquad (6.2)$$

The gas concentrations in Equation (6.2)are in mol/mol %. The heat contribution by both CO ($12.63\ MJ/Nm^3$)and H_2 ($12.75 MJ/Nm^3$) is almost equal, while that from CH_4 is almost three times that of the CO ($39.82\ MJ/m^3$).

Figure 6.14 shows the HHV values of the biomass gasification producer gas calculated by Equation(6.2)based on gas composition predicted from the 1D model as a function of operation temperature with S/B ratio of 0.53 (Figure 6.14a) and as a function of S/B ratio at operation temperature of 710°C (Figure 6.14b). In the figures, based on experimentally measured gas compositions, the HHV values were calculated and included for comparison. From Figure 6.14, it is found that the HHV values based on the model predicted gas composition were close to those based on the measured gas composition. This was clearly

observed for operation temperatures below 710°C and at 780°C. However, for operation temperatures between 710 and 760°C, the HHV values based on the model predicted gas composition were higher than those based on the measured gas composition.

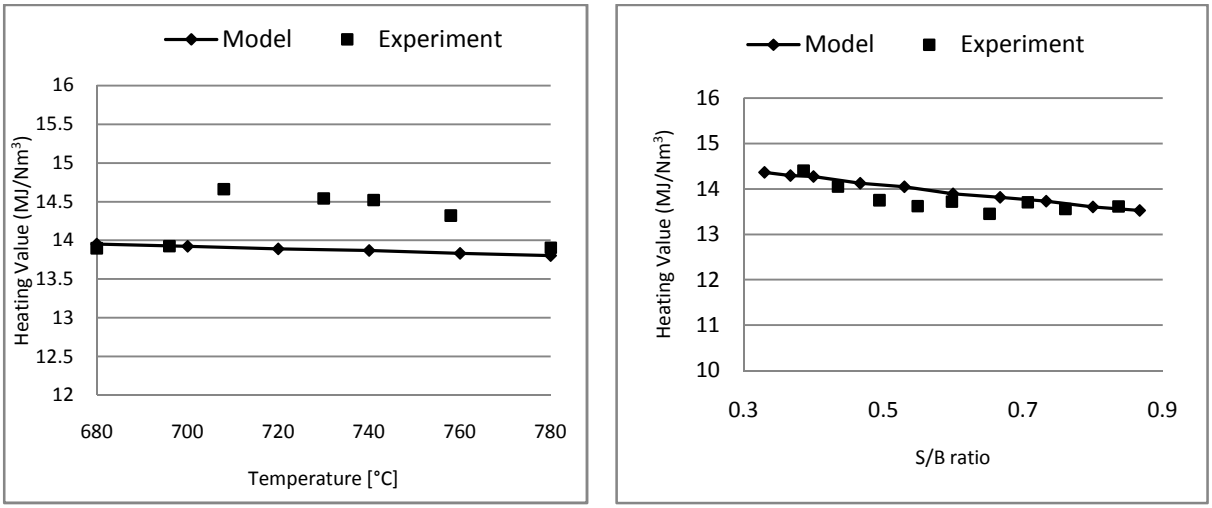

(a) (b)

Figure 6.14: Model predicted HHV of biomass gasification producer gas and comparison with experimental data as a function of operation temperature with S/B ratio of 0.53 (a) and as a function of S/B ratio at operation temperature of 710^{o}C (b).

It was also seen that the HHV values tend to decrease with increase in operation temperature at the given S/B ratio and decrease with S/B ratio at the operation temperature of 710°C. At higher operation temperatures, the gas yield increase but less methane and light hydrocarbons were formed with heavier hydrogen instead. Nevertheless, the HHV values (13-15 MJ/Nm^3) of the producer gas from biomass steam gasification in DFB gasifier are approximately three times those (4-6MJ/m^3) of producer gas from conventional air-blown gasification *(Knoef and Ahrenfeldt, 2005)*.

It had been seen that increase in S/B ratio in the gasification process shifts the equilibrium of the product gases towards H_2 and CO_2 and decreases CO and CH_4 content. The decrease in CO and CH_4 content in the producer gas results in a reduction in the HHV as observed from Figure 6.14(b). The lost energy was consumed to heat up more steam in the gasification with the increase in S/B while all of the other operation parameters retain unchanged.

6.3 Simulation and experimental validation of the developed 2D biomass gasification model

A 1D modelling of biomass gasification had been used to evaluate the effect of the operation conditions on gas composition and temperature profiles in the BFB gasifier during the gasification process as presented in previous sections. These profiles were the average values at a given height of the BFB gasifier. The 2D CFD model was then developed for further studies of BFB gasifier for the synthesis of producer gas, analyzing the profiles of the gaseous species, the flow fields of gas and solids and the distribution of solid fractions in both axial and radial directions but the 2D model is apparently more complicated than the 1D model.

In the 2D model the hydrodynamics were dealt in details with the momentum equations which were explicitly solved by adopting closure laws (as described in Chapter 4 and 5) whereas in the 1D model the hydrodynamic behaviour was described by semi-empirical relations. In 2D model an additional term for the contribution of the turbulence behaviour in the gas phase mixture of the momentum equation had been described by the turbulence model. Thus the limitation in flow behaviour due to the assumption made by the semi-empirical relations in the 1D model are improved in the 2D model with the flow structure that are generally more appropriate. The momentum equations allow determination of the heat and mass transfer as well as the degree of gas and solid mixing. In addition, this 2D model considers two fluid phases of gas and solid, where the solid phase was modelled by finite volume Eulerian granular model (i.e. KTGF model) to simulate gas-solid collision. The gas solid mixing in the 2D model was influenced by the axial dispersion of the fluidization agent and the lateral dispersion of the solid biomass feed and the non-uniform distributions of solids void fraction vary across the BFB gasifier and hence affect the gasification reactions rates. Therefore, the 2D model can be used for better understanding and optimization of the gasification process. In order to achieve convergence of the solution for the 2D model, small time steps (in an order of 10^{-3}s or less) were required and hence solving the 2D model took longer computation time.

Though more sophisticated 2D CFD model improves the modelling efforts for better understanding of the gasification process, simplifications were needed for the CFD solutions to reduce computation time. Further the closure relations were not simple with several

equations that contains more terms and sub-models were solved simultaneously with the uncertainty of semi-empirical parameters.

The following section presents the simulation results from the 2D biomass gasification model presented in Chapters 4 and 5 and the results were compared with the experimental data for validation. In the 2D model simulation, all of the materials (gas species and solid biomass particles) were assigned appropriate properties from standard thermodynamic tables. The properties of the gas species (density, ρ, viscosity, μ, thermal conductivity, λ, specific heat capacity , C_p) were determined as a function of phase composition and temperature which vary with reaction location. These properties were then used to calculate the effective properties of the gas mixture by applying tools in ANSYS FLUENT 12.1 (incompressible ideal gas law for ρ, kinetic theory law for λ and mass-weighted mixing law for μ and C_p). The operating conditions employed for the 2D model are well defined in Chapter 5.

6.3.1 Validation of the developed 2D model

The 2D model developed for the biomass steam gasification in a BFB gasifier in Chapter 5 has been validated with four simulations with varying operating conditions in which two simulations were carried out for two operation temperatures (680^{o}C and 780^{o}C) at a constant S/B ratio of 0.53 and 1 atmospheric pressure. In the other two simulations a constant operating temperature of 710^{o}C was chosen and two S/B ratios were used, one lower value of 0.33 and one high value of 0.84. These operation conditions in the 2D model simulations were the same as those used for 1D model simulation for comparison. The simulation results of 2D model were compared with the 1D model along with the measured data obtained from the experiments described in Section 6.1.1 as shown in Table 6.4. In the Table 6.4 the descriptor 'Wet' refers to the producer gas containing steam while the descriptor 'Dry' refers to the moisture free producer gas. More detailed simulation results of gas composition profiles from the 2D model are presented in Figures 6.15 to 6.18.

Table 6.4: Results of average gas concentrations of the producer gas at the gas exit from the gasifier predicted from the 1D model and the 2D model and those measured from biomass gasification experiments.

Species	CAPE Experiment mole fraction (mol/mol %)		Model prediction, mole fraction (mol/mol %)							
			1D Model		2D Model					
					Average at the exit		Bed centre at the exit		Average valuetaken from radial axis (0.025 to 0.2m)	
	Wet	Dry	Wet	Dry	Wet	Dry	Wet	Dry	Wet	Dry
T: 680°C and S/B ratio: 0.53										
CO	24.42	40.1	28.1	38.5	21.71	39.7	21.37	44.5	23.8	40.1
H_2	12.59	20.67	13.1	17.9	9.40	18.3	9.54	17.9	10.2	17.8
CO_2	14.42	23.67	21.0	28.8	14.44	27.2	14.57	22.6	15.75	27.1
CH_4	9.84	15.56	10.9	14.9	8.08	14.8	8.04	15.0	8.86	14.9
H_2O	39.1	n/a	27.0	n/a	46.37	n/a	46.4	n/a	41.4	n/a
T: 780°C and S/B ratio: 0.53										
CO	28.7	37.3	28.6	35.7	24.2	34.0	23.0	32.3	26.7	36.1
H_2	27.7	36.0	22.6	28.2	22.4	31.2	22.8	32.1	22.0	30.7
CO_2	10.9	14.2	18.4	23	16.1	22.5	16.6	23.4	15.7	21.3
CH_4	8.9	11.6	10.5	13.1	8.8	12.3	8.6	12.1	9.3	12.6
H_2O	23.8	n/a	20.0	n/a	28.4	n/a	25.3	n/a	22.3	n/a
T: 710°C and S/B ratio: 0.33										
CO	31.4	44.2	29.7	40.2	26.32	42.62	28.1	41.89	27.52	41.0
H_2	17.3	24.4	18.0	24.4	20.46	28.44	19.62	29.24	24.29	29.9
CO_2	10.7	15.0	14.7	19.9	8.14	14.18	9.32	13.88	8.1	12.9
CH_4	11.6	16.4	11.4	15.5	9.89	14.76	10.04	14.9	10.7	15.17
H_2O	29.0	n/a	26.2	n/a	35.2	n/a	33.3	n/a	29.92	n/a
T: 710°C and S/B ratio: 0.84										
CO	18.6	32.7	19.4	33.8	17.9	34.3	17.9	33.6	18.9	34.8
H_2	18.2	32.0	17.2	30.0	16.9	32.3	16.9	31.7	17.8	32.9
CO_2	12.4	21.8	12.9	22.5	10.9	20.8	11.6	21.8	12.5	19.3
CH_4	7.74	13.6	7.8	13.6	6.5	12.5	6.7	12.6	7.1	12.4
H_2O	43.1	n/a	42.6	n/a	47.8	n/a	46.8	n/a	41.1	n/a

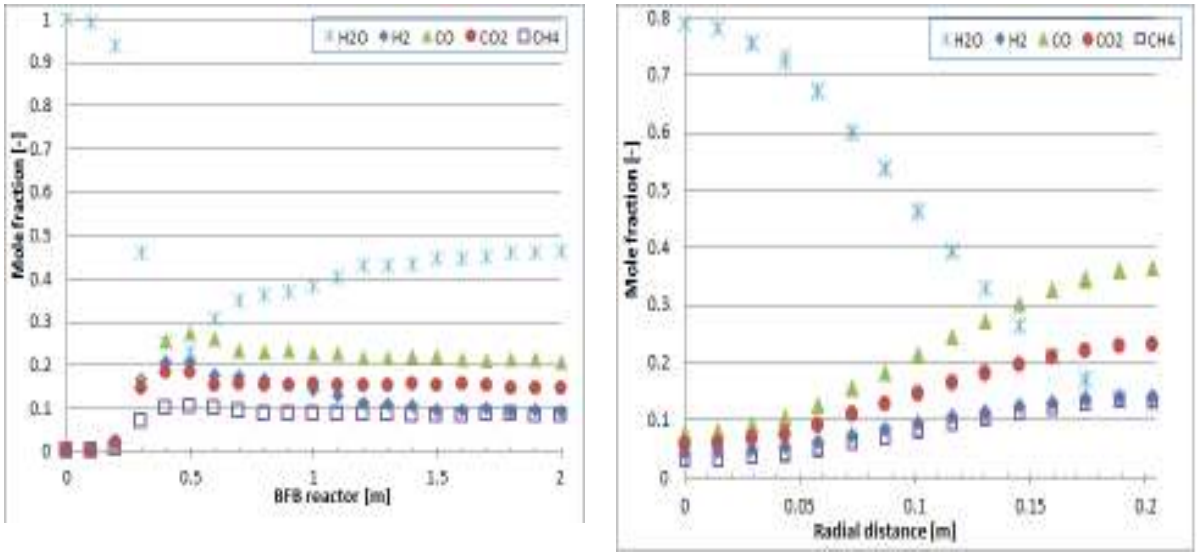

(a) (b)

Figure 6.15: The 2D model simulated profiles of gas composition of the producer gas (wet basis) at the centre-line of the bed along the gasifier height (a) and along the radial distance from one side to another side of the gasifier at the exit corresponding to z = 2m (b), at fixed biomass feeding rate of 15 kg_{dry}/h and a constant S/B ratio of 0.53. Operating temperature and pressure: 680°C and 1 atm.

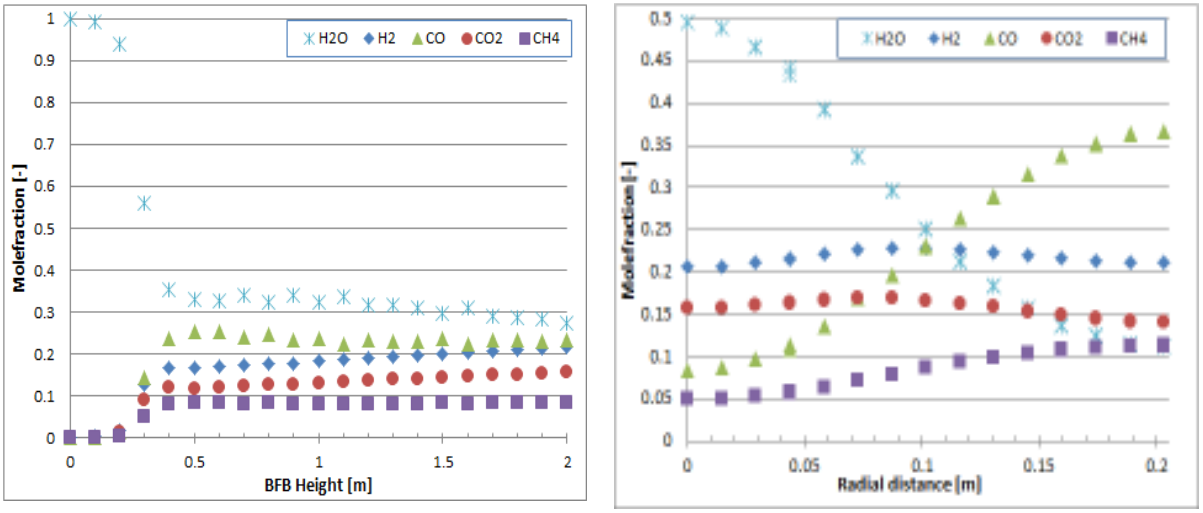

(a) (b)

Figure 6.16: The 2D model simulated profiles of gas composition of the producer gas (wet basis) at the centre-line of the bed along the gasifier height (a) and along the radial distance from one side to another side of the gasifier at the exit corresponding to z = 2m (b), at fixed biomass feeding rate of 15 kg_{dry}/h and a constant S/B ratio of 0.53. Operating temperature and pressure: 780°C and 1 atm.

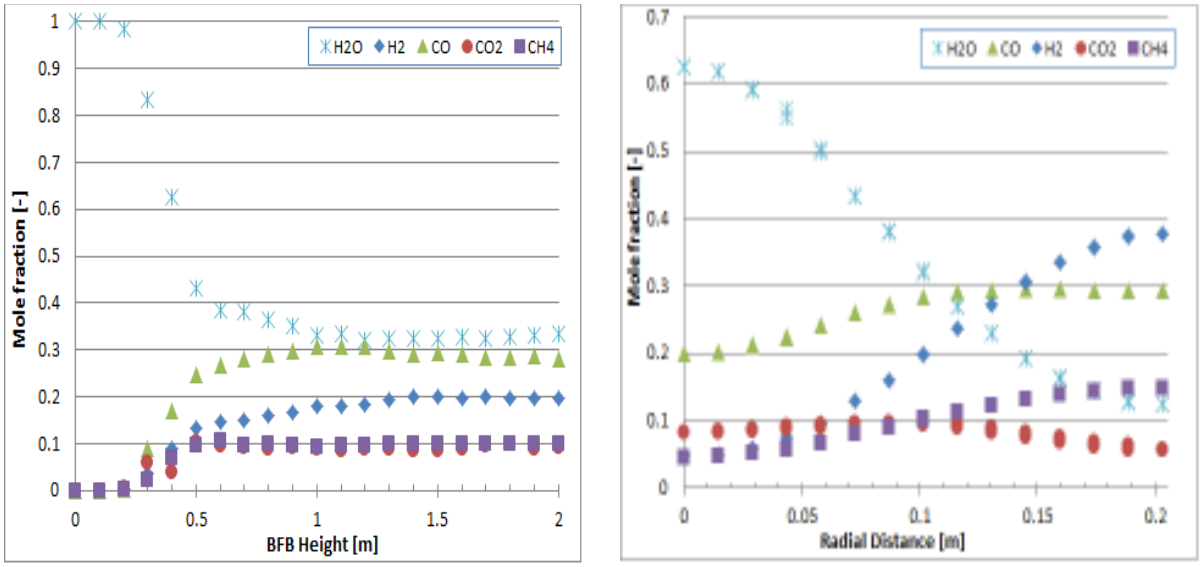

(a) (b)

Figure 6.17: The 2D model simulated profiles of gas composition of the producer gas (wet basis) at the centre-line of the bed along the gasifier height (a) and along the radial distance from one side to another side of the gasifier at the exit corresponding to z = 2m (b), at fixed biomass feeding rate of 15 kg_{dry}/h and operating temperature of 710^{o}C and 1 atm. The S/B ratio: 0.33.

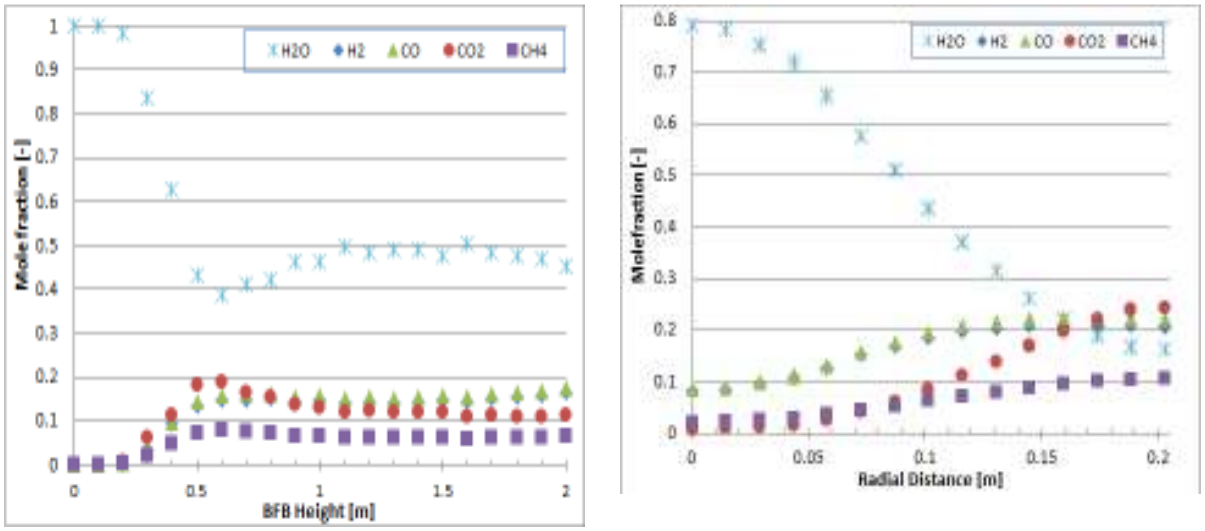

(a) (b)

Figure 6.18: The 2D model simulated profiles of gas composition of the producer gas (wet basis) at the centre-line of the bed along the gasifier height (a) and along the radial distance from one side to another side of the gasifier at the exit corresponding to z = 2m (b), at fixed biomass feeding rate of 15 kg_{dry}/h and operating temperature of 710^{o}C and 1atm. The S/B ratio: 0.84.

Figure 6.15a shows the 2D model simulated profile of gas composition of the producer gas (wet basis) along the gasifier height and Figure 6.15b shows the profile of producer gas composition along the radial distance from one side to another side of the gasifier at the exit. The above results were obtained for fixed biomass feeding rate of 15 kg_{dry}/h and a constant S/B ratio of 0.53 at operating temperature of 680°C and 1 atmospheric pressure. Similar results from the 2D model simulation are shown in Figure 6.16 for operating temperature of 780°C. The 2D model simulation results for two different S/B ratios at operating temperature of 710°C and 1 atmospheric pressure are presented in Figure6.17 for S/B ratio of 0.33 and in Figure 6.18 for S/B ratio of 0.84. For the simulation in Figure 6.18, the $k-\varepsilon$ turbulence viscous model was used. From the simulation results shown in Figures 6.15 to 6.18, significant variations in compositions of the producer gas can be observed within the gasifier.

At the bottom of the BFB bed below the feed point within the gasifier, only steam (H_2O) was present and, due to the superficial velocity being higher than the minimum fluidization velocity, bed bubbling starts with complete mixing of the initial pyrolysis gas components with the steam. At this point the concentration of H_2O decreases and that of the producer gas increases along the height of the gasifier. The average concentration of H_2O from the 2D simulation results shows a decreases from 46.4% at 680°C to 28.4% (mol/mol) at 780°C on the gasifier top (gas exit) which had a discrepancy of about 4-6% (mol/mol) compared to the experimental data at constant S/B ratio of 0.53.

Along the radial distance from one side to another side of the gasifier at the exit (Figures 15b, 16b, 17b and 18b), it was observed that the concentrations of H_2O are non-symmetrical with its values being the highest on one side decreasing along the radial distance towards the other side of the gasifier. This was due to the lateral dispersion of feed biomass in the horizontal direction with the axial dispersion of inlet steam in the vertical direction along the height of the BFB gasifier.

From the results presented in Table 6.4, it can be seen that the average concentrations of H_2 increases from 18.3% to 31.2% (mol/mol) on dry basis when the gasification temperature was increased from 680 to 780°C at constant S/B ratio of 0.53 which is similar to the 1D model and experimental data. During the same range of operating temperature, the concentrations of CO decreases from 39.7% to 34% (mol/mol on dry basis) and that of CO_2 decreases from 27.2% to 22.5% (mol /mol on dry basis), respectively. Though these trends look similar to the 1D model, there is a discrepancy of about 3.7 mol/mol% for CO and 2.7 mol/mol% CO_2 in

the same range of operating temperature. The average concentration of the CH_4 at the exit agrees closely to that of the 1D model and the experimental results between these two temperatures. However the producer gas composition from the centre of the exit closely matches the 1D model value and the experimental data.

Similar to the 1D simulation, the 2D results for a fixed operating temperature of 710°C and varying the S/B ratio from 0.33 to 0.84 agreed closely to that of the 1D model and the experimental results. The average producer gas composition at the top of the gasifier contains for the operating temperature of 710°C and S/B ratio of 0.33 had 28.4% H_2, 42.6% CO, 14.2% CO_2 and 14.8% CH_4 (mol/mol) on dry basis whereas the H_2O at 35.2%(mol/mol).The 2D model simulated concentrations of CO and CH_4 were, respectively, about 3.2% and 0.5% (mol/mol on dry basis) lower than the measured values for S/B ratios examined (0.33 to 0.84) whereas the 1D model simulated values were 2.1% (mol/mol) lower for CO and 0.4% (mol/mol) lower for CH_4than the 2D model (on dry basis). In the meantime, the CO_2 concentration from the 2D model was about 0.8% (mol/mol) lower than the experimental data (0.33 to 0.84) and that from the 1D model at S/B ratio of 0.33 and 0.84 are 4.9% value and 0.7% (mol/mol) higher than the experimental value respectively on dry basis. The concentration of H_2 from the 2D model at 0.33 and 0.84 S/B ratios were higher than the experimental data by 4% and 0.3% (mol/mol) respectively and that from the 1D model in comparison with the experimental showed equal concentration at S/B ratio of 0.33 and 2% (mol/mol) decrease at S/B ratio of 0.84 (dry basis).

6.3.2 Influence of temperature on the producer gas composition

The Figures (6.19- 6.23) show the profiles of mole fractions of producer gas species (in the sequential order of H_2O, H_2, CO_2, CO and CH_4) along the BFB gasifier for different elapsed time from 5s to 40 minutes, when the simulation were conducted at operating temperature of 780^oC, S/B ratio of 0.53 and under atmospheric pressure.

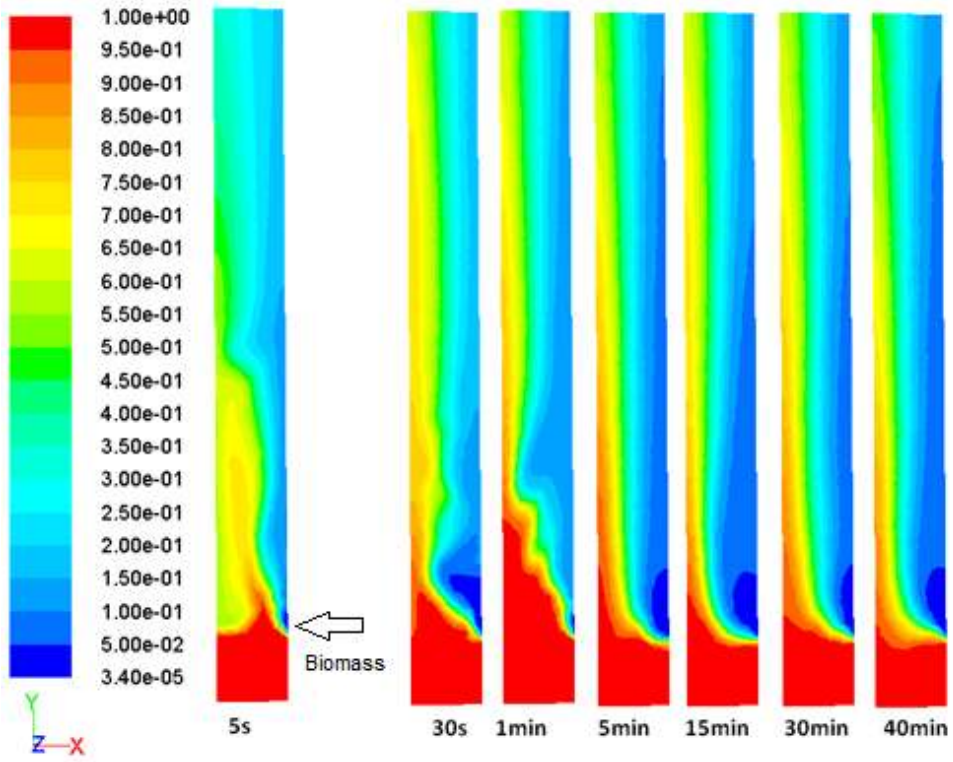

Figure 6.19: The 2D model predicted H_2O distributions along the BFB operated at 780^{o}C, 0.53 S/B ratio and 1 atmospheric pressure at different elapsed time.

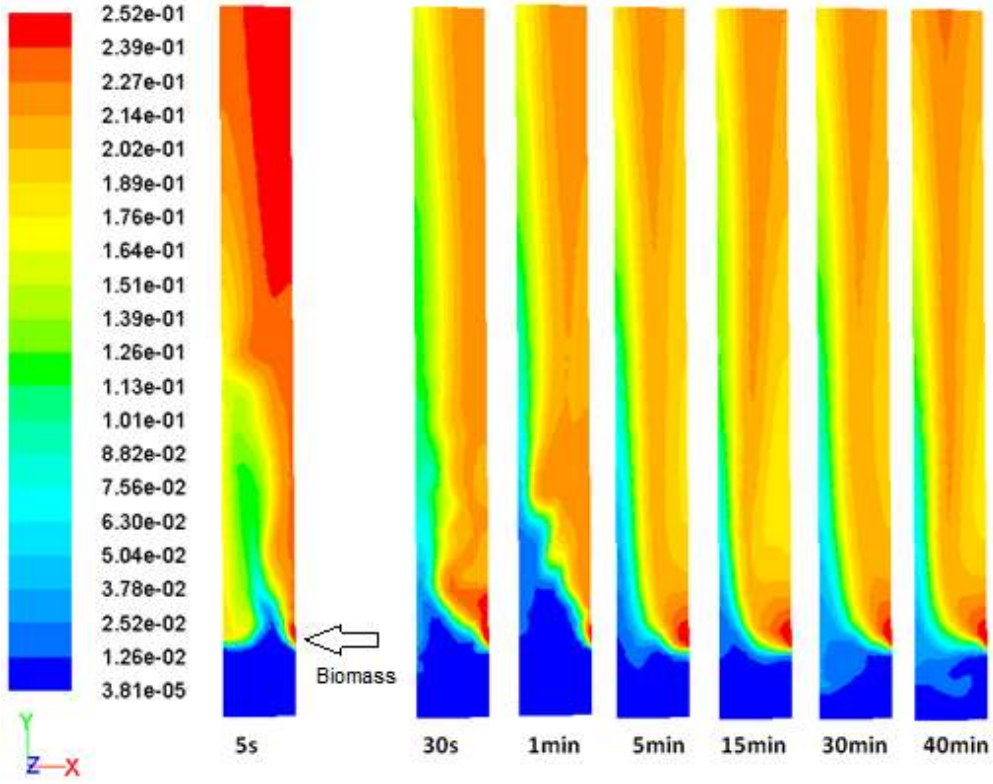

Figure 6.20: The 2D model predicted H_2 distributions along the BFB operated at 780^{o}C, 0.53 S/B ratio and 1 atmospheric pressure at different elapsed time.

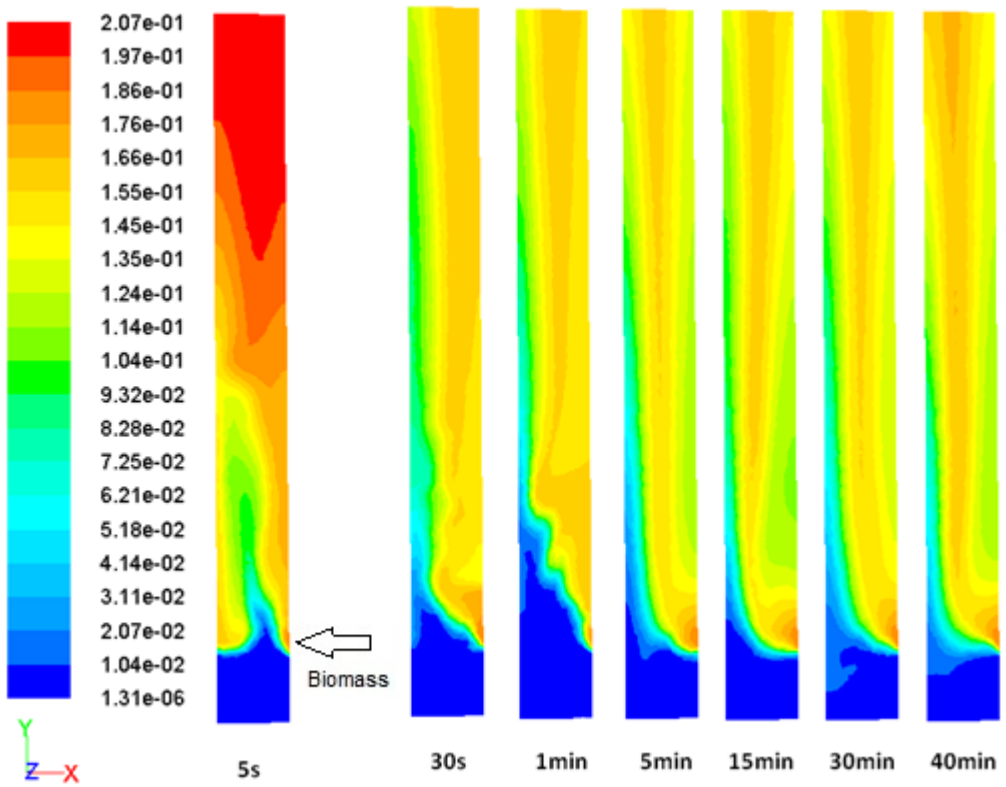

Figure 6.21: The 2D model predicted CO_2 distributions along the BFB operated at 780^{o}C, 0.53 S/B ratio and 1 atmospheric pressure at different elapsed time.

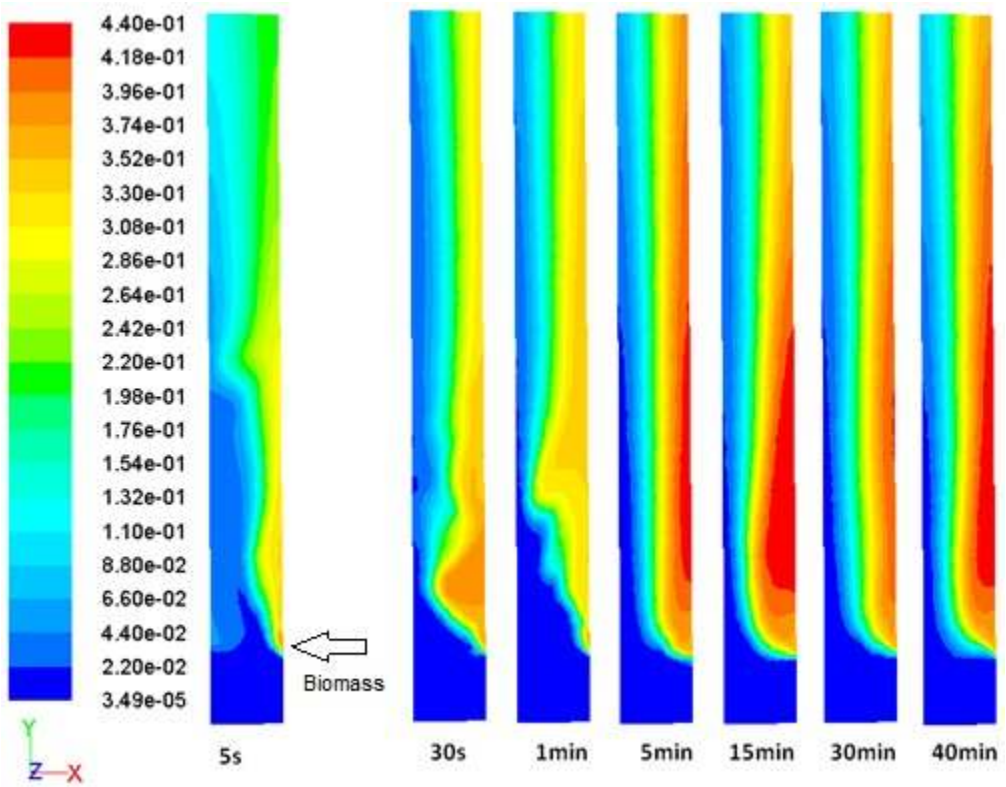

Figure 6.22: The 2D model predicted CO distributions along the BFB operated at 780^{o}C, 0.53 S/B ratio and atmospheric pressure at different elapsed time.

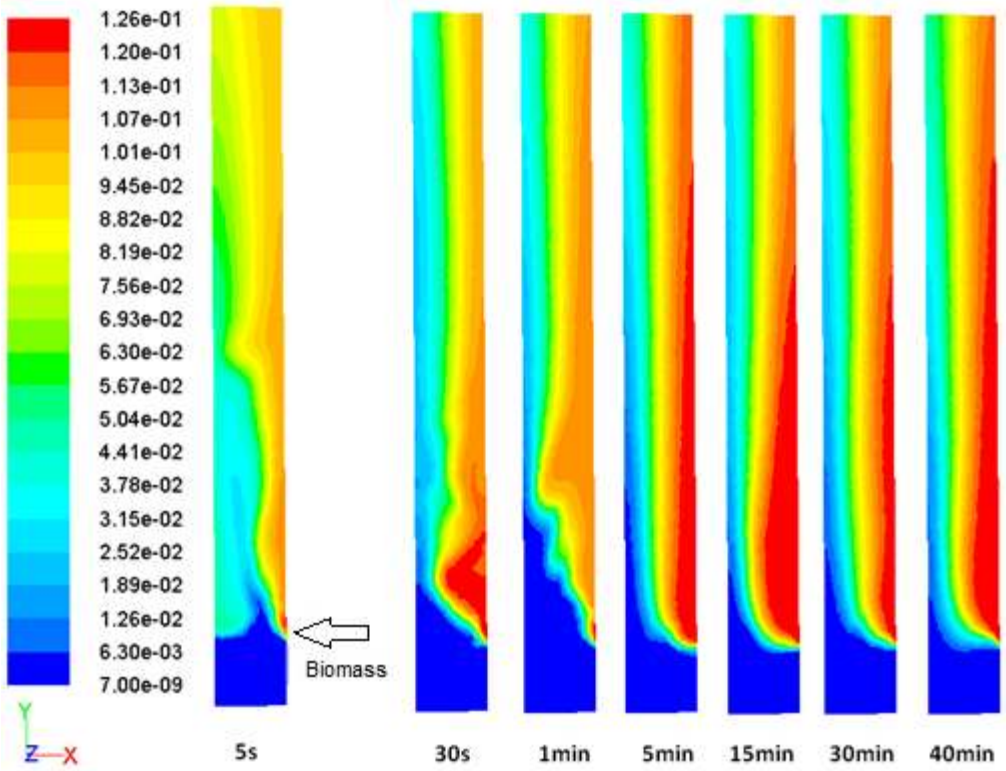

Figure 6.23: The 2D model predicted CH_4 distributions along the BFB operated at 780^{o}C, 0.53 S/B ratio and 1 atmospheric pressure at different elapsed time.

In the simulation, the bed was initially filled with sand at the operating temperature (780^{o}C in this case). Then the steam was fed from the bottom of the BFB gasifier while the biomass was fed from the side of the BFB at a height of 0.2m where instant pyrolysis happens when the biomass was in contact with the hot bed material. The compositions of gases and chars at the biomass feeding point were determined by the pyrolysis reaction model and the product distribution coefficients as described in Chapter 3. The heat was provided by the hot bed material and the instant pyrolysis products of biomass was well-mixed at the bottom along with the injected steam. Though the system was well-mixed, the lateral dispersion of the pyrolysis product from one side of the BFB gasifier directed the axial dispersion of steam flow from the bottom to move towards the other side of the wall allowing large volume of H_2O on one side of the BFB gasifier. This effect can be seen from the simulation results as shown in Figure 6.19.

The concentration of CO_2 and H_2 increased initally during the start of the simulation, due to fast exothermic Water Gas-Shift reaction favouring forward reactions and hence the CO concentrations decreased as can be seen in Figure 6.20- 6.22. The H_2 concentration was

always high near the feed port due to the Water Gas-Shift reaction. The other enothermic reactions such as Steam Gasifcation and Steam Methane Reforming reactions, though at slow reactions rates,also contribute to the increase in concentration of H_2 over time and along the height of the bed to the top of thegasifier. The formed CO_2 from initial pyrolysis and the Water Gas-Shift reaction decreases with elapsed time due to the forward Bouduard reaction which consumes $CO_2$and reaches a steady concentration as shown in Figure 6.21.

It was observed that the concentration of CO was high (Figure 6.22) near the feeding port and in the centre of the bed after 5minutes when the Steam Gasification reaction proceedsfavouring forward products. From this point on the concentration of CO continues increasing in these regions over the time. Both Bouduard reaction and Steam Methane Reforming reaction take about 15-20 minutes for completion when operated of 780^{o}C and hence more CO were formed in the centre of the bed and gets diluted along the top of the gasifier. As described in previous sections for the 1D model simulations, both the exothermic Methanation reaction which proceeds in backward direction and the endothermic Steam Methane Reforming reaction in the forward direction consume CH_4 thus the CH_4 concentration decrease. However, the concentration of CH_4 was increased (Figure 6.23) at the feeding point where a significant amont of CH_4 was produced from the initial pyrolysis.

The Figure 6.24 show the profiles of mass fractions of char particles along the BFB gasifier for different elapsed time from 5s to 40 minutes, when the simulation were conducted at operating temperature of 780^{o}C, S/B ratio of 0.53 and under atmospheric pressure. It can be seen that the char particles are mostly on the bottom of the BFB bed where mixing degree of solids (bed material) and char particles are well distributed over entire solid bed during the time interval. Initially the fraction of char forming in the bed increases over first five minutes and later the consumption of char increases as time progresses. The amount of char dispersed on the freeboard is relatively lower. Similar effects were observed with the 1D model where the concentration char is mostly localised near the bed. When simulating with a single perforated inlet stream at very low superficial velocity close to the mimimum fluidiation, the solids flow turns around gradually so that the binary solid particles (sand +char) eventually reach a flow pattern ascending at the centre and descending near the walls. Such portions of bubbles enhance the particles under going up and down motion, thus favoring a strong particle recirculation all over the bed.

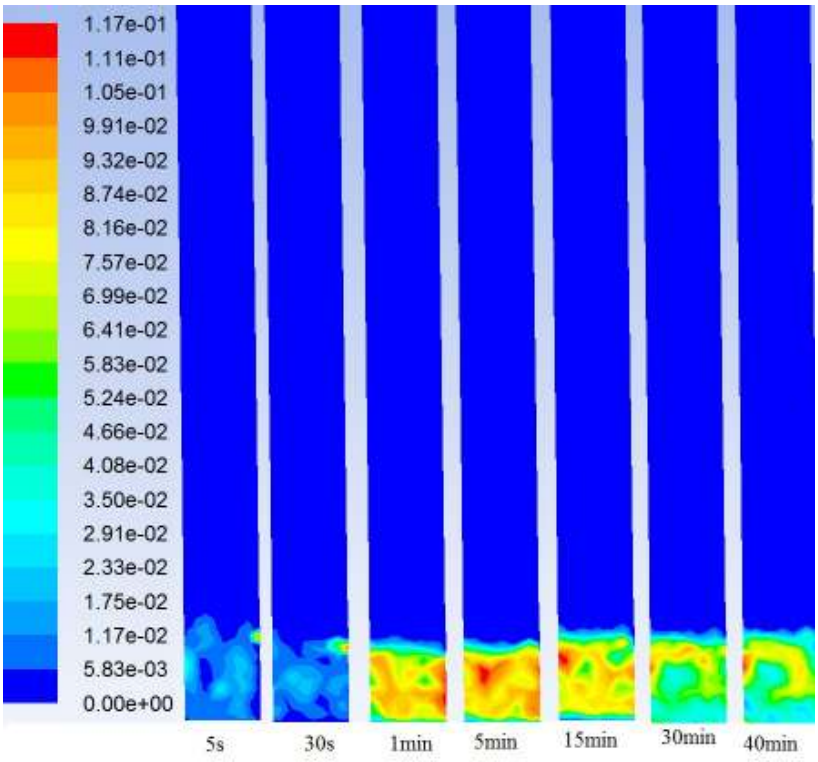

Figure 6.24: The 2D model predicted Char particles distributions along the BFB operated at 780^{o}C, 0.53 S/B ratio and 1 atmospheric pressure at different elapsed time.

6.3.3 Effects of S/B ratio

The 2D model had been employed to investigate the effects of operating conditions on the distributions of the producer gas from biomass steam gasification in the BFB gasifier. The Simulation results for a higher S/B ratio of 0.84 are shown in Figures 6.25 to 6.29 for the gas concentration distribution within the gasifier in the sequential order of H_2O, H_2, CO, CO_2 and CH_4 for different elapsed time from 5s to 40 minutes. The simulation were conducted at operating temperature 710^{o}C and atmospheric pressure.

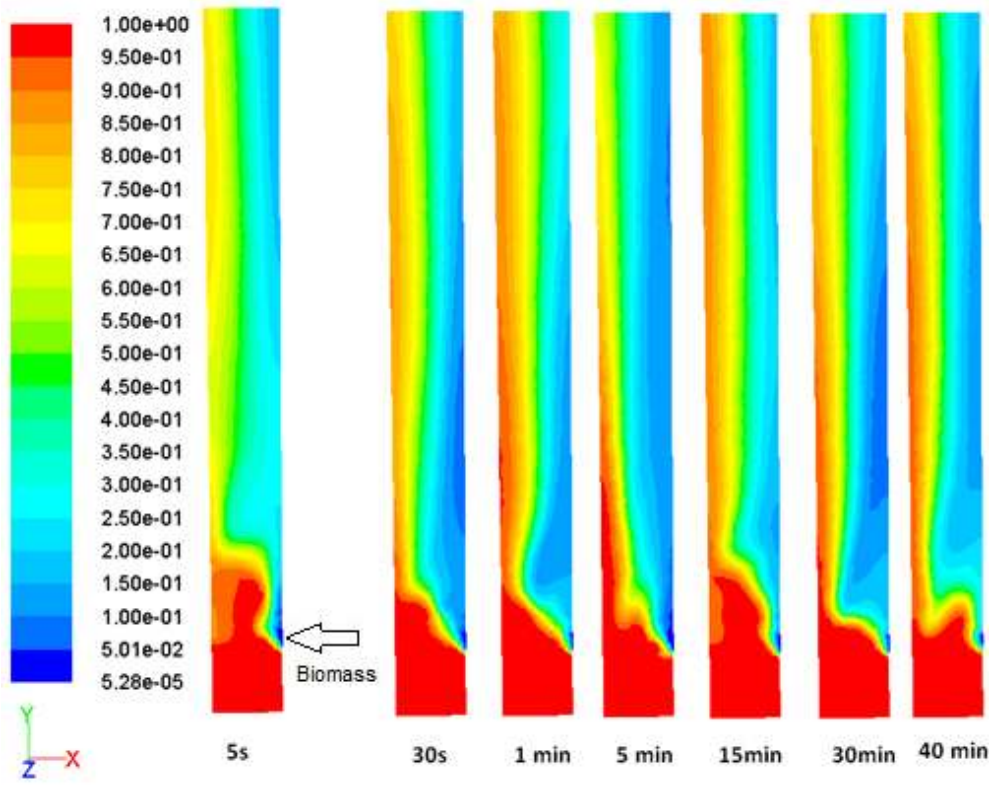

Figure 6.25: The 2D model predicted H_2O distributions along the BFB operated at 710^{o}C, 0.84 S/B ratio and 1 atmospheric pressure at different elapsed time.

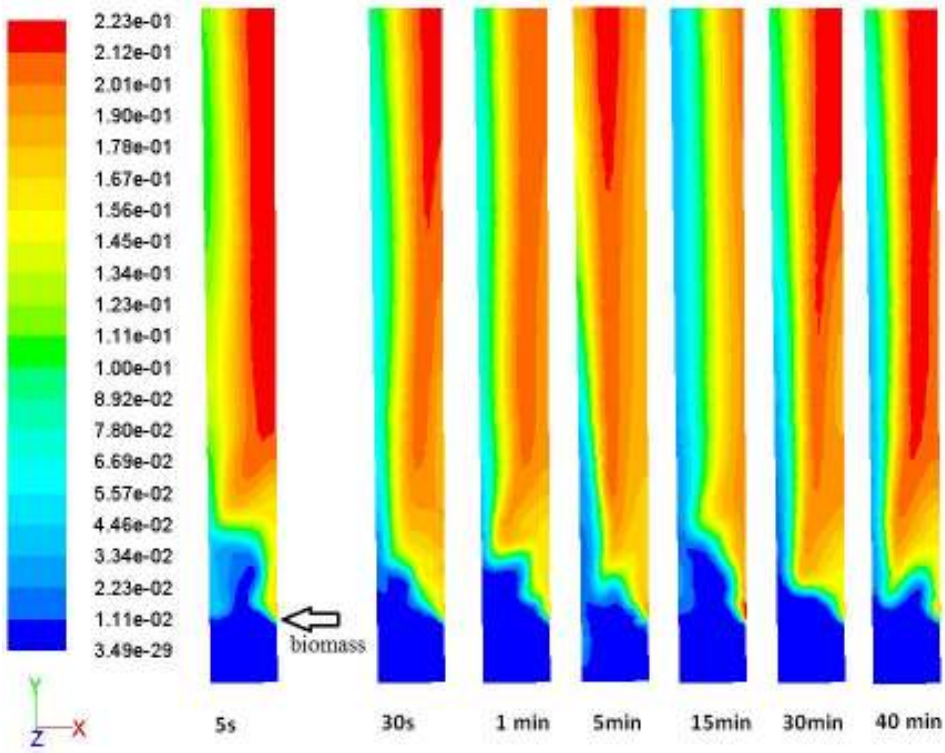

Figure 6.26: The 2D model predicted H_2 distributions along the BFB operated at 710^{o}C, 0.84 S/B ratio and 1 atmospheric pressure at different elapsed time.

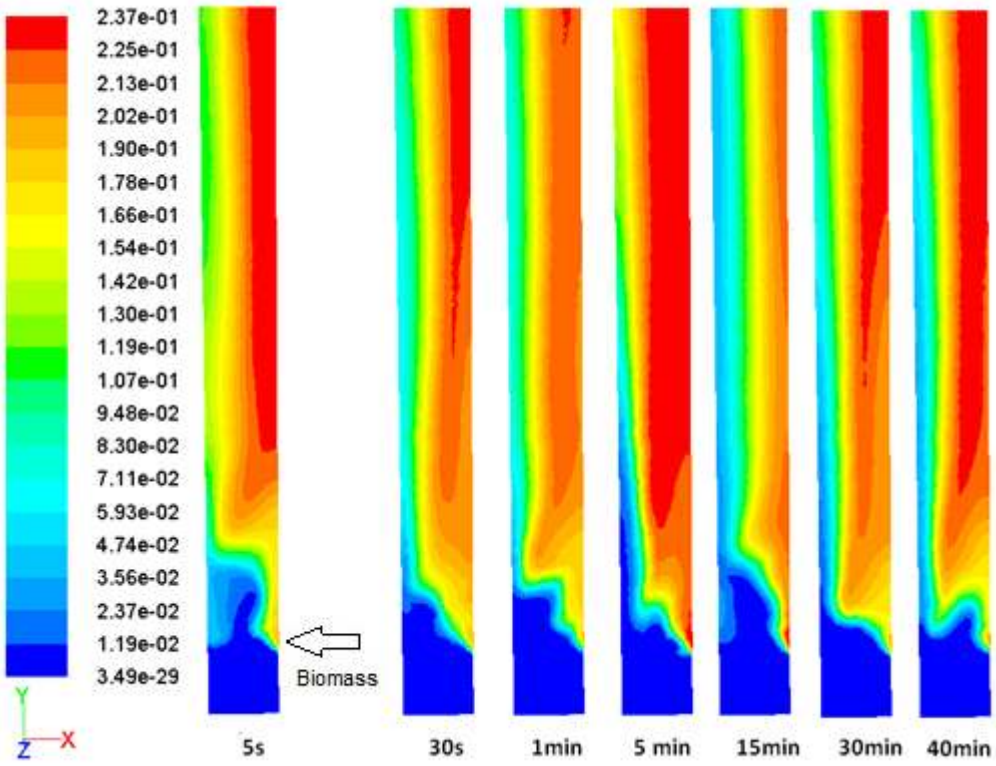

Figure 6.27: The 2D model predicted CO distributions along the BFB operated at 710^{o}C, 0.84 S/B ratio and 1 atmospheric pressure at different elapsed time.

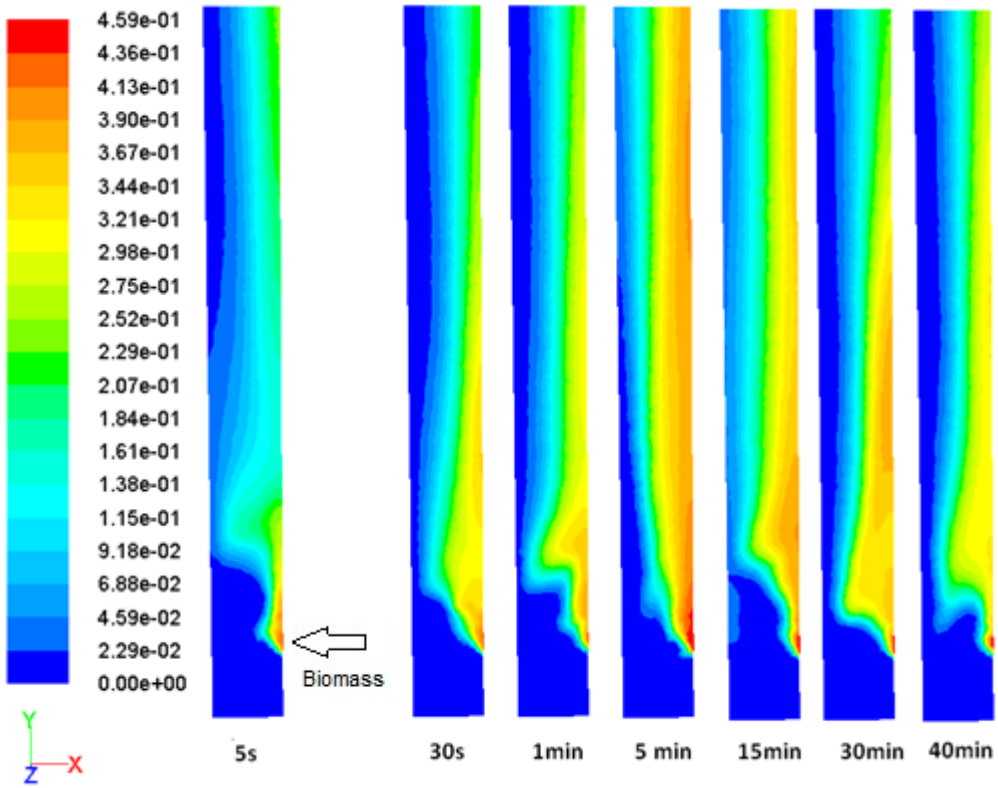

Figure 6.28: The 2D model predicted CO_2 distributions along the BFB operated at 710^{o}C, 0.84 S/B ratio and 1 atmospheric pressure at different elapsed time.

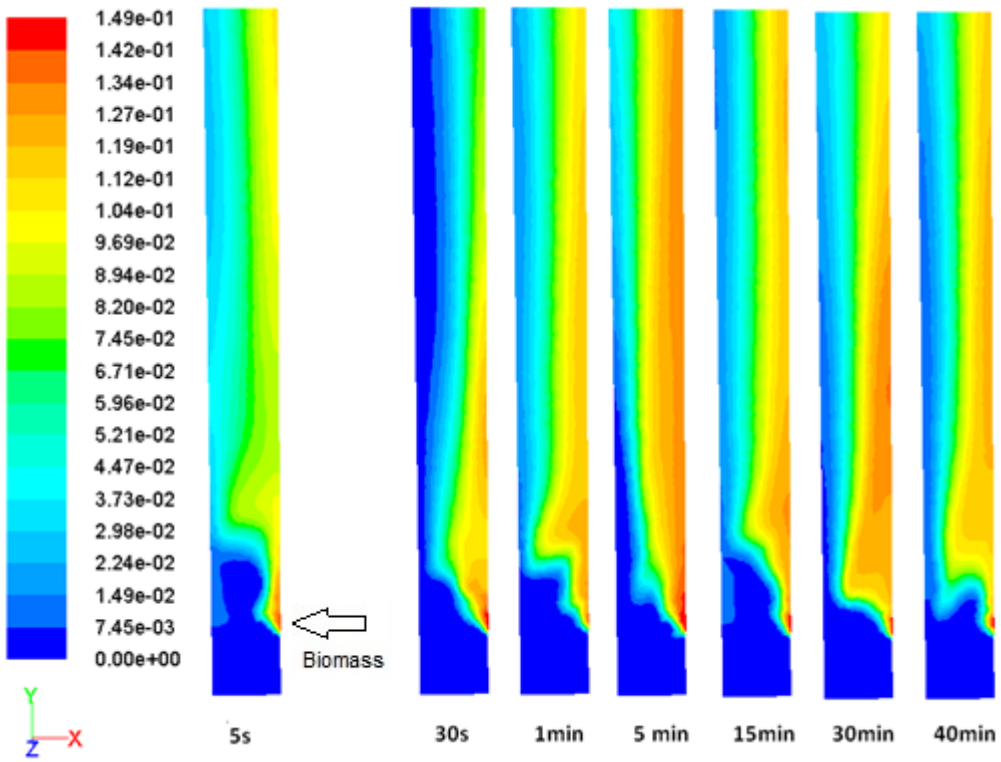

Figure 6.29: The 2D model predicted CH_4 distributions along the BFB operated at 710^{o}C, 0.84 S/B ratio and 1 atmospheric pressure at different elapsed time.

With higher S/B ratio, the high H_2O content in the gasification process influences Water Gas-Shift reaction (Equation 3.16) at low temperature compared with its equilibrium constants, favouring forward reaction and thus forming more of $H_2$and CO_2 in the bottom zone of the gasifier. The Steam Gasification reaction (Equation 3.15) and Steam Methanation Reforming reaction (Equation 3.19) favour forward rections forming more H_2 and CO along the height of the gasifier. Hence the overall H_2 concentration increased over time and along the gasifier height as seen in Figure 6.26. The concentration of CO increased significantly for the same reason as that of H_2 along the height of the gasifier (Figure 6.27). For the CO_2, its concentration is high near the biomass feeding point and increased with elasped time due to Water Gas-Shift reaction, However, the CO_2concentration decreased along the height of the gasifierdue to the Boudard reaction (Figure 6.28). From Figure 6.29, it is found that the CH_4 concentration was high at the biomass feeding point due to devolatisation of biomass in the initial pyrolysis, but the CH_4 concentration decreases along the height of the gasifier as a result of Methanation reaction and Steam Methane Reforming reaction which consume CH_4.

6.4 Conclusion

Experiments of biomass steam gasification were performed in this study in a 100 kW DFB gasifier at operating temperature from 680 to 780°C and S/B ratio between 0.33 and 0.84. The biomass feeding rate was 15 kg/h. For validation of the initial pyrolysis model, separate experiments were conducted also in the above DFB gasifier with nitrogen replacing steam thus only pyrolysis occurred in the gasifier. In all of the experiments, gas samples were collected from the top of the BFB gasifier and analyzed using a micro GC.

The developed 1D model for biomass steam gasification in a BFB gasifier had been numerically solved to predict compositions of producer gas, under various operating conditions of temperature and S/B ratio. The developed 1D model was validated by comparison of the simulation results with the experimental data for the same operating conditions as in the experiments. It had been found that the predicted gas compositions from the 1D model simulations were in close agreement with the experimental data for the biomass steam gasification in the BFB gasifier which reaches steady state conditions.

After the validation, the 1D model was used to examine the effects of operating conditions, including steam/biomass ratio and gasification temperatures, on the producer gas compositions and yield of char along the gasifier height and the gas compositions at the gasifier exit. In addition, the flow regimes (bubble and the emulsion phases) were examined along the BFB gasifier under the above the operating condition.

Finally the developed 2D CFD model embedded with the gasification model that describes two phase (gas-solid) hydrodynamics based on the KTGF was also validated with the same data obtained from the above experiments. The 2D model can predict the profiles of gas composition both along the gasifier height and along radial directions of the gasifier for given operating conditions. The average gas compositions at the gasifier exit simulated from the 2D model were also in close agreement with the experimental data and the results from the 1D model. However, in general, more accurate average values were predicted from the 1D model than the 2D model. The possible reason could be the underestimate of the effect of biomass feeding in the horizontal direction which is counter-action with the vertical steam flow. Under this action, the steam moves heavily towards one side of the spatial co-ordinate. Hence the gasification reaction along the radial co-ordinates varies widely resulting in uneven producer gas composition at the exit of BFB gasifier.

Therefore, it was concluded that the 1D model was suitable for simulation of gasification rate and gas compositions at the gasifier exit. This model is most useful for investigation on the effects of operating conditions on the gasification performance. However, the 2D model is useful for better understanding of the gasification process and the gas distribution with the gasifier.

6.5 References

Altafini, C.R., Wander, P.R., Barreto, R.M., 2003. Prediction of the working parameters of a wood waste gasifier through an equilibrium model. Energy Conversion and Management 44, 2763–2777.

Bird, R.B., Stewart, W.E., Lightfoot, E.N., 2002. Transport Phenomena, second ed. Wiley, New York.

Bridgwater, A.V., 2003. Renewable fuels and chemicals by thermal processing of biomass. Chemical Engineering Journal 91, 87-102.

Bull, D.R., 2008. Performance Improvements to a Fast Internally Circulating Fluidised Bed (FICFB) Biomass Gasifier for Combined Heat and Power Plants University of Canterbury, New Zealand

Chan, W.R., Kelbon, M., Krieger, B.B., 1985. Modelling and experimental verification of physical and chemical process during pyrolysis of a large biomass particle. Fuel 64, 1505-1515.

Corella, J., Sanz, A., 2005. Modeling circulating fluidized bed biomass gasifiers. A pseudo-rigorous model for stationary state. Fuel Processing Technology 86, 1021–1053.

Curtiss, C.F., Bird, R.B., 1999. Multicomponent Diffusion. Industrial & Engineering Chemistry Research 38, 2515-2522.

Di Blasi, C., 2002. Modeling intra- and extra-particle processes of wood fast pyrolysis. AIChE Journal 48, 2386-2397.

Franco, C., Pinto, F., Gulyurtlu, I., Cabrita, I., 2003. The study of reactions influencing the biomass steam gasification process. Fuel 82, 835-842.

Garcia, L., Salvador, M.L., Arauzo, J., Bilbao, R., 1998. Influence of catalyst weight/biomass flow rate ratio on gas production in the catalytic pyrolysis of pine sawdust at low temperatures. Industrial & Engineering Chemistry Research 37, 3812-3819.

Gil, J., Corella, J., Aznar, M.P., Caballero, M.A., 1999. Biomass gasification in atmospheric and bubbling fluidized bed: Effect of the type of gasifying agent on the product distribution. Biomass and Bioenergy 17, 389-403.

Knoef, H., Ahrenfeldt, J., 2005. Handbook biomass gasification. BTG Biomass Technology Group.

Li, X.T., Grace, J.R., Lim, C.J., Watkinson, A.P., Chen, H.P., Kim, J.R., 2004. Biomass gasification in a circulating fluidized bed. Biomass and Bioenergy 26, 171-193.

Lv, P.M., Chang, J., Wang, T.J., Wu, C.Z., Tsubaki, N., 2004. A kinetic study on biomass fast catalytic pyrolysis. Energy & Fuels 18, 1865-1869.

Niklasson, F., Thunman, H., Johnsson, F., Leckner, B., 2002. Estimation of Solids Mixing in a Fluidized-Bed Combustor. Ind. Eng. Chem. Res. 41, 4663-4673.

Patnaik, P., 2004. Dean's Analytical Chemistry Handbook 2nd ed. McGraw-Hill

Paviet, F., Bals, O., Antonini, G., 2007. Kinetic Study of Various Chars Steam Gasification. Journal of Chemical Reactor Engineering Vol. 5: A80.

Poling, B.E., Prausnitz, J.M., O'Connell, J.P., 2001. Properties of Gases and Liquids (5th Edition). McGraw-Hill.

Ragland, K.W., Aerts, D.J., Baker, A.J., 1991. Properties of Wood for Combustion Analysis. Bioresource Technology 37, 161-168.

Rapagnà, S., Jand, N., Kiennemann, A., Foscolo, P.U., 2000. Steam gasification of biomass in a fluidised bed of olivine particles. Biomass and Bioenergy 19, 187-197.

Senneca, O., 2007. Kinetics of pyrolysis, combustion and gasification of three biomass fuels. Fuel Processing Technology 88, 87-97.

Wang, X.Q., Kersten, S.R.A., Prins, W., van Swaaij, W.P.M., 2005a. Biomass pyrolysis in a fluidized bed reactor. Part 1: Literature review and model simulations. Industrial & Engineering Chemistry Research 44, 8773-8785.

Wang, X.Q., Kersten, S.R.A., Prins, W., van Swaaij, W.P.M., 2005b. Biomass pyrolysis in a fluidized bed reactor. Part 2: Experimental validation of model results. Industrial & Engineering Chemistry Research 44, 8786-8795.

Zainal, Z.A., Ali, R., Lean, C.H., Seetharamu, K.N., 2001. Prediction of performance of a downdraft gasifier using equilibrium modeling for different biomass materrials. Energy Conversion and Management 42, 1499-1515.

Chapter 7

Conclusion and recommendations

In this thesis, a comprehensive literature review was firstly conducted to evaluate the existing models for solid fuel gasification in fluidized bed gasifiers with the objective to develop a mathematical model for biomass steam gasification in a BFB gasifier. From the literature review, it is found that each type of the models reported has advantages and disadvantages with different approaches to handle the complicated processes involving hydrodynamics, heat and mass transfer including the chemical reactions. Based on the literature review, two mathematical models are developed for the simulation of biomass steam gasification in the BFB gasifier: 1D non-isothermal reaction kinetics model and 2D CFD model embedded with reaction kinetics and hydrodynamics characteristics. The 1D model is relatively simpler compared to the 2D model thus is more suitable for sensitivity analysis for operation conditions and gasifier optimization while the 2D model can be used for better understanding of the gasification process and prediction of product distribution within the gasifier.

In order to model the biomass gasification process, literature review was conducted to understand and quantify the biomass gasification process with steam as gasification agent at elevated temperatures. The gasification process consists of two stages: initial pyrolysis and subsequent gasification reaction process. The initial pyrolysis process occurred at high temperatures for a very short duration at the bottom of the gasifier where the biomass was fed into the gasifier and mixed with the hot bed material. In the initial pyrolysis process, the biomass was degraded into volatile gaseous components, char and a low quantity of tar. In literature, the pyrolysis kinetics have been found to vary with biomass feedstock under the same operating conditions, and this pyrolysis stage of the biomass gasification had been modelled using a semi-empirical method, mostly using experimental data from coal gasification. The products of the pyrolysis process have significant influence on the subsequent gasification process and final producer gas yield and composition. In the present work, the kinetics of biomass initial pyrolysis was modelled based on measured data from experiments in a 100kW DFB gasifier. It has been found that the product yield and distribution is a function of pyrolysis temperature. The function describing the char conversion in the initial pyrolysis makes it possible to accurately model the pyrolysis and subsequent gasification process.

In the second stage of the gasification process, reactions occur among the gasification agent (steam), the volatile gases and the char. Although tar was also generated in the initial pyrolysis, the quantity of the tar was much less and the tar related reactions were much slower than those of the volatile gas and char, therefore, the tar related reactions were not included in the gasification model The producer gas from biomass steam gasification mainly was assumed to consist of CO, H_2, CO_2, CH_4 and H_2O in the model, and the reactions involving these gas components were Steam Gasification reaction, Water Gas-Shift reaction, Methanation reaction, Bouduard reaction, and Steam Methane Reforming reaction.

In the developed 1D model, the kinetics of biomass gasification reactions were mathematically quantified and integrated with gas-solid hydrodynamics, mass and energy balances within the gasifier. For the simulation of fluid hydrodynamics, two-phase theory of gases and solids (bubble phase and emulsion phase) were employed and the governing hydrodynamic correlations reported from literature were used. In literature, the reported models used the kinetics rates of fossil fuels or those obtained from a particular biomass species. In addition, the gasifier configuration and operation conditions also have significant effect on the gasification kinetics. In the biomass steam gasification in the BFB gasifier, the reaction kinetics was dependent on temperature, S/B ratio and fluid hydrodynamics in the bed. In the developed model, the effect of temperature on the reaction kinetics was described by the Arrhenius equations. The mixing effect of solid and gas was modelled separately for the bubble phase and emulsion phase with different mass transfer mechanisms. The bubble-emulsion mass transfer coefficients along with semi-empirical hydrodynamic closure correlations from the literatures were used in the present model giving proper closures for the modelling. In the developed model, the influence of generated gas from the gasification reactions was also considered through the mixing effect in the fluidized bed. From analysis of reactant contact level in different flow phases, it was assumed that the Water Gas-Shift reaction and Steam Methane Reforming reaction are the only gas phase reactions in the bubble phase and all reactions are possible in the emulsion phase.

For solving the developed 1D biomass steam gasification model in the BFB reactor, numerical methods were employed using a solver function from the PDE modules of Matlab software with properly defined initial and boundary conditions. The converge of the solution within the range of set values and a relative error corresponding to 0.01% were achieved by setting relative and absolute tolerance to about 10^{-4} and 10^{-6} respectively.

To better understand the biomass gasification and to predict the gas distribution in the gasifier, a 2D model was also developed in this study which was built in the CFD software which considered multiphase fluid flow, balances of energy, mass and momentum as well as gasification reactions. In the 2D model, the constitutive equations were explicitly described for the gas phase, the solid phase and the mixed gas-solid phase in incorporation with finite volume Eulerian granular modelling approach (i.e. KTGF model). The gasification reactions were facilitated with Arrhenius kinetics using the ANSYS FLUENT 12.1's laminar finite-rate reaction model and the turbulence-chemistry model was used to describe the coupling of reaction finite-rate reaction model. At S/B ratio above 0.6, the fluid flow is in the transient between laminar and turbulent and the $k-\varepsilon$ turbulence viscous model was used whereas at low S/B ratio below 0.6, the fluid flow was more likely to be laminar thus the laminar viscous model was used in the modelling of fluid hydrodynamics. The interaction between the solid particles and the gas with associated energy, called the granular temperature, was modelled using the KTGF model. The varying granular temperature were used to compute the solids properties such as solid shear viscosity, solid bulk viscosity and the solids pressure involved in the momentum transfer. The developed 2D model was solved using transient-state pressure based ANSYS solver. Improvement in the convergence was achieved by initially simulating using the cold flow where the momentum, energy, and mass balance were solved without chemical reactions, but including the gas species. Furthermore, to stabilize the solution, the under-relaxation factors for pressure, momentum, granular temperature and volume fractions were reduced resulting in the decrease of the residual. The time step for solving the model was chosen at 0.001s with maximum number of iterations set as 20 which would give a convergence criterion of 10^{-3} while the residuals of the species, velocity components and the volume fraction were in the range of 10^{-6}-10^{-4}.

To validate the developed 1D and 2D models for the biomass steam gasification in a BFB gasifier, experiments were undertaken in a 100 kW DFB gasifier at operating temperature of 680 – 780^{o}C, pressure at 1 atm and S/B ratio of 0.33 -0.84. In these experiments, the biomass feeding rate was fixed at 15 kg/h. Separate experiments were also conducted for validation of the initial pyrolysis model in which nitrogen was used to replace steam as gasification agent thus only pyrolysis occurred in the reactor. From the model validation results, it has been found that the predicted gas compositions from the initial pyrolysis model and the 1D gasification models are in close agreement with the experimentally measured data. The initial pyrolysis model showed that the concentration of CO, CO_2 and CH_4 decreases within the

operating temperature range from 680-780^{o}C while the H_2 increases. However in the predicted model the discrepancies varies between ±1.0% (mol/mol) for H_2, ±0.8% (mol/mol) for CO, ±0.6% (mol/mol) for CO_2 and ±0.3% (mol/mol) for CH_4 from the experimental values on dry basis.

The discrepancies of the gas concentrations in the 1D model in relation to the experimental values are less than 2% (mol/mol on dry basis) for CO, CH_4 and for H_2 and CO_2 were less than 4.5% (mol/mol) and 8 % (mol/mol) respectively. For both experimental and simulation results the H_2 increases and CO_2,CO and CH_4 decreases markedly as the operating temperature increases from 680 to 780°C. The 1D model was then employed to investigate the effects of operating conditions (temperatures and S/B ratio) on the gas compositions. The effect of increase in S/B ratio shows discrepancies of less than 2.7% (mol/mol on dry basis) for all of the gas species between the 1D model and the experimental values. From the results, it was concluded that the model can provide detailed information on the gas composition at different gasification temperatures and allows for different operating scenarios to be examined. The effects of increasing the operating temperature above 680°C favours forward reactions (except Methanation reaction) producing more concentration of H_2 ,CO and lesser quantity of CO_2. However above 825^{o}C, the Water Gas-Shift reaction shifts towards reactants by consuming H_2 and the rate of Methanation reaction increases producing more char. These findings show that the optimal range for steam gasification reaction is between 680-825^{o}C. The effects with increasing the S/B ratio favours forward reaction shift for the Steam Methane Reforming reaction, Water Gas-Shift reaction and Steam Gasification reactions which favours the production of H_2 while CO decreases due to the Water Gas-Shift reaction and CO_2 is consumed in the Bouduard reaction. However the increase in S/B ratio dilutes the producer gas.

The developed 2D CFD model embedded with the gasification reactions was also validated with the same data obtained from the above experiments. The discrepancies in relation to the experimental values for the temperature variations were less than 5% (mol/mol) for all of the gas species except for CO_2 which varies by 8.6% (mol/mol) at 780^{o}C and S/B ratio of 0.53 (dry basis). However, the variation in the S/B ratios in the gasifier between the 2D model and the experimental data shows smaller discrepancies that are less than 4% (mol/mol on dry basis) for all the gas species. In this 2D model, the species concentration profiles of biomass gasification products were predicted in both the axial and radial directions of the gasifier. The average gas compositions at the gasifier exit simulated from the 2D model for the operating

temperature ranges 680 to 780°C were also in agreement with the experimental data and the results from the 1D model. However, in general, more accurate average values were predicted from the 1D model than the 2D model.

In commercial BFB gasifiers lateral dispersion of the volatile gases during the initial pyrolysis can be important in the subsequent gasification process and final gas composition. The simulation results from the developed 2D model show that due to the very fast release of volatile gases and the high volatile content in the biomass fuel, the gas components and the fed steam may not be uniformly mixed around the feed port. Under this action, the steam moves heavily towards one side of the spatial co-ordinate. Hence the gasification reaction along the radial co-ordinates varies widely resulting in uneven producer gas composition at the exit of BFB reactor. In conclusion, the gasification behaviour of biomass gasification in a BFB gasifier is strongly affected by the gas-solid mixing (fluid-dynamics) and the chemical reactions involved. Further to improve the reliability of the model, the species concentration profile and the fluid dynamics characteristics along the gasifier have to be validated which requires advanced experimental setup.

From literature, it has been reported that the producer gas composition and tar content from biomass steam gasification are significantly affected by operating temperature and S/B ratio, and thus including tar and its reactions in modelling is desirable in future. The knowledge of the chemistry of tar generation and conversion has to be significantly studied and improved, as well as the effects of temperature, solids concentration and gas composition in the bed on the tar reactions. The reaction kinetics of different types of biomass has to be experimentally studied and validated rigorously to improve the BFB gasification reaction. To support a reliable model, measurements are required for the gas composition, gas yield and tar content both from the whole gasification process and from the initial pyrolysis. Char conversion in gasification is another area for further investigation and this should be modelled in a more rigorous way to quantify the effect of operating conditions on the char conversion rate during the gasification process.

A two-phase model was used to describe the gas phase in the bed, whereas solid mixing model was applied for the char mixing in the bed. It was shown that pyrolysis is an important step in the overall gasification model. Better results were obtained by developing a pyrolytic products distribution function of operating temperature in a semi-empirical way from experiments. However the product distribution function needs to be improved with rigorous experiments with wide range of data and along the spatial co-ordinates thereby increasing the

extend of testing and validating the model. Thus much has to be done to develop reliable computational models and thus the heating value of product fuel gas. The gasification models, developed based on the pyrolysis gasification kinetic models, were able to predict the variation of total gas yield with S/B ratio and temperature. The H_2 increases and CO_2, CO and CH_4 decreases markedly as the operating temperature increases from 680 to 780°C at constant S/B ratio, however the concentration of CO is higher in the operating temperature range. On the other hand, with increase in S/B ratio from 0.33 to 0.84, the CO and CH_4 concentration decreased and that of H_2 increases and CO_2 increases in the producer gas.

The developed biomass gasification models can be improved by validating the concentration, temperature, velocity, pressure of both the gas and solids along the axial and time coordinates with the experimental data. Also the model can be improved by including the circulation of bed materials in the model which influences the mixing behaviour of the solid and gas and hence the gas composition of the producer gas. However the inclusion of solid circulation of bed materials in the 2D CFD model can make the model very complicated. The mixing of incoming bed materials and out-flowing producer gas in the upper part of the BFB gasifier is the key area for consideration. The pressure drop and pressure profile within the gasifier also needs careful consideration as the pressure will affect the gas properties and gas flow. In addition, the char combustion in the CFB reactor and the heat integration within the complete gasifier systems is very important for the model development of the integrated system.

Appendix A

Matlab code for non-stoichiometric equilibrium for initial pyrolysis

```
function fn = Chemeq_NonStoi_temp(x)
global n Mwood T mass_gas Win NC
% Temperature of the reaction in [K].Range b/n 300 - 1300[k]
R = 8.314;     % Gas Constant
if nargin  == 0;
    x = ones(1,8);
end

% To calculate the heat capacity...
% Taken from .taken from Perry Handbook of Chemical
% Engineers. The Order of Parameters for the compounds are H2, CO, CO2, H2O
% CH4, C,O2
%
A = [3.249 3.376 5.457 3.470 1.702 1.771 3.64];
B = [0.422e-3 0.557e-3 1.047e-3 1.450e-3 9.081e-3 0.771e-3 5.06E-04];
C = [0 0 0 0 -2.164e-6 0 0];
D = [0.083e5 -0.031e5 -1.157e5 0.121e5 0 -0.867e5 -2.27E+04];
Go_f298 = [0 -137169 -394359 -228572 -50460 0 0];
Ho_f298 = [0 -110525 -393509 -241818 -74520 0 0];

% Stoichiometric Co-efficient           Reactions
%     H2 CO CO2 H2O CH4 C O2
nu = [1, 1, 0, -1,  0, -1, 0;...      % C  + H2O --> CO + H2
      1,-1, 1, -1,  0,  0, 0;...      % CO + H2O --> CO2+ H2
     -2, 0, 0,  0,  1, -1, 0;...      % C  + 2H2 --> CH4
      0, 2,-1,  0,  0, -1, 0;...      % C  + CO2 --> 2CO
      3, 1, 0, -1, -1,  0, 0;...      % CH4+ H2O --> CO + 3H2
      0, 2, 0,  0,  0, -2,-1;...      % 2C + O2  --> 2CO
      2, 0, 1, -2,  0, -1, 0];        % C + 2H2O--> CO2+ 2H2

Tatm = 298.15;
del_A = A*nu';
del_B = B*nu';
del_C = C*nu';
del_D = D*nu';
del_Go_f298 = Go_f298*nu';
del_Ho_f298 = Ho_f298*nu';
J(n,:) = del_Ho_f298 - (del_A * Tatm + del_B/2*Tatm^2 + del_C/3*Tatm^3-
del_D/Tatm)* R;
I(n,:) = -((del_Go_f298-J(n,:))/(R*Tatm)+del_A*log(Tatm)+ del_B/2*Tatm +
del_C/6*Tatm^2+del_D/(2*Tatm^2));
Keq(n,:) = exp((-J(n,:)/(R*T(n)))+ del_A*log(T(n))+ del_B/2*T(n) +
del_C/6*T(n)^2+del_D/(2*T(n)^2) + I(n,:));

delG (n,:) = -log(Keq(n,:))*R*T(n);%

% Columns 1.H2  2.CO 3.CO2 4.H2O 5.CH4 6.C 7.O2
% Gibbs enthalpy of formation of species i
GFt(n,1:7)=0;

GFt(n,2)=(delG(n,6)-nu(6,6)*GFt(n,6)-nu(6,7)*GFt(n,7))/nu(6,2);
%Gibbs enthalpy of formation of CO [J/mol]
GFt(n,3)=(delG(n,4)-nu(4,2)*GFt(n,2)-nu(4,6)*GFt(n,6))/nu(4,3);
%Gibbs enthalpy of formation of CO2 [J/mol]
```

```
GFt(n,5)=(delG(n,3)-nu(3,6)*GFt(n,6)-nu(3,1)*GFt(n,1))/nu(3,5);
%Gibbs enthalpy of formation of CH4 [J/mol]
GFt(n,4)=(delG(n,5)-nu(5,1)*GFt(n,1)-nu(5,2)*GFt(n,2)-
nu(5,5)*GFt(n,5))/nu(5,4);  %Gibbs enthalpy of formation of H2O [J/mol]

% GFt(2)=-199539.4;   %Unit Conversion to J/mol - H2O
% GFt(3)=-188930.4;   %Unit Conversion to J/mol - CO
% GFt(4)=-395709;     %Unit Conversion to J/mol - CO2
% GFt(5)=0;

%mass of components H2, CO, CO2, H2O, CH4, CO2
NH2  =x(1);          %Mole of H2O
NCO  =x(2);          %Mole of carbon monoxide
NCO2 =x(3);          %Mole of carbon dioxide
NH2O =x(4);          %Mole of hydrogen5%
NCH4 =x(5);          %Mole of methane
Lg_C =x(6);          %La grangian for Carbon
Lg_O =x(7);          %La grangian for Oxygen
Lg_H =x(8);          %La grangian for Hydrogen

% The Composition of Wood in weight percent.
% C - 51.6% H - 6.2% O - 43.2% CH(1.44)O(0.66)
Mw_C = 14.2;       % Molecular weight of char
Mw_wood = 24;       % Molecular weight of biomass
Nwood= Mwood/Mw_wood;%Mole of biomass
NC =Win/Mw_C;          %Mole of Carbon
Mw_vol= mass_gas/(Nwood-NC);   % Molecular weight of volatiles
f(1)=mass_gas/Mw_vol*(4*NCH4+2*NH2+2*NH2O)+0.2*NC-1.44*Nwood;
%Hydrogen Mass Balance
f(2)=mass_gas/Mw_vol*(NH2O+NCO+2*NCO2)+0.13*NC-0.66*Nwood;
%Oxygen Mass Balance
f(3)=mass_gas/Mw_vol*(NCH4+NCO+NCO2)+NC-1*Nwood;                %Carbon
Mass Balance
f(4)=GFt(n,1)/R/T(n)+log(NH2/sum(x(1:5)+1.0*NC))+2*Lg_H/R/T(n);
%H2 Gibbs
f(5)=GFt(n,2)/R/T(n)+log(NCO/sum(x(1:5)+1.0*NC))+Lg_C/R/T(n)+Lg_O/R/T(n);
%CO Gibbs
f(6)=GFt(n,3)/R/T(n)+log(NCO2/sum(x(1:5)+1.0*NC))+2*Lg_O/R/T(n)+Lg_C/R/T(n)
; %CO2 Gibbs
f(7)=GFt(n,4)/R/T(n)+log(NH2O/sum(x(1:5)+1.0*NC))+2*Lg_H/R/T(n)+Lg_O/R/T(n)
; %H2O Gibbs
f(8)=GFt(n,5)/R/T(n)+log(NCH4/sum(x(1:5)+1.0*NC))+Lg_C/R/T(n)+4*Lg_H/R/T(n)
; %CH4 Gibbs
fn = [f(1),f(2),f(3),f(4),f(5),f(6),f(7),f(8)];



% Calling function

function non_linear_eq_solver_NonStoi_Temprang
close all
clear all
global n Mwood T Win mass_gas NC

T = 953:5:1053;%input('Enter the Reactor temperature in the Range between
700-1165 [K] :');
Mwood = 15;%input('Enter the Biomass feed rate in [Kg/hr] :')*1000;%kg
Matrix =[0.41621 0.4973 0.1801 0.0656 0.0051 11508 202070 2820];
```

```
for n=1:length(T)
% Pyrolysis from "Modeling circulating fluidized bed biomass gasifiers.
[t1,z] =ode113(@initialpyrolysis,[0 1],[1 0 0 0]);

% Material balance
m_tar = Mwood*z(end,3)                  % Rate of tar into the reactor by
devolatilization, [kg/s]
Win = Mwood*z(end,4)                    % Rate of char into the reactor by
devolatilization, [kg/s]
mass_gas=Mwood*z(end,2);    % [Kg/s]

InitialGuess = Matrix;
options=optimset('Display','iter','TolFun',1e-
32,'MaxFunEvals',10000,'MaxIter',10000);
[x,fval,exitflag] = fsolve(@Chemeq_NonStoi_temp,InitialGuess,options);
Eflag(n)=[exitflag];
yh2=x(1)/sum(x(1:5));   %mol frac hydrogen
yco=x(2)/sum(x(1:5));   %mol frac carbon monoxide,exitflag
yco2=x(3)/sum(x(1:5));  %mol frac carbon dioxide
yh2o=x(4)/sum(x(1:5));  %mol frac h2o
ych4=x(5)/sum(x(1:5));  %mol frac of methane
Lg_C=x(6) ;%La grangian for Carbon
Lg_O=x(7); %La grangian for Oxygen
Lg_H=x(8); %La grangian for Hydrogen

fn(n,:)=fval;
mol(n,:) =[x(1:5) NC];
molfr(n,:) =[yh2 yco yco2 yh2o ych4];
Matrix=x;
end

Eflag
fn
mol

figure(1)
hold on
grid on
box on
H=plot(T-273,molfr(:,1),'.r');
K=plot(T-273,molfr(:,2),'.g');
L=plot(T-273,molfr(:,3),'.b');
M=plot(T-273,molfr(:,4),'.c');
N=plot(T-273,molfr(:,5),'.k');

legend([H,K,L,M,N],'H2','CO','CO2','H2O','CH4');
title('Molfraction of Pyrolysis products in Biomass Gasification');
xlabel('Temperature in [C]');
ylabel('massfraction');
%%  Pyrolysis of wood (pine Radiata)
function [dxp] = initialpyrolysis(z,x)
        Te=T(n);
% Taken from "Modeling chemical and Physical processes of wood and biomass
% pyrolysis ", Progress in Energy and Combustion Science, Colomba Di Blasi_
% and From " A model of Wood flash pyrolysis in fluidised bed reactor,
% Renewable Energy 30 (2005) 377-392, Zhongyang Luo _, Shurong Wang, Kefa
% Cen...in.... \\ENGCAD1\pgo26$\My Documents\Pyrolysis\Printed

% Reaction Schema for thermal decomposition of wood
%            k1
```

```
%       Wood --->     gas
%                   k4 ^
%              k2       |
%       wood --->     tar
%                      |
%             k3     k5 v
%       wood --->    char
%  Rxn 1,2,3,5 based on Chan et al
%  Rxn   Pre-exp factor ko(1/s)     Act.Energy Ea(KJ/mole)  del Hr (KJ/KG)
%   1      1.30*10^8                        140
%   2      2.00*10^8                        133
%   3      1.08*10^7                        121
%   4      3.09*10^6                        108
%   5      1.48*10^6                        144
%
dwood = -(1.08e7*exp(-121000/8.314/Te)+2e8*exp(-
133000/8.314/Te)+1.3e8*exp(-140000/8.314/Te))*x(1);
dgas = 1.3e8*exp(-140000/8.314/Te)*x(1)+3.09e6*exp(-108000/8.314/Te)*x(3);
dtar = 2e8*exp(-133000/8.314/Te)*x(1)-3.09e6*exp(-108000/8.314/Te)*x(3)-
1.48e6*exp(-144000/8.314/Te)*x(3);
dchar = 1.08e7*exp(-121000/8.314/Te)*x(1)+1.48e6*exp(-
144000/8.314/Te)*x(3);
dxp = [dwood; dgas;dtar; dchar];
end
end
```

Matlab code for one dimensional biomass gasification function

```
function pdebfb_newTestcorrect
close all; clear all
%%
%   Reaction 1: Heterogeneous Water-Gas Shift Reaction                    %
%                K1                                                       %
%   C(s) + H2O <---> CO + H2   %
%   Reaction 2: Hydrogenation Gasification
%                K2
%   C(s) + 2H2 <---> CH4        Del G= -15.4 KJ/mol & 21.9 KJ/mol @ 400 &
750 Deg C
%   Reaction 3: Boudouard Equation
%                K3
%   C(s) + CO2 <---> 2CO        Del G= 53.8 KJ/mol & -8.2 KJ/mol @ 400 &
750 Deg C
%   Reaction 4: Steam Reforming of Methane
%                K4
%   CH4  + H2O <---> CO + 3H2   Del G= 54.9 KJ/mol & -32.7 KJ/mol @ 400 &
750 Deg C
%   Reaction 5: Homogeneous Water-Gas Shift Reaction
%                K5
%   CO  + H2O  <---> CO2 + H2    Del G= -14.3 KJ/mol & -2.6 KJ/mol @ 400 &
750 Deg C
%%
tic
datestr(now)
in = 1;
% Independent Variables
T=780+273;                              % Operating Temperature [K]
Tatm = 298;                             % Reference temperature [K]
P = 101325*1.0;                         % Operating Pressure [Pa or N/m^2 or
kg/m/s^2]
R = 8.314;                              % Rate Constant [J/(mol.K)]
g = 9.81;                               % Acceleration due to gravity [m/s^2]
D1=0.15e-4*(T/273)^1.75;                % effective diffusion coefficient
[m^2/s]
A_cs = pi*0.1^2;                        % C.S Area of the bed [m^2]
Dt= 0.2;                                % bed diameter[m]
H= 2;                                   % Height of the bed [m]
V_r=A_cs*H;                             % Volume of the reactor [m^3]
feed=15./3600;                          % Feed rate of biomass [kg/s]
Mwsand=60.085;                          % Molecular weight of sand kg/Kmol
Mwchar= 14.2;                           % Molecular weight of char kg/Kmol
Msand= 12;                              % weight of sand used in the
reactor[kg]
Bsand=700/3600;                         % Sand flow rate [kg/s]
SFR = 8/3600;                           % Steam Feed Rate Kg/s
SB=SFR/feed;                            % Steam to biomass ratio
dp=275e-6;                              % Diameter of particles (sand)[m]
rho_g=(P/1000)/R/T/(1/18);             % Density of gas species [kg/m^3]
rho_s=1600;                             % density of sand (particles)[kg/m^3]
V_s=Msand/rho_s;                        % Volume of the bed [m^3]
rho_b=360;                              % density of biomass[kg/m^3]
rho_c=rho_b*30/100;                     % density of char (particles)[kg/m^3]
Us= Bsand/rho_s/A_cs;                  % m/s
meu=1.98*10^(-5)*(T/300)^(2/3);         % Viscosity of gas species [Pa.s]
residence_time = Msand/Bsand;           % s
time_res =1/((1/(1.08e7*exp(-121000/8.314/T)))+...
    (1/(2e8*exp(-133000/8.314/T)))+(1/(1.3e8*exp(-140000/8.314/T))));
```

```
dpc= 2e-3;                              % Diameter of char[m]
np=5;
phi= (1+np*dp/dpc)^2;
eta_p=0.95;
eta_fb=0.8;
eta_rad=1/(1/eta_p+(1/phi*(1/eta_fb-1)));

% Fast Pyrolysis from "Modeling circulating fluidized bed biomass
gasifiers.
[t1,z] =ode113(@fastpyrolysis1,[0 time_res],[feed 0 0 0]);
% Material balance
m_tar = z(end,3);  % Rate of tar into the reactor by
devolatilization,[kg/s]
Win = z(end,4);    % Rate of char into the reactor by devolatilization,
[kg/s]
mass_gas=z(end,2); % Mass of volatile gases[Kg/s]

% Fast Pyrolysis distribution function (y=m*x^b) derived from experimental
work
%       H2      CO          CO2         CH4
m=[1.33531E-16 18006450.34 2480.823701 443126.516];
b=[5.726819409 -1.870949006 -0.69559076 -1.494493718];
Mw_fp=[2 28 44 16];        % Molecular weight of H2,CO,CO2,CH4  [kg/kmol]
yi=m.*T.^b/100;            % Molefraction of Volatiles from Fast pyrolysis
Avg_Mol_wt=sum(yi.*Mw_fp); % Average molecular weight of volatiles
[kg/kmol]
n_gas=mass_gas/Avg_Mol_wt; % molar volatile gases[kmol/s]
n_steam=SFR/18;            % molar steam flow rate kmol/s
n_char= Win/Mwchar;        % molar char flow kmol/s
ug= (n_gas+n_steam)/(P/T/R/1000)/A_cs; % velocity of gas stream [m/s]
C_tot=P/T/R/1000;          % Total gas concentration in the BFB kmol/m^3
C_st=n_steam/V_r;          % concentration of steam in the BFB (kmol/m^3.s)
V_steam = SFR/rho_g
V_g= n_gas/(C_tot-C_st);   % volume flowrate of gas (m^3/s)
C_h2=n_gas*yi(1)/V_g;      % concentration of H2 from fp(kmol/m^3)
C_co=n_gas*yi(2)/V_g;      % concentration of CO from fp(kmol/m^3)
C_co2=n_gas*yi(3)/V_g;     % concentration of CO2 from fp(kmol/m^3)
C_ch4=n_gas*yi(4)/V_g;     % concentration of CH4 from fp(kmol/m^3)
C_h2o=C_st;                % concentration of H2O in the BFB (kmol/m^3)
Mw=[2 28 44 18 16 ];        % Molecular weight of H2,CO,CO2,CH4  [kg/kmol]
Ci0=[C_h2 C_co C_co2 C_h2o C_ch4];  %(kmol/m^3)
Avg_Mw=sum(Ci0/sum(Ci0).*Mw); % Molecular weight [kg/kmol]
rho_g=(P/1000)/R/T/(1/Avg_Mw);% Density of gas species [kg/m^3]
Ar= dp^3*rho_g*(rho_s-rho_g)*g/meu^2;  % Archimedies number (-)
nd= 48;                    % no.of nozzles  % Number of holes in the
distributor
umf = meu*((27.2^2+0.0408*Ar)^0.5-27.2)/rho_g/dp; % Minimum fluidisation
velocity [m/s]
dbm=1.64*(A_cs*(ug-umf))^0.4;    % Maximum Bubble Diameter, DbM [m]
db0=0.347*(A_cs*(ug-umf)/nd)^0.4;% Initial Bubble Diameter, Db0 [m]

%  %% check within fluidizing regime
%  Ub=ug-umf+0.711*(g*d_b)^0.5;                        % Bubble Velocity
[m/s]
%         eta_b= (ug-umf)/(Ub-umf);                          %Volume
fraction of the Bubble phase
%         Re_s=eta_b*rho_g*dp*(ug)/meu;
% Cd=24/Re_s*(1+0.15*Re_s^0.687);
% Ut=sqrt(4*g*dp*(rho_s-rho_g)/3/rho_g/Cd);
%
%          if (ug < umf)
```

```
%             disp('steam velocity must be greater than the minimum
fluidising velocity')
%         elseif (ug > Ut)
%             disp('steam velocity must be less than the terminal
velocity')
%             return
%         else
%          end
%% Diffusion
% umf = meu*((27.2^2+0.0408*Ar)^0.5-27.2)/rho_g/dp;    % Minimum
fluidisation velocity
d_b=db0;
Ub=ug-umf+0.711*(g*d_b)^0.5;                          % Bubble Velocity [m/s]
eta_b= (ug-umf)/(Ub-umf);
DEL =  (ug-umf)/Ub;                                  % Volume fraction of the
Bubble phase, DEL
fw=0.38;
Emf=0.4025+603.7*dp ;
Dsr1=fw^2*Emf*eta_b*d_b*Ub^2/3/umf; %m^2/s
Dsr=3/16*eta_b/(1-eta_b)*umf*d_b/Emf;%m^2/s
Dmb= diffusion(Ci0, T);
Dme= diffusion(Ci0,T);
%%
% To calculate the heat capacity.. taken from Perry Handbook of Chemical
% Engineers. The Order of Parameters for the compounds are
%           H2,         CO,    CO2,     H2O       CH4,       C      N2
O2
A =     [3.249      3.376   5.457    3.470      1.702   1.771   3.280
3.639];
B =     [0.422e-3 0.557e-3 1.047e-3 1.450e-3 9.081e-3 0.771e-3 0.593e-3
0.506e-3];
C =     [0          0       0         0     -2.164e-6       0       0
0];
D =     [0.083e5 -0.031e5 -1.157e5  0.121e5     0     -0.867e5  0.040e5 -
0.227e5];
Go_f298 = [0        -137169 -394359   -228572   -50460        0       0
0]; % [KJ/Kmol]
Ho_f298 = [0        -110525 -393509   -241818   -74520        0       0
0]; % [KJ/Kmol]

A_i =[3.616e1 1.517e4 4.189e-3 7.301e-2]; %Values of reaction kinetic
constants [1/s]
E =[77390 121620 19210 36150];            %and activation energy for the
chemical reactions [J/mol]

% Stoichiometric Coefficents of the reactions involved in the order of
% the components
%    H2,CO,CO2,H2O,CH4,C
nu =[0, 2,-1,  0,  0,-1; ... C(s) + CO2 <---> 2CO
     1, 1, 0, -1,  0,-1; ... C(s) + H2O <---> CO + H2
    -2, 0, 0,  0,  1,-1; ... C(s) + 2H2 <---> CH4
     3, 1, 0, -1, -1, 0; ... CH4  + H2O <---> CO + 3H2
     1,-1, 1, -1,  0, 0];... CO   + H2O <---> CO2 + H2
del_A = A(1:6)*nu';
del_B = B(1:6)*nu';
del_C = C(1:6)*nu';
del_D = D(1:6)*nu';
del_Go_f298 = Go_f298(1:6)*nu'; % [KJ/Kmol]
del_Ho_f298 = Ho_f298(1:6)*nu'; % [KJ/Kmol]
del_Ab = A(1:5)*nu(4:5,1:5)';
del_Bb = B(1:5)*nu(4:5,1:5)';
```

```
del_Cb = C(1:5)*nu(4:5,1:5)';
del_Db = D(1:5)*nu(4:5,1:5)';
del_Go_f298b = Go_f298(1:5)*nu(4:5,1:5)'; % [KJ/Kmol]
del_Ho_f298b = Ho_f298(1:5)*nu(4:5,1:5)'; % [KJ/Kmol]

J = del_Ho_f298 - (del_A * Tatm + del_B/2*Tatm^2 + del_C/3*Tatm^3-
del_D/Tatm)* R;  % [KJ/Kmol]
I = -((del_Go_f298-J)/(R*Tatm)+del_A*log(Tatm)+ del_B/2*Tatm +
del_C/6*Tatm^2+del_D/(2*Tatm^2));%[-]
Jb = del_Ho_f298b - (del_Ab * Tatm + del_Bb/2*Tatm^2 + del_Cb/3*Tatm^3-
del_Db/Tatm)* R;  % [KJ/Kmol]
Ib = -((del_Go_f298b-Jb)/(R*Tatm)+del_Ab*log(Tatm)+ del_Bb/2*Tatm +
del_Cb/6*Tatm^2+del_Db/(2*Tatm^2));%[-]

m =0; % Parameter corresponding to symmetry. slab = 0; Cylindrical =1;
x = linspace(0,2,60);
t = linspace(0,040*60,60);
dx= x(2)-x(1);
 [Ds, eta_b, Ub,Ue,d_b]= diffusionsr(x);

sol = pdepe(m,@pdebfbpde,@pdebfbic,@pdebfbbc,x,t);

%% Matlab Function Reference - pdepe
% Solve initial-boundary value problems for systems of parabolic and
% elliptic partial differential equations (PDEs) in one space variable and
% time.

% SYNTAX sol = pdepe(m,pdefun,icfun,bcfun,xmesh,tspan)
%        sol = pdepe(m,pdefun,icfun,bcfun,xmesh,tspan,options)

% Arguments
% m         A parameter corresponding to the symmetry of the problem. m can
%           be slab = 0, cylindrical = 1, or spherical= 2.
% pdefun    A handle to a function that defines the components of the PDE.
% icfun     A handle to a function that defines the initial conditions.
% bcfun     A handle to a function that defines the boundary conditions.
% xmesh     A vector [x0, x1, ..., xn] specifying the points at which a
%           numerical solution is requested for every value in tspan. The
%           elements of xmesh must satisfy x0 < x1 < ... < xn. The length
%           of xmesh must be >= 3.
% tspan     A vector [t0, t1, ..., tf] specifying the points at which a
%           solution is requested for every value in xmesh.The elements of
%           tspan must satisfy t0 < t1 <... < tf. The length of tspan must
%           be >= 3.
% options   Some options of the underlying ODE solver are available in
%           pdepe: RelTol, AbsTol, NormControl, InitialStep, and MaxStep.
%           In most cases, default values for these options provide
%           satisfactory solutions.
%%
c1 = sol(:,:,1);
c2 = sol(:,:,2);
c3 = sol(:,:,3);
c4 = sol(:,:,4);
c5 = sol(:,:,5);
c6 = sol(:,:,6);
c7 = sol(:,:,7);
c8 = sol(:,:,8);
c9 = sol(:,:,9);
c10 = sol(:,:,10);
c11 = sol(:,:,11);
```

```
T_b=sol(:,:,12);
T_e=sol(:,:,13);
T_p=sol(:,:,14);
c12=c1+c2+c3+c4+c5+c6+c7+c8+c9+c10; % totalgas

figure
hold on
grid on
box on
M1 = plot(t1,z(:,1),'d-r','MarkerFaceColor','r','MarkerSize',6);
N1 = plot(t1,z(:,2),'o-g','MarkerFaceColor','g','MarkerSize',6);
O1 = plot(t1,z(:,3),'^-b','MarkerFaceColor','b','MarkerSize',6);
P1 = plot(t1,z(:,4),'v-c','MarkerFaceColor','c','MarkerSize',6);
legend([M1,N1,O1,P1],'Weight fraction of wood',...
'weight fraction of total Gas',...
'weight fraction of tar',...
'weight fraction of char',-1);
title('Molefraction on Pyrolysis for 1 sec','Fontsize',18);
xlabel('Time [s]  --->','FontSize',18);
ylabel('W_{i}/W_{0}  ---->','FontSize',18);


figure
subplot(3,2,1)
plot(x*(ug-umf), Ds)
xlabel('x*(ug-umf) [m^2/s]--->','FontSize',16);
ylabel('D_{rs} [m^2/s]---->','FontSize',16);

 subplot(3,2,2)
plot(d_b, Ds)
xlabel('d_b[m] --->','FontSize',16);
ylabel('D_{rs} [m^2/s]---->','FontSize',16);
subplot(3,2,3)
plot( eta_b,Ds)
xlabel('eta_b [-]  --->','FontSize',16);
ylabel('D_{rs} [m^2/s]---->','FontSize',16);


subplot(3,2,4)
plot(Ub, Ds)
xlabel('Ub [m/s] --->','FontSize',16);
ylabel('D_{rs} [m^2/s] ---->','FontSize',16);

subplot(3,2,5)
plot(eta_b, x)
xlabel('eta_b [-] --->','FontSize',16);
ylabel(' x [m] ---->','FontSize',16);
subplot(3,2,6)
plot(Ue, Ds)
xlabel('Ue[m] --->','FontSize',16);
ylabel('D_{rs} [m^2/s] ---->','FontSize',16);figure
pp = min(size(c1));
subplot(2,2,1)
size(x)
size(t)
size(sol(:,:,1))
surf(x(1:pp),t(1:pp)./60,c1(1:pp,:),...
'LineStyle','none')
xlabel('Distance x')
ylabel('Time t [min]')
```

```
zlabel('C_H_2(Bubble phase)')

subplot(2,2,3)
surf(x(1:pp),t(1:pp)./60,c2(1:pp,:),...
'LineStyle','none')
xlabel('Distance x')
ylabel('Time t[min]')
zlabel('C_C_O(Bubble phase)')

subplot(2,2,2)
surf(x(1:pp),t(1:pp)./60,c6(1:pp,:),...
'LineStyle','none')
xlabel('Distance x')
ylabel('Time t [min]')
zlabel('C_H_2(Emulsion phase)')

subplot(2,2,4)
surf(x(1:pp),t(1:pp)./60,c7(1:pp,:),...
'LineStyle','none')
xlabel('Distance x')
ylabel('Time t')
zlabel('C_{CO}(Emulsion phase)')

figure
subplot(2,1,1)
surf(x(1:pp),t(1:pp)./60,c3(1:pp,:),...
'LineStyle','none')
xlabel('Distance x')
ylabel('Time t[min]')
zlabel('C_{CO2}(Bubble phase)')

subplot(2,1,2)
surf(x(1:pp),t(1:pp)./60,c8(1:pp,:),...
'LineStyle','none')
xlabel('Distance x')
ylabel('Time t[min]')
zlabel('C_{CO2}(Emulsion phase)')

figure
subplot(2,2,1)
surf(x(1:pp),t(1:pp)./60,c4(1:pp,:),...
'LineStyle','none')
xlabel('Distance x')
ylabel('Time t[min]')
zlabel('C_{H2O}(Bubble phase)')

subplot(2,2,3)
surf(x(1:pp),t(1:pp)./60,c9(1:pp,:),...
'LineStyle','none')
xlabel('Distance x')
ylabel('Time t[min]')
zlabel('C_{H2O}(emulsion phase)')

subplot(2,2,2)
surf(x(1:pp),t(1:pp)./60,c5(1:pp,:),...
'LineStyle','none')
xlabel('Distance x')
ylabel('Time t[min]')
zlabel('C_{CH4}(Bubble phase)')
```

```
subplot(2,2,4)
surf(x(1:pp),t(1:pp)./60,c10(1:pp,:),...
'LineStyle','none')
xlabel('Distance x')
ylabel('Time t[min]')
zlabel('C_{CH4}(Emulsion phase)')

figure
surf(x(1:pp),t(1:pp)./60,c11(1:pp,:),...
'LineStyle','none');
xlabel('Distance x')
ylabel('Time t[min]')
zlabel('C_C(Emulsion phase)')

figure
subplot(2,2,1)
surf(x(1:pp),t(1:pp)./60,c1(1:pp,:)+c6(1:pp,:),...
'LineStyle','none');
xlabel('Distance x')
ylabel('Time t[min]')
zlabel('C_{H2}')

subplot(2,2,3)
surf(x(1:pp),t(1:pp)./60,c2(1:pp,:)+c7(1:pp,:),...
'LineStyle','none')
xlabel('Distance x')
ylabel('Time t[min]')
zlabel('C_C_O')

subplot(2,2,2)
surf(x(1:pp),t(1:pp)./60,c3(1:pp,:)+c8(1:pp,:),...
'LineStyle','none')
xlabel('Distance x')
ylabel('Time t[min]')
zlabel('C_{CO2}')

subplot(2,2,4)
surf(x(1:pp),t(1:pp)./60,c4(1:pp,:)+c9(1:pp,:),...
'LineStyle','none')
xlabel('Distance x')
ylabel('Time t[min]')
zlabel('C_{H2O}')
figure
surf(x(1:pp),t(1:pp)./60,c5(1:pp,:)+c10(1:pp,:),...
'LineStyle','none')
xlabel('Distance x')
ylabel('Time t[min]')
zlabel('C_{CH4}')
total_gas=c1(1:pp,:)+c2(1:pp,:)+c3(1:pp,:)+c4(1:pp,:)+c5(1:pp,:)+c6(1:pp,:)
+c7(1:pp,:)+c8(1:pp,:)+c9(1:pp,:)+c10(1:pp,:);


figure
subplot(3,2,1)
surf(x(1:pp),t(1:pp)./3600,(c1(1:pp,:)+c6(1:pp,:))./total_gas,...
'LineStyle','none');
xlabel('Distance x')
ylabel('Time t[hr]')
zlabel('C_{H2}')
```

```
subplot(3,2,3)
surf(x(1:pp),t(1:pp)./3600,(c2(1:pp,:)+c7(1:pp,:))./total_gas,...
'LineStyle','none')
xlabel('Distance x')
ylabel('Time t[hr]')
zlabel('C_C_O')

subplot(3,2,2)
surf(x(1:pp),t(1:pp)./3600,(c3(1:pp,:)+c8(1:pp,:))./total_gas,...
'LineStyle','none')
xlabel('Distance x')
ylabel('Time t[hr]')
zlabel('C_{CO2}')

subplot(3,2,4)
surf(x(1:pp),t(1:pp)./3600,(c4(1:pp,:)+c9(1:pp,:))./total_gas,...
'LineStyle','none')
xlabel('Distance x')
ylabel('Time t[hr]')
zlabel('C_{H2O}')

subplot(3,2,5)
surf(x(1:pp),t(1:pp)./3600,(c5(1:pp,:)+c10(1:pp,:))./total_gas,...
'LineStyle','none')
xlabel('Distance x')
ylabel('Time t[hr]')
zlabel('C_{CH4}')

subplot(3,2,6)
surf(x(1:pp),t(1:pp)./3600,c11(1:pp,:),...
'LineStyle','none');
xlabel('Distance x')
ylabel('Time t[hr]')
zlabel('C_C(Emulsion phase)')

figure
subplot(3,2,1)
surf(x(1:pp),t(1:pp)./3600,(c1(1:pp,:)+c6(1:pp,:))./c12(1:pp,:),...
'LineStyle','none');
xlabel('Distance x')
ylabel('Time t[hr]')
zlabel('C_{H2}')

subplot(3,2,3)
surf(x(1:pp),t(1:pp)./3600,(c2(1:pp,:)+c7(1:pp,:))./c12(1:pp,:),...
'LineStyle','none')
xlabel('Distance x')
ylabel('Time t[hr]')
zlabel('C_C_O')

subplot(3,2,2)
surf(x(1:pp),t(1:pp)./3600,(c3(1:pp,:)+c8(1:pp,:))./c12(1:pp,:),...
'LineStyle','none')
xlabel('Distance x')
ylabel('Time t[hr]')
zlabel('C_{CO2}')

subplot(3,2,4)
```

```
surf(x(1:pp),t(1:pp)./3600,(c4(1:pp,:)+c9(1:pp,:))./c12(1:pp,:),...
'LineStyle','none')
xlabel('Distance x')
ylabel('Time t[hr]')
zlabel('C_{H2O}')

subplot(3,2,5)
surf(x(1:pp),t(1:pp)./3600,(c5(1:pp,:)+c10(1:pp,:))./c12(1:pp,:),...
'LineStyle','none')
xlabel('Distance x')
ylabel('Time t[hr]')
zlabel('C_{CH4}')

figure
subplot(2,2,1)
surf(x(1:pp),t(1:pp)./3600,(c1(1:pp,:)+c6(1:pp,:))./(c12(1:pp,:)-
c4(1:pp,:)-c9(1:pp,:)),...
'LineStyle','none');
xlabel('Distance x')
ylabel('Time t[hr]')
zlabel('y_{H2}')

subplot(2,2,2)
surf(x(1:pp),t(1:pp)./3600,(c2(1:pp,:)+c7(1:pp,:))./(c12(1:pp,:)-
c4(1:pp,:)-c9(1:pp,:)),...
'LineStyle','none')
xlabel('Distance x')
ylabel('Time t[hr]')
zlabel('y_C_O')

subplot(2,2,3)
surf(x(1:pp),t(1:pp)./3600,(c3(1:pp,:)+c8(1:pp,:))./(c12(1:pp,:)-
c4(1:pp,:)-c9(1:pp,:)),...
'LineStyle','none')
xlabel('Distance x')
ylabel('Time t[hr]')
zlabel('y_{CO2}')

subplot(2,2,4)
surf(x(1:pp),t(1:pp)./3600,(c5(1:pp,:)+c10(1:pp,:))./(c12(1:pp,:)-
c4(1:pp,:)-c9(1:pp,:)),...
'LineStyle','none')
xlabel('Distance x')
ylabel('Time t[hr]')
zlabel('y_{CH4}')

figure
subplot(3,2,1)
surf(x(1:pp),t(1:pp)./3600,(c1(1:pp,:)+c6(1:pp,:)),...
'LineStyle','none');
xlabel('Distance x')
ylabel('Time t[hr]')
zlabel('C_{H2}')

subplot(3,2,3)
surf(x(1:pp),t(1:pp)./3600,(c2(1:pp,:)+c7(1:pp,:)),...
'LineStyle','none')
xlabel('Distance x')
ylabel('Time t[hr]')
zlabel('C_C_O')
```

```
subplot(3,2,2)
surf(x(1:pp),t(1:pp)./3600,(c3(1:pp,:)+c8(1:pp,:)),...
'LineStyle','none')
xlabel('Distance x')
ylabel('Time t[hr]')
zlabel('C_{CO2}')

subplot(3,2,4)
surf(x(1:pp),t(1:pp)./3600,(c4(1:pp,:)+c9(1:pp,:)),...
'LineStyle','none')
xlabel('Distance x')
ylabel('Time t[hr]')
zlabel('C_{H2O}')

subplot(3,2,5)
surf(x(1:pp),t(1:pp)./3600,(c5(1:pp,:)+c10(1:pp,:)),...
'LineStyle','none')
xlabel('Distance x')
ylabel('Time t[hr]')
zlabel('C_{CH4}')

subplot(3,2,6)
surf(x(1:pp),t(1:pp)./3600,total_gas,...
'LineStyle','none');
xlabel('Distance x')
ylabel('Time t[hr]')
zlabel('total gas')

figure
subplot(2,1,1)
surf(x(1:pp),t(1:pp)./60,T_b(1:pp,:),...
'LineStyle','none');
xlabel('Distance x')
ylabel('Time t[min]')
zlabel('T_b(Bubble phase)')

subplot(2,1,2)
surf(x(1:pp),t(1:pp)./60,T_e(1:pp,:),...
'LineStyle','none');
xlabel('Distance x')
ylabel('Time t[min]')
zlabel('T_e(emulsion phase)')

time = t(1:pp)./60;

figure
plot(time,T_b(1:pp,:),'r')
hold on
plot(time,T_e(1:pp,:),'b')
T700=T_e(:,1:pp);
tim700= time;

xlabel('Time in min  --->','FontSize',18);
ylabel('T [K]  ---->','FontSize',18);
mf=(c1(1:pp,:)+c6(1:pp,:))./(c12(1:pp,:)-c4(1:pp,:)-c9(1:pp,:));
mf2=(c2(1:pp,:)+c7(1:pp,:))./(c12(1:pp,:)-c4(1:pp,:)-c9(1:pp,:));
mf3= (c3(1:pp,:)+c8(1:pp,:))./(c12(1:pp,:)-c4(1:pp,:)-c9(1:pp,:));
mf4=(c5(1:pp,:)+c10(1:pp,:))./(c12(1:pp,:)-c4(1:pp,:)-c9(1:pp,:));
```

```
figure

mfa1=(c1(1:pp,:)+c6(1:pp,:))./c12(1:pp,:);
mfa2=(c2(1:pp,:)+c7(1:pp,:))./c12(1:pp,:);
mfa3=(c3(1:pp,:)+c8(1:pp,:))./c12(1:pp,:);
mfa4=(c4(1:pp,:)+c9(1:pp,:))./c12(1:pp,:);
mfa5=(c5(1:pp,:)+c10(1:pp,:))./c12(1:pp,:);
subplot(2,2,[1 3])
L= plot([time(1:10) time(11:3:end)]',[mfa1(1:10,end);
mfa1(11:3:end,end)],'pk');
hold on
M= plot([time(1:10) time(11:3:end)]',[mfa2(1:10,end);
mfa2(11:3:end,end)],'^k');
N= plot([time(1:10) time(11:3:end)]',[mfa3(1:10,end);
mfa3(11:3:end,end)],'*k');
O= plot([time(1:10) time(11:3:end)]',[mfa4(1:10,end);
mfa4(11:3:end,end)],'+k');
S= plot([time(1:10) time(11:3:end)]',[mfa5(1:10,end);
mfa5(11:3:end,end)],'sk');
legend([L,M,N,O,S],'y_H_2','y_C_O','y_C_O_2','Y_H_2_O','y_C_H_4','Orientati
on','horizontal')

xlabel('Time in min  --->','FontSize',12);
ylabel('y_i  ---->','FontSize',12);

subplot(2,2,[2 4])
L=plot([time(1:10) time(11:3:end)]',[mf(1:10,end); mf(11:3:end,end)],'pk');
hold on
M=plot([time(1:10) time(11:3:end)]',[mf2(1:10,end);
mf2(11:3:end,end)],'^k');
N=plot([time(1:10) time(11:3:end)]',[mf3(1:10,end);
mf3(11:3:end,end)],'*k');
O=plot([time(1:10) time(11:3:end)]',[mf4(1:10,end);
mf4(11:3:end,end)],'sk');
legend([L,M,N,O],'y_H_2','y_C_O','y_C_O_2','y_C_H_4')

xlabel('Time in min  --->','FontSize',12);
ylabel('y_i  ---->','FontSize',12);

figure

plot(x,c1(end,:))
title('Solution at t = 2')
xlabel('Distance x')
ylabel('u(x,2)')

H2plot=c1(1:pp,:)./(c12(1:pp,:)-c4(1:pp,:)-c9(1:pp,:));
COplot=c2(1:pp,:)./(c12(1:pp,:)-c4(1:pp,:)-c9(1:pp,:));
CO2plot=c3(1:pp,:)./(c12(1:pp,:)-c4(1:pp,:)-c9(1:pp,:));
CH4plot=c5(1:pp,:)./(c12(1:pp,:)-c4(1:pp,:)-c9(1:pp,:));

figure
subplot(2,2,[1 3])

plot([H2plot(end,1:10) H2plot(end,11:3:end)],[x(1:10) x(11:3:end)]','pk');
title('Bubble phase','FontSize',12)
hold on
plot([COplot(end,1:10) COplot(end,11:3:end)],[x(1:10) x(11:3:end)]','^k');
```

```
plot([CO2plot(end,1:10) CO2plot(end,11:3:end)],[x(1:10)
x(11:3:end)]','*k');
plot([CH4plot(end,1:10) CH4plot(end,11:3:end)],[x(1:10)
x(11:3:end)]','sk');
xlabel('Molefraction y_i  --->','FontSize',12);
ylabel('Height [m]  ---->','FontSize',12);

H2eplot=c6(1:pp,:)./(c12(1:pp,:)-c4(1:pp,:)-c9(1:pp,:));
COeplot=c7(1:pp,:)./(c12(1:pp,:)-c4(1:pp,:)-c9(1:pp,:));
CO2eplot=c8(1:pp,:)./(c12(1:pp,:)-c4(1:pp,:)-c9(1:pp,:));
CH4eplot=c10(1:pp,:)./(c12(1:pp,:)-c4(1:pp,:)-c9(1:pp,:));

subplot(2,2,[2 4])

plot([H2eplot(end,1:10) H2eplot(end,11:3:end)],[x(1:10)
x(11:3:end)]','pk');
title('Emulsion phase','FontSize',12)
hold on
plot([COeplot(end,1:10) COeplot(end,11:3:end)],[x(1:10)
x(11:3:end)]','^k');
plot([CO2eplot(end,1:10) CO2eplot(end,11:3:end)],[x(1:10)
x(11:3:end)]','*k');
plot([CH4eplot(end,1:10) CH4eplot(end,11:3:end)],[x(1:10)
x(11:3:end)]','sk');
legend('y_H_2','y_C_O','y_C_O_2','y_C_H_4')
xlabel('Molefraction y_i  --->','FontSize',12);
ylabel('Height [m]  ---->','FontSize',12);

figure
L=plot([time(1:10) time(11:3:end)]',[mf(1:10,end); mf(11:3:end,end)],'pk');
hold on
M=plot([time(1:10) time(11:3:end)]',[mf2(1:10,end);
mf2(11:3:end,end)],'^k');
N=plot([time(1:10) time(11:3:end)]',[mf3(1:10,end);
mf3(11:3:end,end)],'*k');
O=plot([time(1:10) time(11:3:end)]',[mf4(1:10,end);
mf4(11:3:end,end)],'sk');
legend([L,M,N,O],'y_H_2','y_C_O','y_C_O_2','y_C_H_4')

xlabel('Time in min  --->','FontSize',12);
ylabel('y_i  ---->','FontSize',12);

figure

surf(x(1:pp),t(1:pp)./60,T_p(1:pp,:),...
'LineStyle','none');
xlabel('Distance x')
ylabel('Time t[min]')
zlabel('T_b(Bubble phase)')

figure
subplot(2,2,[1 3])
plot(x(1:pp),c11(end,1:pp));
ylabel('W_{char} [kg] --->','FontSize',14);
xlabel(' x [m] ---->','FontSize',14);
hold on

subplot(2,2,[2 4])
plot( x*(ug-umf),Ds,'r')
```

```
ylabel('Ds  [m^2/s]--->','FontSize',14);
xlabel(' x*(ug-umf) [m^2/s] ---->','FontSize',14);

% %
toc
%% Main Partial differential Equations function definition
function [c,f,s] = pdebfbpde(x,t,cb,DcbDx)
        CH2b=cb(1);              % (kmol/m^3)
        Ccob=cb(2);
        Cco2b=cb(3);
        CH2Ob=cb(4);
        CCH4b=cb(5);
        CH2e=cb(6);
        Ccoe=cb(7);
        Cco2e=cb(8);
        CH2Oe=cb(9);
        CCH4e=cb(10);
        Ccs=cb(11);              %kgchar/Kgsand
        Tb=cb(12);
        Te=cb(13);
        Tp=cb(14);
        C_Tot= sum(cb(1:10)); %(kmol/m^3)
        Mw_gasi=[2 28 44 18 16]';
        Avg_Molwt_g= sum((cb(1:5)/C_Tot).*Mw_gasi)...
            +sum(cb(6:10)/C_Tot.*Mw_gasi);     %kg/kmol
        rho_g= P/R/Tb*Avg_Molwt_g/1000;% Density of gas species [kg/m^3]
        dbm=1.64*(A_cs*(ug-umf))^0.4;    % Maximum Bubble Diameter, DbM [m]
        db0=0.347*(A_cs*(ug-umf)/nd)^0.4;% Initial Bubble Diameter, Db0 [m]
        d_b= dbm-(dbm-db0)*exp(-0.3*x/Dt);                    % Bubble
Diameter, Db [m]
        Ar= dp^3*rho_g*(rho_s-rho_g)*g/meu^2;                 % Archimedies
number (-)
        umf = meu*((27.2^2+0.0408*Ar)^0.5-27.2)/rho_g/dp;    % Minimum
fluidisation velocity [m/s]
        Ub=ug-umf+0.711*(g*d_b)^0.5;                          % Bubble
Velocity [m/s]
        eta_b= (ug-umf)/(Ub-umf);
        DEL =  (ug-umf)/Ub;                                % Volume fraction
of the Bubble phase, DEL
        Ue = umf/(1-DEL);                                     % Emulsion
phase gas Velocity, Ue
% Diffusion
        Dmb= diffusion(cb(1:5),Tb);                           % Diffusion
coeffient of H2,CO,CO2,H2O,CH4 in the gas mixture in bubble phase
        Dme= diffusion(cb(6:10),Te);                          % Diffusion
coeffient of H2,CO,CO2,H2O,CH4 in the gas mixture in emulsion phase

        Dif_b= sum(Dmb'.*cb(1:5)/sum(cb(1:5)));
        Dif_e= sum(Dme'.*cb(6:10)/sum(cb(6:10)));

        Kbc = 4.5 *umf/d_b +5.85*(Dif_b^0.5*g^0.25/d_b^1.25);   % [1/s]
        ubr= 0.711*(g*d_b)^0.5;                               % Rise
velocity of single bubble relative to emulsion solids [m/s]
        Emf=0.4025+603.7*dp ;                                 % Void
fraction at Minimum Fluidisation
        Kce=6.77*(Dif_e*Emf*ubr/d_b^3)^0.5;                   % [1/s]
        Kbe=1/(1/Kbc+1/Kce); %Gas Exchange Coefficient between the Bubble
and emulsion phase,[1/s]

        p_mf = 1.75*(1-Emf)*umf^2*rho_g/Emf^3/dp ...
```

```
             + 150*(1-Emf)^2*meu*umf/Emf^3/dp^2;            % Pressure
drop at minimum fluidisation velocity

% Thermal conductivity of gases is polynomial in temperature and can be
% described by the following equation as in Handbook of Heat Transfer by
% Warren M.Rohsenow, James P.Hartnett and Young I.Cho.
% K = a2+b2*T+c2*T^2+d2*T^3 []
%
% Carbon Dioxide (600<=T<=1000K)  Carbon Monoxide (250<=T<=1050K)   %
Ethane (C2H6) (200<=T<=1000K)
% a2 = 6.085375e-2                a2 = -7.41704398e-4               a2 =
-3.83815197e-2
% b2 =-3.63680275e-4              b2 = 9.87435265e-5                b2 =
5.47282126e-4
% c2 = 1.0134366e-6               c2 = -3.77511167e-8               c2 =
-2.80760648e-6
% d2 =-9.7042356e-10              d2 = -1.99334224e-11              d2 =
8.74854603e-9
% e2 = 3.27864115e-13             e2 = 3.65528473e-14               e2 =
-1.369896e-11
% f2 = 0                          f2 = -1.2427179e-17               f2 =
1.05765043e-14
% g2 = 0                          g2 = 0                            g2= -
3.16347435e-18
% Methane CH4 (200<=T<=1000K)   % Hydrogen (500<=T<=1050K)
% a2 = -1.3401499e-2            % a2 = 1.083105e-1
% b2 = 3.6630706e-4             % b2 = 2.21163789e-4
% c2 = -1.82248608e-6           % c2 = 2.26380948e-7
% d2 = 5.93987998e-9            % d2 = -1.74258636e-10
% e2 = -9.1405505e-12           % e2 = 4.6468625e-14
% f2 = 6.7896889e-15            % f2 = 0
% g2 = -1.95048736e-18
%
%       H2,                 CO,         CO2,         CH4,
C2H6
        a2=[1.083105e-1     -7.41704398e-4   6.085375e-2    -1.3401499e-2
-3.83815197e-2];
        b2=[2.21163789e-4    9.87435265e-5  -3.63680275e-4   3.6630706e-4
5.47282126e-4];
        C2=[2.26380948e-7   -3.77511167e-8   1.0134366e-6   -1.82248608e-6
-2.80760648e-6];
        d2=[-1.74258636e-10 -1.99334224e-11 -9.7042356e-10   5.93987998e-9
8.74854603e-9];
        e2=[4.6468625e-14    3.65528473e-14  3.27864115e-13 -9.1405505e-12
-1.369896e-11];
        f2=[0               -1.2427179e-17          0        6.7896889e-15
1.05765043e-14 ];
        g2=[0                   0                   0       -1.95048736e-18
-3.16347435e-18];

C_to=1;%(P+p_mf)/Tb/R/1000;


K(1:3)=(a2(1:3)+b2(1:3)*Tb+C2(1:3)*Tb^2+d2(1:3)*Tb^3+e2(1:3)*Tb^4+f2(1:3)*T
b^5+g2(1:3)*Tb^6)/1.000;  % [kW/m/K]
        K(4) = 0.094313/1.000; % kW/m/K
        K(5) =
(a2(4)+b2(4)*Tb+C2(4)*Tb^2+d2(4)*Tb^3+e2(4)*Tb^4+f2(4)*Tb^5+g2(4)*Tb^6)/1.0
00;% kW/m/K
```

```
K_e(1:3)=(a2(1:3)+b2(1:3)*Te+C2(1:3)*Te^2+d2(1:3)*Te^3+e2(1:3)*Te^4+f2(1:3)
*Te^5+g2(1:3)*Te^6)/1.000;% kW/m/K
        K_e(4) = 0.094313/1.000;% kW/m/K
        K_e(5) =
(a2(4)+b2(4)*Te+C2(4)*Te^2+d2(4)*Te^3+e2(4)*Te^4+f2(4)*Te^5+g2(4)*Te^6)/1.0
00;% kW/m/K

        Kavg= sum(cb(1:5)/sum(cb(1:5)).*K');            % The average
thermal conductivity of gases {kW/m/K}

        Cp   = R*(A+B*(Tb+Tatm)/2+C/3*(4*((Tb+Tatm)/2)^2-
Tb*Tatm)+D/(Tb*Tatm));  % [KJ/KmolK]
%         dCpTdx = R*(A+B*(DcbDx(12)+Tatm)/2+C/3*(4*((DcbDx(12)+Tatm)/2)^2-
DcbDx(12)*Tatm)+D/(eps+DcbDx(12)*Tatm)).*DcbDx(12);
        Cp_e = R*(A+B*(Te+Tatm)/2+C/3*(4*((Te+Tatm)/2)^2-
Te*Tatm)+D/(Te*Tatm));% [KJ/KmolK]
%         dCpTdx_e =
R*(A+B*(DcbDx(13)+Tatm)/2+C/3*(4*((DcbDx(13)+Tatm)/2)^2-
DcbDx(13)*Tatm)+D/(eps+DcbDx(13)*Tatm)).*DcbDx(13);
        Keq_e= exp((-J/(R*Te))+ del_A*log(Te)+ del_B/2*Te +
del_C/6*Te^2+del_D/(2*Te^2) + I); %[-]
        Keq  = exp((-Jb/(R*Tb))+ del_Ab*log(Tb)+ del_Bb/2*Tb +
del_Cb/6*Tb^2+del_Db/(2*Tb^2) + Ib); %[-]
%         delH_ref= Ho_f298(1:6)*nu';%[KJ/Kmol]
%         delHRx=delH_ref +Cp(1:6)*nu'*Tb;%[KJ/Kmol]
%         delHRx_e=delH_ref +Cp_e(1:6)*nu'*Te;%[KJ/Kmol]

        Cpsand=(57.9588+9.33019*10^(-3)*Te+1834713/Te^2)/Mwsand;    % 0.83
% Specific heat of Sand [KJ/kg/K]
if in== 1
            D2cbDx2(:,in)= zeros(1,14);
            dDmbdx(1:5)= 0;
            dDmedx(1:5)= 0;
else
            DcbDx_prev(:,in)= DcbDx;
            D2cbDx2(:,in)= (DcbDx-DcbDx_prev(:,in-1))/dx;

            Dmb_prev(:,in)=Dmb;
            Dme_prev(:,in)=Dme;
            dDmedx= (Dme-Dme_prev(:,in-1)')/dx;
            dDmbdx= (Dmb-Dmb_prev(:,in-1)')/dx;
end
%         D2cbDx2(12,in);
        dudz=
R*sum(Tb*D2cbDx2(1:5,in)+cb(1:5)*D2cbDx2(12,in)+2*DcbDx(1:5)*DcbDx(12))/((1
.75*(1-DEL)*2*Ub*rho_g/DEL^3/dp)+(150*(1-DEL)^2*meu/DEL^3/dp^2));
        duedz=
R*sum(Te*D2cbDx2(6:10,in)+cb(6:10)*D2cbDx2(13,in)+2*DcbDx(6:10)*DcbDx(13))/
((1.75*(DEL)*2*Ue*rho_g/(1-DEL)^3/dp)+(150*DEL^2*meu/(1-DEL)^3/dp^2));
        dusdz=
R*Msand*sum(Msand*Tp*D2cbDx2(11,in)+Msand*cb(11)*D2cbDx2(14,in)+2*DcbDx(11)
*DcbDx(14))/((1.75*(DEL)*2*Ue*rho_g/(1-DEL)^3/dp)+(150*DEL^2*meu/(1-
DEL)^3/dp^2));
v_s=(Msand/rho_s+Ccs/rho_c);
        C_Tb= sum(cb(1:5).*Cp(1:5)'); % kJ/m^3/K
        C_Te=sum(cb(6:10).*Cp_e(1:5)')+(1-
Emf)/Emf*(Ccs*Cp(6)/Mwchar+Msand*Cpsand)/V_r;% kJ/m^3/K
        C_Tp=Ccs*Cp(6)/Mwchar;
        c = [ones(10,1);1;C_Tb;C_Te; C_Tp];
```

```
        Ks=1.000*(0.0013+0.05*(Te/1000)+0.63*(Te/1000)^2)/1.000; %kW/m/K
        SBcons=5.67*10^(-11); % Stephen boltzmann constant kW m^2 K^4
        Krg= 40.00*SBcons*0.05*Tb^3; % unit?
        Krs= 40.00*SBcons*0.85*Te^3;
        Kss= (1-DEL)*(Krg+ Ks/(Ks/(dp*Krs)+1.43*(1-1.2*(1-DEL))));
        Pr_s= Cpsand*meu/Kss;
        Re_s = rho_g*DEL*abs(Ub-Ue)*dp/meu;
        Nu_s = (7-10*DEL+5*DEL^2)*(1+0.7*Re_s^0.2*Pr_s^(1/3))+(1.33-
2.4*DEL+1.2*DEL^2)*Re_s^0.7*Pr_s^(1/3);
        hs= Nu_s*Kss/dp;
        Sc= meu/D1/rho_g;
             km=2.06*Ub/DEL*Re_s^(-0.575)*Sc^(-2/3);
             f_Ci = ones(1,10).*[Dmb Dme];

        f = [reshape(f_Ci,10,1);Dsr;Kavg;Kss;Ccs/rho_c*Kss].*DcbDx;

        Ac = A_i.*exp(-E/R/Tb);
%[1/s]
        rb(1) = C_Tot*Ac(4)*(CCH4b*CH2Ob - Ccob*CH2b^3/Keq(1));
%[kmol/(m3.s)]  % CH4  + H2O <---> CO + 3H2
        rb(2) = 2780*exp(-1510.7/Tb)*( Ccob*CH2Ob-Cco2b*CH2b/Keq(2));
%[kmol/(m3.s)]  % CO   + H2O <-->  CO2+ H2
        Rb=rb*nu(4:5,1:5);  % kmol/m3/s

        Ac = A_i.*exp(-E/R/Te);
%[1/s]
        re(1) = C_Tot*(1/(1/km+1/Ac(1)))*(Cco2e-1.0*Ccoe^2/Keq_e(1));
%[kmol/(m3.s)]  % C(s) + CO2 <---> 2CO
        re(2) = C_Tot*(1/(1/km+1/Ac(2)))*(CH2Oe-1.0*Ccoe*CH2e/Keq_e(2));
%[kmol/(m3.s)]  % C(s) + H2O <---> CO + H2 6*(1-DEL)/dp *
        re(3) = C_Tot*(1/(1/km+1/Ac(3)))*(CH2e^2-1.0*CCH4e/Keq_e(3));
%[kmol/(m3.s)]  % C(s) + 2H2 <---> CH4 6*(1-DEL)/dp *
        re(4) = C_Tot*Ac(4)*(CCH4e*CH2Oe - Ccoe*CH2e^3/Keq_e(4));
%[kmol/(m3.s)]  % CH4  + H2O <---> CO + 3H2
        re(5) = 2780*exp(-1510.7/Te)*(Ccoe*CH2Oe-Cco2e*CH2e/Keq_e(5));
%[kmol/(m3.s)]  % CO   + H2O <-->  CO2+ H2
        Re=re*nu(:,1:6);  % kmol/m3/s
        Rcs=6*(DEL)/dp*Re(6)*Mwchar*Emf/(1-Emf)*(Msand/rho_s + Ccs/rho_c);
% kg/s

%         Ue

        Wout =1.5*Ccs/residence_time;% kg/s
        s_Ci =[-(Ub-dDmbdx').*DcbDx(1:5)-cb(1:5)*dudz-Kbe*(cb(1:5)-
cb(6:10))+Rb';...
            -(Ue-dDmedx').*DcbDx(6:10)-cb(6:10)*duedz+ Kbe*DEL/Emf/(1-
DEL)*(cb(1:5)-cb(6:10))+Re(1:5)';...
             (Win- Wout)-duedz*cb(11)-Us*DcbDx(11)+Rcs];
%*Msand*A_c*dp*12*cb(11)*1];%

        sp_heat_g=sum(Cp(1:5).*((cb(1:5))'/sum(cb(1:5))));  % [KJ/Kmol/K]
        sp_heat_g_e=sum(Cp_e(1:5).*((cb(6:10))'/sum(cb(6:10)))); %
[KJ/Kmol/K]
%         Th_gr_g=sum(K(1:5).*((cb(1:5))'/sum(cb(1:5))));% kW/m/K
        Th_gr_g_e=sum(K_e(1:5).*((cb(6:10))'/sum(cb(6:10))));% kW/m/K
        H_bc_b=4.5*umf*rho_g*sp_heat_g/d_b/Avg_Molwt_g + ...

5.85*(rho_g*sp_heat_g*Kavg/Avg_Molwt_g)^(1/2)*g^(1/4)/d_b^(5/4); %kW/m3/K
```

```
H_ce_b=6.78*(Emf*Th_gr_g_e*sp_heat_g_e*Ub*rho_g/Avg_Molwt_g/d_b^3)^0.5;%kW/
m3/K
        H_be_inv = (1/H_bc_b)+(1/H_ce_b);
        H_be = 1/H_be_inv; %kW/m3/K


        h_e= Ho_f298(1:5)+Cp_e(1:5)*Te; % Specific enthalpy of gases in
bubble phase %[KJ/Kmol]
        h_c =Ho_f298(6)+Cp_e(6)*Te; % KJ/Kmol
        h_sand= 0+Cpsand*Te; %[KJ/kg]

        dCbdt= -cb(1:5)*dudz-Ub*(DcbDx(1:5))+ Dmb'.*D2cbDx2(1:5,in)+...
                DcbDx(1:5).*dDmbdx'-Kbe*(cb(1:5)-cb(6:10))+Rb';
        dCedt= -cb(6:10)*duedz-Ue*(DcbDx(6:10))+Dme'.*D2cbDx2(6:10,in) ...
                + DcbDx(6:10).*dDmedx'...
                + Kbe*DEL/Emf/(1-DEL)*(cb(1:5)-cb(6:10))+Re(1:5)';
        dCcsdt= Dsr*D2cbDx2(11,in)+Win-Wout-Us*DcbDx(11)-Ccs*duedz+Rcs;

        s_Te=-sum(cb(6:10).*Cp_e(1:5)')*Ue*DcbDx(13)- ...
            (1-Emf)/Emf*(Ccs*Cp(6)/Mwchar+Msand*Cpsand)/V_r*Ue*DcbDx(13)...
            -sum(DcbDx(6:10).*h_e')*Ue- ...
            (1-Emf)/Emf*(DcbDx(11)*h_c/Mwchar)/V_r*Ue...
            -sum(cb(6:10).*h_e')*duedz-...
            (1-Emf)/Emf*((Ccs*h_c/Mwchar+Msand*h_sand)/V_r)*duedz...
            +DEL/(1-DEL)/Emf*H_be*(Tb-Te)+sum(h_e.*Re(1:5))+ ...
            1/Emf/V_r*Rcs*h_c/Mwchar...
            +sum(Dme'.*(DcbDx(6:10)).*Cp_e(1:5)'*DcbDx(13))+...

sum(Dme'.*D2cbDx2(6:10,in).*h_e')+sum(h_e'.*DcbDx(6:10).*dDmedx')...
            +(1-Emf)/Emf*(Dsr*DcbDx(11)*Cp_e(6)/Mwchar/V_r*DcbDx(13)+ ...
            sum(Dsr.*D2cbDx2(11,in).*h_c/Mwchar/V_r))...
            +0/(Emf*v_s*(1-
DEL))*((Cpsand*Msand*0+h_c/Mwchar*Ccs)/residence_time)...
            -Te*(sum(Cp_e(1:5)'.*dCedt)+(1-
Emf)/Emf*(dCcsdt*Cp_e(6)/Mwchar)/v_s);
%sum(delH_ref.*re);

        h_b= Ho_f298(1:5)+Cp(1:5)*Tb; % Specific enthalpy of gases in
bubble phase [KJ/Kmol]

        s_Tb=-sum(cb(1:5).*Cp(1:5)')*Ub*DcbDx(12)-
sum(DcbDx(1:5).*h_b')*Ub...
             -sum(cb(1:5).*h_b')*dudz - H_be*(Tb-Te) + sum(h_b.*Rb)- ...

Tb*sum(Cp(1:5)'.*dCbdt)+sum(Dmb'.*(DcbDx(1:5)).*Cp(1:5)'*DcbDx(12))+...
          sum(Dmb'.*D2cbDx2(1:5,in).*h_b')+sum(h_b'.*DcbDx(1:5).*dDmbdx');


        s_Tc=-Us*h_c/Mwchar*DcbDx(11)-Us*Ccs*Cp_e(6)/Mwchar*DcbDx(14)...
            +A_cs*(hs*(Tb-Tp)+SBcons*eta_rad*(Tb^4-Tp^4))...
            -Rcs*h_c/Mwchar+ ...

Dsr*h_c/Mwchar*D2cbDx2(11,in)+Dsr*Cp(6)/Mwchar*DcbDx(11)*DcbDx(14)...
            -((Ccs*h_c/Mwchar+0*Msand*h_sand))*duedz...
        -Tp*Cp_e(6)/Mwchar*dCcsdt;%sum(delH_ref(4:5).*rb);%

        s = [reshape(s_Ci,11,1);s_Tb;s_Te;s_Tc];
```

```
         in = in+1;

end

%% Function definition for initial conditions
function Init = pdebfbic(x)
                d_b= dbm-(dbm-db0)*exp(-0.3*x/Dt);                    %
Bubble Diameter, Db [m]
        Ub=ug-umf+0.711*(g*d_b)^0.5;                            % Bubble
Velocity [m/s]
        eta_b= (ug-umf)/(Ub-umf);                               % ????
        DEL = eta_b; %  (ug-umf)/Ub;                                  % Volume
fraction of the Bubble phase, DEL
        Init=[DEL*Ci0 (1-DEL)*Ci0 Win T T T];
end

%% Function definition for boundary Conditions
function[pl,ql,pr,qr]=pdebfbbc(xl,cl,xr,cr,t)

        d_b= dbm-(dbm-db0)*exp(-0.3*xl/Dt);                     % Bubble
Diameter, Db [m]
        Ub=ug-umf+0.711*(g*d_b)^0.5;                            % Bubble
Velocity [m/s]
        eta_b= (ug-umf)/(Ub-umf);                               % ????
        Ue = umf/(1-eta_b);                                    % Emulsion phase
gas Velocity, Ue
        DEL = eta_b;

         pl=(cl(1:14)'-[(DEL)*Ci0 (1-DEL)*Ci0 Win*64 T T T]);       % BC:
C_ib-(D_ib/u_b) x (?C_ib)/?z = C_i0 ; C_ie-(D_ie/u_e) x (?C_ie)/?z = C_i0
;T_b=T_in;T_e=T_in
         ql=[-(DEL)*Dmb/Ub -(1-DEL)*Dme/Ue -Dsr/Us 0 0 0];
        pr=zeros(14,1)';
        qr=ones(14,1)';
end
%%  Fast Pyrolysis of wood (pine Radiata)
function [dxp] = fastpyrolysis1(z,x)
        Tpy=T;
% Taken from "Modeling chemical and Physical processes of wood and biomass
% pyrolysis ", Progress in Energy and Combustion Science, Colomba Di Blasi_
% and From " A model of Wood flash pyrolysis in fluidised bed reactor,
% Renewable Energy 30 (2005) 377-392, Zhongyang Luo _, Shurong Wang, Kefa
% Cen...in.... \\ENGCAD1\pgo26$\My Documents\Pyrolysis\Printed

% Reaction Schema for thermal decomposition of wood
%            k1
%       Wood --->     gas
%                  k4 ^
%             k2       |
%       wood --->     tar
%                      |
%            k3     k5 v
%       wood --->    char
%  Rxn 1,2,3,5 based on Chan et al
%  Rxn   Pre-exp factor ko(1/s)     Act.Energy Ea(KJ/mole)  del Hr (KJ/KG)
%   1      1.30*10^8                        140
%   2      2.00*10^8                        133
%   3      1.08*10^7                        121
%   4      3.09*10^6                        108
%   5      1.48*10^6                        144
```

```
%
        dwood = -(1.08e7*exp(-121000/8.314/Tpy)+2e8*exp(-
133000/8.314/Tpy)+1.3e8*exp(-140000/8.314/Tpy))*x(1);
        dgas = 1.3e8*exp(-140000/8.314/Tpy)*x(1)+3.09e6*exp(-
108000/8.314/Tpy)*x(3);
        dtar = 2e8*exp(-133000/8.314/Tpy)*x(1)-3.09e6*exp(-
108000/8.314/Tpy)*x(3)-1.48e6*exp(-144000/8.314/Tpy)*x(3);
        dchar = 1.08e7*exp(-121000/8.314/Tpy)*x(1)+1.48e6*exp(-
144000/8.314/Tpy)*x(3);
                dxp = [dwood; dgas;dtar; dchar];
end

%% Diffusion
function Dm= diffusion(Ci0,T);
        sigmaV = [7.07 18.9 26.9 12.7 24.4];
%    H2,CO,CO2,H2O,CH4
             Mw = [2 28 44 18 16 ];
for Ai = 1:5
for Bi = 1:5
                DAB(Ai,Bi) = 1e-
7*T^1.75*(1/Mw(Ai)+1/Mw(Bi))^0.5/(P/101325)/(sigmaV(Ai)^(1/3)+sigmaV(Bi)^(1
/3))^2;
end
%             Dij(Ai,Ai) = 0;
end
        Dmaint(1:5)=0;
         Ct=sum(Ci0);%1;%
for Ai = 1:5
for Bi = 1:5
if Ci0(Ai)~= 1
                    Dmaint(Bi)= (Ci0(Bi)/DAB(Ai,Bi)/Ct);
                DAB(Ai,Bi);
else
                    Dm(Ai) = 0;
end
                Dm(Ai)= (1-Ci0(Ai)/Ct)/(sum(Dmaint(:))-
(Ci0(Ai)/DAB(Ai,Ai))/Ct);
end
end
end
% Diffusion end
%% Diffusion solids
function [Ds, eta_b, Ub,Ue,d_b]= diffusionsr(x);
         d_b= dbm-(dbm-db0)*exp(-0.3*x/Dt);                % Bubble
Diameter, Db [m]
        Ub=ug-umf+0.711*(g*d_b).^0.5;                       % Bubble
Velocity [m/s]
          eta_b= (ug-umf)./(Ub-umf);                          %          Ue
= umf./(1-eta_b);
Ds=3/16.*eta_b./(1-eta_b).*umf.*d_b./Emf;%m^2/s

end
end
```

2D model Routine for biomass steam gasification in the BFB using the using ANSYS Workbench 12.1

In the simulation of this study, the object was built using the Fluid Flow (FLUENT) analysis system of ANSYS Workbench 12.1 which consists of five components: geometry, mesh, fluent-setup, solutions and results.

Step 1:

Open Ansys workbench and select Fluid Flow (FLUENT) from toolbox customization. The FluidFlow(FLUENT) will appear on the toolbox. Drag the FluidFlow(FLUENT) to the project schematic, where five components of Fluid Flow(FLUENT) will appear as shown below.

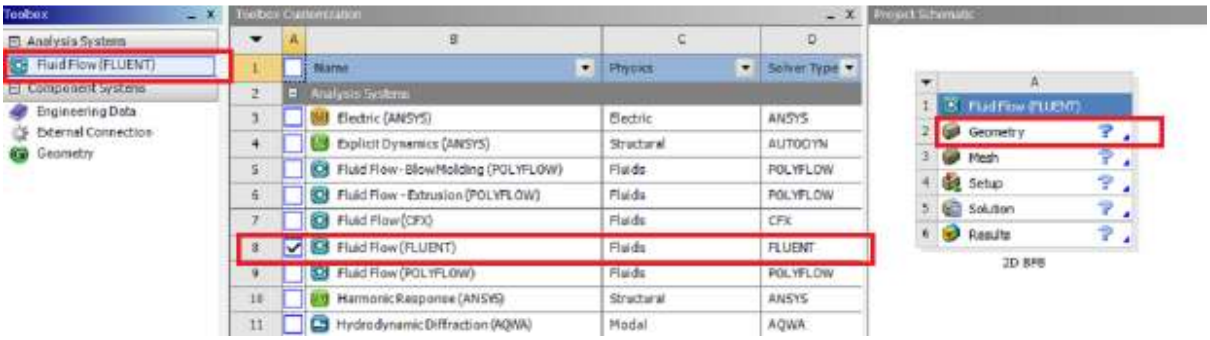

Step 2:

Double click on the "Geometry" to open Design modeler (CAD tool) for defining the geometry of the design problem (2D BFB gasifier of 2m tall and 0.2m inner diameter (I.D.)).

Step 3:

Double click on the "Mesh" to open Meshing (CAD tool) for defining the mesh of the 2D BFB gasifier. ANSYS Workbench Mesh has built-in mesh generators called automatic patch confirming which performs meshing automatically. For finer mesh size as shown in figure a, change the relevance center to "fine" and click 'update'. This creates hexahedral mesh. The boundaries are named in meshing mode. They are defined by creating names by right-clicking on the region where boundary definition is required. By default the boundary is defined as wall. All these are highlighted in red in the below diagram.

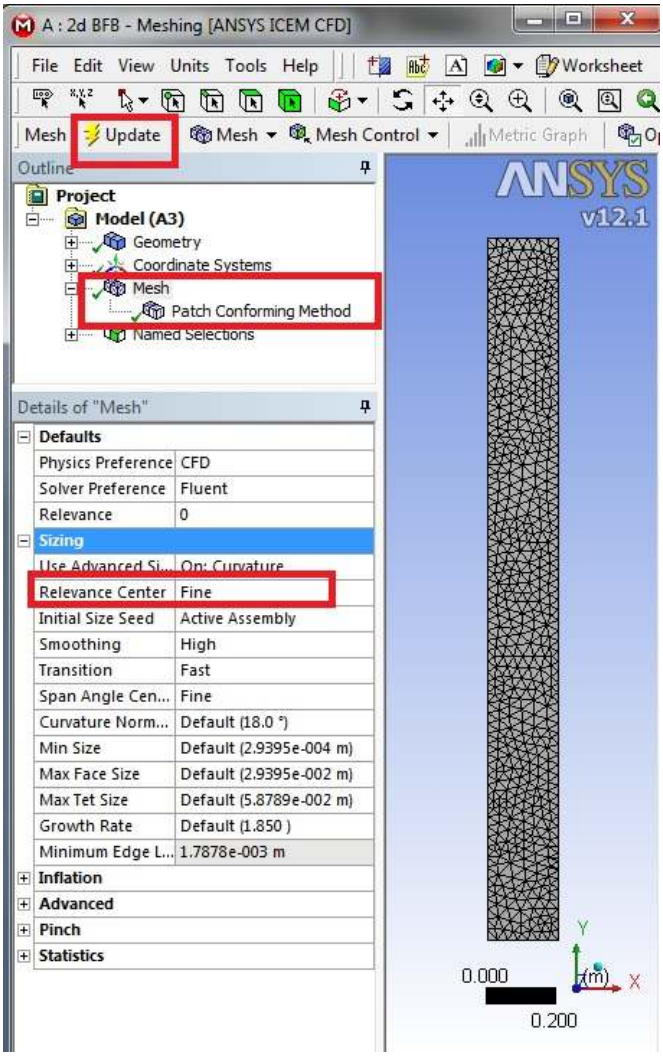

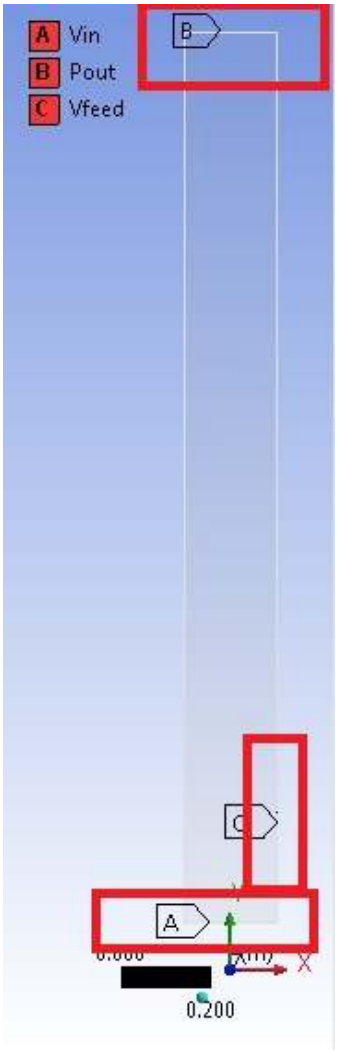

Step 4:

Double click on the “Setup” to open Fluent Launcher (CAD tool) will appear and click ok

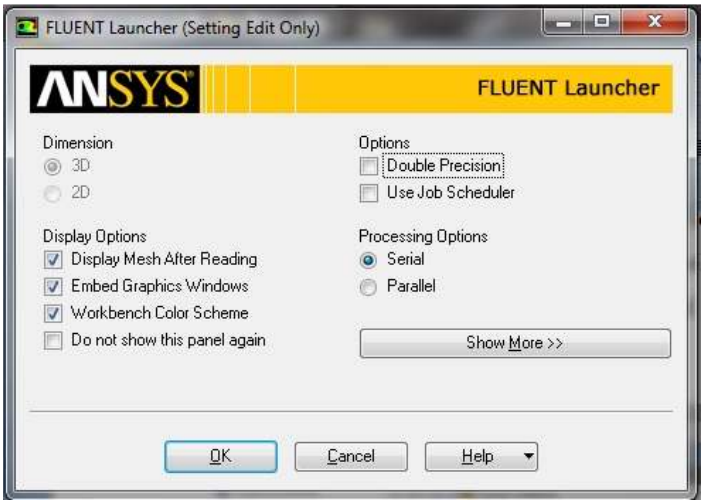

In the Fluent, the 2D BFB gasifier's sub models, materialproperties of gas, solid and their mixture, hydrodynamics parameters, initial and boundary conditions, operating conditions and solvers are defined. The fluent imports the geometry and mesh created from Design modeler and meshing tool.

Step 5:

In the open 'General' from the Problem Setup. Check the mesh and geometry by clicking the 'Check'. Select the solver type as 'Pressure based' and velocity formulation as 'Absolute' and time as 'Transient'. Choose the gravity dialog box and fill the acceleration due to gravity for y direction as -9.81 m/s^2.

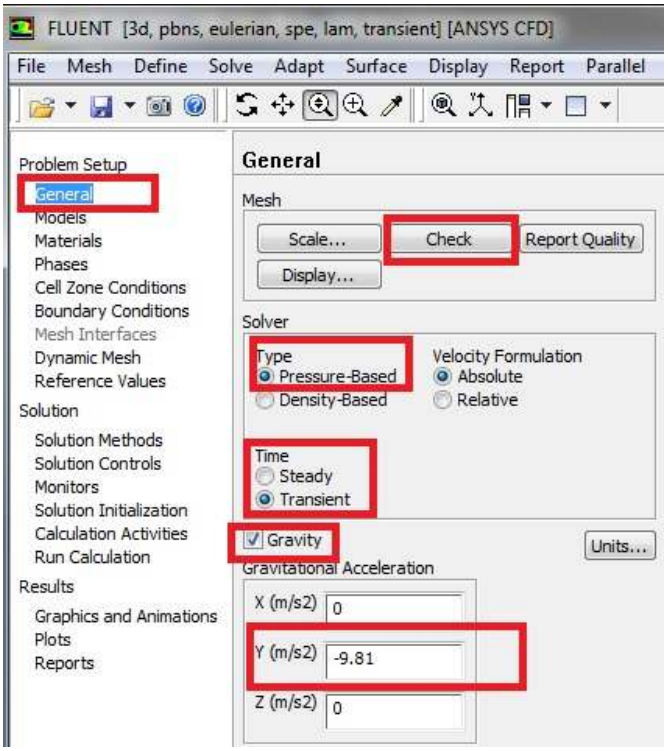

Step 6: **Models**

Choose Eulerian in the Multiphase model, where the number of Eulerian phases is set as 3 and scheme as implicit. Select energy equation from Energy and Laminar model in the Viscous model. In the species model select 'species transport', laminar finite –rate from the turbulence-chemistry interaction, and choose volumetric and particle surface from the Reactions and inlet diffusion from the options as below

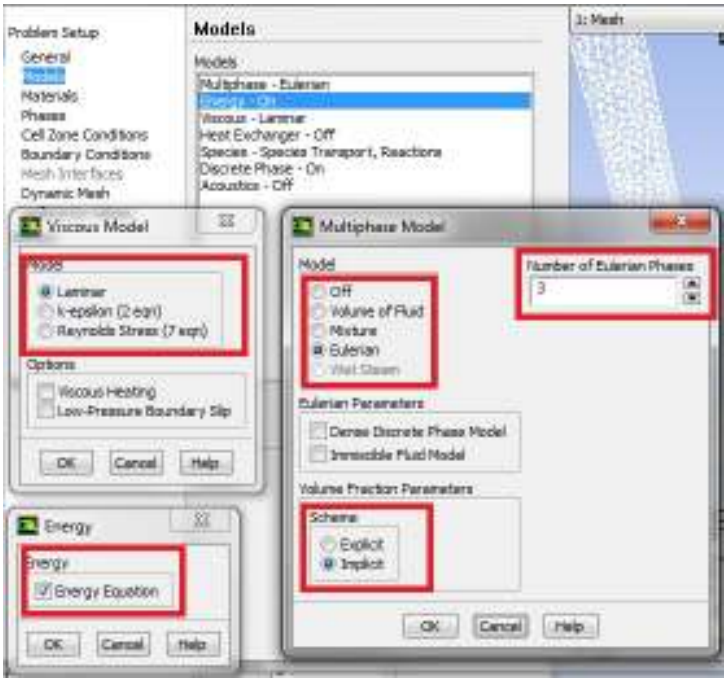

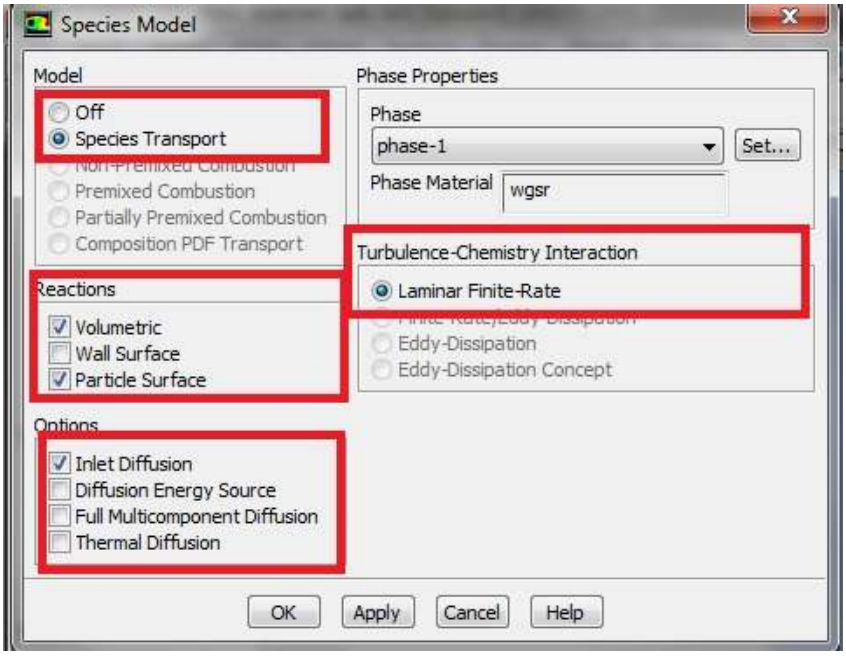

Step 7: Material selections

Click the Fluent Database button to open the Fluent Database Materials panel. Select fluid from the Material Type drop-down list. Copy from the Fluent Database gas, species such as CO, CO_2, H_2O, H_2, CH_4 and solid species C(s) and sand. Select mixture from the Material Type drop-down list and name it as 'wgsr' for the volatile gas. Include the species that is involved in the chemical reactions. In the fluidized bed the solid particles (treated as a fluid) are held in suspension by the volatile gas mixture and steam injected at the bottom of the bed.

Select water-vapor (H_2O) from the Fluent Fluid Materials drop-down list. Enter solids for Name and enter silica for chemical formula and Enter 1600 kg/m^3 for density.

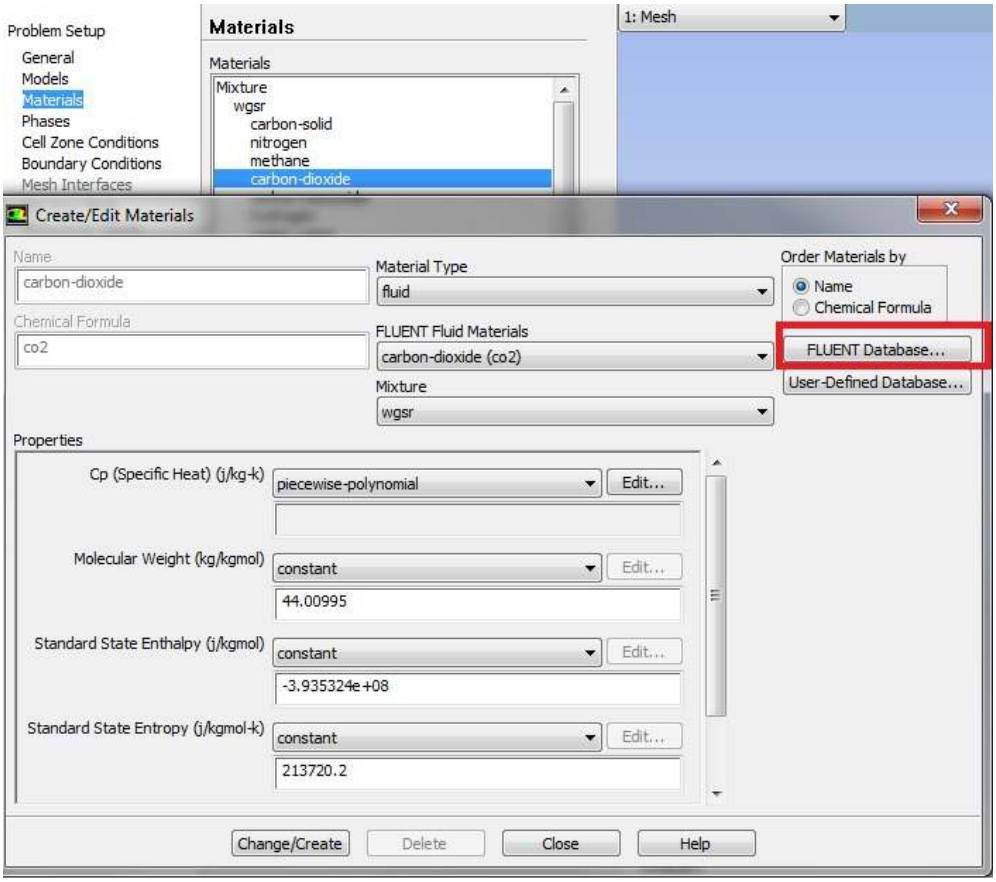

Step 8: Phase selections

In defining the multiphase system three Eulerian phases where selected in which the phase 1 is selected as the primary phase and ‘wgsr’ is selected from the Phase panel. While the secondary solid phases 2 and 3 are Granular and ‘solids’ and ‘C(s)’ from the Phase Material panel. The primary and the secondary phases has ‘edit’ panel to define the properties such as density, specific heat, thermal conductivity, viscosity and mass diffusivity of the primary phase whose values can be added directly and the detailed in Table 5.2.

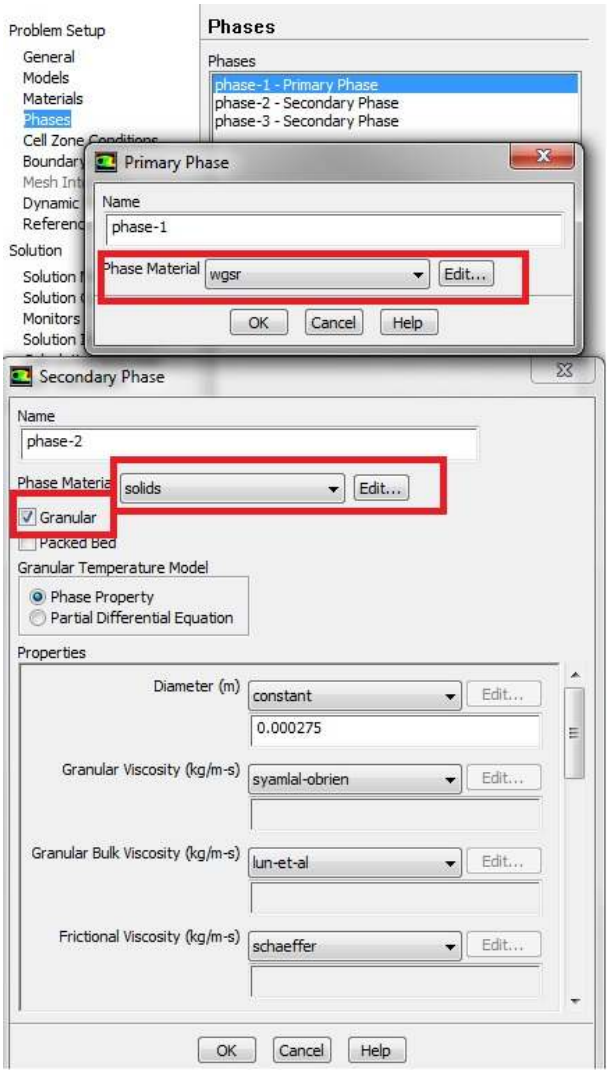

Step 9: Defining Reactions

The properties of the primary phase also have listed two more important properties: Reaction and Mechanism. The gasification reactions in the BFB are defined here. The total number of reactions changed to five and reaction type selected as volumetric. Select from the drop down list to choose the species for the reactants and products, the number of reactants and products for each of the reaction. All the five gasification reactions (Equations 3.15 to 3.19) can be defined in this reactions panel by changing the reaction ID from 1 to 5. The Arrhenius rate group box has the pre-exponential factor, activation energy to load the respective values as given in Table 3.5.

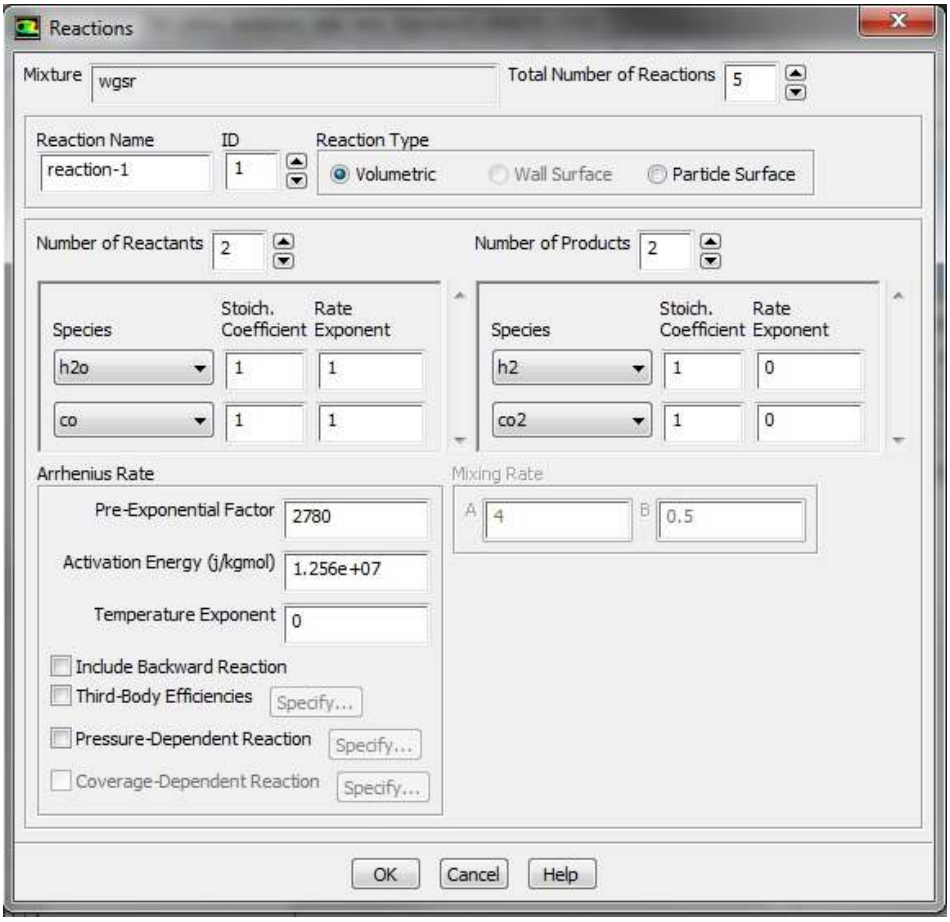

Step 10: Defining interaction between the phases

The interphase momentum and heat transfer between the phases are defined using the interaction panel under the phases defining mode. Clicking the interaction panel on the phase defining mode, the phase interaction dialog box opens where the drag coefficient between the phases can be defined for the momentum interphase. Likewise for the heat interaction are defined from the ‘heat’ panel in the phase interaction.Click the Collisions tab and enter 0.8 for Constant Restitution Coefficient.

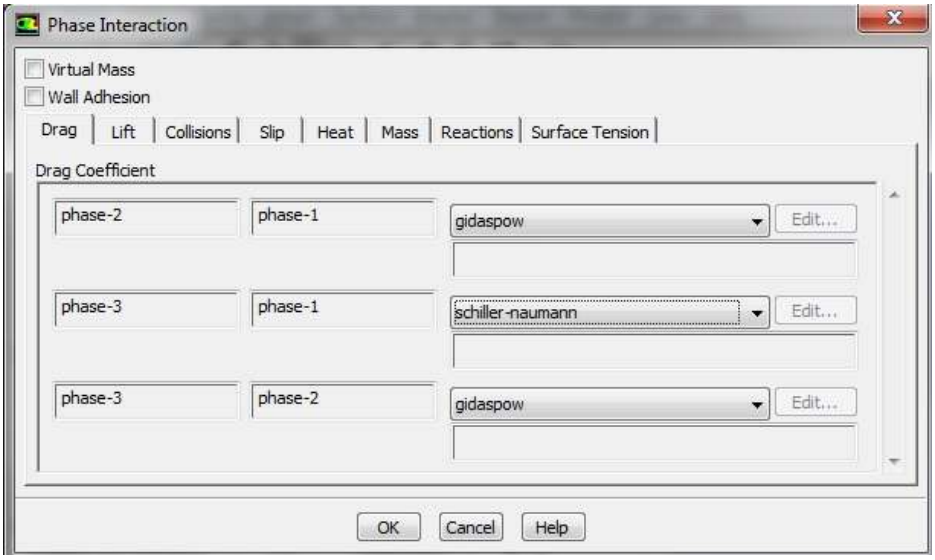

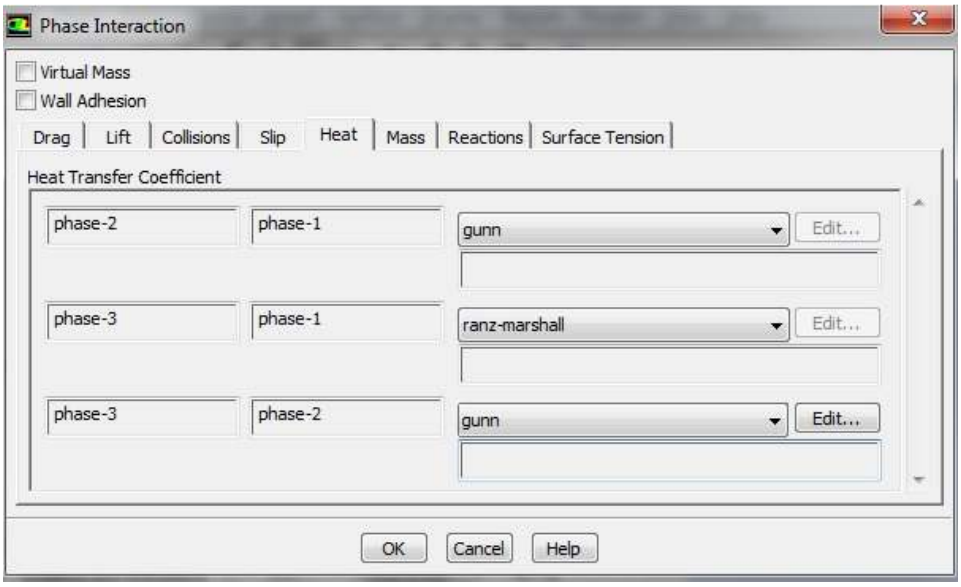

Step 11: Boundary Conditions

The boundary conditions are defined as velocity inlet from the bottom for steam, lateral velocity inlet of feed biomass as pyrolytic products and the outlet on the top of the BFB as pressure outlet. In both the inlets the velocity of gas mixture (primary phase), the momentum, thermal and species fields are defined, while the secondary phase these fields are zero as shown in figure. The outlet of the BFB is defined as atmospheric pressure.

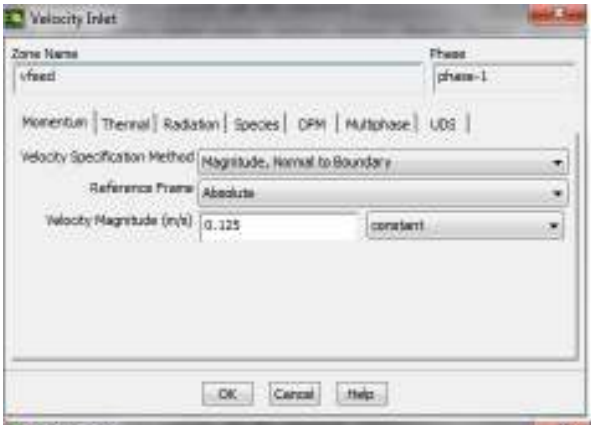
Velocity Inlet
Zone Name
vfeed
Phase
phase-1
Momentum | Thermal | Radiation | Species | DPM | Multiphase | UDS
Velocity Specification Method
Magnitude, Normal to Boundary
Reference Frame
Absolute
Velocity Magnitude (m/s)
0.125
constant
OK
Cancel
Help


Velocity Inlet
Zone Name
vfeed
Phase
phase-1
Momentum | Thermal | Radiation | Species | DPM | Multiphase | UDS
Temperature (k)
constant
OK
Cancel
Help

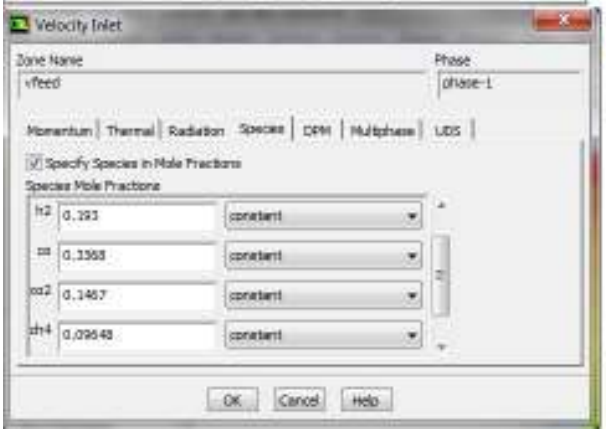
Velocity Inlet
Zone Name
vfeed
Phase
phase-1
Momentum | Thermal | Radiation | Species | DPM | Multiphase | UDS
Specify Species in Mole Fractions
Species Mole Fractions
h2
0.193
constant
co
0.1368
co2
0.1467
ch4
0.09648
OK
Cancel
Help


Velocity Inlet
Zone Name
vfeed
Phase
phase-2
Momentum | Thermal | Radiation | Species | DPM | Multiphase | UDS
Velocity Specification Method
Magnitude, Normal to Boundary
Reference Frame
Absolute
Velocity Magnitude (m/s)
0
constant
Granular Temperature (m2/s2)
0.0001
constant
OK
Cancel
Help

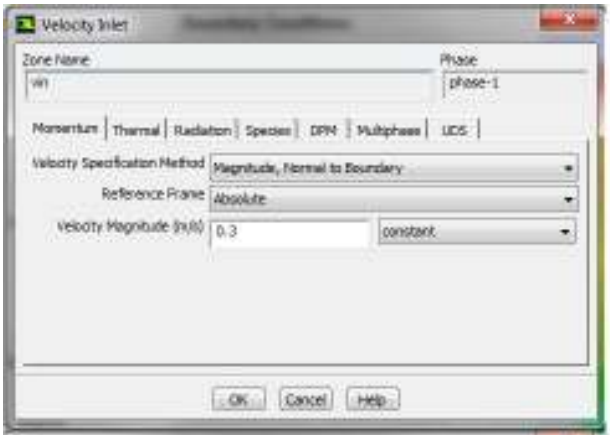
Velocity Inlet
Zone Name
vin
Phase
phase-1
Momentum | Thermal | Radiation | Species | DPM | Multiphase | UDS
Velocity Specification Method
Magnitude, Normal to Boundary
Reference Frame
Absolute
Velocity Magnitude (m/s)
0.3
constant
OK
Cancel
Help


Velocity Inlet
Zone Name
vin
Phase
phase-1
Momentum | Thermal | Radiation | Species | DPM | Multiphase | UDS
Specify Species in Mole Fractions
Species Mass Fractions
h2o
1
constant
h2
0
co
0
co2
0
OK
Cancel
Help


Velocity Inlet
Zone Name
vin
Phase
phase-1
Momentum | Thermal | Radiation | Species | DPM | Multiphase | UDS
Temperature (k)
973
constant
OK
Cancel
Help


Velocity Inlet
Zone Name
vin
Phase
phase-2
Momentum | Thermal | Radiation | Species | DPM | Multiphase | UDS
Volume Fraction
0
constant
OK
Cancel
Help

Step 11: Adaption

A small Region Adaption will be adapted in order to create a register so that the solid volume fraction can be patched to a bed height of 0.2 m in the BFB. The input coordinates are chosen as 0 for X Min and Y Min respectively and 0.2 for X Max and Y Max respectively. Click Mark. FLUENT will report the number of cells marked for adaption in the console.

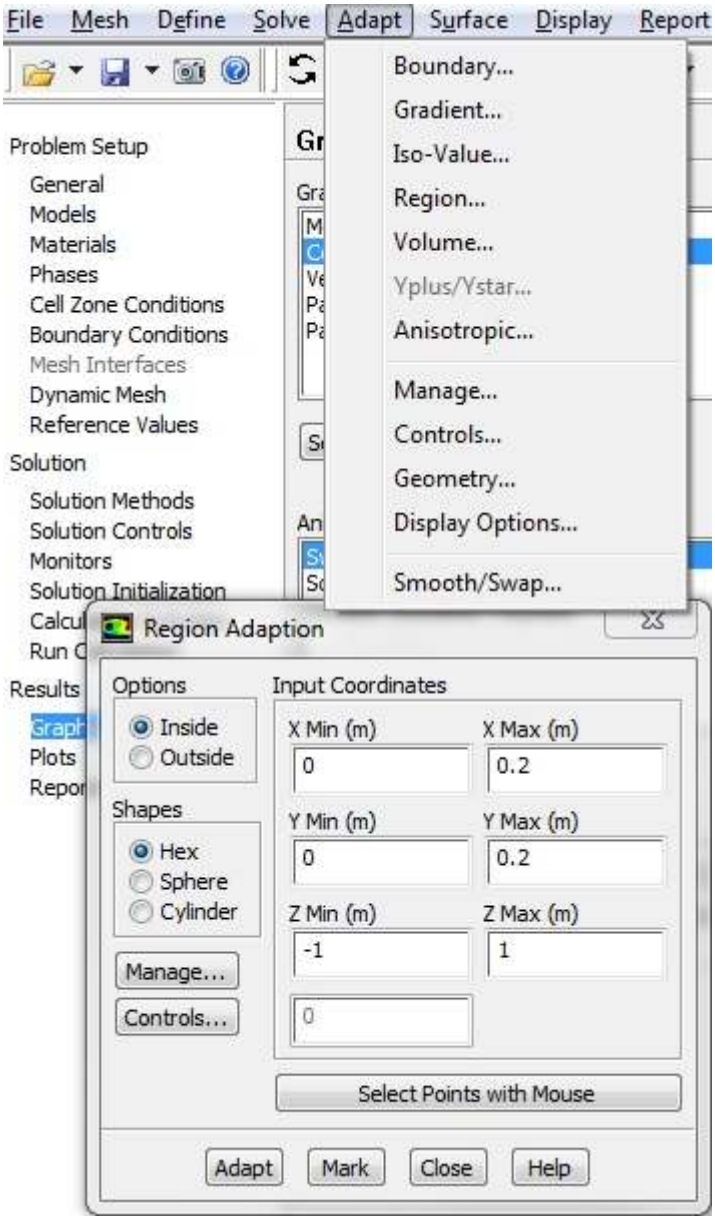

Step 12: Solution controls

The solution controls were given by the under relaxation factors as shown in Table 5.2.

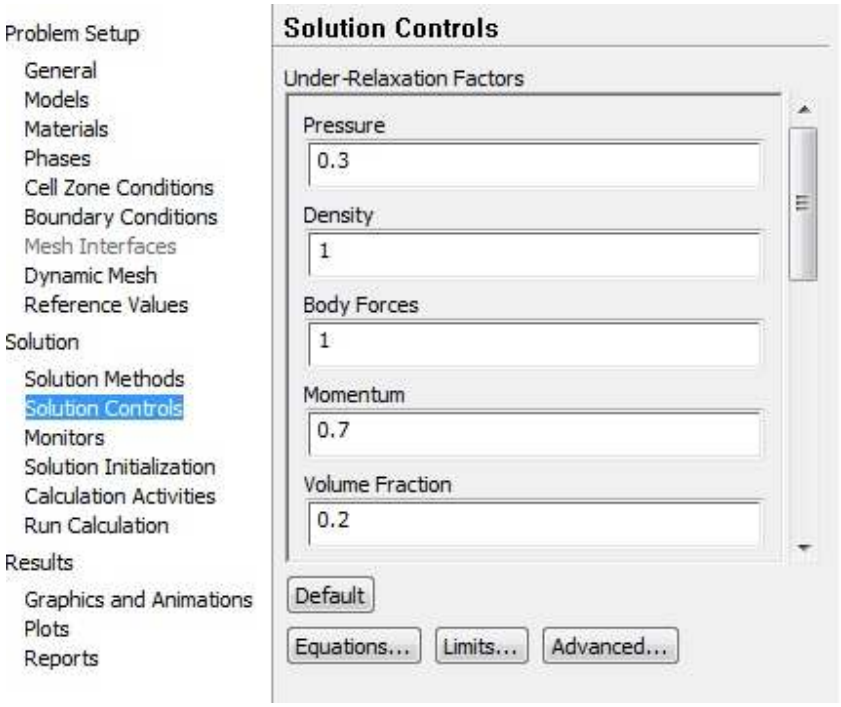

Step 13: Solution Methods

The solution Methods were given by Phase Coupled Simple scheme as shown in Table 5.2. In the spatial discretization, the gradient is least square cell based, while the momentum, volume fraction, energy and species are all first order upwind.

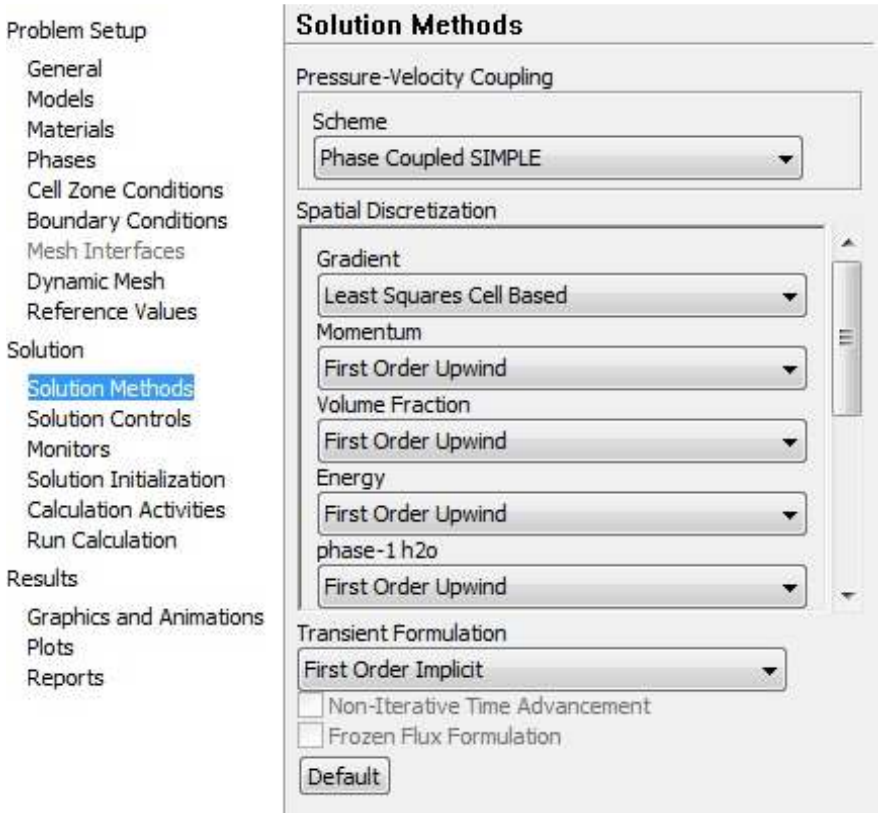

Step 14: Solution Initialization

The initial values are generated by selecting all zones from the computation region and initializing using the initialize panel.

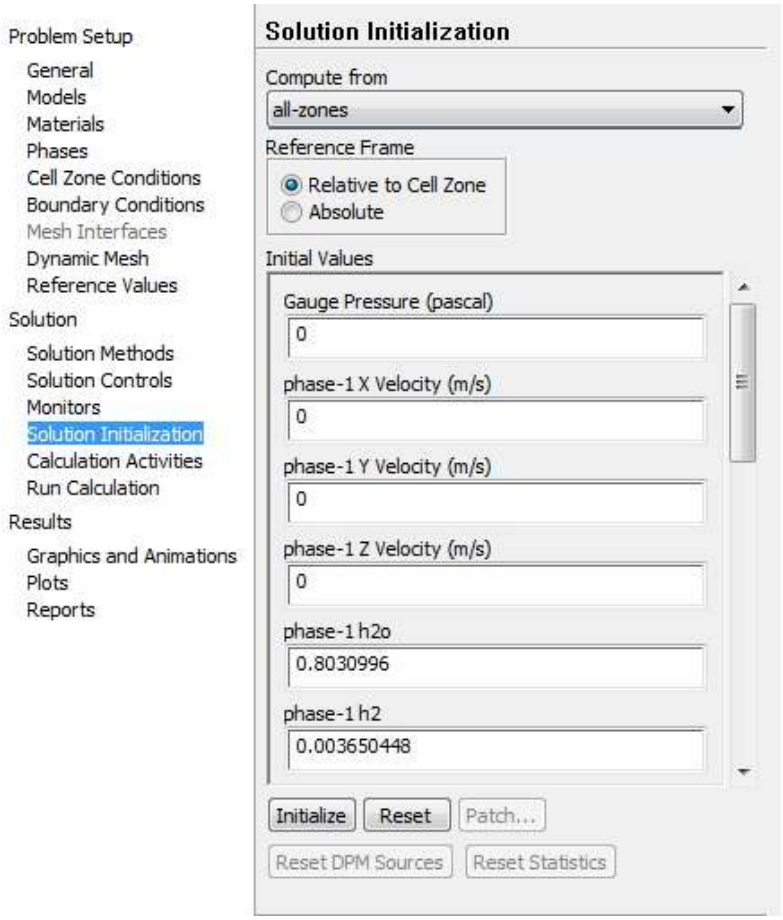

Step 15: Patch the initial sand bed configuration.

In the Patch panel, select the volume fraction from the variable selection list,hexahedron-r0 from the registers to patch selection list and enter 0.52 for value and finally click patch

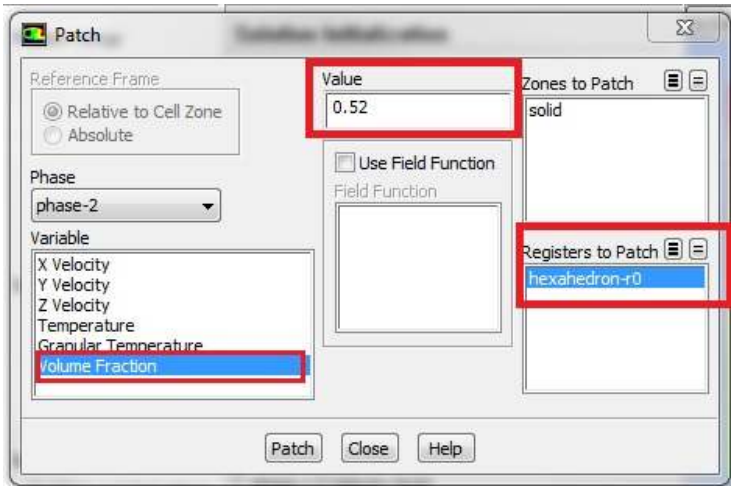

After initializing the entire domain of your flow field, different initializationvalues for particular variables can be enter into different cells. This is known as patchingand is generally used if you have multiple fluid zones that you want to patch withdifferent values.

Step 16: Run Calculation

For a good convergence smaller time steps were required and hence in solving this proposed model, the time step was set as 0.001s with maximum number of iterations set as 20.